NUMERICAL SOLUTIONS FOR CASSON AND WILLIAMSON NANOFLUIDS OVER A STRETCHING SHEET

KHO YAP BING

MASTER OF SCIENCE

UNIVERSITI MALAYSIA PAHANG

UNIVERSITI MALAYSIA PAHANG

DECLARATION OF THESIS AND COPYRIGHT

Author's Full Name : KHO YAP BING

Date of Birth : 7 JUN 1990

Title : NUMERICAL SOLUTIONS FOR CASSON AND

WILLIAMSON NANOFLUIDS OVER A STRETCHING

SHEET

Academic Session : MASTER OF SCIENCE

I declare that this thesis is classified as:

☐ CONFIDENTIAL (Contains confidential information under the Official Secret Act 1997)*

☐ RESTRICTED (Contains restricted information as specified by the organization where research was done)*

☑ OPEN ACCESS I agree that my thesis to be published as online open access (Full Text)

I acknowledge that Universiti Malaysia Pahang reserve the right as follows:

1. The Thesis is the Property of Universiti Malaysia Pahang
2. The Library of Universiti Malaysia Pahang has the right to make copies for the purpose of research only.
3. The Library has the right to make copies of the thesis for academic exchange.

Certified by:

_____   _____
(Student's Signature)   (Supervisor's Signature)

_____   _____
New IC/Passport Number   Name of Supervisor
Date: Date:

NOTE : * If the thesis is CONFIDENTIAL or RESTRICTED, please attach with the letter page 2 from the organization with the period and reasons for confidentiality or restriction.

SUPERVISOR'S DECLARATION

We hereby declare that we have checked this thesis and in our opinion, this thesis is adequate in terms of scope and quality for the award of the degree of Master of Science in Mathematics.

_____
(Supervisor's Signature)

Full Name   :

Position   :

Date   :

_____
(Co-supervisor's Signature)

Full Name   :

Position   :

Date   :

STUDENT'S DECLARATION

I hereby declare that the work in this thesis is based on my original work except for quotations and citation which have been duly acknowledged. I also declare that it has not been previously or concurrently submitted for any other degree at Universiti Malaysia Pahang or any other institutions.

_____

(Student's Signature)

Full Name   : KHO YAP BING

ID Number   : MSE15003

Date   :

NUMERICAL SOLUTIONS FOR CASSON AND WILLIAMSON NANOFLUIDS OVER A STRETCHING SHEET

KHO YAP BING

Thesis submitted in fulfillment of the requirements

for the award of the degree of

Master of Science

Faculty of Industrial Sciences & Technology

UNIVERSITI MALAYSIA PAHANG

May 2018

ACKNOWLEDGEMENT

First of all, praise be to God. I give thanks to Him for all the blessings and good health that He has given me in completing this work.

I wish to express my most sincere gratitude to my principal supervisor, Dr. Zulkhibri Ismail and his senior colleague who collaborated in the present research, Associate Professor Dr. Mohd Zuki Salleh, for their patient guidance, endless encouragement, knowledge shared, wise decisions made and financial support given during my master's study, all of which have been crucial for the success of this research. I truly appreciate the contribution they have made from first day I entered the faculty. I will always remember the valuable lessons they have taught me and the commitment they have given to nurturing and shaping my future path.

I would like to thank to my co-supervisor, Ms Norhafizah Md Sarif for her help and useful suggestions. My deepest thanks and appreciation also go to my seniors, Abid Hussanan and Muhammad Khairul Annuar Mohamed for their consistent assistance and teaching. Without their effort, this thesis would not have been possible. I would also like to thank the member of staff of at the Faculty of Industrial Sciences and Technology, UMP who had helped me in various ways.

My sincere gratitude goes to my dearest parents, my siblings, my relatives and my friends. I shall forever remain indebted for the love, care, support and sacrifice they have given me especially during course of my study which have provided the strength for me from the beginning until the end.

.

ABSTRAK

Bendalir tak Newtonan mempunyai karakter yang unik kerana tidak mematuhi hukum kelikatan Newtonan. Dengan sifat reologi, persamaan klasik Navier-Stokes tidak lagi sesuai untuk mentakrifkan keseluruhan bendalir tak Newtonan. Bendalir tak Newtonan boleh ditakrifkan mengikut beberapa kategori seperti elastik likat, kelikatan kebergantungan masa dan kelikatan tak Newtonan. Contoh bendalir adalah seperti minyak, sos, pasta makanan, cat dan larutan koloid. Bendalir tak Newtonan mendapat perhatian kerana prestasi yang cemerlang di dalam industri dan penggunaan teknologi jika dibandingkan dengan bendalir Newtonan. Dalam kajian ini, terdapat dua bendalir tak Newtonan iaitu bendalir nano Casson dan Williamson yang dipilih untuk diselidik. Sementara itu, beberapa syarat sempadan dikaji iaitu suhu dinding malar, pemanasan Newtonan dan syarat gelincir. Syarat lain yang dipertimbangkan adalah kesan radiasi terma, medan magnet dan keliangan media. Model yang dicadangkan untuk setiap permasalahan adalah bergantung kepada sistem persamaan menakluk yang tertakluk kepada syarat awal dan syarat sempadan. Kemudian, pembolehubah tak berdimensi diperkenalkan untuk menurunkan persamaan menakluk kepada bentuk tak berdimensi. Seterusnya, penyelesaian berangka persamaan pembezaan biasa diselesaikan dengan menggunakan kaedah Luruan. Penyesaian ini mestilah asimptot dan perlu memenuhi syarat awal dan syarat sempadan. Perbandingan kes kelikatan dijalankan untuk mengesah kajian yang dijalankan adalah tepat dan dipercayai. Penyelesaian berangka untuk profil halaju, suhu dan kepekatan diplot secara grafik dan dibincangkan dengan pelbagai parameter. Pekali geseran kulit, nombor Nusselt dan nombor Sherwood setempat juga diselidik dan diperiksa. Keputusan menunjukkan bahawa profil halaju menurun secara signifikan dengan peningkatan parameter Casson dan Williamson. Selain itu, dapat diperhatikan bahawa parameter tidak boleh melebihi nilai kritikal, di mana bendalir akan kehilangan karakter. Dalam kajian ini didapati bendalir tak Newtonan mempunyai konduktiviti pemindahan haba yang lebih baik daripada bendalir asas. Parameter pemanasan Newtonan juga meningkatkan suhu dinding di dalam aliran bendalir lembaran tegang. Penyelesaian fizikal parameter pemanasan Newtonan juga dianalisa. Penyelesain berangka yang diperoleh dalam kajian ini amat penting dalam mengesahkan asas aliran disebabkan piawanan ketepatan untuk kaedah anggaran, analitik dan eksperimen.

ABSTRACT

The unique characteristic of non-Newtonian fluids is that they do not obey the Newtonian law of viscosity. With the rheological behaviour properties, the classical Navier Stokes equations are no longer appropriate to define all the non-Newtonian fluids. Non-Newtonian fluids can be defined in several categories like visco-elastic, time-dependent viscosity and non-Newtonian viscosity. Such fluids are oils, ketchup, food paste, paints and colloidal solutions. Non-Newtonian fluids have gained much attraction due to their better performance in industrial and technological applications compared to Newtonian fluids. In this study, there are two types of non-Newtonian fluids, namely, the Casson and Williamson nanofluids, were selected to be investigated. Meanwhile, several types of boundary conditions studied were constant wall temperature, Newtonian heating and slip conditions. Other conditions considered were thermal radiation effect, magnetic field and porosity of the medium. The proposed model for each problem would depend on the system of governing equations subject to the imposed initial and boundary conditions. Then, suitable non-dimensional variables were introduced to reduce the governing equations into the dimensionless form. Next, the numerical solutions of ordinary differential equations were solved using the Shooting method. These solutions must be asymptotic and must meet the imposed initial and boundary conditions. The comparison for viscous case was conducted to verify that the results of the present study would be reliable and accurate. The numerical solutions of velocity, temperature and concentration profiles were plotted graphically and discussed with different parameters. The skin friction coefficient, local Nusselt number and Sherwood number also have been studied and examined. Results showed that the velocity profile had decreased significantly with increase in Casson and Williamson parameters. The wall temperature increased when Casson and Williamson parameters increased. Besides, it is noticed that these parameter must not exceed the critical values respectively; otherwise, the fluid lost its characteristics. The non-Newtonian fluids in the present study were found to have better conductivity in heat transfer compared with base fluids. Also, the Newtonian heating parameter leads increase the wall tempearature in the fluid fow over a stretching sheet. The physical solutions for Newtonian heating parameter were also analysed. The numerical solutions obtained in the present study would be important in the validations of fundamental flow because of the accuracy standards for approximate method, analytical and experimental method.
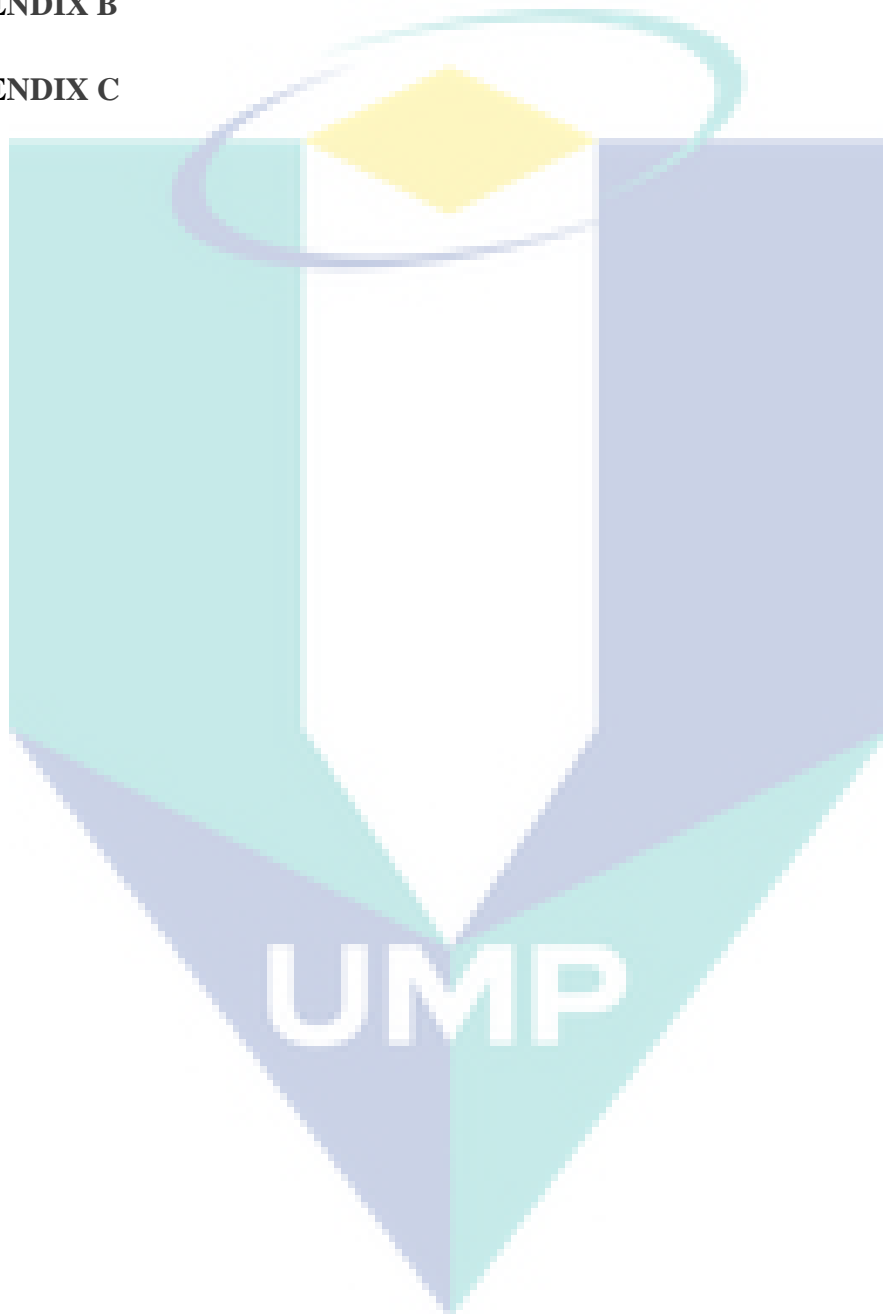
TABLE OF CONTENT

LIST OF TABLES

LIST OF FIGURES

LIST OF SYMBOLS

a	Positive constant for stretching rate
B	Thermal slip parameter
B^*	Thermal slip factor
B_o	Induced magnetic field
C	Volumetric volume expansion coefficient
C_f	Local skin friction coefficient
C_W	Concentration near the plate
C_∞	Concentration far away from the plate
D	Mass diffusivity
D_B	Brownian diffusion coefficient
D_T	Thermophoresis diffusion coefficient
f	Dimensionless stream function
h_s	Heat transfer coefficient
K	Porosity parameter
k	Thermal conductivity
k_1	Permeability of the porous medium
k^*	Mean absorption coefficient
Le	Lewis number
M	Magnetic parameter

Nb	Brownian parameter
Nc	Heat capacities ratio
Nbt	Diffusivity ratio
Nt	Thermophoresis parameter
Nu	Local Nusselt number
Pr	Prandtl number
q_r	Radiative heat flux
R	Radiation parameter
Sc	Schmidt number
Sh	Sherwood number
T	Nanofluid temperature
T_W	Temperature of the fluid inside the boundary layer
T_∞	Ambient temperature
u, v	Velocity components along x and y axes
$U_W(x)$	Stretching sheet velocity

Greek symbols

α_m	Nanofluid thermal diffusivity
β	Casson nanofluid parameter
δ	Velocity slip parameter
δ^*	Velocity slip factor
ρ	Density of nanofluid
σ	Electricity conductivity

σ^*	Stefan Boltzmann constant
ν	Kinematic viscosity
$(\rho c_p)_f$	Effective heat capacity of nanoparticle
λ	Williamson nanofluid parameter
ψ	Stream function
μ	Dynamic viscosity
τ_w	Shear stress surface
θ	Dimensionless temperature
ϕ	Dimensionless concentration
Γ	Time constant

Subscripts

w	Condition at wall
∞	Condition at infinity

LIST OF ABBREVIATION

CWT   Constant Wall Temperature

MHD   Magnetohydrodynamic

NH   Newtonian heating
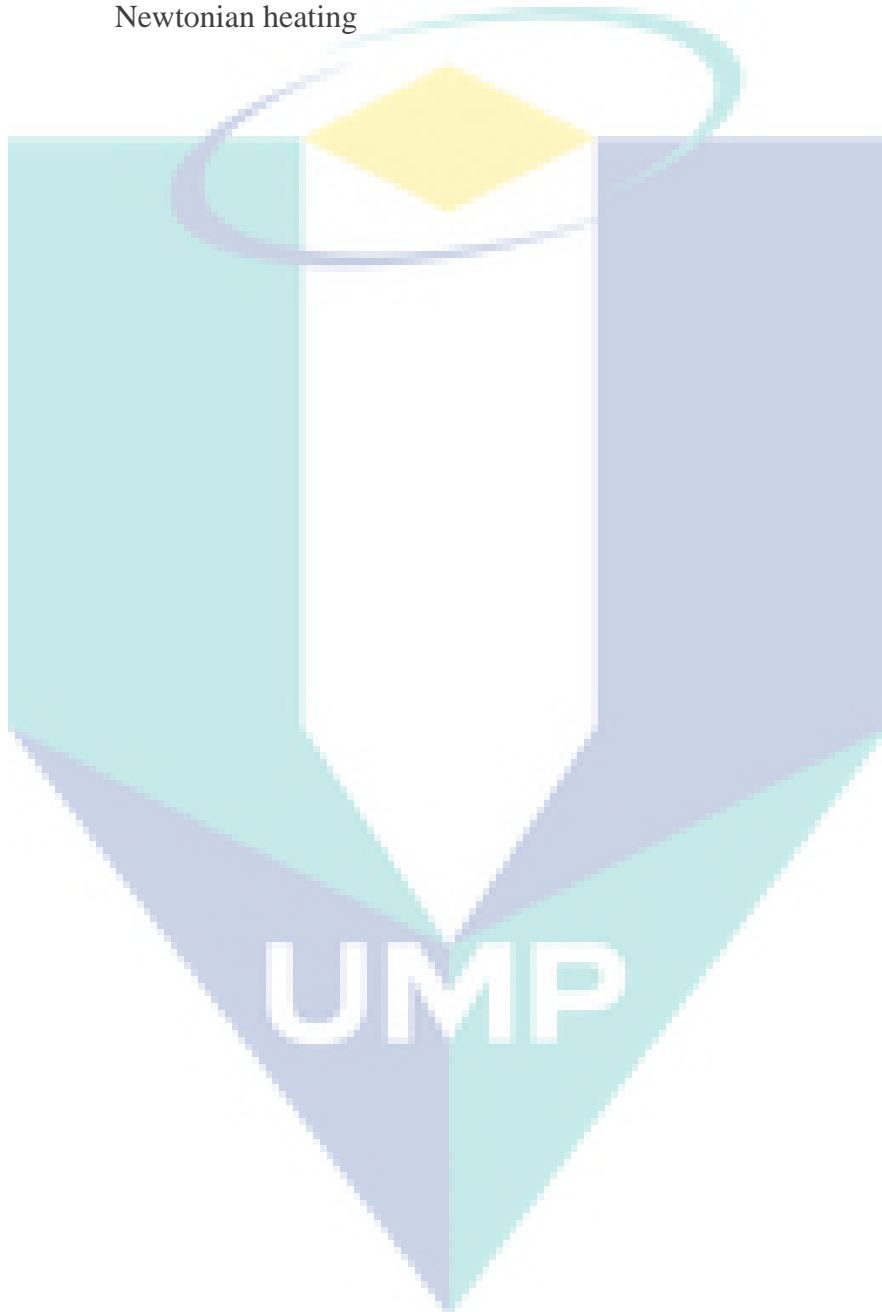
CHAPTER 1

INTRODUCTION

1.1   Introduction

In this chapter, two types of non-Newtonian fluids, namely Casson and Williamson nanofluids are studied. Section 1.2 discusses the background of this research while the problem statement is given in Section 1.3. Meanwhile, Section 1.4 highlights the objectives and scope of the research. Section 1.5 which describes the methodology and the methods used to perform and solve the governing equations. Next, Section 1.6 presents the significance of the study. Lastly, Section 1.7 provides the outline of the thesis.

1.2   Research Background

The life of human lives never goes far from applying the flow of non-Newtonian fluid models. Non-Newtonian fluid models have play important roles in the basic daily needs of humans as the concept is applied in medical sciences, engineering and the industry. The outcome from such models can be observed everywhere and in many processes such as food ingredients their preparation, blood circulation, cosmetic products, and paper production (Taylor et al, 2013). In recent years, the issue of nanofluids has become popular and has been widely discussed and investigated due to the vast accredited to the potential properties and characteristics of the nanofluids such as thermal conductivity, viscosity, and heat transfer rate. Scientists and researchers have uncovered the application of nanofluids and believe that they would benefit the human lives and future development in science and research. The term 'nanofluid' was first coined by Choi (1995) in the thermal science community. Since then, this issue has attracted who have published numerous articles discussing nanofluids in publications on heat transfer and thermal science. For the past few years, articles on nanofluids have

1

rapidly increased. For example, based on Google Scholar search (2012 - 2016), the number of citations for nanofluids in journals dramatically increased from less than 100 citations per year in 2012 to more than 170 in 2013 before dropping slightly to approximately 170 in the following year but continued to increase above 170 in 2015 and finally soaring up almost two-fold and nearly reached 340 citations per year in 2016 (see Figure 1.1).
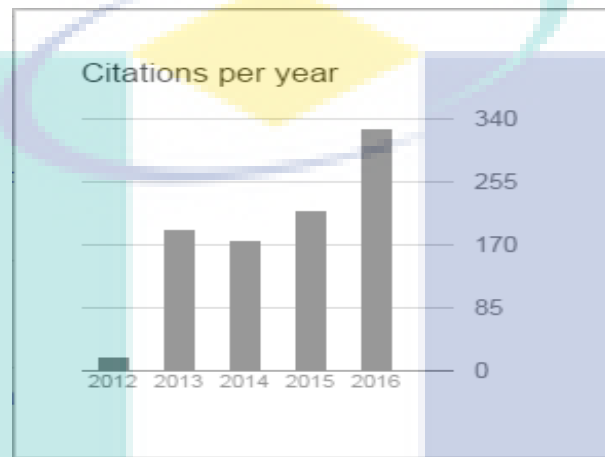
Figure 1.1 Citations for the term "nanofluids".

The applications of nanofluids used in medicine especially in cancer treatment and control of fluid motion. Nanofluids are also applied in both heating and cooling process systems ranging from the cooling of wrapped integrated circuits at a small scale to the transfer in nuclear reactors at a large scale. Nanofluids are also used in cooling the microchips in electrical devices (e.g., desktop computer) because of their high thermal conductivity properties. Besides, nanofluids can also be used as detergent to clean up oil spills and stains. Nanofluids behave as different from base fluids in term of classical concepts of spreading and adhesion on solid surfaces (Wong & Leon, 2009). Because there is not a single constitutive equation that can describe all the properties or rheological behaviour of non-Newtonian fluids, some researchers have introduced new models of non-Newtonian fluids such as the Williamson fluid, Casson fluid, Jeffrey fluid in order to imitate their performance better. The relevant contributions of non-Newtonian fluids flow have been explored by Akbar et al. (2011); Hayat and Ali (2008); Magyari and Keller (1999); Mustafa and Khan (2015); Krishnamurthy et al. (2016) and Nadeem and Hussain (2014).

2

The flow of non-Newtonian fluids involves the absorption or loss of heat since heat transfer exists when there is a difference in temperature between two objects and it. It is a physical act of thermal energy being exchanged and the dissipation of heat between two systems. The temperature is defined as the available amount of thermal energy while the movement of thermal energy is represented by the flow of heat transfer. The heat transfer problem has been concern in studies by many researchers (see Das et al. 2006; Cebeci & Bradshaw, 2012; Haq et al. 2014; Gorla & Gireesha 2016; Bhatti and Rashidi, 2016). There are three ways to transfer heat: (1) conduction; (2) convection; and, (3) radiation. Conduction is the transfer of energy in the form of electricity or heat from an atom to another within an object through direct contact. Solids transfer energy is the most efficient compared to transfer of energy through liquids and gases since the arrangement of molecules in solids are tightly packed and closer together. Convection is the transfer of energy by the actual movement of warmed matter in fluids or gases through the movement of currents. Radiation is the energy transferred directly by electromagnetic wave through space or any transparent medium. Radiation is different from the other two ways of heat transfer because radiation does not rely upon any contact between the heat sources. For example, the sun releases heat through radiation and the heat energy is subsequently transferred heat across the solar system. The random movement of molecules and atoms in a matter directly causes thermal radiation while the movement of charged protons and electrons results in the emission of electromagnetic radiation. All objects radiate thermal energy based on their temperature. The higher the temperature of materials, the more they will radiate thermal energy. As the nanofluid flows over a stretching sheet, the collision between nanoparticles and wall surface of a plate releases the thermal heat which affects its reaction. The flow of incompressible viscous fluid towards a stretching sheet is important in some technological applications such as polymer extrusion, fiber glass production, and paper manufacturing. Based on the study by Mahapatra and Gupta (2001), the final quality of these cases depends on the rate of heat transfer at stretching sheet. In fact, many journals have published the investigations on heat transfer flow over a stretching surface set with varying problem such as non-Newtonian of power law fluid, velocity varying linearly flow, boundary layer flow, stagnation point, and slip condition.

Magnetohydrodynamics (MHD) is also a subject of subjects' interest in this study as due to the presence of electrically conducted fluids motion in magnetic field. The idea of implementing MHD had been introduced by Hannes Alfven who won the Nobel Prize in 1970. As noted by Shima et al. (2009), the magnetic nanofluids cause magneto dielectric effect (a mechanism of reversibly forming particle agglomerate chains) which affects the thermal conductivity. In addition, a reversible approach to dynamically control friction between the moving parts can be manipulated by a stable magnetic fluid. There are several electromagnetic nanofluid applications, for instance, in solar energy harvesting, medical treatment, and random lasers. Besides, fluid flow through porous media is a subject that receives much interest in the academia which concerns how fluids behave when passing through a porous medium. Normally, a porous medium is most often characterized by its porosity. The concept of porous medium has been applied in many areas, especially applied sciences and engineering like filtration, bio-remediation, and biology, among others. This is due to its properties of electrical conductivity, permeability and tensile strength. Much of research on fluid flow through a porous medium can be found in Lapwood (1948), Saffman and Taylor (1958), Vafai (1984), and Ahmad and Pop (2010). Many researchers studied their problems with no-slip condition. However, no-slip condition is inadequate when the fluid is particulate such as suspensions, emulsions and polymer solutions. Due to its micro or even smaller size, the behaviour of the fluids flow is opposite of or deviates form that of no-slip condition. The nanofluidic flow is categorized as the so-called slip length because the slip length is exhibited when it goes part against the solid surface. Thus, the no-slip condition may not be appropriate for the nano scale instead, a certain degree of tangential slip must be allowed. The relevant works can be found in studies by Yoshimura and Prud'homme (1988), Majumder et al. (2005), Gad-el-Hak (1999) and Aly (2015).

In mathematical modelling, a well-defined physical problem for convective boundary flow can be described by the governing equations which are then subjected to the boundary conditions. Generally, there are several types of boundary conditions used in heat transfer problem. Based on the literature study, it has been discovered that there are a few common boundary conditions such as ramped wall temperature, prescribed surface heat flux or convective boundary conditions. However, these assumptions may fail to work in some practical solutions where the heat transfer from the surface is taken

to be directly proportional to the local surface temperature. This is because some of the flows are defined as conjugate convective flow and proportional to the local surface temperature like Newtonian heating. This work had first been carried out by Merkin (1994) on free convection boundary flow over a vertical plat immersed in viscous fluid. Then, this boundary condition was evaluated by other researchers in their numerical or analytical study as in convective heat transfer problems. The development and application for Newtonian heating can be found in some engineering applications such as in heat exchanger, heat management appliances, and engine cooling. The problems considered as Newtonian heating under different conditions can be found in the works of Salleh et al. (2010), Lesnic et al. (1999), and Narahari and Ishak (2011).

In this study, two types of non-Newtonian fluids were examined, namely, the Casson and the Williamson nanofluids. Their detailed description will be provided in the following subsections.

1.2.1 Nanofluids

In the past century, convective heat transfer fluids (e.g., water and kerosene) played a crucial role in several applications in the engineering field and industrial sectors (e.g., chemical production, power generation, and microelectronics). However, these fluids had been analysed with low thermal conductivities and thus, resulted in limited heat transfer capabilities. In order to meet demands, the idea of nanofluids was introduced and to replace fluids with lower thermal conductivity. Generally, a fluid that possesses the nanometer sized of particles is called a nanofluid. According to Taylor et al. (2013), nanofluids are the colloidal suspension of nanoparticles with sizes between 1 and 100 nm which are available in conventional base fluids like water, glycols and oil. Normally, nanoparticles used in the fluids are typically made up of carbon nanotubes (CNTs), metals (e.g., Au, Cu, Al, Ag and Fe) or oxides (e.g., CuO, Al_2O_3, TiO_2 and SiO_2). Due to the unique properties of the nano-sized particles, nanofluids are found to have great potential in the application of heat transfer in many fields such as engineering, process system, biomedical and cooling system. After the term nanofluid was introduced by Choi (1995) and Eastman et al. (1996), it has since then become famous and gained much interest from researchers. Consequently, the study of nanofluids has shown rapid growth in recent years.

Nanofluids have many advantages and show great potential. Compared to solid-liquid convention of heat transfer, it has been evident that nanofluid performs better in high particular surface area and causes a rise in temperature gradient between nanoparticles and the fluid. Furthermore, nanofluids have greater dispersion stability within the presence of Brownian motion particles. Brownian motion or pedesis is the random manner in which particles are suspended in a fluid, whether in gas or liquid moves. This phenomenon is due to the collision between the particles and atoms in a gas or liquid moving at high speed. Jang and Choi (2004) have suggested that the smaller the size of particles, the higher the random motion would be. As a result, the convection effects become dominant which causes the conductivity of the nanofluid to increase. Hence, to achieve better conductivity, the size of the particle must be as small as possible. Furthermore, nanofluids save more energy in pumping power compared to base fluids to achieve equivalent temperature gradient intensification. Nanofluids are also well known for having adjustable properties such as thermal conductivity and surface wettability which depend on the particle concentration to suit the different applications. A study by Sivashanmugam (2012) has concluded that the nanofluid produces a large increase in the heat transfer coefficient as well as an increase in the number of nanoparticles concentration. An investigation of nanofluids by (Das et al. 2006) higlighted four specific features as below:

i.   Unstandardized enhancement in thermal conductivity. The criterion of most concern in nanofluid would be the abnormal rise in thermal conductivity, exceeding the expectations and predictions by any theory.

ii. Stability. Nanofluids could be used as a stabilizing agent because of their stability.

iii. Less concentration with Newtonian behaviour. Eventhough in low concentration of nanoparticles, large enhancement in thermal conductivity would still be achievable and completely maintain Newtonian behaviour in nanofluids. Thus, the viscosity rise would be nominal and the resulting pressure drop would increase only marginally.

iv. The dependence on nanoparticles size. In generally, the smaller the size of nanoparticles, the greater the surface area, and the higher enhancement of thermal conductivity observed.

Ever since the first work carried out by Choi (1995) regarding nanofluids, several researchers have adopted the concept and develop problems such as like introducing the new fluid models (e.g., Casson fluid, Williamson fluid, and Jeffrey fluid). Consequently, nanofluids are introduced into these fluid models. Nadeem and Hussain (2014) have concluded that nanoparticles have strong impact on wall temperature after they worked out the problem of heat analysis of Williamson nanofluid. Recently, the effect of chemical reaction and non-linear thermal radiation in Williamson nanofluid was investigated by Prasannakumara et al. (2016). Gorla and Gireesha (2016) noted that the heat transfer rate of Williamson nanofluid would be more efficient than that of the Newtonian fluids after studying the problem of dual solution for stagnation point of Williamson nanofluid. In addition, Haq et al. (2014) have also discovered that skin friction of Casson nanofluid is comparatively higher than Newtonian fluids. Meanwhile, Malik et al. (2014) have studied the behaviour on boundary layer flow of Casson nanofluid over a vertical exponentially stretching cylinder as cylindrical geometry plays an important role in human blood flow. The three dimensional flow of Casson nanofluid was presented by Nadeem et al. (2014) and they have found that the Newtonian nanofluids produce the lower friction and heat transfer rate compared to those of the non-Newtonian nanofluids.

There are still many uncertainties about of nanofluids and yet nanofluids have been fully utilized in the medical treatment, industrial sector and engineering field. Therefore, an improvement in knowledge and technology in this field is vital for the future. Indeed, research in the development and investigation on nanofluids will continue to be conducted with different boundary conditions.

1.2.2 Casson nanofluid

The viscoplastic fluid had been discovered in the 19th century and was first modelled by Bingham in 1922. The model was then introduced into a general framework of continuum mechanics by Oldroyd. Later, the work has since been extended and continued by other researchers especially mathematicians working on different areas as well as experts on analytical and computational methodologies, theoretical development for new and existing applications on viscoplastic flow problem.

The viscoplastic materials are fluids that manifest or deliberately yield stress. The materials only flow like fluid when the yield value exceeds a certain critical value of shear stress. Otherwise, it behaves like a rigid solid and there is no deformation when the yield stress is smaller than the shear stress of a certain amount. In fact, the viscoplastic fluid appears in many situations, including food pastes, some polymer solutions, clays and muds, cosmetic productions, crystallizing lavas, hair gel and others. Consequently, the theory of the fluid has been applied in a wide array of different fields, ranging from chemical industries to food processing and biological fluids. One of the extensions from the viscoplastic fluid model is a Casson fluid model.

The Casson fluid model was pioneered by Casson (1959) who investigated and predicted the flow behaviour of pigment –oil suspensions. Casson fluid model is diluted to a Newtonian fluid if the yield stress is lower than the shear stress. Due to this characteristic, this fluid model has been introduced in modelling of biological fluid flow especially in food products and blood flow. Casson fluid model provides a good approximation to other viscoplastic fluid model like Bingham plastic model. Having investigated the problem of Casson fluid flow through the cardiovascular stenotic blood vessel, Srivastava and Saxena (1994) have concluded that Casson fluid shows better performance when applied to constrict of the small vessel for blood flow due to the non-Newtonian effects. Other than that, it has also been proven as a good approximation for other materials such as chocolate, yogurts, syrups and foams (Dash et al. 2000; Qasim & Noreen, 2014). Eventually, Casson fluid is extended with nanofluids under various conditions, including convective boundary layer, thermal heat transfer, magnetic force and porosity towards stretching surface (Nadeem et al., 2013; Hayat et al., 2012 and Haq et al. 2014).

1.2.3 Williamson nanofluid

At every point, the fluid flows, the viscous stress appears to be in linear proportion to the rate of change of its deformation over time, known as the local strain rate. Therefore, a Newtonian fluid does not depend on the flow's velocity and stress state. In this thesis, pseudoplastic model was selected as the fluid medium in the problem studied. In rheology, it is also considered synonymous with thinning shear whose viscosity decreases under shear strain. More precisely, pseudoplastic fluids that show apparent viscosity or consistency decrease instantaneously with an increase in

8

shear rate. Normally, it is often seen in molten polymer, poly solutions, complex fluids and suspensions, including paint, blood, whipped cream, ketchup and many others (Cross, 1965). For example, like wall paint, it would not drip excessively when it is being applied to the surface and would readily flow off. Besides, blood also considered as thinning shear fluid since the blood viscosity decreases with increased shear strain rate. Williamson fluid was defined by Williamson (1929) in order to look for a medium with pseudoplastic materials flow. Thus, Williamson fluid can also refer to viscoelastic thinning shear fluid. Subsequently, it has been gained plenty of attention from other researchers who studied and investigated the problem utilizing different parameters such as porosity, Brownian motion, slip conditions and so forth. The other relevant works utilizing different conditions can be found through Nadeem and Akram (2010); Ellahi et al. (2013) and Kothandapani and Prakash (2015).

1.2.4 Tiwari and Das Model

According to Brinkman (1952), he had proposed a phase model which using Maxwell-Garnet thermal conductivity and viscosity. Due to the form of phase model, the nanoparticles and the base fluid are considered in the condition of thermal equilibrium and flowing in constant velocity with no slip condition between them. In fact, this model is corresponding to the effect of nanoparticle's volume fraction. In other word, the effectiveness of thermal conductivity would be increase as the the result increase in volume fraction of nanoparticle. Based on the investigations of Jang and Choi (2007), only a little amount of solid volume fraction could enhance the effectiveness of thermal conductivity in the fluid. Thus, the rate of heat transfer which occurs on the wall also will be improved since due to the high thermal conductivity.

The idea of Tiwari and Das model have been applied in this research work for better understanding of the characteristics of thermal conductivity in nanofluid flow.

1.2.5 Shooting Method

In general, most of the study of fluid mechanic problems is modelled in terms of linear or non-linear differential equations. In order to overcome the problems, a shooting method was introduced and it is one of the common techniques for solving boundary value problem. This method is easier to apply and the result obtained is reliable compared to other methods, Morrison et al. (1962), Ha (2001) and Gireesha et

al. (2015). The Shooting method takes advantage of the speed and adaptivity of initial value problems. However, it is not as robust as collocation or finite difference methods. For example, even though the boundary value problem may look as quite well posed and stable, the growing modes of initial value problems may be inherently unstable and may be unnoticeable. Therefore, the comparison of work is necessary. According to the literature review, it can be seen that the Shooting method has been used frequently to determine the numerical solutions for Newtonian or non-Newtonian flow problems, especially in its application in the science and engineering field to solve differential equations. Thus, in this study, trajectories were 'shot' out in different directions until a trajectory with an appropriate boundary value would be obtained. Specifically, the Shooting method is a method to overcome a boundary value problem by reducing it to the initial value problem's solution.

In this thesis, the Shooting method is chosen as the method to determine the numerical solution which was discussed in Section 2.4. The solutions are written in the form of partial differential equation which is then transformed to ordinary differential equation. Besides, the solutions do not calculate the complicated integrals either analytically or numerically. Furthermore, these solutions are obtained by Shooting method that satisfies all the imposed boundary and initial conditions as well as governing equations.

1.2.6   Boundary Layer Theory

The concept of boundary layer was first coined by Ludwig Prandtl (Schlichting, 1979) and it is important due to the effects of viscosity where the layer of the fluid in the immediate vicinity of a bounding surface, especially in the study of physics and fluid mechanics. Prandtl had showed that fluid flow past a body can be divided into two main parts after performing the experiments in combination with together the theoretical considerations. The major part is defined as inviscid since it concerns a free stream of fluid which is far from the surface of an object. On the other hand, the minor is called the boundary layer. Since this part is a thin layer adjacent to the object surface in which the effects of viscosity are felt, the friction effects is significant and cannot be ignored (Burmeister, 1993; Acheson, 1990).

Simultaneously, there are two types of layer which can be found in the boundary layer, namely the velocity boundary layer and thermal boundary layer (Ozisik, 1985). For better understanding, let us consider a fluid past over a plate sheet as shown in Figure 1.1. The interaction between the fluid and the surface of the plate sheet will produce a region which is known as velocity boundary layer. The y-component velocity u rises from zero at the surface with no slip condition to an asymptotic value U_∞. Additionally, the thickness of velocity boundary layer δ_h is characterized by the velocity gradient and shear stress. Further, there is a formation of a region called the thermal boundary layer as a result of the changes of temperature between the fluid and the surface area. The thickness of the layer is represented as δ_T and the temperature changes from the surface value T_s to T_∞ at $y = 0$ as the outer flow. Thermal boundary layer is characterized by the temperature gradient and the rate of heat transfer.
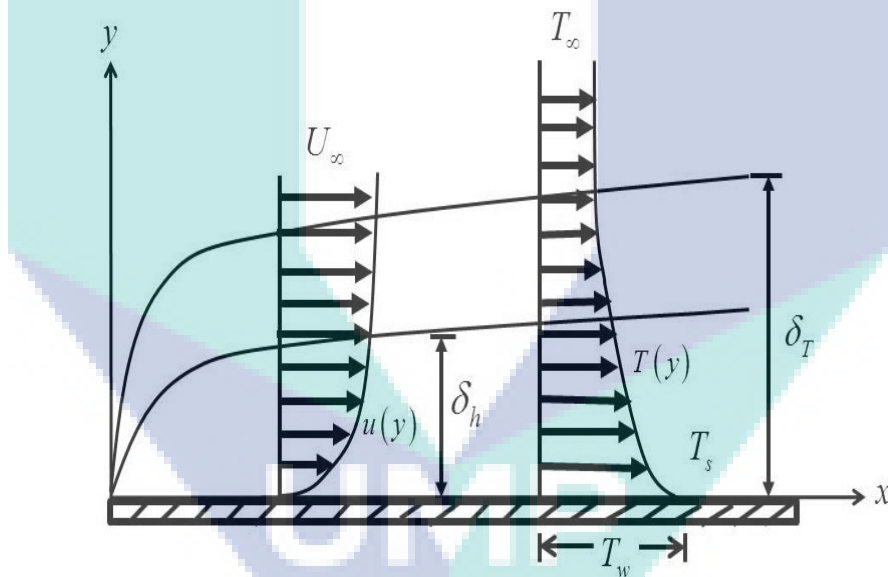
Figure 1.2 Formation of the boundary layer.

(Incropera et al., 2006; Kreith et al., 2010).

The application of the theory of boundary layer is common especially when it involves the problem of fluid flow and heat transfer. One of the reasons is that equations of boundary layer are parabolic and it is easier to solve compared to other forms like elliptic or hyperbolic Navier-Stokes equations. However, the boundary layer equations are valid only up to the separation point. The relevant work involving the

boundary layer theory is found in a study by Bejan, 2013; Cebeci and Bradshaw, 1988 and Ahmad, 2009.

1.3   Problem Statement

In general, there exist many published journals regarding non-Newtonian fluids. However, numerical solutions with Newtonian heating by the Shooting method are rarely available in literature. This is because treating numerically the mathematical models of Newtonian heating is more complicated and consumes much of time in shooting the acceptable or appropriate value in a certain range. Even though numerical solutions are as accurate as analytical solutions, numerical solutions are easier to perform prediction as comparing the finding results are more feasible. Furthermore, the accuracy standard for the Shooting method is reliable and believable. The major purpose of this thesis is to figure out the numerical solutions for the steady flow of different types of nanofluids under several conditions. Thus, this study will explain in detail the following problems.

(i)   How does the Casson nanofluid behave in the problem of several situations (involving thermal radiation, magnetohydrodynamics, porous medium) over a stretching sheet with Constant wall temperature (CWT) and Newtonian heating (NH)?

(ii)   How the Williamson nanofluid behaves in the problem of slip condition over a stretching sheet?

(iii)   How does the Williamson nanofluid behave in the problem of several situations (involving thermal radiation, magnetohydrodynamics, porous medium) past over a stretching sheet with Constant wall temperature (CWT) and Newtonian heating (NH)?

1.4   Scope and Objective of Research

In this study, the two dimensional of steady and incompressible fluids flow over a stretching sheet were studied. The objectives of the present study are to analyze mathematical model of non-Newtonian nanofluid with various effects and different boundary conditions. This study can be divided into three problems:

(i) Thermal radiation effect on MHD and heat transfer flow of Casson nanofluid model in the presence of porous medium by Constant wall temperature and Newtonian heating.

(ii) Slip conditions effects on flow and heat transfer of Williamsom nanofluid over stretching sheet.

(iii) Thermal radiation effect on MHD and heat transfer flow of Williamson nanofluid model by Constant wall temperature and Newtonian heating.

1.5   Research Methodology

The physical problems of the objectives are expressed in mathematical formulation and then they are modelled using the fundamental equations of fluid dynamics. The derived parameters of each problem in the governing equations include continuity, momentum, energy and concentrations equations, as well as imposed initial values and boundary conditions. Moreover, the Boussinesq and Rosseland approximations are used in the development of some parameters governing equations. A set of appropriate non-dimensional variables for every problem is then introduced and transformed into non-dimensional form. Then, the Shooting method is carried out with velocity, temperature and concentration stated as numerical solutions. Skin friction coefficient, local Nusselt number and Sherwood number are evaluated as well.

For better understanding of each problem, the exact solutions are computed numerically and the result for all the parameters is shown graphically. The Maple-13 software is used to plot the variable profiles and indicated in tabular form. All the numerical results through the Shooting method are compared with existing solutions available in the literature in order to verify the accuracy of the present analysis. The effects of the pertinent flow parameters are noted in the variable profiles in terms of velocity, temperature, nanoparticle fraction, temperature wall gradient, skin friction coefficient and Sherwood number.

1.6   Significance of the Study

Nowadays, non-Newtonian fluid is part of important subjects in science and technology. With the enhancement of nano-technology, nanofluids improve the thermal conductivity in flow, which is extremely beneficial to the medical and engineering sectors.

In the engineering and technology sector, the convective heat transfer of nanofluids has great impact in the heating and cooling system, power generation and chemical processes. Due to the excellent thermal conductivity, heat energy can be effectively transferred in the nanofluid systems. As a result, nanofluids can be potentially applied in various industries, including heavy industry, manufacturing industry, nuclear energy harvesting and others, for heating or cooling purposes. The studies of nanofluid application are reported by Riehl and dos Santos (2012), Verma and Tiwari (2015), Shama et al. (2015), Wu and Zhao (2013) and Gupta et al. (2012).

Medically, nanofluids could improve the adsorption or transportation of drugs in a patient based on its advanced mass transfer property. In cancer therapeutics, nano-sized iron particles can be transported to the tumour tissues without damaging nearby nerve tissues or organs in the patient's body. The side effects from the drugs can be further reduced with the assistance of magnetic field. Hence, magnetic effect is also one of the studied parameters in the current study.

To develop a better understanding of thermal radiation effect on MHD and heat transfer flow characteristics for Casson and Williamson nanofluids with Newtonian heating, this thesis explores the nanofluid flow behavior including the effects of the parameters such as radiation parameter, thermophoresis parameter, Lewis number, Prandtl number, etc. This helps in explaining and verifying the experimental results for future studies.

1.7   Literature Review

This topic provides a literature review on the problems outlined in the objectives respectively. Section 1.7.1 provides the literature regarding the effect of thermal radiation on MHD with heat and mass transfer flow in Casson nanofluid over a stretching sheet by Constant Wall Temperature (CWT) and Newtonian heating (NH). The literature for slip conditions on flow and heat transfer analysis of Williamson nanofluid past over a stretching sheet is presented in Section 1.7.2. Section 1.7.3 discusses about the literature for thermal radiation effect on MHD flow and heat transfer of Williamson nanofluid over a stretching sheet with Constant Wall Temperature (CWT) and Newtonian heating (NH).

1.7.1 Thermal Radiation and MHD on Flow and Heat Transfer in Casson Nanofluid

It is well known that convectional fluids such as water, ethylene glycol and engine oil used in many industrial processes are poor heat conductors due to their low thermal conductivities. To overcome this situation, Choi (1995) introduced the idea of nanofluids. Nanofluid is a new class of fluid created by scattering nano/micro-sized materials (nanoparticles, nanofibers, nanotubes, nanowires, nanorods and nanosheets) in conventional heat transfer fluids. The convective heat transfer flow over boundary layer of non-Newtonian fluids has been widely investigated in several applications of the engineering fields. Due to its higher complexity compared to Newtonian fluids, many of non-Newtonian fluid models were proposed to solve the problems. One of the models is Casson nanofluid. Casson (1995) first introduced this model to investigate the behaviour flow of pigment oil suspensions. In fact, Casson fluid is a plastic fluid and requires a higher shear stress (as long as the value is bigger than the yield stress) so that it can start the flow in the system. Nanofluids are believed to be able to significantly enhance thermal conductivity greatly. Thus, the combination of this model with nanofluid has attracted the attention from some researchers due to its unique charaterictics and functions and has the potential in certain industry application, good approximation for biological fluids and other materials. Amongst them, Buongiorno (2006) published a survey article on the convective transport in nanofluids. Ahmed and Pop (2010) examined mixed convection flow of nanofluid past a vertical plate embedded in a porous medium. Bachok et al. (2010) presented numerical solutions for boundary layer flow past a moving surface when nanofluid is flowing. Yacob et al. (2011) studied the boundary layer flow of a nanofluid over a stretching/shrinking sheet with convective boundary condition. Chamkha and Aly (2011) used implicit finite difference method and analyzed the effect of heat generation or absorption on the steady free convection flow of a nanofluid over permeable vertical plate with suction or injection. Noghrehabadi et al. (2012) studied partial slip effects on the boundary layer flow of a nanofluid past a stretching sheet with constant wall temperature. Likewise, Rana and Bhargava (2012) studied the same problem by considering flow over a nonlinearly stretching sheet. Anwar et al. (2012) also investigated nanofluids flow over a nonlinearly stretching sheet. Meanwhile, Mahdy (2012) studied mixed convection flow together with heat transfer in nanofluids due to stretching sheet. Qasim et al.

(2013), studied heat and mass transfer phenomenon in nanofluids with convective boundary conditions whereas Matin and Pop (2013) investigated force convection flow of a nanofluid through a porous channel with chemical reaction. Later, Loganathan and Vimala (2014) obtained numerical solution of unsteady nanofluids flow that lies over vertical flat plate with accretion or ablation at the leading edge.

Recently, Ganga et al. (2016) studied the thermal radiation effects on hydromagnetic flow of nanofluids and found the analytic solutions by using homotopy analysis and numerical method by the fourth order Runge-Kutta method. The physical properties of fluids could be controlled by varying the application of magnetic field in medical treatment like cancer therapy. Hussain et al. (2015) had studied the problem on magnetohydrodynanmics (MHD) boundary layer flow of Casson nanofluid with convective and viscous dissipation conditions. He concluded that the greater the value of Casson parameter, the lower the temperature and concentration of nanoparticles. The result was in good agreement with Khalid el at. (2015) since they also had examined the problem of MHD effects and convective heat transfer flow on Casson nanofluid with the presence of porous medium. The MHD effect on three dimensional Casson fluid flow porously over a stretching sheet were investigated by Mahanta and Shaw (2015). By using the Spectral Relaxation Method, they concluded that Casson fluid parameter and porosity parameter reduce the velocity profiles. Meanwhile, Nadeem et al. (2014) investigated the combined effects of magnetic field and partial slip on an obliquely striking Casson fluid over a stretching plate. The magnetic parameter has opposite influence on skin friction components and causes the tangential velocity profiles to drop. The heat transfer rate is enhanced while the induced magnetic field increased as indicated by the investigation carried out by Raju et al. (2016) after they solved the problem on homogeneous–heterogeneous reactions and the effects of induced magnetic field on stagnation flow in Casson fluid. Hayat et al. (2016) also conducted an investigation on magnetic field with mixed convection flow of Casson nanofluid. Another study was performed by Hamad et al. (2011) who investigated the effects of magnetic field on heat transfer flow of a nanofluids laid over a vertical semi-infinite flat plate. Likewise, the same problem extended by Chamkha and Aly (2011) by including heat absorption and generation effects. Meanwhile, Ellahi (2013) found analytical solution for MHD flow of non-Newtonian nanofluids inside a pipe with temperature dependent viscosity. Similarly, Qasim et al. (2014) used water as conventional base

fluid with magnetite (Fe_3O_4) nanoparticles and studied MHD heat transfer in ferrofluid over a stretched cylinder with given heat flux and slip condition. Sheikholeslami et al. (2014) studied MHD heat transfer with thermal radiation inside an enclosure of semi annulus. Sheikholeslami et al. (2015) and Sheikholeslami et al. (2016) considered the magnetic fields effects on nanofluids flow with and without considering the thermal radiation in a semi annulus. Hussanan et al. (2016) examined by unsteady MHD flow and heat transfer in some nanofluids over an accelerated vertical plate in a porous medium. Few other attempts made in this direction are contributed by Krishna et al. (2014); Haq et al. (2014); Ibrahim and Makinde (2015) and Ramzan (2015).

There are many process involving heat and mass transfer as long as there is temperature difference between two objects. The study of heat and mass transfer is important because of its extensive application in engineering fields such as chemical, electrical, and mechanical, among others. One of the factors to enhance the rate of heat transfer is the amount of nanoparticles in fluids. Utilization of nanofluids as a coolant in radiator or cooling mechanism is more effective compared to using base fluids since the thermal conductivity of metal nanoparticles (Al_2O_3, TiO_2) are higher than that of base fluids like water, engine oil, etc. (Hayat et al. 2016). Radiation is one of the methods to transfer heat energy. Unlike conduction and convection, radiation independently transfers heat energy and carries electromagnetic wave. Raju et al. (2016) analyzed the problem of MHD effect with thermal radiation on Casson fluid over a stretching sheet who then concluded that raising the value of heat source parameter also enhances heat transfer rate and Casson fluid performs better in transferring heat than Newtonian fluid. Hayat et al. (2015) who examined the effect of thermal radiation on mixed convection flow of Casson nanofluid over a stretching plate found that the thickness of boundary layer increases with the increase the thermal radiation parameter, internal heat generation and heat transfer Biot number. Ibrahim and Makinde (2015) had examined the effect of slip and convective boundary condition on MHD stagnation point flow and heat transfer in Casson nanofluid over a stretching sheet. Haq et al. (2014, a), Haq et al. (2014, b) studied the problem of MHD effects and heat transfer flow on Casson nanofluid and carbon nanotube (CNT) past over a permeable shrinking sheet respectively. All of them totally agreed that Casson fluid has higher heat transfer rate and skin friction compared to water based fluids.

An exponentially stretching sheet or cylinder have gained massive attention from many researchers due to its applications in flow meter design, piping, polymer extrusion, fibre technology, casting systems and many others. All the above research however, focus on Newtonian fluid (such as water, ethylene glycol and engine oil) containing nanoparticles. Keeping this view, Malik et al. (2014) studied the boundary layer flow of Casson nanofluids over a vertical exponentially stretching cylinder. Haq et al. (2014) examined the effects of convective heat transfer on two dimensional MHD flow of Casson nanofluid over an exponentially permeable shrinking sheet. Nadeem et al. (2014) extended the same problem for three dimensional flows by taking linearly stretching sheet instead of an exponentially shrinking sheet. Heat transfer analysis in a Williamson nanofluid over a stretching sheet was studied by Nadeem and Hussain (2014). Hayat et al. (2015) studied heat transfer in a Jeffrey fluid containing nanoparticles over a stretching cylinder. Recently, Nadeem et al. (2014) discussed the problem of MHD three-dimensional boundary layer flow of Casson nanofluid past a linearly stretching sheet with convective boundary condition. They mentioned that the stretching parameter reduces the velocity profile in both directions as well as decreases the behaviour for temperature and nanoparticle fraction profiles. Sarojamma and Vendabai (2015) conducted an analysis of magnetic field and heat transfer effects on the steady boundary layer flow on Casson nanofluid over an exponentially stretching vertical cylinder. In the meantime, Abolbashari et al. (2015) used the Optimal Homotopy Analysis Method (OHAM) to solve the problem of entrophy generation for Casson nanofluid over a stretching sheet. Likewise, Qing et al. (2016) studied similar problem with Casson nanofluid flow over a stretching/shrinking sheet by Successive linearization method (SLM). Other related problems with Casson nanofluid can be referred to Akbar and Khan (2015), Mustafa and Khan (2015), Raju and Sandeep (2016), Malik et al. (2016) and Kumaran and Sandeep (2017).

Casson fluid model has been categorised as rheological model for many fluids like blood and chocolate. Casson fluid exhibits a yield stress and behaves as a solid if the shear stress is less than the yield stress. It deforms to liquid when shear stress is greater than yield stress and vice versa. As a continuous work, the aim of the present study is to determine the thermal radiation effects on MHD flow with heat and mass transfer in Casson nanofluid over a stretching sheet with Newtonian heating (NH).

1.7.2 Slip Conditions on Flow and Heat Transfer Analysis of Williamson Nanofluid

Nanofluid has been discovered and discussed by many researchers due to its unique properties and well known as the suspended colloidal liquid with nano-size metallic or non-metallic particles. Generally, nanofluids enhance thermal conductivity whether in cooling down or heating up compared to other normal base fluids like water, kerosene and the like. Some researchers like Xuan and Roetzel (2000), Turkyilmazoglu (2012), Kakac and Pramuanjaroenkij (2009) and Roy et al. (2004) who studied the heat transfer flow with nanofluids, stated that even in the presence of low concentration of nanoparticles, the suspensions can enhance thermal conductivity up to 20%. The enhancement of thermal conductivity mainly depends on some factors like the material of particles, shape/size of particles, temperature of the fluid material, and so on. The purpose of heat transfer coefficient is to determine the factor in forced convection cooling or heating application, like the heat exchange process involved in electrical engine systems. Moreover, heat transfer coefficient proposed in correlation with the stagnation point of some parameter such as Nusselt number, Reynolds number, Prandlt number and nozzle aspect ratio, and heat source spacing.

There are many models of non-Newtonian fluids that are grouped property wise like polar fluids, visco-inelastic or elastic fluids and micro structure fluids. In the work of Krishnamurthy et al. (2016), Williamson nanofluid is categorized as visco-inelastic fluids. Blasius (1950) initially studied the problem of velocity boundary layer on a flat plat followed by Sakiadis (1961) who investigated the theoretical aspect of approximate and exact method for performance of boundary layer flow through a flat surface. Next, Ramesh et al. (2015) had studied the convective boundary condition on Blasius and Sakiadis flows with Williamson fluid. Prior to that, Khan and Khan (2014) carried out the investigation on boundary layer flows of Williamson fluid by using homotopy analysis method (HAM). He found that the thickness of boundary layer decreases as Williamson parameter increases. Later, Nadeem and Hussain (2016) analyzed the problem on Williamson nanofluid with MHD flow over a heated surface and found out that the thermal conductivity of Williamson fluid is lower than the MHD Williamson nanofluid.

Thermal energy occurs when there is a temperature difference between objects. Heat transfers in non-Newtonian fluids have become common and important in some fields such as reactor cooling systems, electronic packing and so on. Kurtcebe and Erim (2002) studied the problem of turbine cooling application with heat transfer in non-Newtonian visco-inelastic fluid and concluded that the upper limit of visco-inelastic parameter depends to the Reynolds number. The heat transfer analysis flow in nanofluids over a stretching sheet is important and crucial for the optimum quality of the final product especially in polymer extrusion production. Ibrahim and Shankar (2013) studied the heat transfer and MHD boundary layer flow in nanofluid past over a stretching sheet. Krishnamurthy et al. (2016) investigated the effect of chemical reaction on melting heat transfer and MHD boundary layer flow of Williamson nanofluid. Meanwhile, the flow features and convective heat transfer of Cu-water nanofluids were investigated by Xuan and Li (2003). According to their findings, the heat transfer feature increases as the volume fraction of nanoparticles increases. With the same Reynolds number, the suspended nanoparticles show higher heat transfer coefficient and remarkably enhance heat transfer process compared to the base fluid. Heris et al. (2006) carried out the experiment on convective heat transfer laminar flow over oxide nanofluid with boundary condition of constant wall temperature. They concluded that there are several factors to enhance the heat transfer for nanofluid, as well as increase the chaotic movements of nanoparticles, thermal conductivity, interactions and fluctuations.

Slip condition is considered since the presence of nanoparticles causes the interface of slip velocity between fluid and solid boundary. Yang (2009) had presented the viscous flow over a solid surface with slip boundary condition. The interfacial interaction between fluid and solid is reflected by slip condition contributed by the interaction of intermolecular and roughness of wall surface. Noghrehabadi et al. (2012) studied the problem of the partial slip boundary condition effect on nanofluids with prescribed wall temperature over a stretching sheet. The Nusselt and Sherwood number decreases as the velocity slip parameter increases. Malvandi et al. (2014) conducted an examination on the slip effects of nanofluids in unsteady stagnation point over a stretching sheet. In their work, an increase in the values of slip parameter caused the values of skin coefficient to drop. The slip and no slip conditions on the laminar nanofluids by forced convection were numerically studied by Raisi et al. (2011). They

found out that only higher Reynolds number affects the rate of heat transfer as slip velocity coefficient increases. Amanulla et al. (2017) had studied on MHD Williamsom nanofluid from an isothermal sphere due to the thermal and momentum slip effects.

1.7.3 MHD Flow and Heat Transfer Analysis of Williamson Nanofluid with Thermal Radiation

Recently, the investigation on different model of nanofluids has attracted the attention of many researchers. The term nanofluid, refers to fluid with suspended nanoparticles. It is a type of fluid that consists of tiny particles, hence providing a very large surface area that favours the transferring of heat energy. The pioneer works of Choi attracted the attention of researchers, eventually leading to wide investigation in nanofluids with other factors like heat and mass transfer, passing a stretching sheet or vertical plate, radiation and thermal effect and magnetic field (Venkateswarlu and Narayana, 2015; Reddy, 2014; Sreenivasulu et al. 2015). Compared to particles of others sizes, nanoparticles have larger surface area and have great potential in heat enhancement due to the smaller particles suspended in the fluids (Xuan and Li, 2000). Some researchers had discovered that nanofluid has about 40% higher thermal conductivity compared to base fluid. This characteristic is very useful in some industry application such as in cooling and solidifications system (Nadeem & Hussain, 2014). Meanwhile, Burgiono (2006) presented the three models using different convective transport of nanofluid and with the boundary condition as the constant wall temperature. In many industry processes, heat transfer plays an important role as the transferred input energy or the removed output energy in the process. Yang et al. (2005) had uncovered the properties of convective heat transfer of nanoparticle in laminar flow. The results showed that the nanoparticle increases the heat transfer coefficient of the fluid system in laminar. Another researcher, Trisakri and Wongwises (2007) explained the reasons how suspended nanoparticles can enhance the heat transfer of conventional fluids and provided a guide line for future research. Wen et al. (2009) performed a research on heat transfer applications of nanofluids and identified the limiting factors for further development.

Williamson nanofluid, one of the non-Newtonian heating fluids, is a viscoelastic shear thinning fluid. It is potentially applied in biological engineering to estimate the occurrence of mass and heat transfer in the vessels such as diffusion of nutrients in

blood, hemodialysis and others (Kothandapani and Prakash, 2015). It become famous after Williamson (1929) made an investigation on the medium for pseudoplastic materials flow. Nadeem and Hussain (2014) analyzed the two-dimensional flow of heat transfer on Williamson nanofluids. They found that Lewis number only appears in volume fraction equation when the velocity transformation is dependent on thermal diffusivity; otherwise, Schmidt number will appear, and vice versa. The homotopy analysis method (HAM) was used in their research to obtain the solutions. Prasannakumara et al. (2016) presented the chemical reaction effects on Williamson nanofluids slipped over a stretching sheet in the presence of embedded porous medium. In their results, the skin coefficient is higher in the presence of velocity, thermal and solutal slip for Williamson parameter. The work is extended by Krishnamurthy et al. (2016) by considering the factor of boundary layer flow of MHD and melting heat transfer. A study on the effect of thermal radiation parameter and magnetic field on the peristaltic motion of Williamson nanofluids in a tapered asymmetric channel was conducted by Kothandapani and Prakash (2015). Meanwhile, Bhatti and Rashidi (2016) studied the effect of the combined effects of thermo-diffusion and thermal radiation on Williamson nanofluid over a porous stretching sheet. Ramesh et al. (2015) studied the convective boundary condition on Sakiadis and Blasius flows of Williamson fluid while Akbar et al. (2015) investigated the peristaltic flow of a Williamson nanofluid in an asymmetric channel.

As the fluid is conducted by fluid dynamics, the fluid motion induces currents, eventually producing Lorentz body force on the fluid. This phenomenon of electrically conducting fluids is called Magnetohydrodynamics (MHD). The effects of thermal radiation and magnetic field have given significant impact on nanofluids flow. And this issue has been discovered by Sheikholeslami et al. (2015) who presented the effect of thermal radiation on MHD nanofluid flow and heat transfer by means of two phase model. Recently, an analysis to inspect the numerical investigation of MHD flow of Williamson fluid model over a sheet with variable thickness was performed by Salahuddin et al. (2016). Prior to that, Narayana et al. (2015) had examined the effect of the nanoparticles on MHD boundary layer flow over a stretching surface with the effect of viscous dissipation. In the meantime, Hayat et al. (2015) conducted an investigation on MHD steady flow of viscous Copper water nanofluids caused by a rotating disk. The use of electrically conducting fluids under the influence of magnetic fields in various

industries has led to a renewed interest in investigating hydromagnetic flow and heat transfer in different geometries. Kumari et al. (2012) fully developed free convective flow of a Williamson fluid in a vertical channel under the effect of a magnetic field. Sparrow and Cess (1961) studied the effect of magnetic field on free convection heat transfer. In their study, there is a moderate effect (10-15%) on heat transfer compared to other results without MHD. Although the problem with correlations to MHD would be studied by many different researchers later, Hossain and Pop (1996) formulated the MHD boundary layer flow and heat transfer on a continuous moving wavy surface. The flow and heat transfer characteristics are substantially altered by some specific values of magnetic parameter. Azizian et al. (2014) investigated the flow of magnetite nanofluids with the presence of magnetic field on laminar convective heat transfer. In their research, the magnetite nanofluids can be increased significantly (up to 300%) when a magnetic field was applied. When larger magnetic flux gradient is applied, the larger local heat transfer coefficient enhancement occurs. There are many fluid engineering processes involving flow over a continuously stretching or shrinking surface and it is very important in such processes as polymer extrusion, plastic films and wires drawing, production of glass fiber and paper, liquid films in condensation process and many others (Turkyilmazoglu, 2012). He carried out the exact analytical solutions for heat and mass transfer of MHD slip flow in water-based nanofluids containing Cu, Ag, CuO, Al_2O_3 and TiO_2 and he found the results in an excellent agreement with those available in the literature. Rashidi et al. (2014) investigated the buoyancy effect on MHD flow of nanofluid over a stretching sheet in the presence of thermal radiation while Khan et al. (2012) studied the unsteady free convection boundary-layer flow of a nanofluid along a stretching sheet with thermal radiation in the presence of magnetic field. Reddy et al. (2017) had studied the characteristics of MHD and heat transfer flow of Williamson nanofluid with variable thickness and variable conductivity. They have noticed that the rate of cooling is much faster for the coolant material having small thermal conductivity parameter.

Thermal radiation still exists even though there is a small flow of convection heat transfer coefficient. Thermal radiation is significant in controlling heat transfer process like in polymer processing industry. Sheikholeslami et al. (2015) studied the effect of thermal radiation on MHD nanofluid flow and heat transfer between two horizontal rotating plates. The result showed that concentration of boundary layer

thickness decreases with the increase of radiation parameter. Further, a study by Bhatti and Rashidi (2016) examined the combined effects of thermo-diffusion and thermal radiation on Williamson nanofluid over a porous stretching sheet. They concluded that the large values of thermal radiation parameter and thermophoresis parameter enhance the temperature profile. Haq et al. (2015) considered the effects of velocity and thermal slip with thermal radiation on MHD stagnation point flow of nanofluid over a stretching sheet. In the present work, the constant wall temperature (CWT) was taken into account. There are many industrial heat exchanger applications that include the condition of CWT, such as the condensation or evaporation of fluid on the outer surface of conduits. The assumption of CWT can be justified if the heat transfer coefficient in the inner surface is lower than in the outer surface (Mohamad, 2003). Renksizbulut et al. (2006) also considered the condition of CWT in slip-flow and heat transfer in rectangular microchannels. The constant-wall-temperature convective heat-transfer characteristics of a gaseous flow model in two-dimensional micro and nano-channels were hydrodynamically and thermally investigated by Hadjiconstantinou and Simek (2002).

Stretching sheet happens when the velocity at the boundary is far from a fixed point. Also, it is widely applied and important in some engineering processes such as polymer extrusion, glass fiber production, manufacturing of foods and paper. The rate of heat transfer for stretching sheet is crucial for the final quality of a product (Sarif et al. 2013). Gorla and Gireesha (2016) studied the Dual solutions for stagnation point flow and convective heat transfer of a Williamson nanofluid past a stretching or shrinking sheet while Nadeem et al. (2013) examined the two dimensional flow of Williamson fluid model over a stretching sheet. Meanwhile, Salleh et al. (2010) studied the steady boundary layer flow and heat transfer over a stretching sheet with Newtonian heating. As a continuation, in the present study, the objective of studying the thermal radiation and magnetic effect on Williamson nanofluids flow and heat transfer analysis over a stretching sheet was proposed. The analysis for constant wall temperature (CWT) and Newtonian heating (NH) is included in this paper for comparison purposes. The governing nonlinear equations are reduced into ordinary differential equations using the similarity transformation and they are then solved numerically using the Shooting method.

1.8   Thesis Outline

There are six chapters in this thesis. The outline of this thesis is as follows:

Chapter 1 is preliminary with general introduction of the background, model of non-Newtonian nanofluids, boundary layer, problem statement, objective and scope of studies, significance of the research study and literature review of related published work and divided into three parts corresponding to each problem.

Meanwhile, Chapter 2 discusses the governing equations and methodology. The numerical method of the shooting technique is carried out to solve the governing ordinary differential equations.

In Chapter 3 of this thesis, the problem of thermal radiation effect on MHD of Casson nanofluid and heat transfer over a stretching sheet is explained. Two boundary conditions examined, namely, constant wall temperature (CWT) and Newtonian heating (NH), are described. Firstly, the mathematical formulation of the governing equations in terms of continuity, momentum, energy and concentration is presented. Then, an explanation of how the mathematical formulation was subjected the equations to the corresponding initial and boundary conditions, is provided. The way that problem was written in dimensionless form and then solved by the Shooting method to obtain numerical results for the velocity, temperature and concentration profiles, is also shown in this chapter. These solutions were found to have satisfied all imposed initial and boundary conditions. Subsequently, a comparison was made with published works in the literature to determine the validity of the present solutions. In this chapter, numerical results for the velocity, temperature and concentration profiles for various parameters are graphically presented accordingly. In addition to that, the skin friction coefficient, local Nusselt number and Sherwood number are also presented in tabular forms and discussed. In the next chapter, the Williamson nanofluid is considered.

Chapter 4 presents the slip conditions on flow and heat transfer analysis of Williamson nanofluid over a stretching sheet. Presentation of the results begins with a mathematical formulation including the derivation of momentum equation with velocity and thermal slip parameter, energy and concentration equations. Through similar transformations, this chapter illustrates how the governing equations were then

transformed into non-linear ordinary equations. Then, these solutions are presented graphically and the parameters are discussed.

In chapter 5, the examination of the effect of thermal radiation on heat transfer in MHD flow of Williamson nanofluid over a plate embedded in a porous medium is discussed. There are two cases considered, CWT and NH. Numerical solutions for the velocity, temperature and concentration profiles obtained using the same method applied as described in the previous chapter and graphically. The solutions were found to have satisfied all imposed initial and boundary conditions as well as asymptotic at all times. The skin friction coefficient, local Nusselt number and Sherwood number are obtained are also given.

Finally, Chapter 6 is the summary of this thesis with the conclusions and possible recommendations for future study included. References, appedices and publications are also provided.

CHAPTER 2

PROBLEM FORMULATION AND NUMERICAL METHOD

2.1   Introduction

This chapter and the following chapters will discuss how mathematical formulation model obtain the numerical solutions. Initially, the derivations of the problem in the form of partial differential equations (PDEs) are reduced to ordinary differential equations (ODEs). Then, the resulting system of ODEs is solved through the Shooting method and through the Maple software.

In this work, there were two models of nanofluids considered, namely, the Casson and Williamson nanofluids. Some of the parameters such as radiation parameter, magnetic parameter, and Prandtl number were also included into the governing equations respectively. The physical quantities of skin friction coefficient, local Nusselt number and Sherwood number were also studied thoroughly. Besides that, three different boundary conditions were studied: constant wall temperature (CWT), Newtonian heating (NH) and slip conditions. In this chapter, only the mathematical formulation of Casson nanofluid will be described and explained. However, not all problem formulations are discussed in this chapter but will be highlighted in the following chapters.

2.2   Governing Equations

In this analysis, a steady two dimensional boundary layer flow of a non-Newtonian Casson nanofluid over a stretching surface embedded in a porous medium was considered. The sheet stretched along x-axis with a velocity $U_w = ax$ at $y = 0$, where $a > 0$ was a constant. A constant magnetic field was applied normal to the sheet, whereas induced magnetic field was neglected by assuming low magnetic Reynolds

number (see Figure 3.1). Further, the temperature T constant wall temperature T_w near the sheet and ambient temperature T_∞ was considered. No gravity effect considered because it was assumed that the flow occur on horizontal stretching plate, thus $g = 0$.

The thermal diffusivity of nanofluid was given by α_m where it was defined as $\dfrac{k}{\left(\rho C_P\right)_f}$.
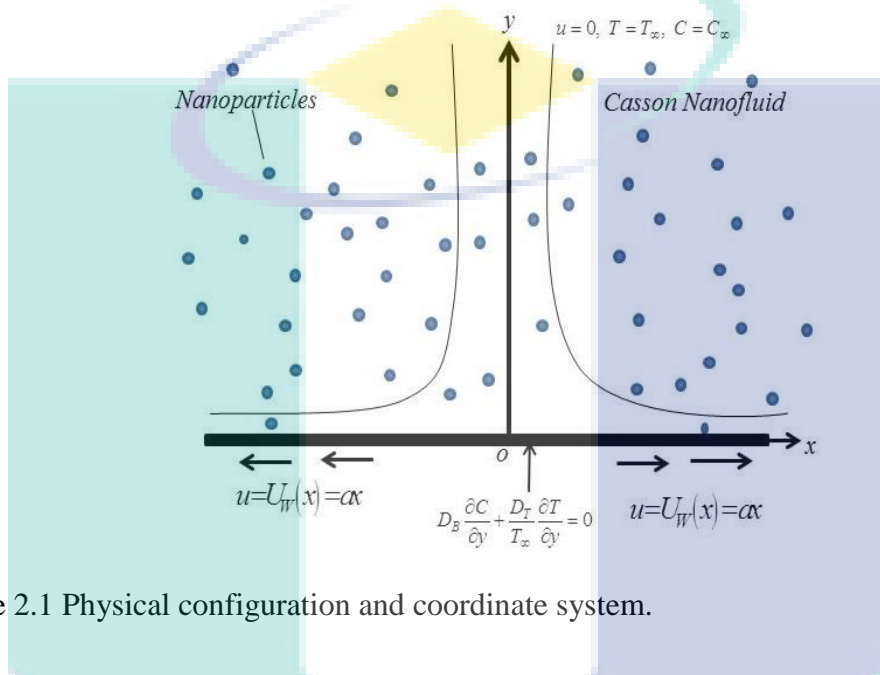
Figure 2.1 Physical configuration and coordinate system.

According to Mustafa and Junaid (2015), the rheological equation of state for isotropic and incompressible flow of Casson nanofluid is given as follow:

$$\tau_{ij} = 2\left(\mu_B + \frac{P_y}{\sqrt{2\pi}} \right)e_{ij}, \ \pi > \pi_c$$

$$2\left(\mu_B + \frac{P_y}{\sqrt{2\pi_c}} \right)e_{ij}, \ \pi < \pi_c \tag{2.1}$$

where μ_B is the plastic dynamic viscosity of the non-Newtonian fluid, P_y is the yield stream of fluid, π is the product of the component of deformation rate and itself, namely, $\pi = e_{ij}e_{ij}$, e_{ij} is the (i, j) component of the deformation rate, and π_c is a critical value of π based on non-Newtonian model. Using the Boussineq approximation, the boundary layer flow of a Casson nanofluid was governed as follows:

Continuity equation:

$$\frac{\partial u}{\partial x} + \frac{\partial v}{\partial y} = 0 \qquad\qquad 2.2$$

Momentum equation:

$$u\frac{\partial u}{\partial x} + v\frac{\partial u}{\partial y} = v\left(1+\frac{1}{\beta}\right)\frac{\partial^2 u}{\partial y^2} - \frac{\sigma B_o^2}{\rho}u - \left(1+\frac{1}{\beta}\right)\frac{v}{k_1}u, \qquad 2.3$$

Energy equation:

$$u\frac{\partial T}{\partial x} + v\frac{\partial T}{\partial y} = \alpha_m\frac{\partial^2 T}{\partial y^2} + \tau\left[D_B\frac{\partial C}{\partial y}\frac{\partial T}{\partial y} + \frac{D_T}{T_\infty}\left(\frac{\partial T}{\partial y}\right)^2\right] - \frac{1}{(\rho C_P)_f}\frac{\partial q_r}{\partial y}, \qquad 2.4$$

Concentration equation:

$$u\frac{\partial C}{\partial x} + v\frac{\partial C}{\partial y} = D_B\frac{\partial^2 C}{\partial y^2} + \frac{D_T}{T_\infty}\frac{\partial^2 T}{\partial y^2}. \qquad 2.5$$

subject to boundary conditions with Constant wall temperature (CWT) and Newtonian heating (NH),

$$u = U_W(x) = ax,\ v = 0,\ T = T_w\ \text{(CWT) or } \frac{\partial T}{\partial y} = -h_s T\ \text{(NH), at } y = 0,$$
$$u \to 0,\ v \to 0,\ T \to T_\infty,\ C \to C_\infty\ \text{as } y \to \infty. \qquad 2.6$$

2.3 Similarities Transformations

Firstly, the PDEs must be reduced in terms of ODEs. The reason is that several independent variables such as x and y would be complicated to solve. However, through similarity transformation, the simplification of mathematical formulation would be easily achievable. For the sake of this purpose, the stream function $\psi(x,y)$ is defined as

$$u = \frac{\partial \psi}{\partial y},\ v = -\frac{\partial \psi}{\partial x} \qquad\qquad 2.7$$

Accoring to Nadeem et al. (2014), the velocities of u and v for the linear problem along x and y directions, respectively, was given as

$$\psi = (av)^{\frac{1}{2}} xf(\eta),\ \eta = \left(\frac{a}{v}\right)^{\frac{1}{2}} y \qquad\qquad 2.8$$

Besides, Pohlhausen (1921) defined the dimensionless variable for the temperature $\theta(\eta)$ and concentration $\phi(\eta)$ as

$$\theta(\eta) = \frac{T - T_\infty}{T_W - T_\infty} \qquad \qquad 2.9$$

$$T = \theta(\eta)(T_W - T_\infty) + T_\infty \qquad \qquad 2.10$$

$$\phi(\eta) = \frac{C - C_\infty}{C_W - C_\infty} \qquad \qquad 2.11$$

$$C = \phi(\eta)(C_W - C_\infty) + C_\infty \qquad \qquad 2.12$$

2.3.1 Continuity Equation

In solving the equation (2.1), $u\dfrac{\partial u}{\partial x}$ and $v\dfrac{\partial u}{\partial y}$ had to be differentiated, respectively.

$$
\begin{aligned}
u &= \frac{\partial \psi}{\partial y} \\
&= \frac{\partial \psi}{\partial \eta} \cdot \frac{\partial \eta}{\partial y} \\
&= \frac{\partial}{\partial \eta}\left((av)^{\frac{1}{2}} x f(\eta)\right) \frac{\partial}{\partial y}\left(\left(\frac{a}{v}\right)^{\frac{1}{2}} y\right) \qquad \qquad 2.13 \\
&= \left((av)^{\frac{1}{2}} x f'(\eta)\right)\left(\frac{a}{v}\right)^{\frac{1}{2}} \\
&= ax f'(\eta)
\end{aligned}
$$

$$
\begin{aligned}
\frac{\partial u}{\partial x} &= \frac{\partial}{\partial x}\left(ax f'(\eta)\right) \\
&= a f'(\eta)
\end{aligned} \qquad \qquad 2.14
$$

$$
\begin{aligned}
v &= -\frac{\partial \psi}{\partial x} \\
&= -\frac{\partial}{\partial x}\left((av)^{\frac{1}{2}} x f(\eta)\right) \qquad \qquad 2.15 \\
&= -(av)^{\frac{1}{2}} f(\eta)
\end{aligned}
$$

$$\frac{\partial v}{\partial y} = \frac{\partial v}{\partial \eta} \cdot \frac{\partial \eta}{\partial y}$$

$$= \frac{\partial}{\partial \eta}\left(-(av)^{\frac{1}{2}} f(\eta)\right) \frac{\partial}{\partial y}\left(\left(\frac{a}{v}\right)^{\frac{1}{2}} y\right)$$

2.16

$$= -(av)^{\frac{1}{2}} f'(\eta)\left(\frac{a}{v}\right)^{\frac{1}{2}}$$

$$= -af'(\eta)$$

Hence, the equations (2.15) and (2.17) were substituted into equation (2.1):

$$\frac{\partial u}{\partial x} + \frac{\partial v}{\partial y} = af'(\eta) + \left(-af'(\eta)\right)$$

$$= 0$$

From the above formulation, the continuity equation was proven.

2.3.2 Momentum Equation

To solve the equation (2.2), $u\dfrac{\partial u}{\partial x}$, $v\dfrac{\partial u}{\partial y}$ and $\dfrac{\partial^2 u}{\partial y^2}$ had to be differentiated, respectively.

$$u\frac{\partial u}{\partial x} = axf'(\eta).af'(\eta)$$

$$= a^2 xf'^2(\eta)$$

2.17

$$v\frac{\partial u}{\partial y} = v\frac{\partial u}{\partial \eta} \cdot \frac{\partial \eta}{\partial y}$$

$$= v\frac{\partial}{\partial \eta}\left(axf'(\eta)\right) \frac{\partial}{\partial y}\left(\left(\frac{a}{v}\right)^{\frac{1}{2}} y\right)$$

2.18

$$= -(av)^{\frac{1}{2}} f(\eta).axf''(\eta)\left(\frac{a}{v}\right)^{\frac{1}{2}}$$

$$= -a^2 xf(\eta) f''(\eta)$$

31

$$\frac{\partial^2 u}{\partial y^2} = \frac{\partial}{\partial \eta}\left(\frac{\partial u}{\partial y}\right) \cdot \frac{\partial \eta}{\partial y}$$

$$= \frac{\partial}{\partial \eta}\left(\frac{\partial u}{\partial \eta} \cdot \frac{\partial \eta}{\partial y}\right) \cdot \frac{\partial \eta}{\partial y}$$

$$= \frac{\partial}{\partial \eta}\left(\frac{\partial}{\partial \eta}\left(axf'(\eta)\right) \cdot \frac{\partial}{\partial y}\left(\sqrt{\frac{a}{v}}y\right)\right) \cdot \frac{\partial \eta}{\partial y}$$

2.19

$$= \frac{\partial}{\partial \eta}\left(axf''(\eta) \cdot \sqrt{\frac{a}{v}}\right) \cdot \sqrt{\frac{a}{v}}$$

$$= axf'''(\eta) \cdot \sqrt{\frac{a}{v}} \cdot \sqrt{\frac{a}{v}}$$

$$= \frac{a^2}{v}xf'''(\eta)$$

Thus, the equations (2.18), (2.19) and (2.20) were substituted into equation (2.2),

$$a^2 xf'^2(\eta) + \left(-a^2 xf(\eta)f''(\eta)\right) = v\left(1+\frac{1}{\beta}\right)\frac{a^2}{v}xf'''(\eta) - \frac{\sigma B_o^2}{\rho}\left(axf'(\eta)\right)$$

$$-\left(1+\frac{1}{\beta}\right)\frac{v}{k_1}\left(axf'(\eta)\right)$$

By dividing $a^2 x$, the following should be obtained:

$$f'^2(\eta) - f(\eta)f''(\eta) = \left(1+\frac{1}{\beta}\right)f'''(\eta) - \frac{\sigma B_o^2}{a\rho}f'(\eta) - \left(1+\frac{1}{\beta}\right)\frac{v}{ak_1}f'(\eta)$$

By rearranging the position and substitute $M = \frac{\sigma B_o^2}{a\rho}$ and $K = \frac{v}{ak_1}$, the following should

be obtained:

$$\left(1+\frac{1}{\beta}\right)f'''(\eta) + f(\eta)f''(\eta) - f'^2(\eta) - \left(\frac{\sigma B_o^2}{a\rho} + \left(1+\frac{1}{\beta}\right)\frac{v}{ak_1}\right)f'(\eta) = 0$$

$$\left(1+\frac{1}{\beta}\right)f'''(\eta) + f(\eta)f''(\eta) - f'^2(\eta) - \left(M + \left(1+\frac{1}{\beta}\right)K\right)f'(\eta) = 0$$

2.20

2.3.3 Energy Equation

For solving the equation (2.3), $\frac{\partial T}{\partial x}$, $\frac{\partial T}{\partial y}$, $\frac{\partial^2 T}{\partial y^2}$, $\frac{\partial C}{\partial y}$ and $\frac{\partial q_r}{\partial y}$ had to be differentiated, respectively.

32

$$\frac{\partial T}{\partial x} = \frac{\partial T}{\partial \eta} \frac{\partial \eta}{\partial x}$$

$$= \frac{\partial}{\partial \eta}\left(\theta(\eta)(T_W - T_\infty) + T_\infty\right)\frac{\partial}{\partial x}\left(\left(\frac{a}{v}\right)^{\frac{1}{2}} y\right) \qquad 2.21$$

$$= (T_W - T_\infty)\theta'(\eta).(0)$$

$$= 0$$

$$\frac{\partial T}{\partial y} = \frac{\partial T}{\partial \eta} \frac{\partial \eta}{\partial y}$$

$$= \frac{\partial}{\partial \eta}\left(\theta(\eta)(T_W - T_\infty) + T_\infty\right)\frac{\partial}{\partial y}\left(\left(\frac{a}{v}\right)^{\frac{1}{2}} y\right) \qquad 2.22$$

$$= (T_W - T_\infty)\theta'(\eta)\left(\frac{a}{v}\right)^{\frac{1}{2}}$$

$$= \sqrt{\frac{a}{v}}(T_W - T_\infty)\theta'(\eta)$$

$$\frac{\partial^2 T}{\partial y^2} = \frac{\partial}{\partial \eta}\left(\frac{\partial T}{\partial y}\right).\frac{\partial \eta}{\partial y}$$

$$= \frac{\partial}{\partial \eta}\left(\sqrt{\frac{a}{v}}(T_W - T_\infty)\theta'(\eta).\frac{\partial}{\partial y}\left(\left(\frac{a}{v}\right)^{\frac{1}{2}} y\right)\right) \qquad 2.23$$

$$= \sqrt{\frac{a}{v}}(T_W - T_\infty)\theta''(\eta)\sqrt{\frac{a}{v}}$$

$$= \frac{a}{v}(T_W - T_\infty)\theta''(\eta)$$

$$\frac{\partial C}{\partial y} = \frac{\partial C}{\partial \eta} \frac{\partial \eta}{\partial y}$$

$$= \frac{\partial}{\partial \eta}\left(\phi(\eta)(C_W - C_\infty) + C_\infty\right)\frac{\partial}{\partial y}\left(\left(\frac{a}{v}\right)^{\frac{1}{2}} y\right) \qquad 2.24$$

$$= (C_W - C_\infty)\phi'(\eta).\left(\frac{a}{v}\right)^{\frac{1}{2}}$$

$$= \sqrt{\frac{a}{v}}(C_W - C_\infty)\phi'(\eta)$$

33

According to Rosseland's approximation [Hussanan et al. (2013); Hussanan et al. (2015)], the radiative heat flux is simplified as

$$q_r = -\frac{4\sigma^*}{3k^*}\frac{\partial T^4}{\partial y} \qquad\qquad 2.25$$

where σ^* and k^* are the Stefan-Boltzmann and mean absorption coefficient, respectively. By expanding T^4 in a Taylor series about T_∞ and ignoring the higher order terms, the following would be obtained:

$$T^4 \simeq 4TT_\infty^3 - 3T_\infty^4. \qquad\qquad 2.26$$

By differentiation of equation (2.26), we obtained the term as below

$$\begin{aligned}\frac{\partial q_r}{\partial y} &= \frac{\partial}{\partial y}\left(-\frac{4\sigma^*}{3k^*}\frac{\partial T^4}{\partial y}\right)\\ &= -\frac{16\sigma^* T_\infty^3}{3k^*}\frac{\partial^2 T}{\partial y^2} \qquad\qquad 2.27\\ &= -\frac{16\sigma^* T_\infty^3}{3k^*}\cdot\frac{a}{v}(T_W - T_\infty)\theta''(\eta)\end{aligned}$$

Hence, the above equations (2.22), (2.23), (2.24), (2.25) and (2.28) were substituted into equation (2.3) to obtain this:

$$axf'(\eta).(0) + \left(-(av)^{\frac{1}{2}} f(\eta)\right)\left(\sqrt{\frac{a}{v}}(T_W - T_\infty)\theta'(\eta)\right)$$

$$= \alpha_m\left(\frac{a}{v}(T_W - T_\infty)\theta''(\eta)\right) - \frac{1}{(\rho C_p)_f}\left(-\frac{16\sigma^* T_\infty^3}{3k^*}\cdot\frac{a}{v}(T_W - T_\infty)\theta''(\eta)\right)$$

$$+ \tau\left[D_B\left(\sqrt{\frac{a}{v}}(T_W - T_\infty)\theta'(\eta)\right)\left(\sqrt{\frac{a}{v}}(C_W - C_\infty)\phi'(\eta)\right) + \frac{D_T}{T_\infty}\left(\sqrt{\frac{a}{v}}(T_W - T_\infty)\theta'(\eta)\right)^2\right]$$

Then, simplifying it to be:

$$-a(T_W - T_\infty)f(\eta)\theta'(\eta) = \alpha_m\frac{a}{v}(T_W - T_\infty)\theta''(\eta) + \frac{a}{v}\frac{16\sigma^* T_\infty^3}{3k^*(\rho C_p)_f}(T_W - T_\infty)\theta''(\eta)$$

$$+ \left[\tau D_B\left(\frac{a}{v}(T_W - T_\infty)(C_W - C_\infty)\phi'(\eta)\theta'(\eta)\right) + \tau\frac{D_T}{T_\infty}\frac{a}{v}(T_W - T_\infty)^2\theta'^2(\eta)\right]$$

By dividing $a(T_W - T_\infty)$, the following should be obtained:

$$-f(\eta)\theta'(\eta) = \frac{\alpha_m}{v}\theta''(\eta) + \left(\frac{\tau D_B}{v}(C_W - C_\infty)\phi'(\eta)\theta'(\eta)\right) + \frac{\tau D_T}{vT_\infty}(T_W - T_\infty)\theta'^2(\eta)$$

$$+\frac{1}{v}\frac{16\sigma^* T_\infty^3}{3k^*(\rho C_P)_f}\theta''(\eta)$$

Because $\alpha_m = \dfrac{k}{(\rho C_P)_f}$, then $(\rho C_P)_f = \dfrac{k}{\alpha_m}$ and this could be substituted into following

equation:

$$\frac{\alpha_m}{v}\theta''(\eta) + \frac{4}{3}\frac{1}{v}\frac{4\sigma^* T_\infty^3}{k^*\frac{k}{\alpha_m}}\theta''(\eta) + \left(\frac{\tau D_B}{v}(C_W - C_\infty)\phi'(\eta)\theta'(\eta)\right) + \frac{\tau D_T}{vT_\infty}(T_W - T_\infty)\theta'^2(\eta)$$

$$+f(\eta)\theta'(\eta) = 0$$

By rearrange the equation, the following should be obtained:

$$\frac{\alpha_m}{v}\theta''(\eta) + \frac{4}{3}\frac{\alpha_m}{v}\frac{4\sigma^* T_\infty^3}{k^* k}\theta''(\eta) + \left(\frac{\tau D_B}{v}(C_W - C_\infty)\phi'(\eta)\theta'(\eta)\right) + \frac{\tau D_T}{vT_\infty}(T_W - T_\infty)\theta'^2(\eta)$$

$$+f(\eta)\theta'(\eta) = 0$$

$$\frac{\alpha_m}{v}\left(1 + \frac{4}{3}\frac{4\sigma^* T_\infty^3}{k^* k}\right)\theta''(\eta) + \left(\frac{\tau D_B}{v}(C_W - C_\infty)\phi'(\eta)\theta'(\eta)\right) + \frac{\tau D_T}{vT_\infty}(T_W - T_\infty)\theta'^2(\eta)$$

$$+f(\eta)\theta'(\eta) = 0$$

Finally, by introducing these symbols, $R = \dfrac{4\sigma^* T_\infty^3}{k^*\alpha}$, $\Pr = \dfrac{v}{\alpha_m}$, $Nb = \dfrac{\tau D_B}{v}(C_W - C_\infty)$ and

$Nt = \dfrac{\tau D_T}{vT_\infty}(T_W - T_\infty)$, then the equation became:

$$\frac{1}{\Pr}\left(1 + \frac{4}{3}R\right)\theta''(\eta) + Nb\phi'(\eta)\theta'(\eta) + Nt\theta'^2(\eta) + f(\eta)\theta'(\eta) = 0 \qquad 2.28$$

2.3.4 Concentration Equation

In order to solve the equation (2.4), $\dfrac{\partial C}{\partial x}$ and $\dfrac{\partial^2 C}{\partial y^2}$ had to be differentiated,

respectively.

$$\frac{\partial C}{\partial x} = \frac{\partial C}{\partial \eta}\frac{\partial \eta}{\partial x}$$

$$= \frac{\partial}{\partial \eta}\left(\phi(\eta)(C_W - C_\infty) + C_\infty\right)\frac{\partial}{\partial x}\left(\left(\frac{a}{v}\right)^{\frac{1}{2}}y\right) \qquad 2.29$$

$$= (C_W - C_\infty)\phi'(\eta).(0)$$

$$= 0$$

$$\frac{\partial^2 C}{\partial y^2} = \frac{\partial}{\partial \eta}\left(\frac{\partial C}{\partial y}\right).\frac{\partial \eta}{\partial y}$$

$$= \frac{\partial}{\partial \eta}\left(\sqrt{\frac{a}{v}}(C_W - C_\infty)\phi'(\eta)\right).\frac{\partial}{\partial y}\left(\left(\frac{a}{v}\right)^{\frac{1}{2}}y\right) \qquad 2.30$$

$$= \sqrt{\frac{a}{v}}(C_W - C_\infty)\phi''(\eta).\sqrt{\frac{a}{v}}$$

$$= \frac{a}{v}(C_W - C_\infty)\phi''(\eta)$$

Hence, the above equations (2.30) and (2.31) were substituted into equation (2.4) to obtain this:

$$axf'(\eta).(0) + \left(-(av)^{\frac{1}{2}}f(\eta)\right)\left(\sqrt{\frac{a}{v}}(C_W - C_\infty)\phi'(\eta)\right)$$

$$= D_B\left(\frac{a}{v}(C_W - C_\infty)\phi''(\eta)\right) + \frac{D_T}{T_\infty}\left(\frac{a}{v}(T_W - T_\infty)\theta''(\eta)\right)$$

$$-a(C_W - C_\infty)f(\eta)\phi'(\eta) = D_B\left(\frac{a}{v}(C_W - C_\infty)\phi''(\eta)\right) + \frac{D_T}{T_\infty}\left(\frac{a}{v}(T_W - T_\infty)\theta''(\eta)\right)$$

By dividing $a(C_W - C_\infty)$ and $\frac{D_B}{v}$, the following should be obtained:

$$-\frac{v}{D_B}f(\eta)\phi'(\eta) = \phi''(\eta) + \frac{D_T}{D_B T_\infty}\frac{(T_W - T_\infty)}{(C_W - C_\infty)}\theta''(\eta)$$

$$\phi''(\eta) + \frac{v}{D_B}f(\eta)\phi'(\eta) + \frac{D_T}{D_B T_\infty}\frac{(T_W - T_\infty)}{(C_W - C_\infty)}\theta''(\eta) = 0$$

Lastly, by introducing the symbol, $Sc = \dfrac{v}{D_B}$, so that the equation would become:

$$\phi''(\eta) + Scf(\eta)\phi'(\eta) + \frac{Nt}{Nb}\theta''(\eta) = 0 \qquad\qquad 2.31$$

2.3.5 Formulation of Boundary Conditions

As we mentioned in Section 2.2 to Section 2.3, the equations (2.2), (2.3), (2.4) and (2.5) were subjected to equation (2.6), therefore the dimensionless equations (2.20), (2.28) and (2.31) would be bound by the following conditions:

$$u = U_W(x) = ax,\ v = 0,\ T = T_w \text{ (CWT) or } \frac{\partial T}{\partial y} = -h_s T \text{ (NH), at } y = 0,$$

$$u \to 0,\ v \to 0,\ T \to T_\infty,\ C \to C_\infty \text{ as } y \to \infty.$$

Firstly, the boundary conditions were considered $y = 0$, then $\eta = \left(\dfrac{a}{v}\right)^{\frac{1}{2}} y = 0$. When $u = U_W(x) = ax$ and $\eta = 0$, the new conditions would become:

$$
\begin{aligned}
u &= ax \\
\frac{\partial \psi}{\partial y} &= ax \\
axf'(0) &= ax \\
f'(0) &= \frac{ax}{ax} \\
&= 1
\end{aligned}
\qquad\qquad 2.32
$$

Next, when $v = 0$ and $\eta = 0$, the condition would become:

$$
\begin{aligned}
v &= 0 \\
-\frac{\partial \psi}{\partial x} &= 0 \\
-(av)^{\frac{1}{2}} f(0) &= 0 \\
f(0) &= 0
\end{aligned}
\qquad\qquad 2.33
$$

Also, when $\eta = 0$, the condition of temperature would become:

37

$$T = T_W \text{ (Constant Wall Temperature)}$$

$$\theta(0) = \frac{T - T_\infty}{T_W - T_\infty}$$

$$= \frac{T_W - T_\infty}{T_W - T_\infty}$$

$$= 1$$

2.34

$$\frac{\partial T}{\partial y} = -h_s T \text{ (Newtonian Heating)}$$

$$\sqrt{\frac{a}{v}} T_\infty \theta'(0) = -h_s T_\infty \left(\theta(0) + 1 \right)$$

$$\theta'(0) = -h_s \sqrt{\frac{v}{a}} \left(\theta(0) + 1 \right)$$

$$\theta'(0) = -\gamma \left(\theta(0) + 1 \right)$$

2.35

Where $\gamma = h_s \sqrt{\dfrac{v}{a}}$ defined as non-Newtonian conjugate parameter.

Besides, when $\eta = 0$, the condition of temperature would become:

$$C = C_W$$

$$\phi(0) = \frac{C - C_\infty}{C_W - C_\infty}$$

$$= \frac{C_W - C_\infty}{C_W - C_\infty}$$

$$= 1$$

2.36

Next, the boundary conditions were considered when $y \to \infty$. Hence,

$\eta = \left(\dfrac{a}{v} \right)^{\frac{1}{2}} y \to \infty$. When $\eta \to \infty$ and $u \to 0$, the new condition as below would be

obtained:

$$u \to 0,$$

$$axf'(\infty) \to 0,$$

$$f'(\infty) \to 0.$$

2.37

38

For $\eta \to \infty$ and $v \to 0$, the new condition would become:

$$v \to 0,$$
$$-(av)^{\frac{1}{2}} f(\infty) \to 0,$$
$$f(\infty) \to 0.$$

$$2.38$$

Also, $T \to T_\infty$ when $\eta \to \infty$. Thus, there would be a new condition for temperature:

$$T \to T_\infty,$$
$$\theta(\infty)(T_W - T_\infty) + T_\infty \to T_\infty,$$
$$\theta(\infty)(T_W - T_\infty) \to 0,$$
$$\theta(\infty) \to 0.$$

$$2.39$$

Lastly, $C \to C_\infty$ when $\eta \to \infty$. Thus, there would be a new condition for concentration:

$$C \to C_\infty,$$
$$\phi(\infty)(C_W - C_\infty) + C_\infty \to C_\infty,$$
$$\phi(\infty)(C_W - C_\infty) \to 0,$$
$$\phi(\infty) \to 0.$$

$$2.40$$

Thus, the boundary conditions would be obtained after the similarity transformations as follows:

$$f'(0) = 1, \ f(0) = 0, \ \theta(0) = 1 \ (\text{CWT}), \ \theta'(0) = -\gamma(\theta(0) + 1) \ (\text{NH}), \ \phi(0) = 1,$$
$$f'(\infty) \to 0, \ f(\infty) \to 0, \ \theta(\infty) \to 0, \ \phi(\infty) \to 0$$

$$2.41$$

2.3.6 Derivations of Physical Quantities

In the present work, it was interesting to find out the numerical values of skin friction coefficient C_f, local Nusselt number Nu and Sherwood number Sh. The quantities of interest were given as:

$$C_f = \frac{\tau_w}{\rho U_W^2},$$

$$2.42$$

$$Nu = \frac{x q_w}{k T_\infty},$$

$$2.43$$

$$Sh = \frac{xq_m}{D_B(C_W - C_\infty)}.$$ 2.44

Where τ_w was defined as shear stress along the direction of two-dimensions, q_w represented heat flux from the surface of the stretching sheet and q_m belonged to mass flux from the surface of the plate. When $y = 0$, all of them were:

$$\tau_w = \mu\left(\frac{1}{1+\beta}\right)\frac{\partial u}{\partial y},$$ 2.45

$$q_w = -k\frac{\partial T}{\partial y},$$ 2.46

$$q_m = -D_B\frac{\partial C}{\partial y}.$$ 2.47

By substituting the equations (2.45), (2.46) and (2.47) into equations (2.42), (2.43) and (2.44) respectively, the following results would be obtained:

For equation (2.43):

$$C_f = \frac{\tau_w}{\rho U_W^2},$$

$$= \frac{\mu\frac{\partial u}{\partial y}}{\rho U_W^2}$$

$$= \frac{\mu}{\rho}\frac{ax\left(1+\frac{1}{\beta}\right)f''(0)\left(\frac{a}{v}\right)^{\frac{1}{2}}}{(ax)^2}$$

$$= v\frac{ax\left(1+\frac{1}{\beta}\right)f''(0)\left(\frac{a}{v}\right)^{\frac{1}{2}}}{(ax)^2}$$

$$= \frac{\left(\frac{v}{a}\right)^{\frac{1}{2}}\left(1+\frac{1}{\beta}\right)f''(0)}{x}$$

By multiplying with $\left(\text{Re}_x\right)^{\frac{1}{2}}$, then the following should be obtained:

$$x\left(\frac{a}{v}\right)^{\frac{1}{2}}.C_f = \frac{\left(\frac{v}{a}\right)^{\frac{1}{2}}f''(0)}{x}.x\left(\frac{a}{v}\right)^{\frac{1}{2}}$$

$$\left(\text{Re}_x\right)^{\frac{1}{2}} C_f = \left(1+\frac{1}{\beta}\right)f''(0) \qquad 2.48$$

For equation (2.44):

$$Nu = \frac{xq_w}{kT_\infty},$$

$$= \frac{x}{kT_\infty}\left(-k\frac{\partial T}{\partial y}\right)$$

$$= \frac{x}{kT_\infty}\left(-k\sqrt{\frac{a}{v}}(T_\infty)\theta'(0)\right)$$

$$= -x\sqrt{\frac{a}{v}}\theta'(0)$$

By dividing with $\left(\text{Re}_x\right)^{\frac{1}{2}}$, then the following should be obtained:

$$\frac{Nu}{\left(\text{Re}_x\right)^{\frac{1}{2}}} = -\frac{x\sqrt{\frac{a}{v}}\theta'(0)}{x\left(\frac{a}{v}\right)^{\frac{1}{2}}} \qquad 2.49$$

$$= -\theta'(0)$$

For equation (2.45):

$$Sh = \frac{xq_m}{D_B\left(C_W - C_\infty\right)}$$

$$= \frac{x}{D_B\left(C_W - C_\infty\right)}\left(-D_B\frac{\partial C}{\partial y}\right)$$

$$= \frac{x}{D_B\left(C_W - C_\infty\right)}\left(-D_B\sqrt{\frac{a}{v}}\left(C_W - C_\infty\right)\phi'(0)\right)$$

$$= -x\sqrt{\frac{a}{v}}\phi'(0)$$

By dividing with $\left(\mathrm{Re}_x\right)^{\frac{1}{2}}$, then the following should be obtained:

$$\frac{Sh}{\left(\mathrm{Re}_x\right)^{\frac{1}{2}}} = -\frac{x\sqrt{\frac{a}{v}}\phi'(0)}{x\left(\frac{a}{v}\right)^{\frac{1}{2}}} \qquad\qquad 2.50$$

$$= -\phi'(0)$$

where $\mathrm{Re}_x = \frac{xU_W(x)}{v}$ was the local Reynolds number. Thus, our skin friction coefficient, heat transfer rate and mass flux transfer rate were given as $\left(\mathrm{Re}_x\right)^{\frac{1}{2}}C_f$, $\frac{Nu}{\left(\mathrm{Re}_x\right)^{\frac{1}{2}}}$ and $\frac{Sh}{\left(\mathrm{Re}_x\right)^{\frac{1}{2}}}$, respectively.

2.4 Numerical Method: Shooting Method

A two point boundary value problem (BVP) would be formed once there were attempts to solve these equations (2.21), (2.29) and (2.32) through numerical procedure. However, through the Shooting method, the BVP was converted into an initial value problem (IVP). The reason of using the Shooting method is because this method could diagnose the applicable initial conditions for a related IVP which would give accurate solution to the BVP. This method was applied in Maple programming language based on dissolve command and shoot implementation. In this method, the new variables for the velocity components, temperature and concentration profiles, would be introduced.

42

Firstly, the third-order system for the momentum equation was reduced to a first-order system to obtain the following:

$$
\begin{aligned}
f &= f, \\
f' &= p, \\
f'' &= p' = q, \\
f''' &= p'' = q'.
\end{aligned}
$$

2.51

Next, the second-order system was reduced to a first-order system for the energy equation and concentration equation, respectively:

$$
\begin{aligned}
\theta &= \theta, \\
\theta' &= r, \\
\theta'' &= r'.
\end{aligned}
$$

2.52

and

$$
\begin{aligned}
\phi &= \phi, \\
\phi' &= s, \\
\phi'' &= s'.
\end{aligned}
$$

2.53

where primes referred to the derivative with respect to η. Therefore, a new equation of momentum (2.54), energy (2.55), and concentration (2.56) would be formed and expressed as follows:

$$
\left(1+\frac{1}{\beta}\right)q' + fq - p^2 - (M+K)p = 0
$$

2.54

$$
\frac{1}{\Pr}\left(1+\frac{4}{3}R\right)r' + Nb(s)(r) + Nt(r)^2 + pr = 0
$$

2.55

$$
s' + Sc(f)(s) + \frac{Nt}{Nb}r' = 0
$$

2.56

And the new boundary conditions for the above three equations would be given as follows:

$$
f(0)=0,\ p(0)=1,\ \theta(0)=1\ \text{(CWT)},\ r(0)=-\gamma\left(1+\theta(0)\right)\ \text{(NH)},\ \phi(0)=0,
$$
$$
p(\infty)\to 0,\ \theta(\infty)\to 0,\ \phi(\infty)\to 0\ \text{ as } y\to\infty.
$$

2.57

Based on ODEs (2.21), (2.29), and (2.32), the summation of the highest order for the three equations would be seven, which means that there must be seven initial values to run the Shooting method. Nevertheless, three out of seven values were missing and the values were:

$$q(0) \Rightarrow f'',$$
$$r(0) \Rightarrow \theta',$$
$$s(0) \Rightarrow \phi'.$$

Because the values of $q(0)$, $r(0)$ and $s(0)$ representing f'', θ' and ϕ', respectively, had been missing, choose such values were chosen by using trial and error technique, the fourth order Runge-Kutta method was used to obtain the solution. From the solution obtained, it had to be determined whether the solution had satisfied the boundary condition at the endpoints by checking the velocity, temperature and concentration profiles. If the profiles had satisfied the boundary conditions at the endpoints asymptotically, it would mean that the solution obtained was valid and would significantly benefit the current study. The same procedure was repeated with other assumed values of $q(0)$, $r(0)$ and $s(0)$ for the same values of parameters used. The programming works are shown in Appendix A of this thesis by using *Maple 13* software. Figure 2.2 below shows the general flow diagram for the computations of Shooting method for problems discussed in this thesis.
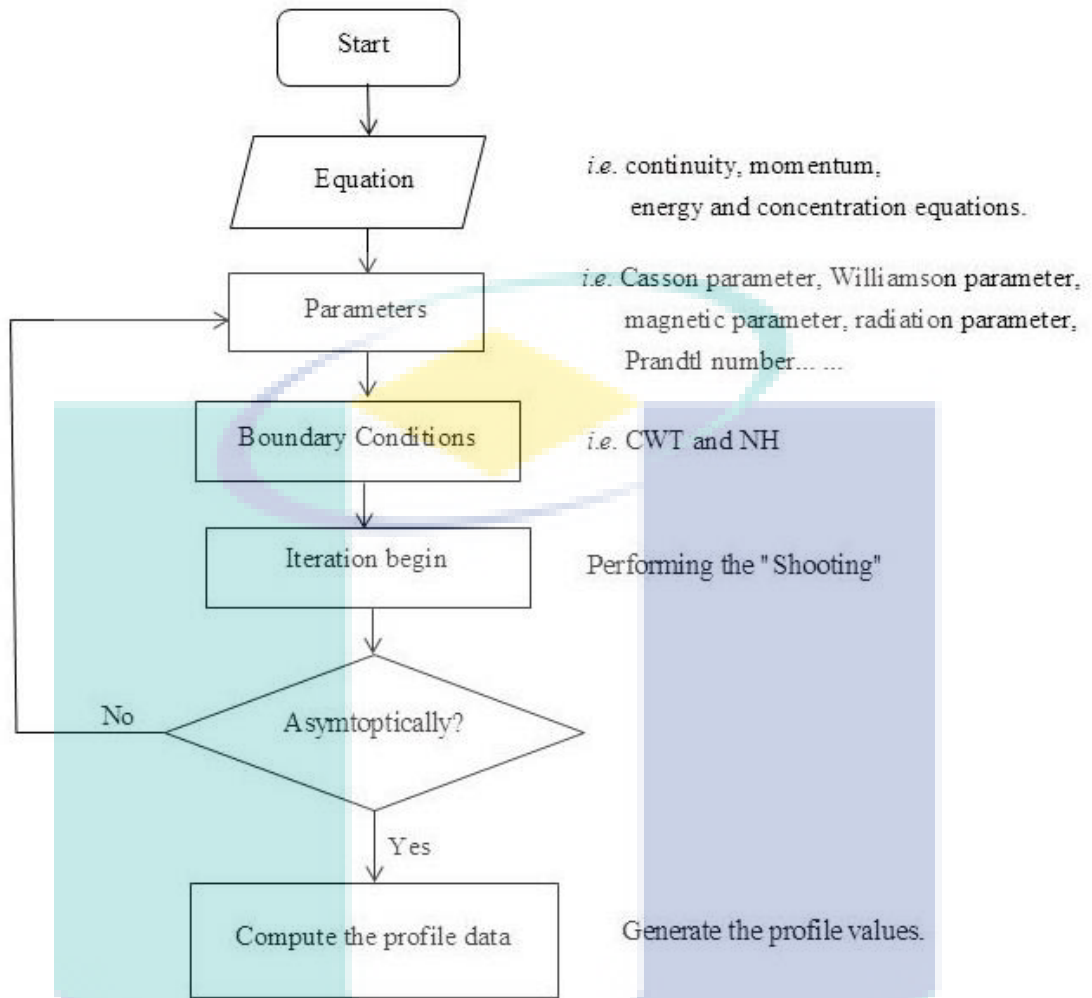
Figure 2.2 Flow diagram for the Shooting method.

CHAPTER 3

EFFECT OF THERMAL RADIATION ON MHD FLOW AND HEAT TRANSFER IN CASSON NANOFLUID OVER A STRETCHING SHEET

3.1   Introduction

Generally, problems involving thermal radiation and magnetohydrodynamic (MHD) flow with heat and mass transfer are very common in industry processes. The main reason is that a lot of engineering processes occur at higher temperature and the knowledge of radiation in heat transfer leads to significant contribution to equipment design such as nuclear power plants, gas turbine, transportation and communication devices like satellites, aircraft, space vehicles and even for war equipment like missiles. Sivaiah et al. (2010) has mentioned that the effects of thermal radiation play an important role in operations at high temperature. The related problem has been discussed by researchers in different fields as mentioned in the literature review section.

This chapter will focus on the effect of thermal radiation on magnetohydrodynamic (MHD) heat and mass transfer flow in Casson nanofluid over a stretching sheet with the presence of porous medium. Two different boundary conditions, namely, Constant wall temperature (CWT) and Newtonian heating (NH), were examined. The results of viscous fluid was first carried out to compare to the findings by Khan and Pop (2010), Gorla and Sidawi (1994), Wang (1989). Besides that, the porous medium may be applied in petroleum refineries, movement of oil, water and gas for purification and filtration.

In the current work, the basic of boundary layer equations (momentum, energy and concentration) are transformed into the non-dimensional forms and then from partial differential equation to ordinary differential equation. Subsequently, the appropriate results are carried out via the Shooting method. The numerical solutions are

obtained for the velocity, temperature and concentration profiles, as well as the skin friction coefficient, local Nusselt number and local Sherwood number. The features of flow and heat characteristics for several parameters with various given values are analyzed and presented with graphical results. The parameters considered are Casson fluid, magnetic, porosity, radiation, Prandtl number, Brownian motion, thermophoresis and Lewis number.

3.2 Mathematical Formulation

In this chapter, the problem formulation of the Casson nanofluid over a stretching sheet and boundary conditions for constant wall temperature and Newtonian heating are presented and derived in Section 2.2 and 2.3, which in Chapter 2. The non-linear equations (2.2), (2.3) and (2.4) were subjected to boundary conditions (2.41) are solved numerically using shooting method. The purpose of this study is to focus on the effects of thermal radiation and heat transfer flow MHD in the presence of porous medium for Casson nanofluid over a stretching sheet.

3.2.1 Results and Discussion for Constant Wall Temperature (CWT)

The non-linear ordinary differential equations were of third order in f, second order in θ and ϕ, reduced into simultaneous ordinary equations. With the initial conditions of $\eta \to \infty$, the value of $f'(\eta)$, $\theta(\eta)$ and $\phi(\eta)$ could be obtained. Thus, unknown initial conditions $\eta = 0$ were obtained by using the Shooting method and the initial values for boundary value problem were assumed. The calculated boundary values should be similar to the real boundary values; hence, the calculated boundary values should be as close as possible to the real boundary values. In this study, there was no consideration of variation in temperature, velocity and concentration where large infinity condition was employed but finite value for η. The value of $\eta_{\max} = 12$, which was sufficient to achieve asymptotic boundary conditions for all parameter values considered, was chosen. Table 3.1 shows the comparison values of $-\theta'(0)$ with previous results. It concludes that this method worked efficiently and the results presented here are accurate.

Table 3.1 Comparison of results for the Nusselt number $-\theta'(0)$ when $R = K = M = Nb = Nt = 0$, $\beta = \infty$, $Le = 1$.

Pr	Khan and Pop (2010)	Gorla and Sidawi (1994)	Wang (1989)	Present study
0.20	0.1691	0.1691	0.1691	0.1698
0.70	0.4539	0.5349	0.4539	0.4539
2.00	0.9113	0.9114	0.9114	0.9113
7.00	1.8954	1.8905	1.8954	1.8954
20.00	3.3539	3.3539	3.3539	3.3539

This section includes the study of thermal radiation effect on MHD and heat transfer flow of Casson nanofluid with embedded porous medium. The parameters involved were Casson parameter β, magnetic parameter M, porosity parameter K, radiation parameter R, Prandlt number Pr, Brownian motion parameter Nb, thermophoresis parameter Nt and Sc number. The effects of these parameters on the temperature $\theta(\eta)$, velocity $f'(\eta)$, and concentration $\phi(\eta)$ profiles are shown graphically based on Figure 3.1 to 3.19 including the concentration wall temperature, Sherwood number and skin friction coefficient. The numerical results for these parameters are given in Table 3.2.

The effects of Casson parameter β on velocity $f'(\eta)$ and temperature $\theta(\eta)$ are shown in Figures 3.1 and 3.2 respectively. It was found that an increase in Casson parameter β had led to decreasing velocity $f'(\eta)$ field while increasing the temperature $\theta(\eta)$. To increase the Casson parameter β, yield stress was reduced, which means that Casson fluid behaved like Newtonian fluid $(\beta \to \infty)$. Thus, it is concluded that Casson fluid's velocity was greater than Newtonian fluid. Figures 3.3 and 3.4 show the magnetic parameter M effects on velocity $f'(\eta)$ and temperature $\theta(\eta)$, respectively. It was discovered that the velocity $f'(\eta)$ field had decreased as the magnetic parameter M increased. The reason is that when magnetic parameter M increased, it would also cause the Lorentz force to increase. This force would oppose the fluid motion due to the application of transverse magnetic field which would always

result in a resistive force that would tend to resist the fluid flow. Meanwhile, Figure 3.4 shows that an increase in the magnetic parameter M led to an increase in temperature $\theta(\eta)$. Further, this enhancement would be very significant near the sheet; however this effect would be almost negligible away from the sheet. Figures 3.5 and 3.6 illustrate different values of the porous medium. From Figure 3.5, it can be seen that the variation in velocity profile decreased as porosity parameter K increased. Figure 3.6 shows that increasing the porosity parameter K led to an increase in thermal boundary layer. Figures 3.7 and 3.8 illustrate the temperature $\theta(\eta)$ and concentration $\phi(\eta)$ fields for different values of Brownian parameter Nb. It was observed that increase in Nb had caused then the temperature $\theta(\eta)$ field to also increase but the concentration $\phi(\eta)$ field to decrease. Because the Brownian motion referred to the movement of nanoparticles, the higher the motion of nanoparticles, the larger the enhancement of thermal conductivity would be. Figures 3.9 and 3.10 indicate the temperature and concentration profiles of thermophoresis parameter, respectively. It was observed that when Nt had increased, the temperature and concentration profiles would also increase. According to Anwar et al. (2013), this phenomenon is due to the larger value of Nb representing a large extent of fluid and thus, causes the thickness of the thermal boundary layer to increase. The same trend would also happen when Nt increases.

The variation of temperature profile by Prandlt number is shown in Figure 3.11. As Pr increased, the temperature distribution would decrease. Figure 3.12 reveals the temperature profile affected by the radiation parameter. Based on the graph, the result shows that when R increased the temperature profile would also increase. Figure 3.13 depicts the effect of Schmidt parameter on concentration profile. The result shows that as the Sc increased, the concentration profile would decrease at all time. This is because when Sc increased, the momentum diffusivity effects would increase which would slow down the effects of mass transfer rate leading to lower concentration profile. Figures 3.14, 3.15 and 3.16 are plotted graphically to describe the effect of Casson nanofluid and magnetic parameter on local Nusselt number, Sherwood number and skin friction coefficient, respectively. Figure 3.14 shows that the skin friction coefficient decreased when the value of β and M had increased. Figures 3.15 and 3.16 show the temperature and concentration gradient would increase with β but the local

Nusselt number and Sherwood number would gradually decrease. The influence of Brownian parameter and thermophoresis parameter on local Nusselt number and Sherwood number is illustrated in Figure 3.17. It can be seen that the dimensionless temperature gradient decreased and remained stagnant when Nb and Nt had increased. Even though concentration gradient would increase when Nb and Nt increased, it was evident that there were was a slight change of heat transfer with the higher value of Nb and Nt. In fact, the larger value of Nb and Nt would enhance the convective mass transfer capability and vice versa, while the smaller value of Nb and Nt would enhance the convective heat transfer capability.

Figure 3.18 indicates the effect of Schmidt number and Prandlt number on dimensionless temperature rate. As the Schmidt number increased, the wall temperature would decrease. However, the wall temperature would increase when Prandtl number was raised. The higher value of Pr would cause the thickness of boundary layer to reduce while the heat transfer rate increased as the wall temperature was constant. Figure 3.19 shows the effect of Prandlt number and radiation parameter on temperature gradient. With increasing Pr value, the local Nusselt number would also increase. However, the rate of heat transfer would decrease once R increased. This is because the thermal diffusivity would cause the heat transfer ability of fluid to be physically reduced.
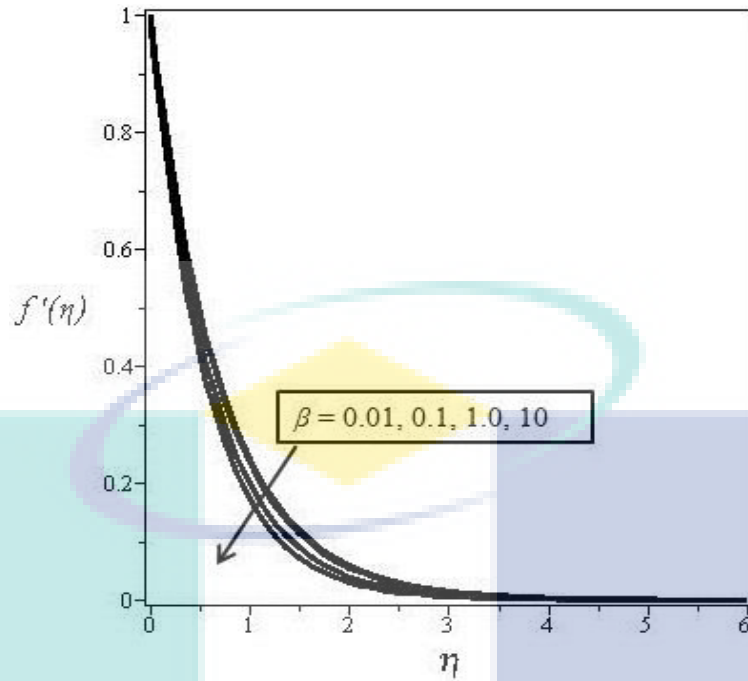
Figure 3.1 Velocity profile for various values of Casson parameter β, when $M = 0.2, K = 2,\ R = 5, Nb = 0.5, Nt = 0.5, Sc = 2$ and $\Pr = 7$.
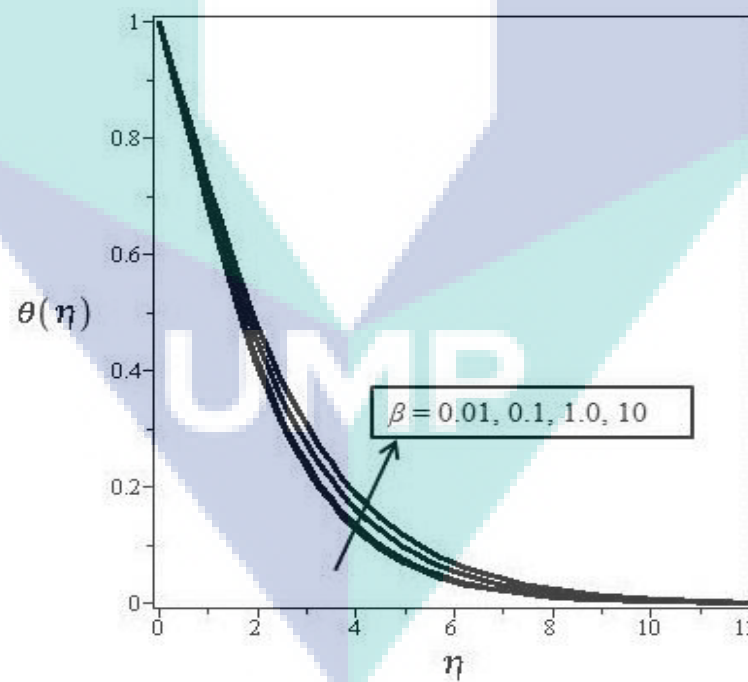
Figure 3.2 Temperature profile for various values of Casson parameter β, when $M = 0.2,\ K = 2,\ R = 5,\ Nb = 0.5,\ Nt = 0.5,\ Sc = 2$ and $\Pr = 7$.
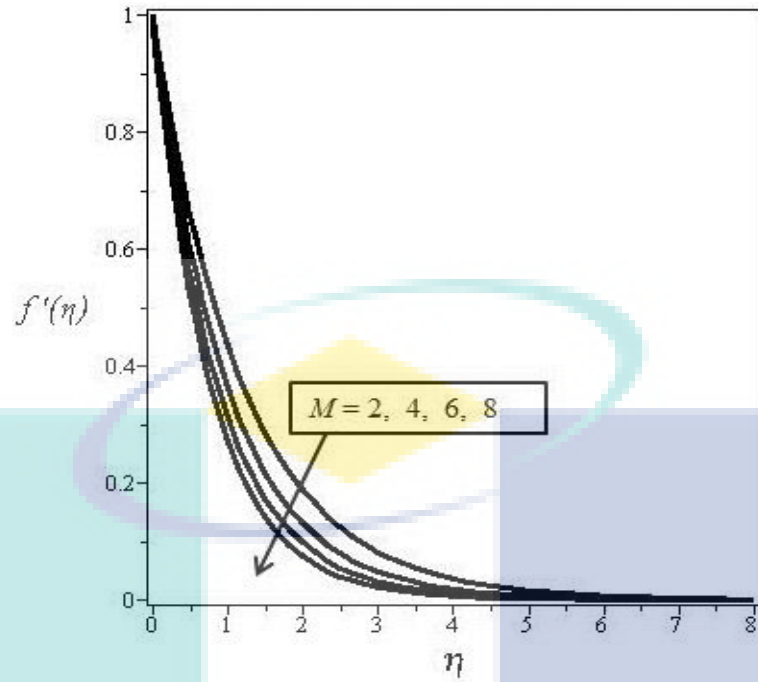
Figure 3.3 Velocity profile for various values of magnetic parameter M, when $\beta = 0.2$, $K = 2$, $R = 5$, $Nb = 0.5$, $Nt = 0.5$, $Sc = 2$ and $\Pr = 7$.
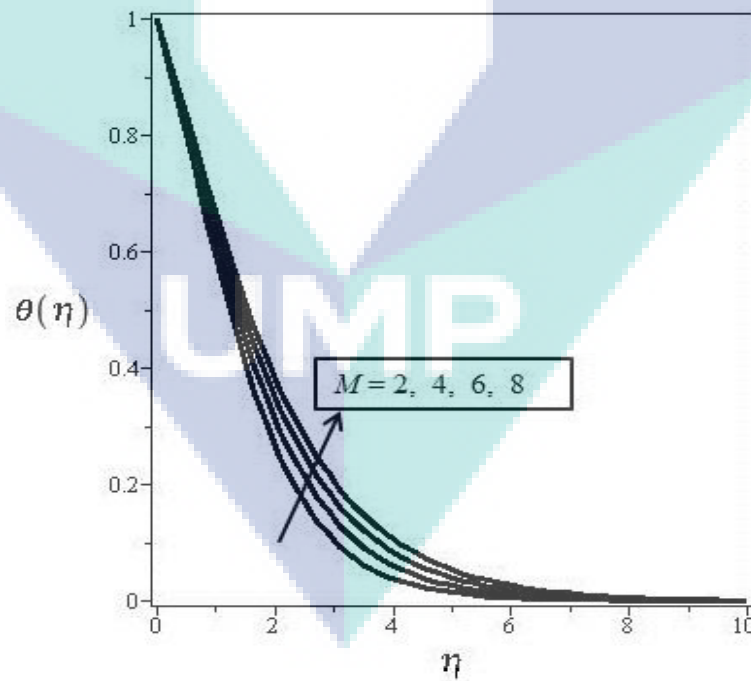
Figure 3.4 Temperature profile for various values of magnetic parameter M, when $\beta = 0.2$, $K = 2$, $R = 5$, $Nb = 0.5$, $Nt = 0.5$, $Sc = 2$ and $\Pr = 7$.
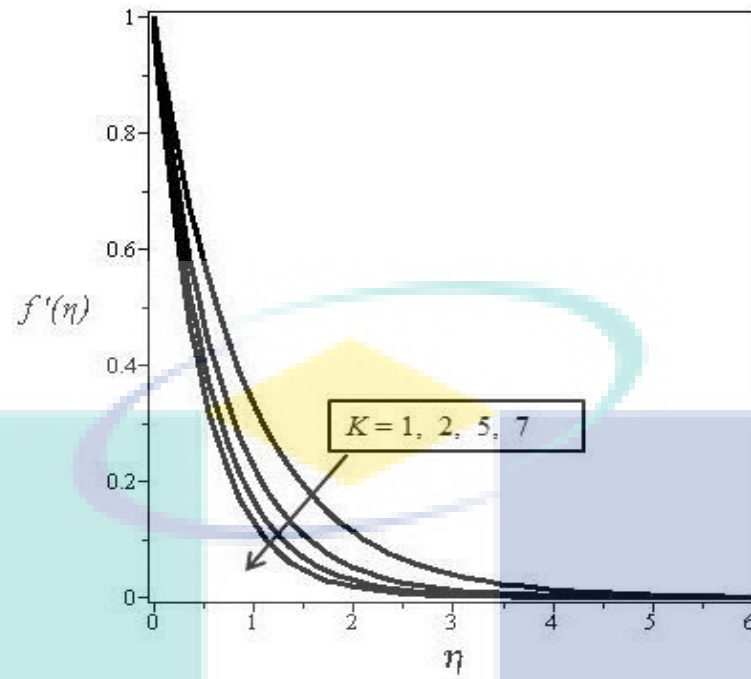
Figure 3.5 Velocity profile for various values of porosity parameter K, when $\beta = 0.2,\ K = 2,\ R = 5,\ Nb = 0.5,\ Nt = 0.5,\ Sc = 2$ and $\mathrm{Pr} = 7$.
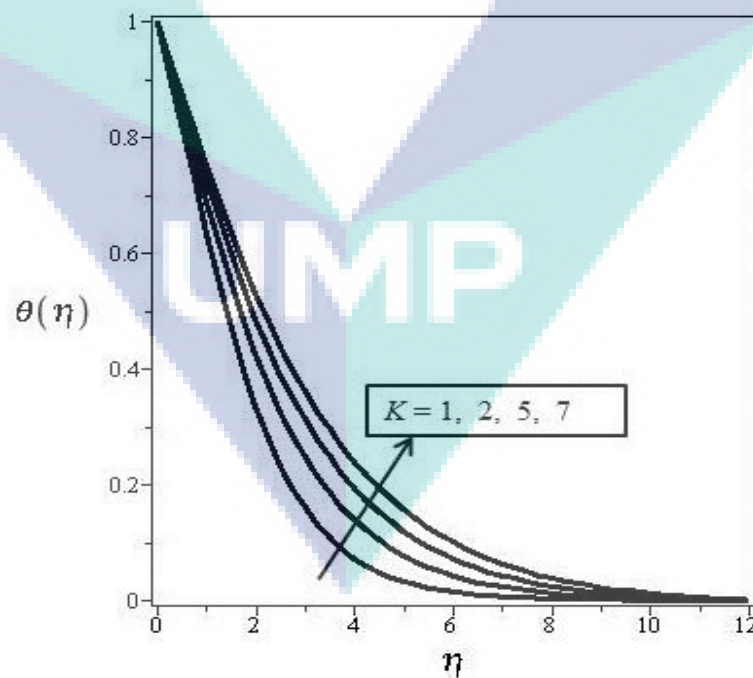
Figure 3.6 Concentration profile for various values of porosity parameter K, when $\beta = 0.2,\ K = 2,\ R = 5,\ Nb = 0.5,\ Nt = 0.5,\ Sc = 2$ and $\mathrm{Pr} = 7$.
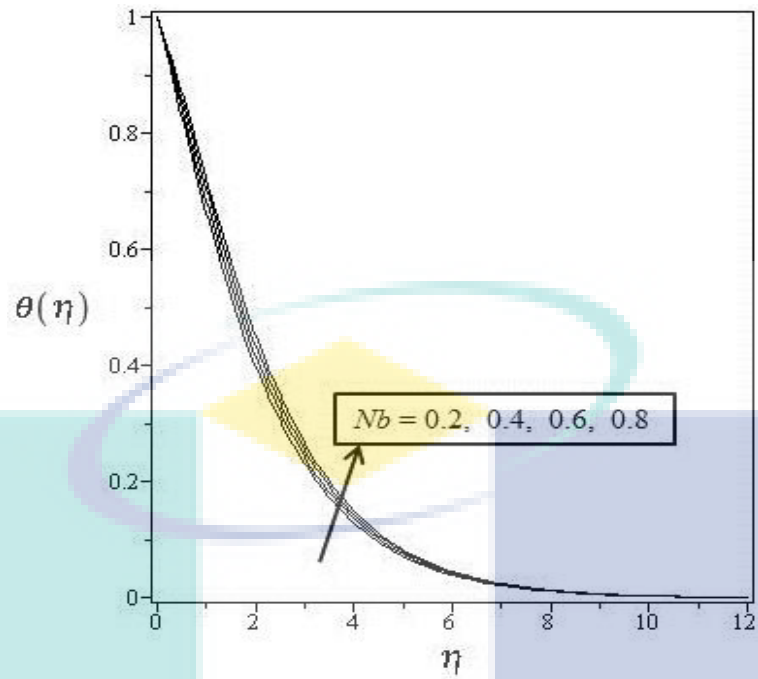
Figure 3.7 Temperature profile for various values of Brownian motion parameter Nb, when $\beta = 0.2$, $K = 2$, $M = 0.2$, $R = 5$, $Nt = 0.5$, $Sc = 2$ and $\Pr = 7$.
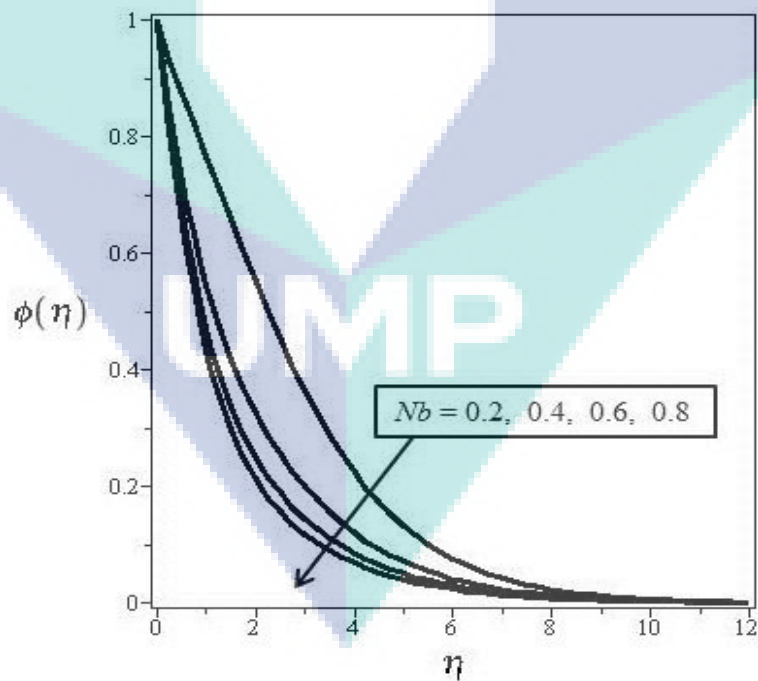
Figure 3.8 Concentration profile for various values of Brownian motion parameter Nb, when $\beta = 0.2$, $K = 2$, $M = 0.2$, $R = 5$, $Nt = 0.5$, $Sc = 2$ and $\Pr = 7$.
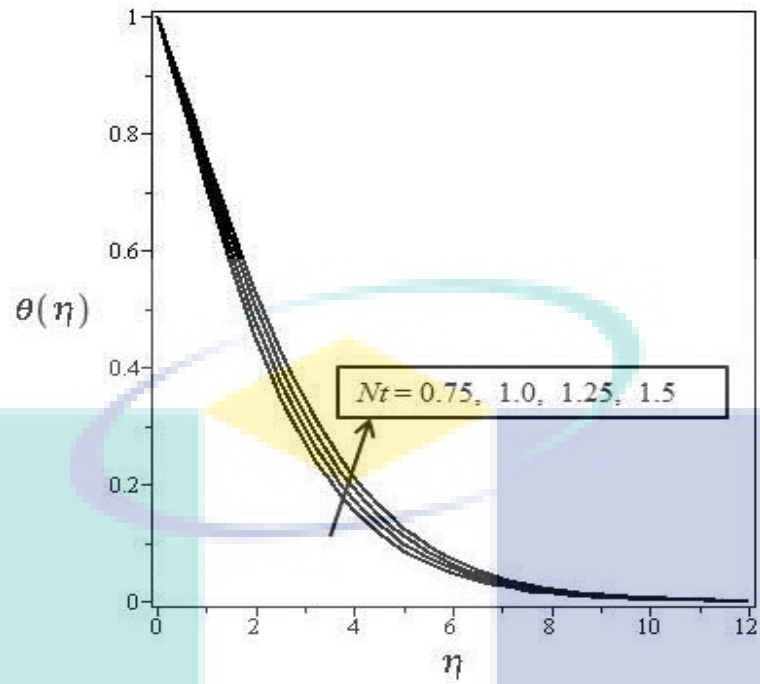
Figure 3.9 Temperature profile for various values of thermophoresis parameter Nt, when $\beta = 0.2$, $K = 2$, $M = 0.2$, $R = 5$, $Nb = 0.5$, $Sc = 2$ and $\Pr = 7$.
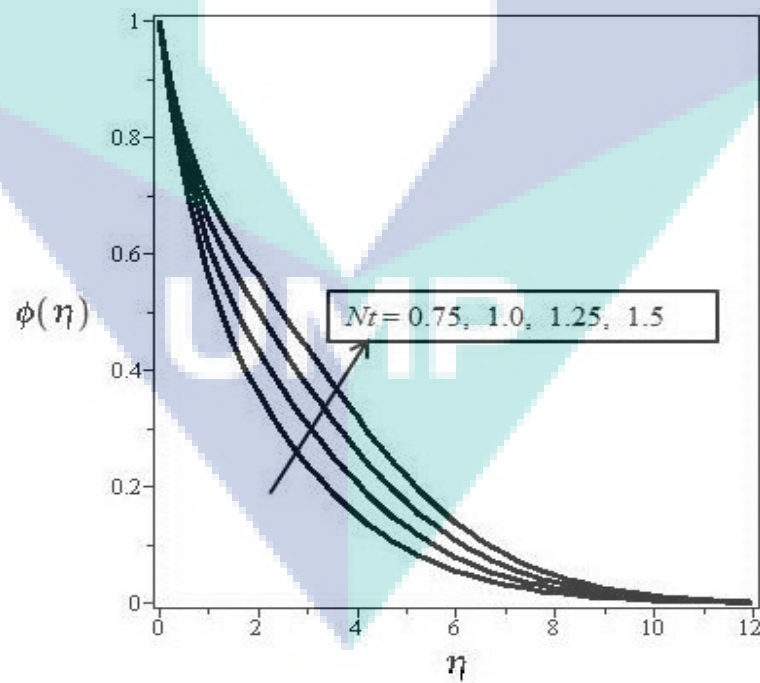
Figure 3.10 Concentration profiles for various values of thermophoresis parameter Nt, when $\beta = 0.2$, $K = 2$, $M = 0.2$, $R = 5$, $Nb = 0.5$, $Sc = 2$ and $\Pr = 7$.
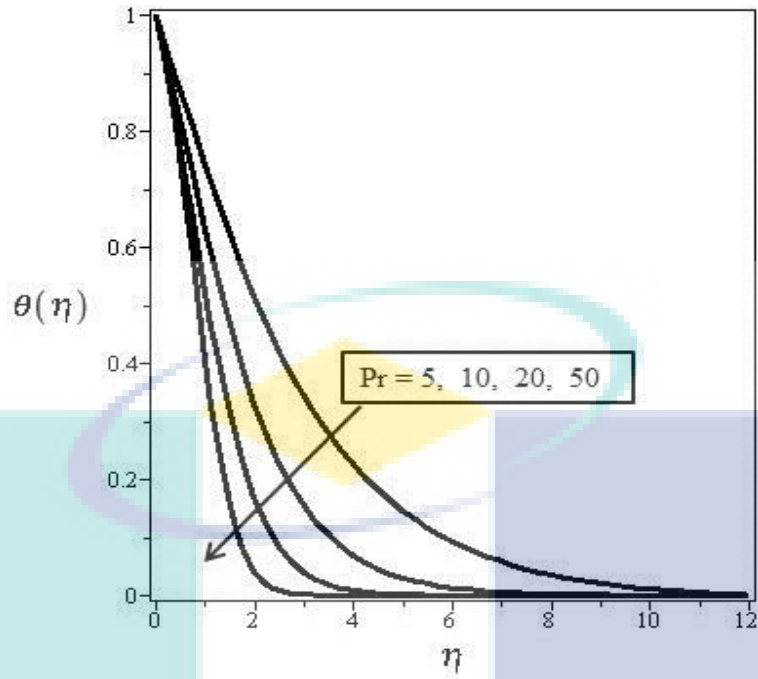
Figure 3.11 Temperature profile for various values of Prandlt number Pr, when $\beta = 0.2,\ K = 2,\ M = 0.2,\ R = 5,\ Nb = 0.5,\ Nt = 0.5$ and $Sc = 2$.
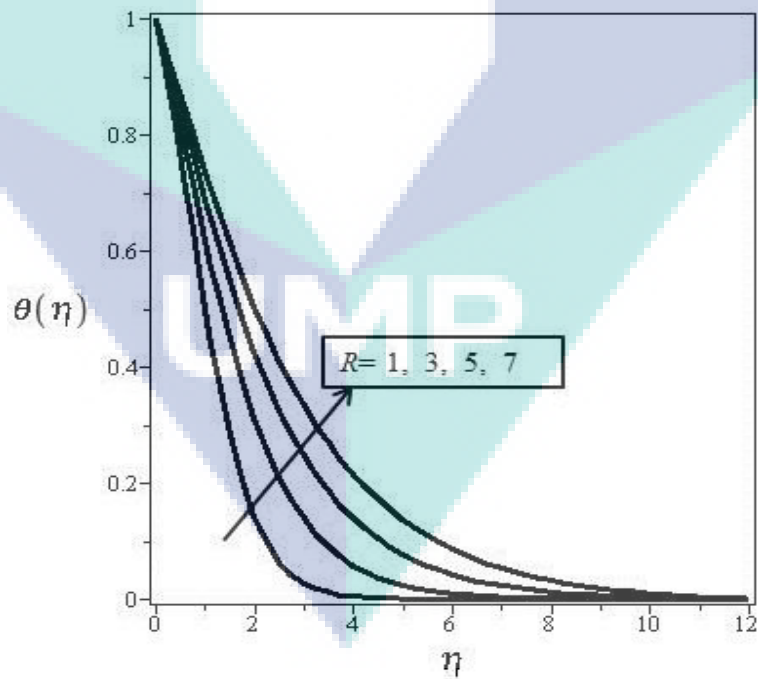
Figure 3.12 Temperature profile for various values of radiation parameter R, when $\beta = 0.2,\ K = 2,\ M = 0.2,\ Nb = 0.5,\ Nt = 0.5,\ Sc = 2$ and $Pr = 7$.
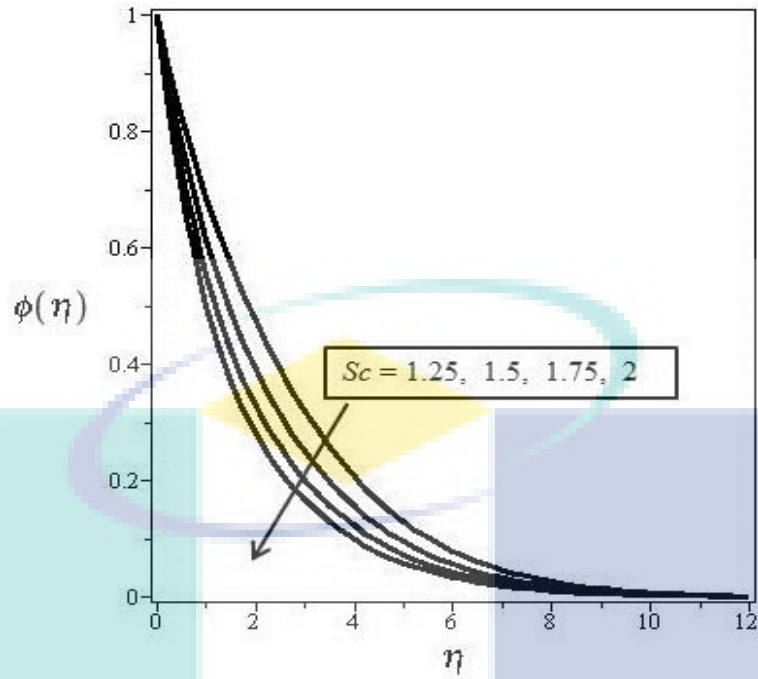
Figure 3.13 Concentration profile for various values of Schmidt number Sc, when $\beta = 0.2,\ K = 2,\ M = 0.2,\ R = 5,\ Nb = 0.5,\ Nt = 0.5$ and $\Pr = 7$.
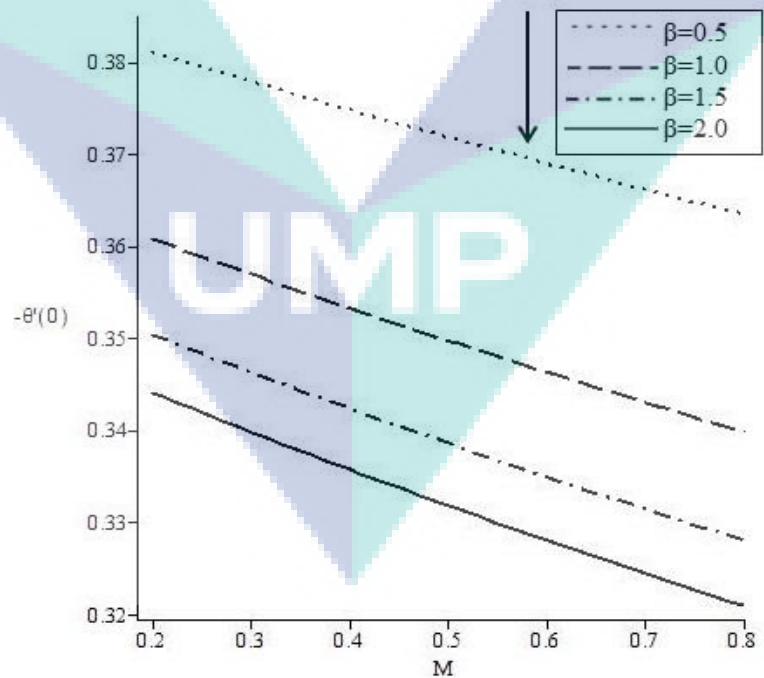
Figure 3.14 The effect of β and M on local Nusselt number.
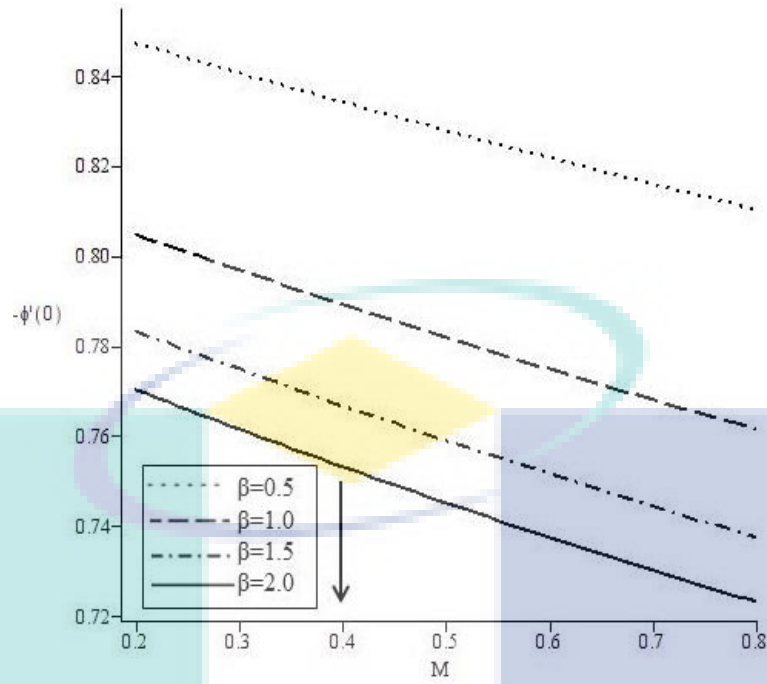
Figure 3.15 The effect of β and M on local Sherwood number.
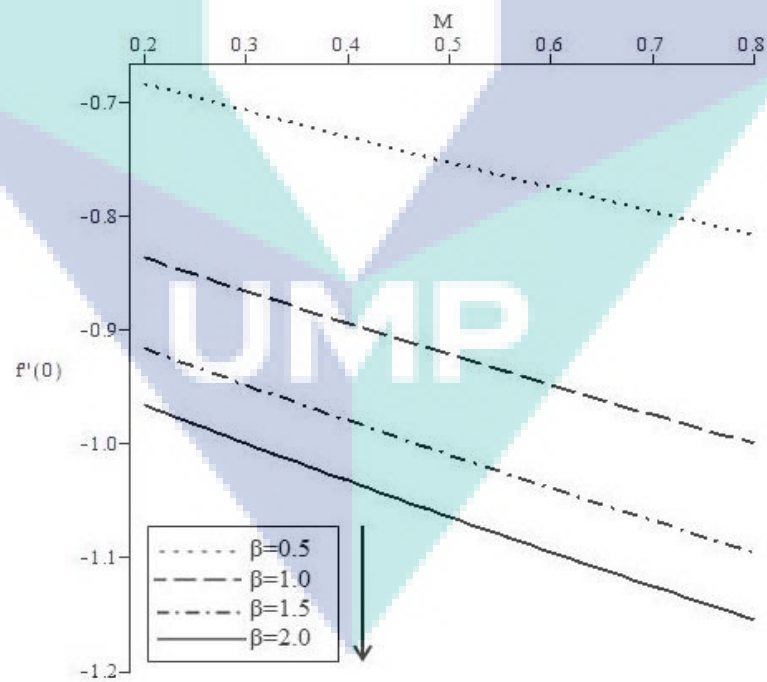
Figure 3.16 The effect of β and M on skin friction coefficient.
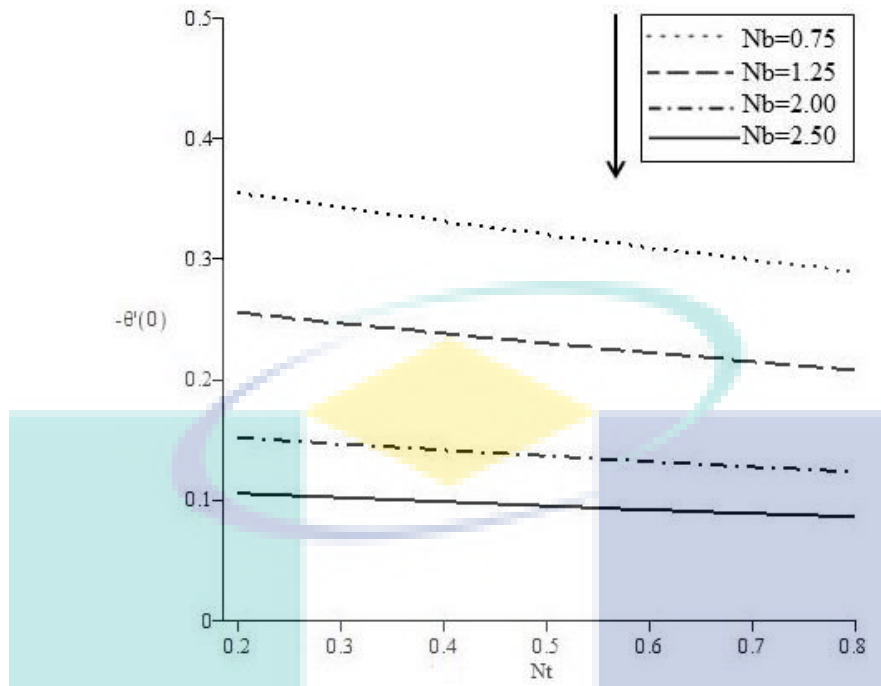
Figure 3.17 The effect of Nb and Nt on local Nusselt number.
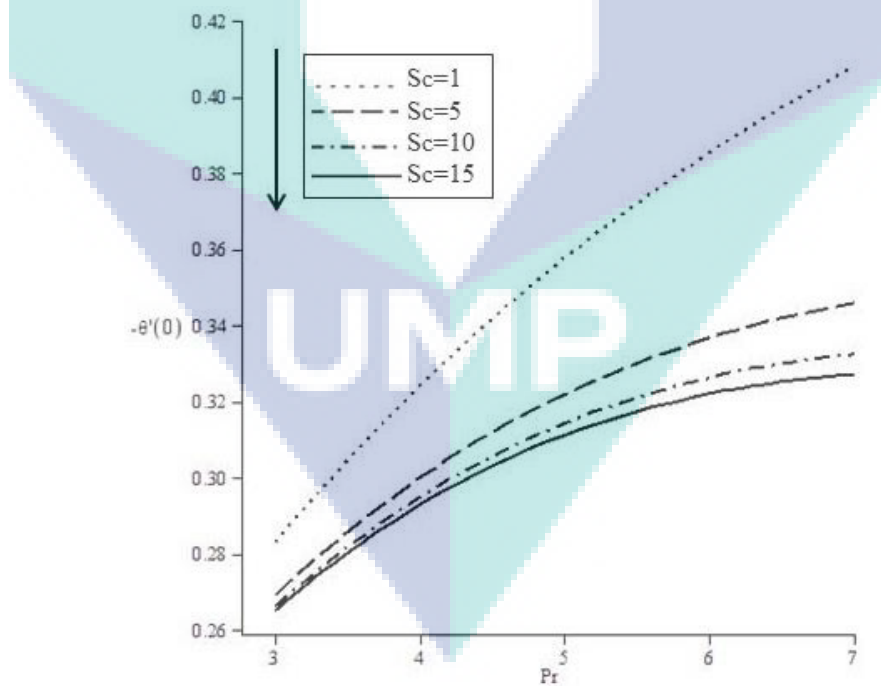
Figure 3.18 The effect of Sc and Pr on local Nusselt number.
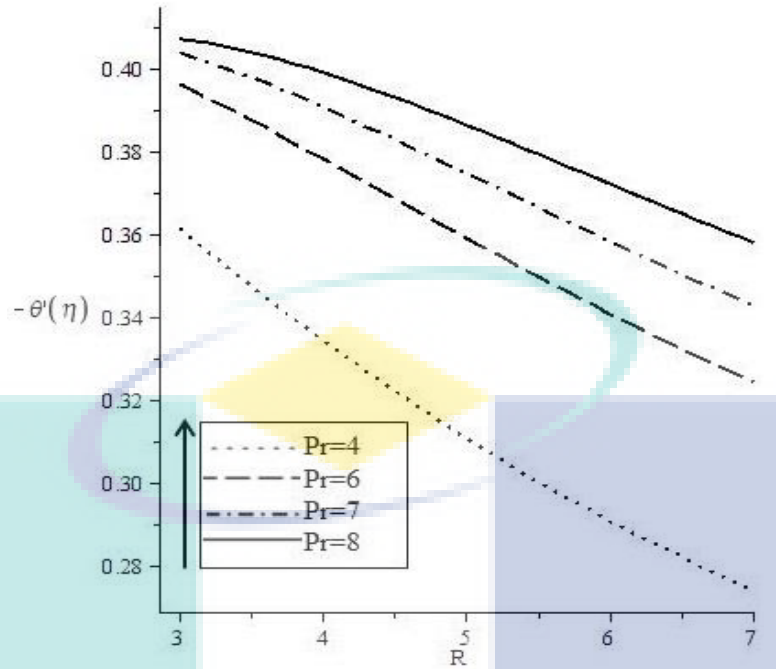
Figure 3.19 The effect of Pr and R on local Nusselt number.

The variation of skin friction coefficient $f''(0)$, temperature gradient $-\theta'(0)$ and concentration gradient $-\phi'(0)$ with respect to Casson nanofluid β, magnetic parameter M, porosity parameter K, Prandlt number Pr, Brownian parameter Nb, thermophoresis parameter Nt, radiation parameter R and Schmidt number Sc are presented in Table 3.2.

3.2.2 Summary

Thermal radiation on MHD flow and heat mass transfer over stretching sheet in Casson nanofluid were studied numerically. The nonlinear ordinary differential equations were solved numerically using the Shooting method. The result of velocity, temperature and concentration profiles are then presented graphically for different values of the pertinent parameters. Also, the skin friction coefficient, local Nusselt number and Sherwood number were the examined with the influence of various parameters. The results are summarized as below:

- For temperature and concentration profiles, the boundary layer thickness increased but the velocity distribution decreased when Casson nanofluid parameter, magnetic parameter and porosity parameter increased.
- Temperature profile decreased when Prandlt parameter number increased.

- When Brownian motion parameter increased, the concentration profile dropped but the temperature profile increased.
- Increase in the thermophoresis parameter resulted in an increase in the temperature and concentration profiles.
- Temperature profile increased when the radiation parameter increased.
- Increasing the values of Schmidt number caused the concentration profile to decrease .
- Skin friction coefficient as well as local Nusselt and Sherwood number decreased at all time as β and M in the fluid increased.
- The increase of Nb and Nt in the fluid caused the local Nusselt number to decrease and Sherwood number to increase.
- The higher the value of Sc and Pr, the higher the temperature gradient would be.
- The higher the value of   and the lower the local Nusselt number would be.

Table 3.2 Numerical values for $\left(1+\dfrac{1}{\beta}\right)f''(0),\ -\theta'(0)$ and $-\phi'(0)$ for different parameters values.

β	M	K	R	Nb	Nt	Sc	Pr	$\left(1+\dfrac{1}{\beta}\right)f''(0)$	$-\theta'(0)$	$-\phi'(0)$
0.01	0.2	2	5	0.5	0.5	2	7	-1.418408	0.290002	
0.10								-1.452270	0.286358	
1								-1.612451	0.269928	
10								-1.758098	0.256149	
0.2	2	2	5	0.5	0.5	2	7	-0.836668	0.360837	
	4							-1.01650	0.337775	
	6							-1.169045	0.319260	
	8							-1.303840	0.303874	
0.2	0.2	1	5	0.5	0.5	2	7	-1.095445	0.327579	
		2						-1.483240	0.283077	
		5						-1.788854	0.253379	
		7						-2.049390	0.231778	
0.2	0.2	2	1	0.5	0.5	2	7		0.349831	0.636292
			3						0.327175	0.624007
			5						0.283077	0.644833
			7						0.247238	0.665772
0.2	0.2	2	5	0.2	0.5	2	7		0.342778	0.282130
				0.4					0.301929	0.585531
				0.6					0.265226	0.683642
				0.8					0.232376	0.730609
0.2	0.2	2	5	0.5	0.75	2	7		0.261561	0.584359
					1				0.242203	0.534969
					1.25				0.224764	0.494762
					1.50				0.209030	0.462188
0.2	0.2	2	5	0.5	0.5	1.25	7		0.301766	0.372734
						1.50			0.293983	0.471341
						1.75			0.287925	0.561497
						2.00			0.283077	0.644833

3.2.3 Results and Discussion for Newtonian Heating (NH)

This section includes the graphical results for velocity $f'(0)$, temperature $\theta(0)$ and concentration $\phi(0)$ profiles for the parameters involved such as Casson nanofluid parameter β, Newtonian heating parameter γ, magnetic parameter M, porosity parameter K, Brownian motion parameter Nb, thermophoresis parameter Nt, Prandtl number Pr, radiation parameter R and Schmidt number Sc, respectively, by using the boundary condition (2.41).

Figures 3.20 and 3.21 illustrate Casson nanofluid effects on the velocity and temperature respectively. Velocity profile would decrease as the Casson nanofluid parameter increased. At the same time, the temperature profile would increase as Casson nanofluid parameter increased. Figure 3.21 and 3.22 present the Newtonian heating parameter effects on temperature and concentration profiles respectively. The profiles would increase when the Newtonian heating parameter increased. This would also lead to an increase in the thickness of boundary layer.

Induced magnetic field would be affected by the velocity and temperature profiles as shown in Figures 3.24 and 3.25. The velocity profile would drop but the temperature profile would increase as the magnetic parameter increased. This is due to the resistive force produced by the magnetic field, reducing the flow motion significantly and causing the retardation in velocity. Figures 3.26 and 3.27 depict the effects of porosity parameter on velocity and temperature profile. The velocity profile would decrease when the porosity parameter increased due the existance of magnetic field. The temperature profile would increase when the porosity parameter increased because the existence of a porous medium would lead to enhanced thermal conductivity and mass transfer rate in the fluid.

The temperature profile would increase when the Brownian motion parameter increased but the concentration profile would decrease as shown in Figures 3.28 and 3.39, respectively. The Brownian motion occured due to the movement of the small sized nanoparticles affecting the heat transfer charateristics. This phenomenon would be important because it could enhance the thermal conductivity of nanofluids. Figures 3.30

and 3.31 illustrate the thermophoresis parameter effects on temperature and concentration profiles. Both profiles would increase when thermophoresis parameter increased. In fact, thermophoresis parameter would be directly proportional to the heat transfer rate coefficient in relation to the hot fluid. Increase in the value of Prandtl number would cause the temperature profile to drop, as shown in Figure 3.32. Meanwhile, Figure 3.33 presents the effect of radiation parameter on temperature and it can be seen that an increase in the value of radiation parameter would cause the temperature profile to increase. This is due to the enhancement of conduction effects in nanofluid as influenced by thermal radiation. From the Figure 3.34, it can also be seen that the concentration profile would decrease as Schmidt number increased.

Figure 3.35 illustrates the effect of Newtonian heating parameter γ and radiation parameter R on temperature wall gradient. An increase in the value of γ would cause the local Nusselt number $-\theta'(0)$ to increase. This is because the radiation parameter would radiate actively at higher temperature; thus, the graph shows high value of R as it increased significantly. Figures 3.36 and 3.37 show the effect of the presence of Casson parameter, magnetic parameter and porosity parameter on local Nusselt number and skin friction coefficient, respectively. Figure 3.36 shows that the temperature wall gradient would increase as these three parameters increased. The thickness of boundary layer also would increase because more heat produce as the fluid motion was resisted by Lorentz force, thus causing a slow down in the fluid motion. Also, there was more friction produced when the magnetic parameter increased. The result can be seen in Figure 3.37. Figure 3.38 presents the critical value of Newtonian heating parameter γ_c and Prandtl number Pr on gradient of wall temperature. It was observed that when $\text{Pr} = 2$, then $\gamma_c = 0.136884$. However, when the value of Pr increased to 7, then $\gamma_c = 0.071840$. The critical value of Newtonian heating parameter on temperature wall gradient would become smaller when Prandtl number increased.
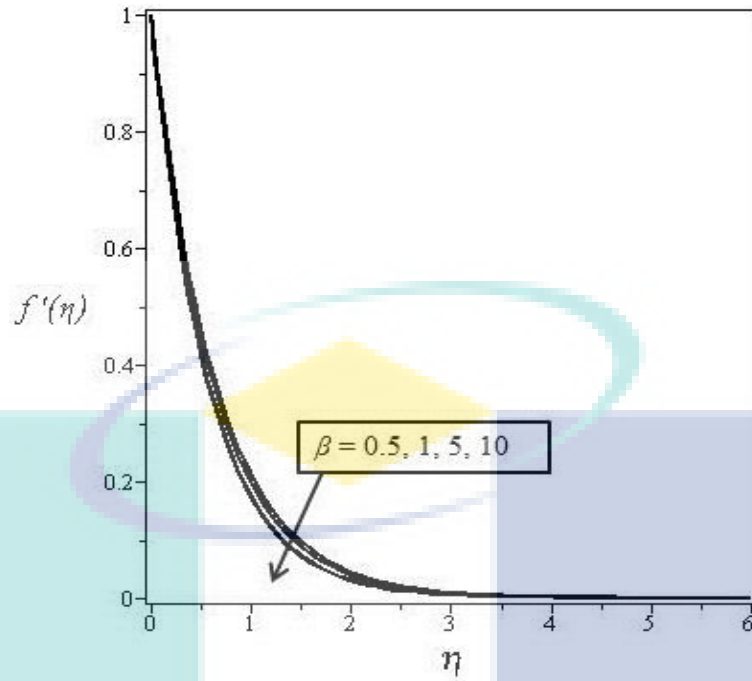
Figure 3.20 Velocity profile for various values of Casson nanofluid β, when $M = 0.2,\ K = 2,\ \gamma = 0.125,\ Sc = 5,\ R = 0.25,\ Nb = 0.5,\ Nt = 0.5$ and $\Pr = 2$.
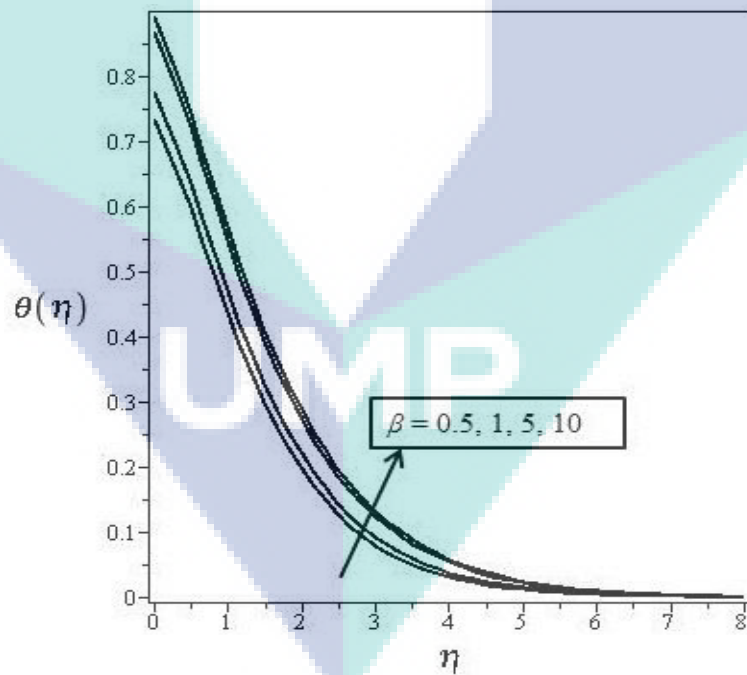
Figure 3.21 Temperature profile for various values of Casson nanofluid β, when $M = 0.2,\ K = 2,\ \gamma = 0.125,\ Sc = 5,\ R = 0.25,\ Nb = 0.5,\ Nt = 0.5$ and $\Pr = 2$.
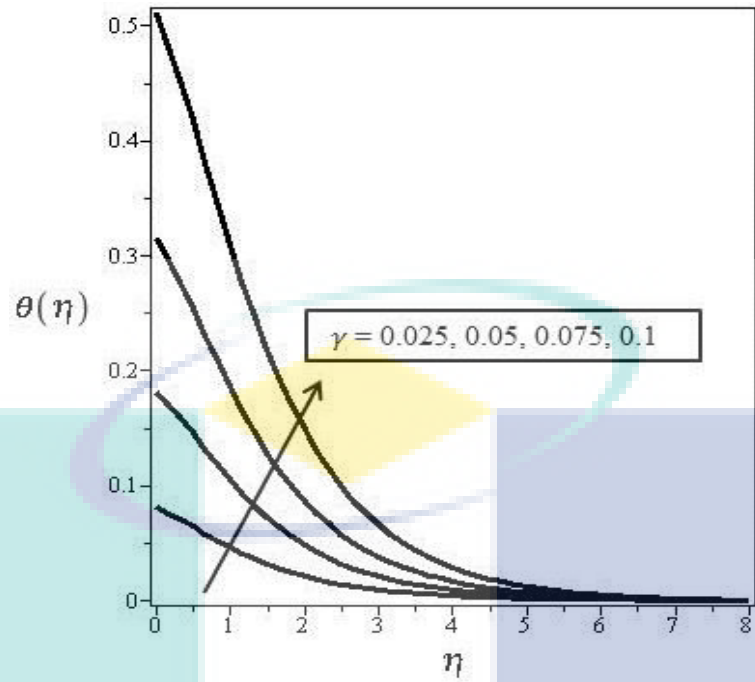
Figure 3.22 Temperature profile for various values of Newtonian heating parameter γ, when $M = 0.2,\ K = 2,\ \beta = 10,\ Sc = 5,\ R = 0.25,\ Nb = 0.5,\ Nt = 0.5$ and $\mathrm{Pr} = 2$.
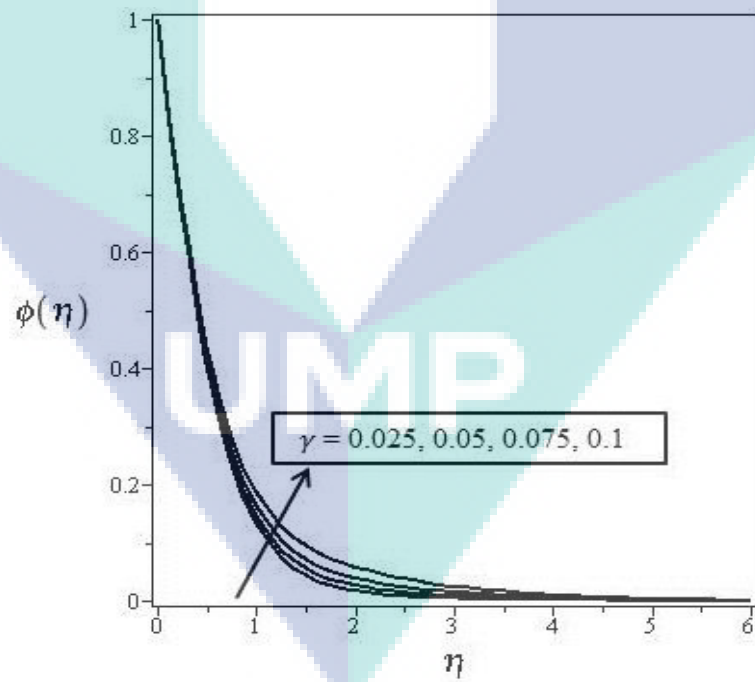
Figure 3.23 Concentration profile for various values of conjugate parameter γ, when $M = 0.2,\ K = 2,\ \beta = 10,\ Sc = 5,\ R = 0.25,\ Nb = 0.5,\ Nt = 0.5$ and $\mathrm{Pr} = 2$.
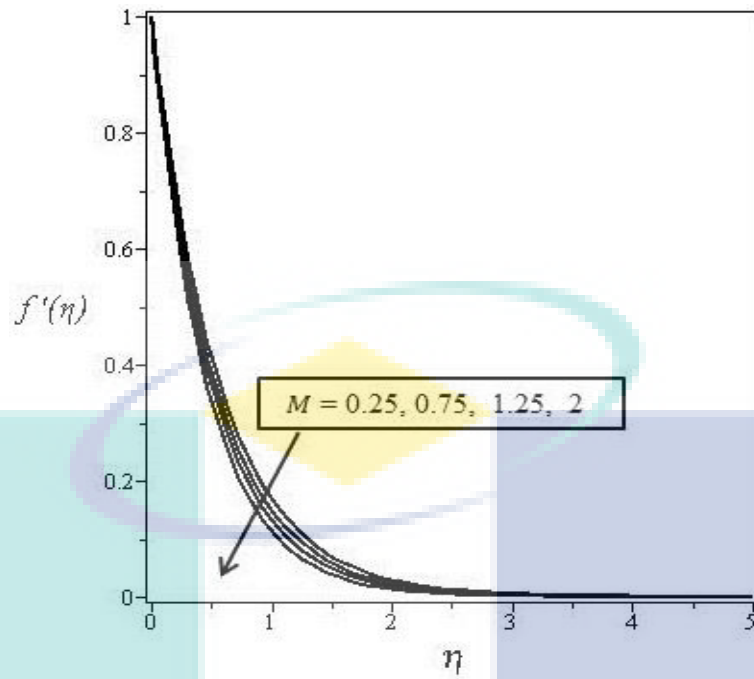
Figure 3.24 Velocity profile for various values of magnetic parameter M, when $K = 2,\ \beta = 10,\ \gamma = 0.115,\ Sc = 5,\ R = 0.25,\ Nb = 0.5,\ Nt = 0.5$ and $\Pr = 2$.
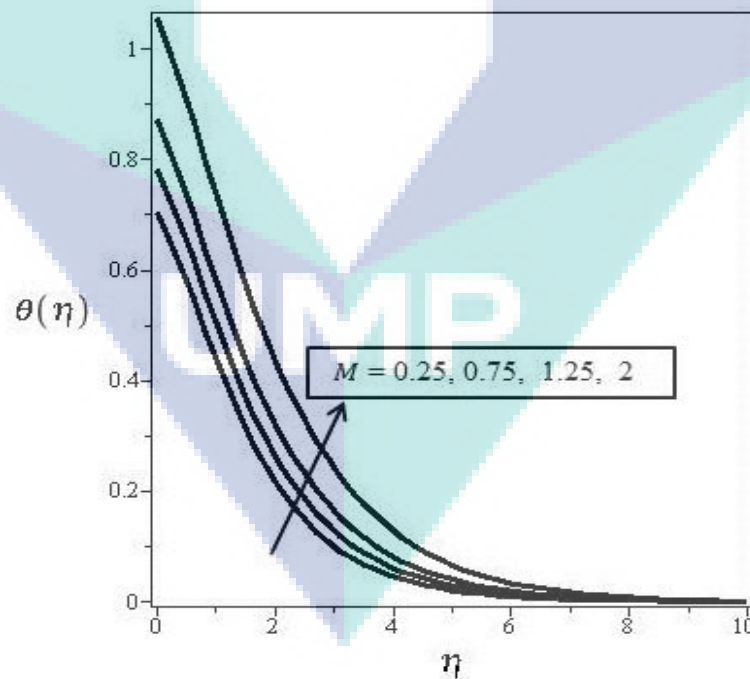
Figure 3.25 Temperature profile for various values of magnetic parameter M, when $K = 2,\ \beta = 10,\ \gamma = 0.115,\ Sc = 5,\ R = 0.25,\ Nb = 0.5,\ Nt = 0.5$ and $\Pr = 2$.
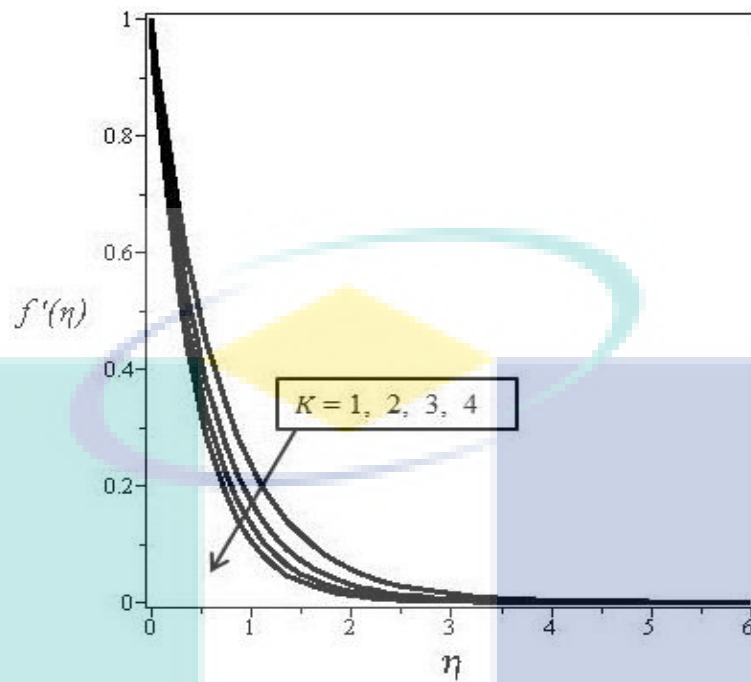
Figure 3.26 Velocity profile for various values of porous medium K, when $M = 2, \beta = 10, \gamma = 0.115, Sc = 5, R = 0.25, Nb = 0.5, Nt = 0.5$ and $\text{Pr} = 2$.
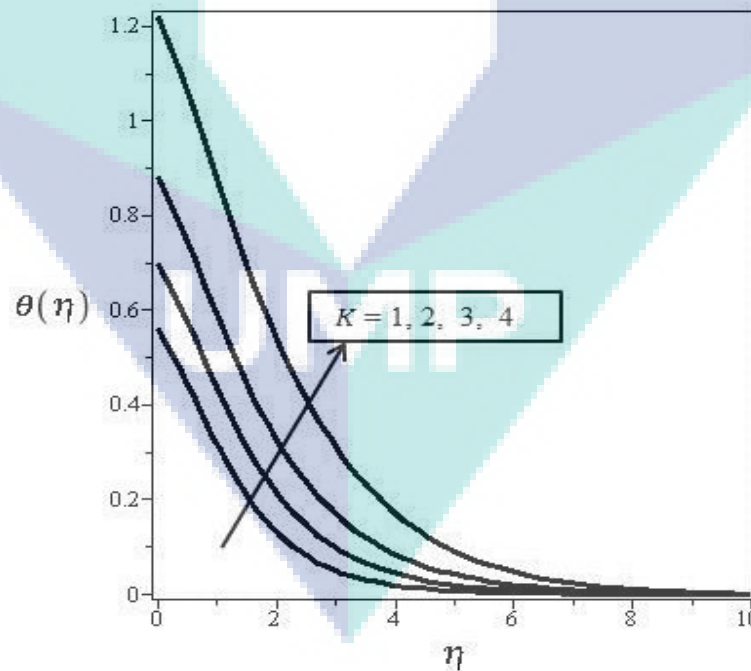
Figure 3.27 Temperature profile for various values of porous medium parameter K, when $M = 2, \beta = 10, \gamma = 0.115, Sc = 5, R = 0.25, Nb = 0.5, Nt = 0.5$ and $\text{Pr} = 2$.
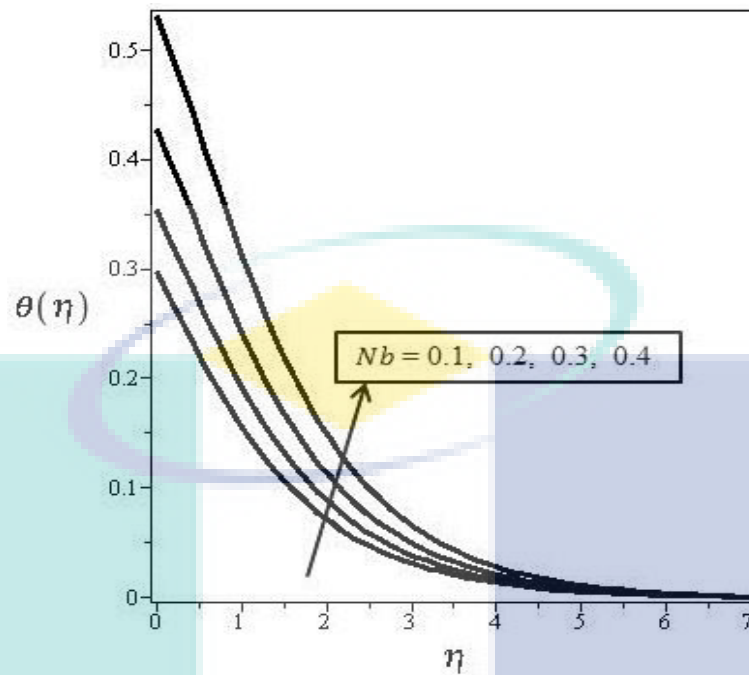
Figure 3.28 Temperature profile for various values of Brownian parameter Nb, when $M = 2,\ \beta = 10,\ K = 2,\ \gamma = 0.115,\ Sc = 5,\ R = 0.25,\ Nt = 0.5$ and $\Pr = 2$.
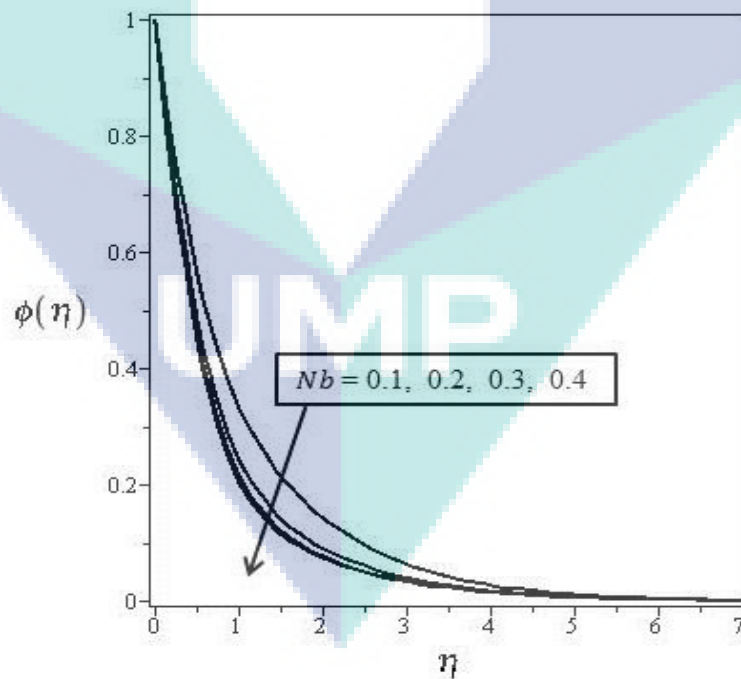
Figure 3.29 Concentration profile for various values of Brownian parameter Nb, when $M = 2,\ \beta = 10,\ K = 2,\ \gamma = 0.115,\ Sc = 5,\ R = 0.25,\ Nt = 0.5$ and $\Pr = 2$.
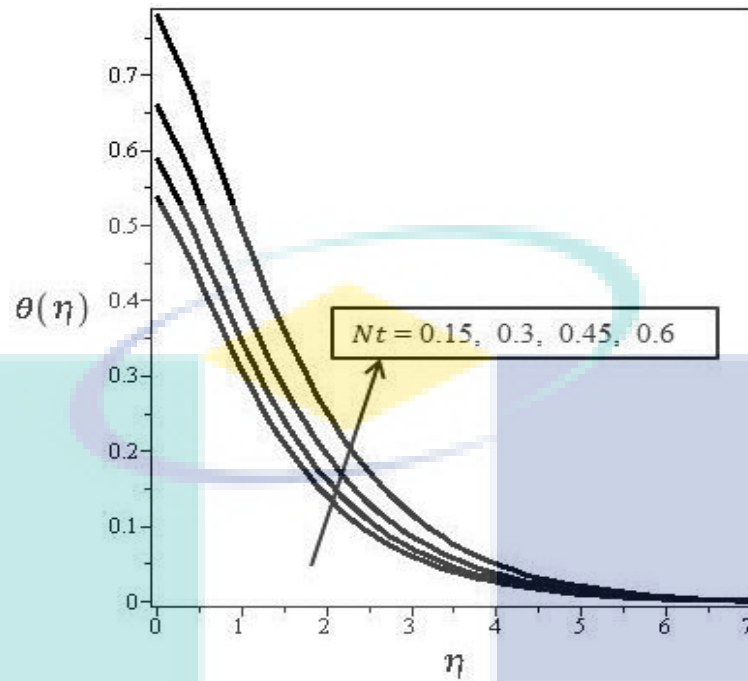
Figure 3.30 Temperature profile for various values of thermophoresis parameter Nt, when $M = 2$, $\beta = 10$, $K = 2$, $\gamma = 0.115$, $Sc = 5$, $R = 0.25$, $Nb = 0.5$ and $\mathrm{Pr} = 2$.
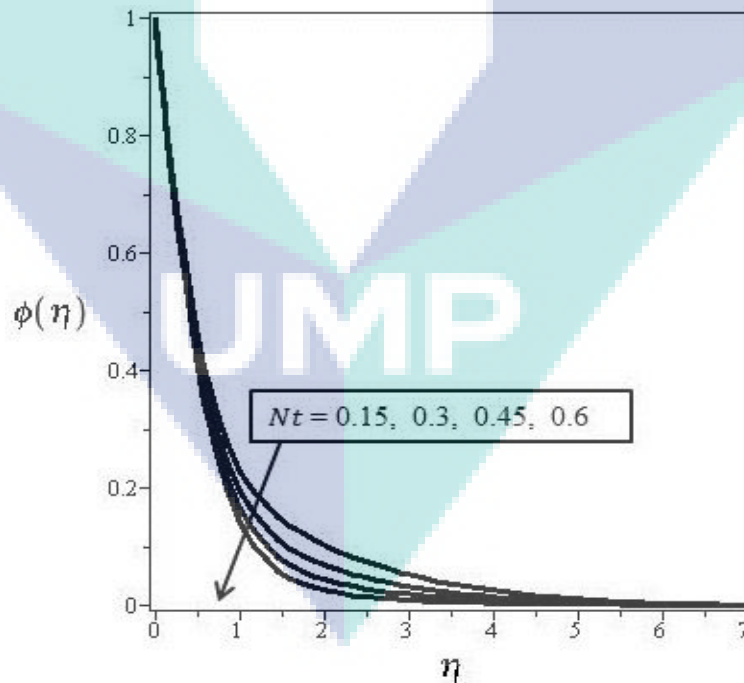
Figure 3.31 Concentration profile for various values of thermophoresis parameter Nt, when $M = 2$, $\beta = 10$, $K = 2$, $\gamma = 0.115$, $Sc = 5$, $R = 0.25$, $Nb = 0.5$ and $\mathrm{Pr} = 2$.
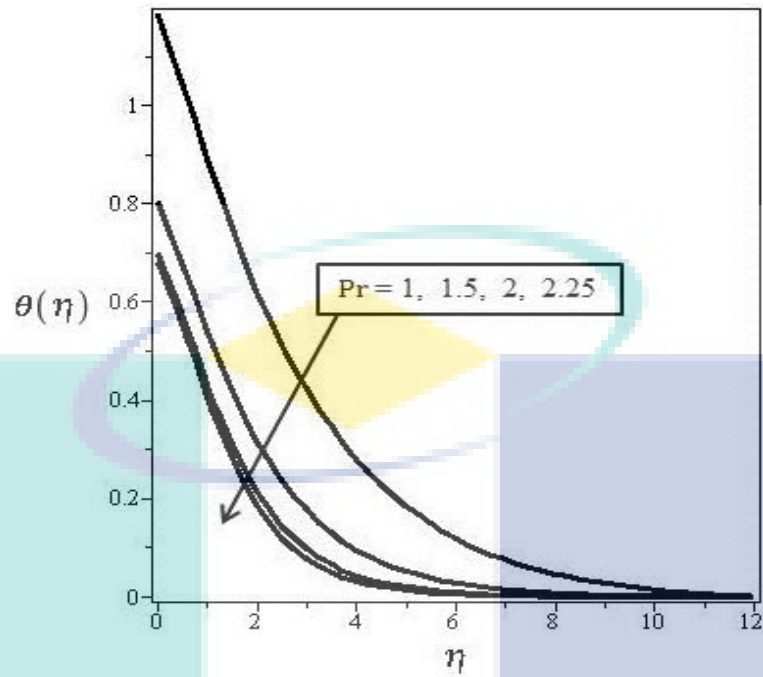
Figure 3.32 Temperature profile for various values of Prandtl number Pr, when $M = 2$, $\beta = 10$, $K = 2$, $\gamma = 0.115$, $Sc = 5$, $R = 0.25$, $Nb = 0.5$ and $Nt = 0.5$.
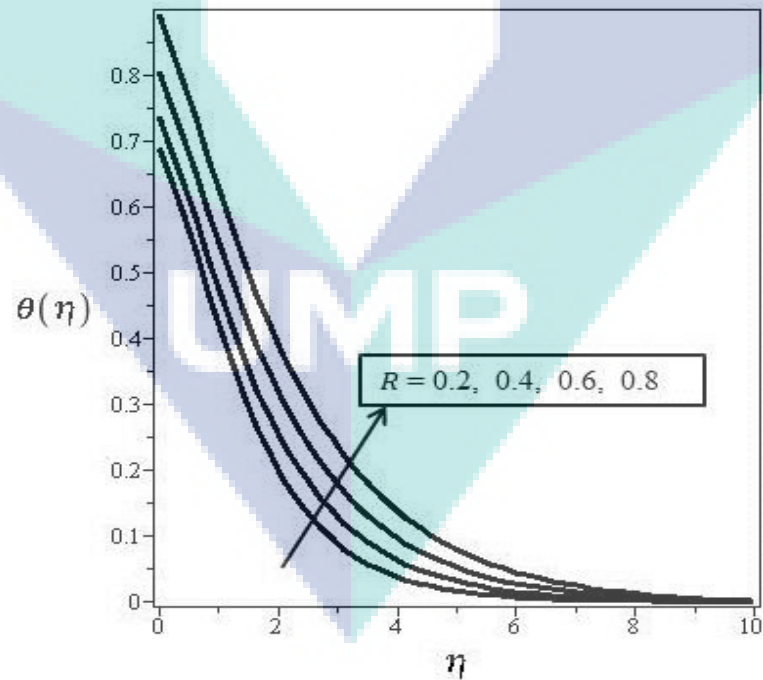
Figure 3.33 Temperature profile for various values of radiation parameter R, when $M = 2$, $\beta = 10$, $K = 2$, $\gamma = 0.115$, $Sc = 5$, $Nt = 0.5$, $Nb = 0.5$ and $Pr = 2$.
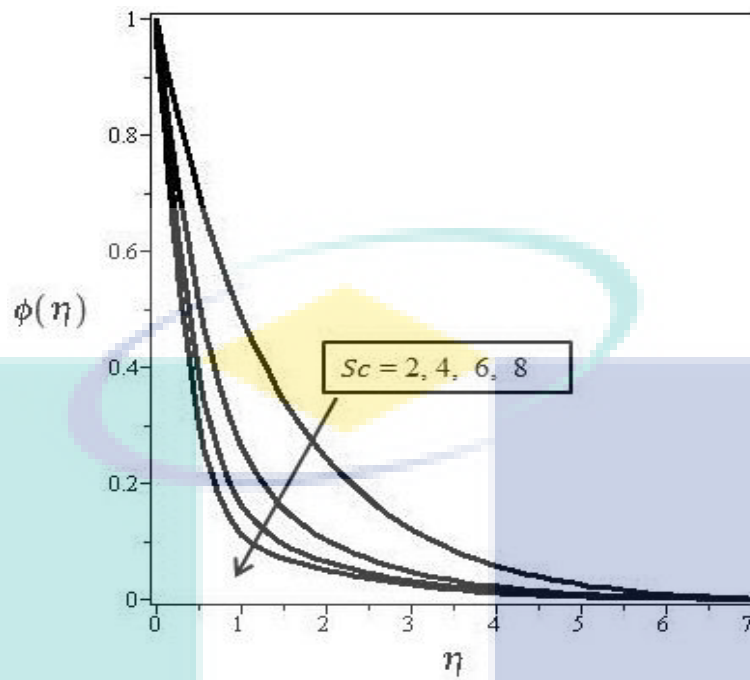
Figure 3.34 Concentration profile for various values of Schmidt number Sc, when $M = 2, \beta = 10, K = 2, \gamma = 0.115, R = 0.25, Nt = 0.5, Nb = 0.5$ and $Pr = 2$.
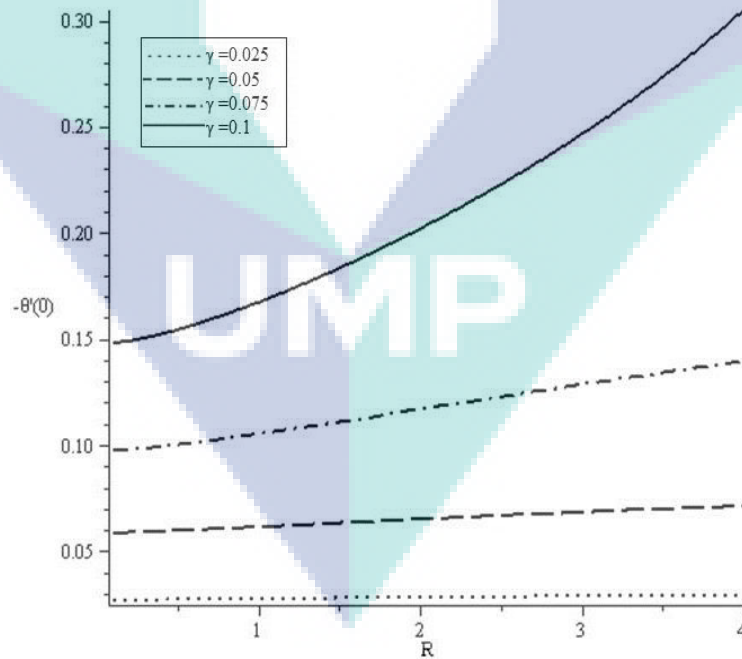
Figure 3.35 The effect of γ and R on local Nusselt number.
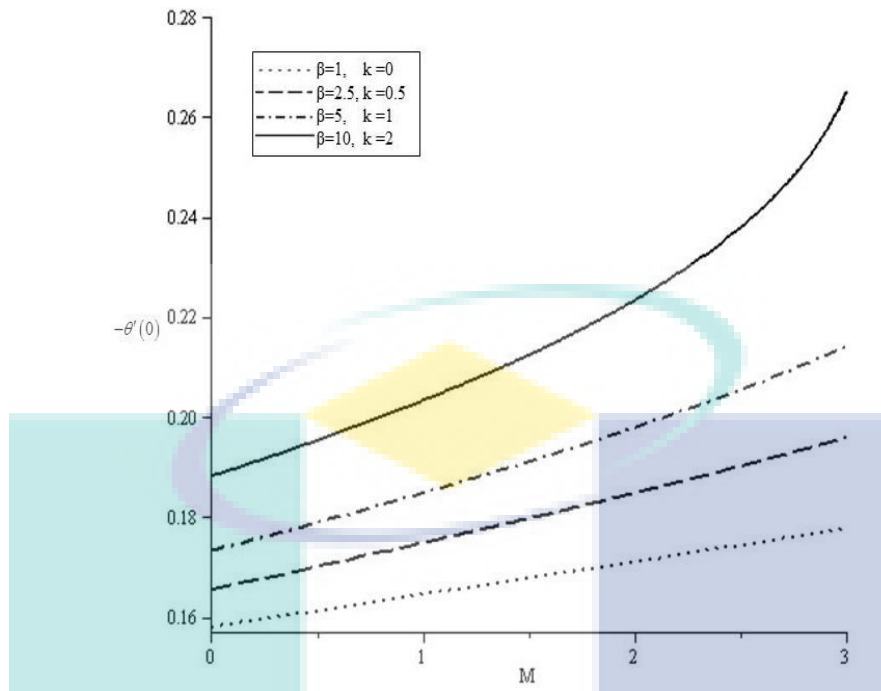
Figure 3.36 The effect of β, K and M on local Nusselt number.
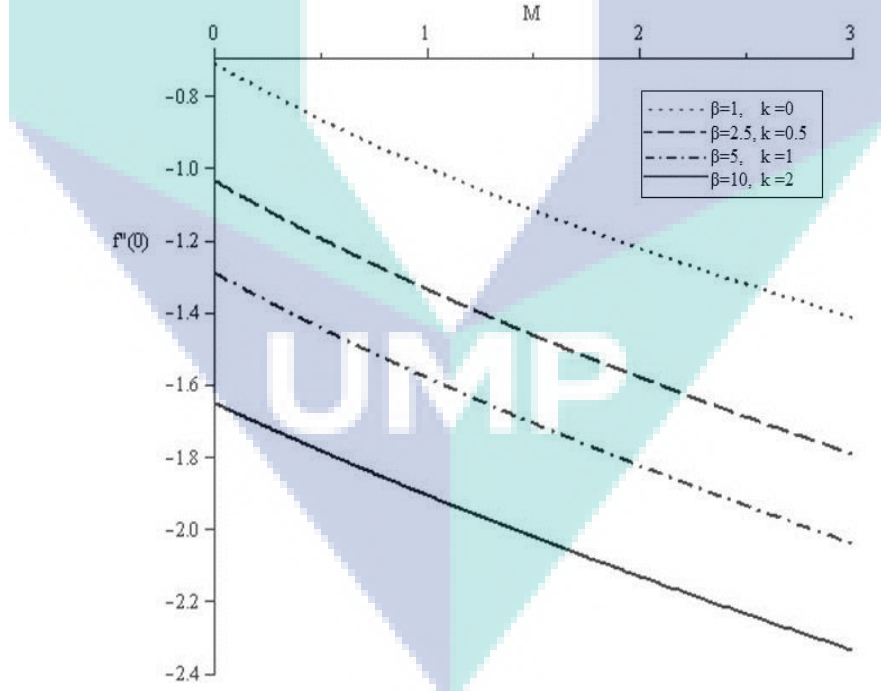
Figure 3.37 The effect of β, K and M on skin friction coefficient.
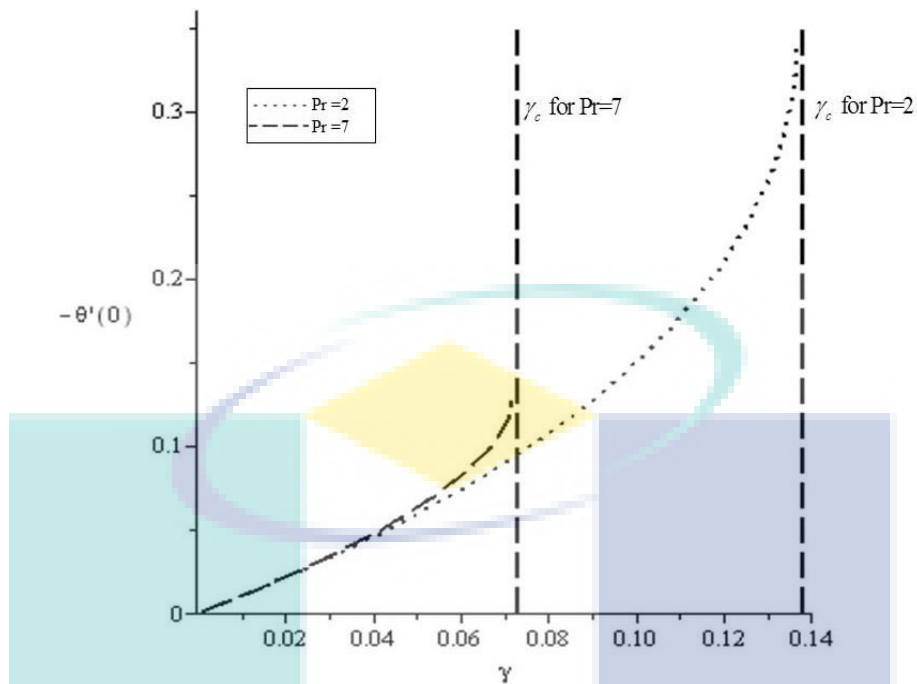
Figure 3.38 Variation of local Nusselt number with critical value of Newtonian heating parameter γ_c when $\mathrm{Pr} = 2$ and 7, respectively.

3.2.4 Summary

Thermal radiation on MHD flow and heat mass transfer over stretching sheet in Casson nanofluid with Newtonian heating were studied numerically. The nonlinear ordinary differential equations were solved numerically using the Shooting method. The result of velocity, temperature and concentration profiles were then presented graphically for different values of the pertinent parameters. Also, the skin friction coefficient, local Nusselt number and Sherwood number were examined with influence of various parameters. The results are summarized as below:

- When the Casson nanofluid parameter increased, magnetic parameter and porosity parameter, the thickness of boundary layer of temperature and concentration profile would also increase but the velocity distribution would decrease.
- Temperature profile would decrease when Prandlt parameter number increased.
- Increase of Brownian motion parameter resulted concentration profile decreases but temperature profile increases.
- An increase in thermophoresis parameter would cause temperature and concentration profiles to decrease.

74

- Temperature profile would increase when the radiation parameter increased.
- Concentration profile would decrease when Schmidt number increased.
- Skin friction coefficient as well as local Nusselt and Sherwood number would decreased at all time as β and M in the fluid increased.
- The thickness of boundary layer would increase as the Newtonian heating parameter and radiation parameter increased.
- The skin friction coeffient would drop and local Nusselt number would rise when the Casson parameter, magnetic parameter and porosity parameter increased simultaneously.
- To obtain a physically appropriate solution, the value of γ must be less than γ_c and with an acceptable range of values of $\Pr$.

Table 3.3 The computation results with all the parameters for local skin friction coefficient, local Nusselt number and local Sherwood number, respectively.

β	M	K	γ	R	Nt	Nb	Sc	Pr	$\left(1+\dfrac{1}{\beta}\right)f''(0)$	$-\theta'(0)$	$-\phi'(0)$
0.5	0.2	2	0.115	0.25	0.5	0.5	5	2	-1.5491	0.2167	
1									-1.6124	0.2218	
5									-1.7320	0.2335	
10									-1.7580	0.2365	
10	0.25	2	0.115	0.25	0.5	0.5	5	2	-1.7709	0.1960	
	0.75								-1.8949	0.2048	
	1.25								-2.0113	0.2152	
	2								-2.1742	0.2365	
10	0.2	1			0.5	0.5	5	2	-1.4459	0.1793	
			0.115	0.25							
		2							-1.7580	0.1952	
		3							-2.0226	0.2163	
		4							-2.2563	0.2554	
10	0.2	2	.025	0.25	0.5	0.5	5	2		0.0270	1.3918
			0.05							0.0590	1.3794
			0.075							0.0986	1.3644
			0.1							0.1511	1.3455
10	0.2	2	0.115	0.2	0.5	0.5	5	2		0.1942	
				0.4						0.1996	
				0.6						0.2076	
				0.8						0.2176	
10	0.2	2	0.115	0.25	0.15	0.5	5	2		0.1769	1.3819
					0.3					0.1827	1.3609
					0.45					0.1909	1.3393
					0.6					0.2048	1.3161
10	0.2	2	0.115	0.25	0.5	0.1	5	2		0.1493	1.0164
						0.2				0.1557	1.2134
						0.3				0.1642	1.2792
						0.4				0.1761	1.3122

CHAPTER 4

SLIP CONDITIONS ON FLOW AND HEAT TRANSFER ANALYSIS OF WILLIAMSON NANOFLUID OVER A STRETCHING SHEET

4.1 Introduction

The existence of slip conditions on interface of nanofluids and the solid boundary is caused by the presence of nanoparticles as reported by Ibrahim and Shankar (2013). Thus, this topic mainly focuses on the slip conditions with heat transfer analysis in Williamson nanofluid flow over stretching sheet. Due to the appearance of dynamic viscosity, velocity and thermal slip factors, two types of slip conditions have been considered, namely velocity and thermal slip parameters. The mathematical formulation has been described well in relation to the slip parameters and through the similarity transformations, the governing equations are transformed into non-linear ordinary differential equations. In addition, the closed form numerical solutions for velocity, temperature and concentration are obtained as well as for skin friction, heat transfer rate and Sherwood number. These solutions have been plotted graphically and discussed for each parameter. The comparison of viscous case has been carried out and computational software Maple-13 has been used to solve the problems.

4.2 Mathematical Formulation

A two-dimensional viscous flow of Williamson nanofluid over a stretching plate where the flow was incompressible and in steady state has been considered. The velocity of surface has been linear and could be represented by $U_w(x) = bx$ while b and x represented the constant and the coordinate measured along the stretching plate, respectively. In addition, y would be the coordinate measured normal to the stretching

plate and flow of nanofluid at $y = 0$. It can be assumed that the wall temperature of $T_w = ax^2 + T_\infty$ and the fraction of nanoparticles C_w would be constant at the stretching surface. When y would be approaching infinity, the ambient values of temperature and nanoparticle fraction would be denoted as T_∞ and C_∞, respectively.
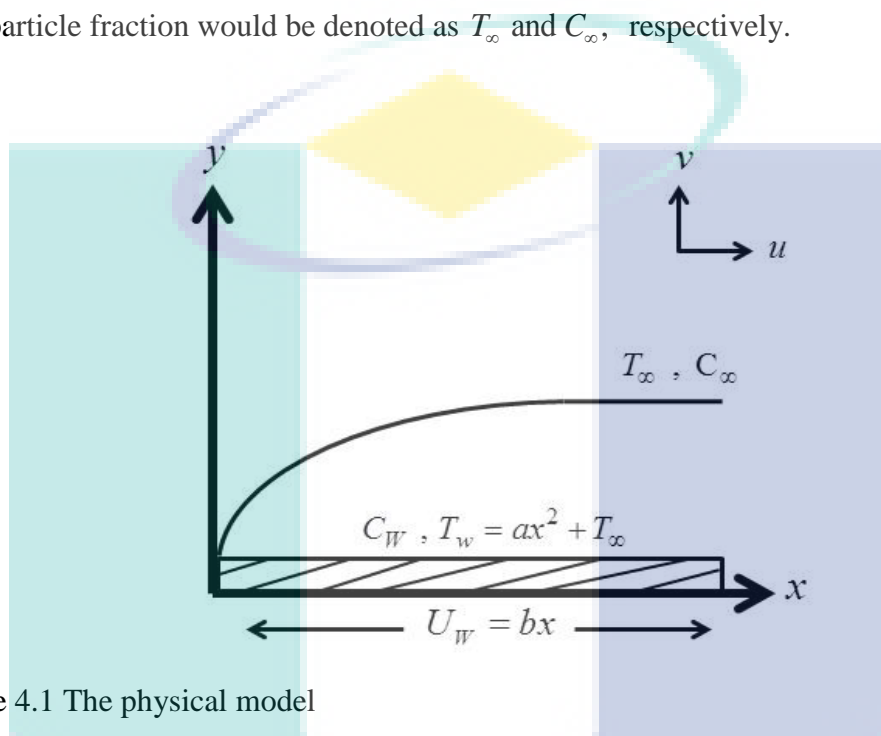
Figure 4.1 The physical model

The constitutive equations of Williamson fluid model are given as:

$$\mathbf{S} = -p\mathbf{I} + \tau \qquad\qquad 4.1$$

in which p is the pressure, $\mathbf{I}$ is the identity vector, τ is the extra stress tensor and $\mathbf{S}$ is Cauchy stress tensor and

$$\tau = \mu\left[1 + \Gamma\chi\right]\mathbf{A}_1 \qquad\qquad 4.2$$

where μ is the limiting velocities at zero, Γ is the time constant, $\mathbf{A}_1$ is first Rivlin-Erickson tensor and χ is defined as follows:

$$\chi = \sqrt{\frac{1}{2}\pi} \qquad\qquad 4.3$$

Based on the Figure 4.1, the two dimensional boundary layer governing equations of non-Newtonian Williamson nanofluid flow would be as follows:

$$u \frac{\partial u}{\partial x} + v \frac{\partial u}{\partial y} = \nu \frac{\partial^2 T}{\partial y^2} + \sqrt{2} \nu \Gamma \frac{\partial u}{\partial y} \frac{\partial^2 T}{\partial y^2} \tag{4.4}$$

$$u \frac{\partial T}{\partial x} + v \frac{\partial T}{\partial y} = \alpha \frac{\partial^2 T}{\partial y^2} + \frac{\rho_p C_p}{\rho C} \left[D_B \frac{\partial C}{\partial y} \frac{\partial T}{\partial y} + \frac{D_T}{T_\infty} \left(\frac{\partial T}{\partial y} \right)^2 \right] \tag{4.5}$$

$$u \frac{\partial C}{\partial x} + v \frac{\partial T}{\partial y} = D_B \frac{\partial^2 C}{\partial y^2} + \frac{D_T}{T_\infty} \frac{\partial^2 T}{\partial y^2} \tag{2.5}$$

With the corresponding boundary conditions would be as below:

$$u = u_w + \delta^* \mu \left(\frac{\partial u}{\partial y} \right), \quad v = 0, \ T = T_w + B^* \frac{\partial T}{\partial y}, \quad C = C_w \ \text{at} \ y = 0. \tag{4.6}$$
$$u \to 0, \ T \to T_\infty, \ C = C_\infty \ \text{as} \ y \to \infty.$$

By following Yasin et al. (2016), the similarity transformations would be as below:

$$u = bx f'(\eta) \tag{4.7}$$

$$v = -\sqrt{b\nu} f(\eta) \tag{4.8}$$

$$\eta = \sqrt{\frac{b}{\nu}} y \tag{2.7}$$

$$\theta(\eta) = \frac{T - T_\infty}{T_w - T_\infty} \tag{2.10}$$

$$\phi(\eta) = \frac{C - C_\infty}{C_W - C_\infty} \tag{2.12}$$

The governing equations then could be reduced to ordinary differential equations by using the following similarity transformations:

$$f'''(\eta) + \lambda f'''(\eta) f''(\eta) + f''(\eta) f'(\eta) - f'^2(\eta) = 0 \tag{4.9}$$

$$\theta''(\eta) + \Pr f(\eta) \theta'(\eta) - 2\Pr f'(\eta) \theta(\eta) + \frac{Nc}{Le} \theta'(\eta) \phi'(\eta) + \frac{Nc}{(Le)(Nbt)} \theta'^2(\eta) = 0 \tag{4.10}$$

$$\phi''(\eta) + Sc f(\eta) \phi'(\eta) + \frac{1}{Nbt} \theta''(\eta) = 0 \tag{4.11}$$

79

Where $\lambda = \sqrt{\dfrac{2b^3}{\nu}}\Gamma x$, $\Pr = \dfrac{\nu}{\alpha}$, $Nc = \dfrac{\rho_p C_p}{\rho C}(C_W - C_\infty)$, $Nbt = \dfrac{T_\infty D_B (C_W - C_\infty)}{D_T (T_W - T_\infty)}$,

$Le = \dfrac{\alpha}{D_B}$, $Sc = \dfrac{\nu}{D_B}$. The f, θ and ϕ would be functions of η and prime denoting

derivatives with respect to η the corresponding boundary conditions would take the

following form:

$$f(0) = 0, \ f'(0) = 1 + \delta f''(0), \ \theta(0) = 1 + B\theta'(0), \ \phi(0) = 1 \quad \text{as } y = 0.$$
$$f'(\infty) = 0, \ \theta(\infty) = 0, \ \phi(\infty) = 0 \quad \text{as } y \to 0.$$

4.12

The physical quantities of interest were skin friction coefficient C_f, local Nusselt

number Nu and local Sherwood number Sh, defined as

$$C_f = \dfrac{\tau_w}{\rho U_W^2}, \quad Nu = -\dfrac{x q_w}{T_W - T_\infty}\dfrac{\partial T}{\partial y}\bigg|_{y=0} \quad \text{and} \quad Sh = -\dfrac{x}{C_w - C_\infty}\dfrac{\partial C}{\partial y}$$

4.13

where the shear stress $\tau_w = \mu\left[\dfrac{\partial u}{\partial y} + \dfrac{\Gamma}{\sqrt{2}}\left(\dfrac{\partial u}{\partial y}\right)^2\right]$. Using the non-dimensional variables,

the following was obtained

$$C_f.\sqrt{\mathrm{Re}} = f''(0) + \dfrac{\lambda}{2}f''^2(0), \quad \dfrac{Nu}{\sqrt{\mathrm{Re}}} = -\theta'(0) \quad \text{and} \quad \dfrac{Sh}{\sqrt{\mathrm{Re}}} = -\phi'(0).$$

4.14

where $\mathrm{Re} = \dfrac{b}{\nu}x^2$ is the local Reynold's number. The detailed explanation of

mathematical formulation for this chapter is providein Appendix C of this thesis.

4.3 Results and Discussion

The non-linear partial differential equations were solved with similarity
transformations and transformed to ordinary differential equations, which were
then derived manually based on the given boundary conditions. Next, the derived
equations were solved by using the Shooting method. Thus, unknown initial conditions
$\eta = 0$ may be obtained by using Shooting method and the initial values for boundary
value problem may be assumed. The calculated boundary values should be similar to
the real boundary values, hence, the values should be as close to the boundary values

are appropriate to consider. In this study, there were no considerations of variation in temperature, velocity and concentration and we assume large infinity condition but finite value for η. the value of $\eta \geq 6$ was chosen because this value would be sufficient to achieve asymptotic boundary conditions for all parameters considered.

Table 4.1 The comparison of local Nusselt number $-\theta'(0)$ for Prandlt number in viscous case.

Pr	Ishak et al. (2009) by Keller Box method	Hayat et al. (2008) by Homotophy Analysis method	Present study by Shooting method
0.72	0.8086	0.808631	0.808834
1	1.0000	1.000000	1.000008
3	1.9237	1.923591	1.923678
10	3.7207	3.721596	3.720671

Based on the comparison with previous results undertaken by other researchers, it was discovered there had been good consensus in the results. Thus, this technique can be concluded to have worked efficiently and the results presented here are accurate and reliable.

This section includes the graphical results for velocity, temperature and concentration profiles for the relevant variables such as velocity slip parameter δ, thermal slip parameter B, non-Newtonian Williamson parameter λ, Prandtl number Pr, heat capacities ratio parameter Nc, diffusivity ratio parameter Nbt, Lewis number Le and Schmidt number Sc, respectively. Figures 4.2, 4.3 and 4.4 depict the various values of velocity slip factor parameter for velocity, temperature and concentration profile respectively. The graphical results show that the value of velocity profile would reduce as the velocity slip factor parameter increased. Meanwhile, the wall temperature would decrease as the velocity slip factor parameter increased. However, the volume fraction of nanoparticles would increase as the velocity slip factor parameter increased. Figures 4.5 and 4.6 illustrate the temperature and concentration profiles on thermal slip parameter. It was found that the wall temperature and volume fraction of nanoparticles had decreased due to an increase in thermal slip parameter. Figures 4.7, 4.8 and 4.9

present several values of non-Newtonian Williamson parameter on velocity, temperature and concentration profile, respectively. As the value of velocity profile decreased, the wall temperature and concentration profiles would increase simultaneously when the Williamson parameter increased. Furthermore, the skin friction coefficient for Williamson nanofluid would get lower as the non-Newtonian Williamson parameter increased. It would be suitable to be used as lubricant in cooling system because the suspended nanoparticles that could keep stay longer in the base fluids would enhance the flow characteristics of nanofluids.

Figure 4.10 shows the Prandlt number on temperature profile. The increment of Prandlt number caused the slow rate in thermal diffusion; thus, the temperature profile was reducing at all times. Figure 4.11 depicts the heat capacities ratio effect on temperature profile. It can be seen that the wall temperature would increase when the heat capacities ratio parameter increased. Also, the boundary layer thickness would decrease in this case. Therefore, the greater the value of radiation parameter, the larger the superficial heat flux would be. Figure 4.12 illustrates the Lewis number on temperature profile. Lewis number would also refer to the thermal to species diffusivity ratio. Lewis number is considered for conditions where the temperature and mass fraction are larger by defining temperature and diffusivities, in which reduced the convective heat transfer. Thus, the wall temperature is decreasing function against Lewis number. Figures 4.13 and 4.14 depicted the different value of diffusivity ratio parameter on temperature and concentration profile respectively. The value of both the profile dropped as the value of diffusivity parameter increases. Figure 4.15 presented the Schmidt number on concentration profile. The value of the profile getting less and lesser as the value of Schmidt number increases.

Figure 4.16 presents the effect of B and Pr on temperature gradient. When the value of Pr was small, the temperature gradient would be high. However, increasing the Prandtl number would lead to a sharp drop in the heat transfer rate. The effect of Nb and Nt on temperature gradient is shown in Figure 4.17. It is clear that the temperature gradient would rise as the value of Brownian motion parameter and thermophoretic parameter increased. Figure 4.18 depicts the effect of Le and Pr on temperature gradient. Based on the diagram, the gradient of wall temperature would

increase when the Prandtl number and Lewis number increased. The skin friction coefficient, gradient temperature and concentration with all the parameters are shown in Table 4.2.
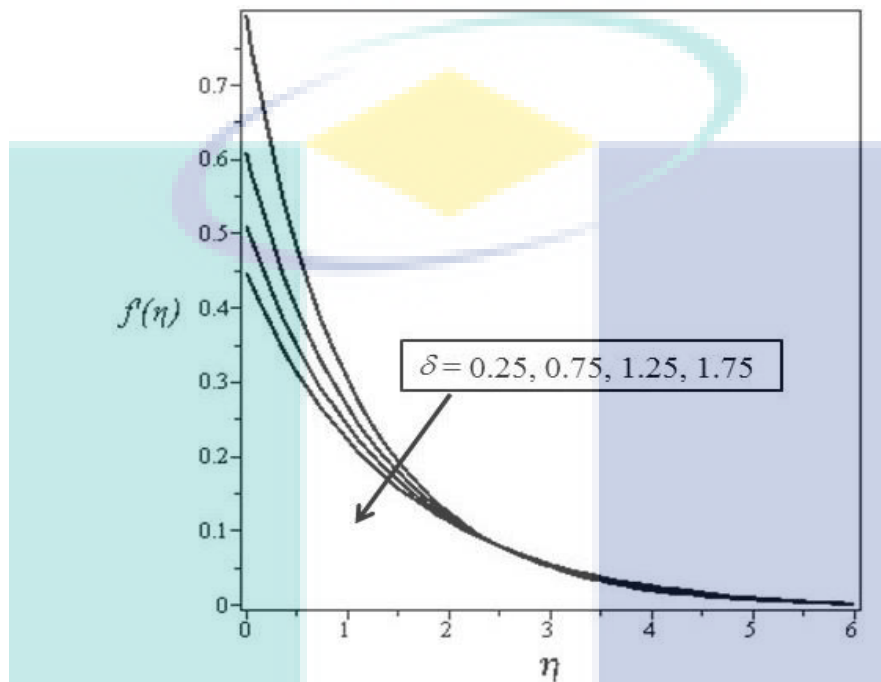
Figure 4.2 Velocity profile for various values of slip parameter δ, when $\lambda = 0.5$, $B = 1$, $Nc = 2.5$, $Nbt = 2$, $Le = 10$, $Sc = 5$ and $\Pr = 7$.
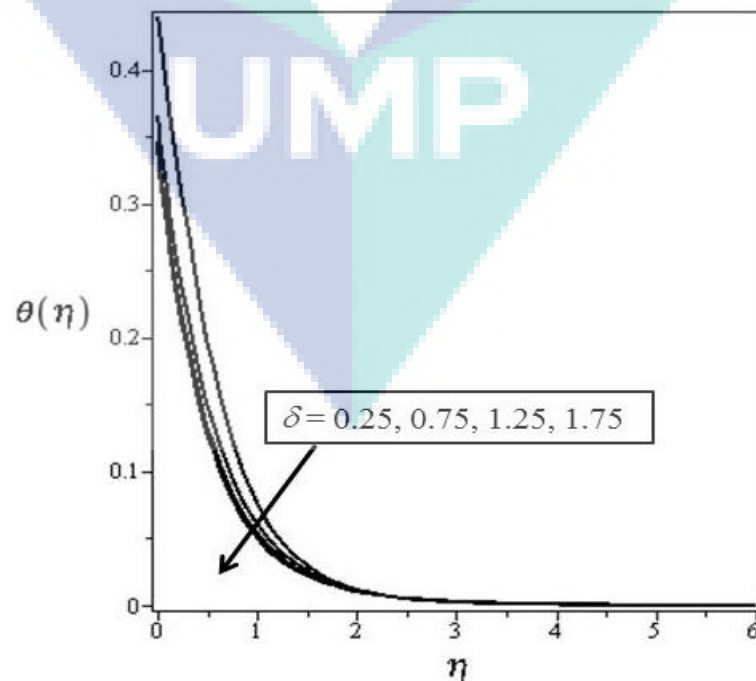
Figure 4.3 Temperature profile for various values of velocity slip parameter δ, when $\lambda = 0.5$, $B = 1$, $Nc = 2.5$, $Nbt = 2$, $Le = 10$, $Sc = 5$ and $\Pr = 7$.
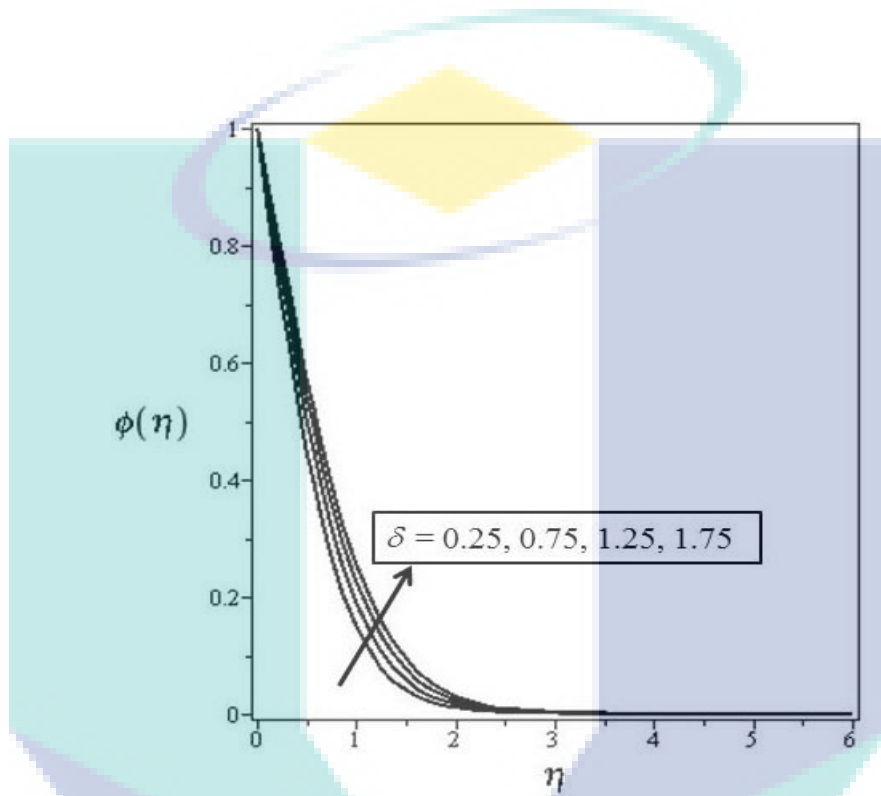
Figure 4.4 Concentration profile for various values of velocity slip parameter δ, when $\lambda = 0.5$, $B = 1$, $Nc = 2.5$, $Nbt = 2$, $Le = 10$, $Sc = 5$ and $\Pr = 7$.
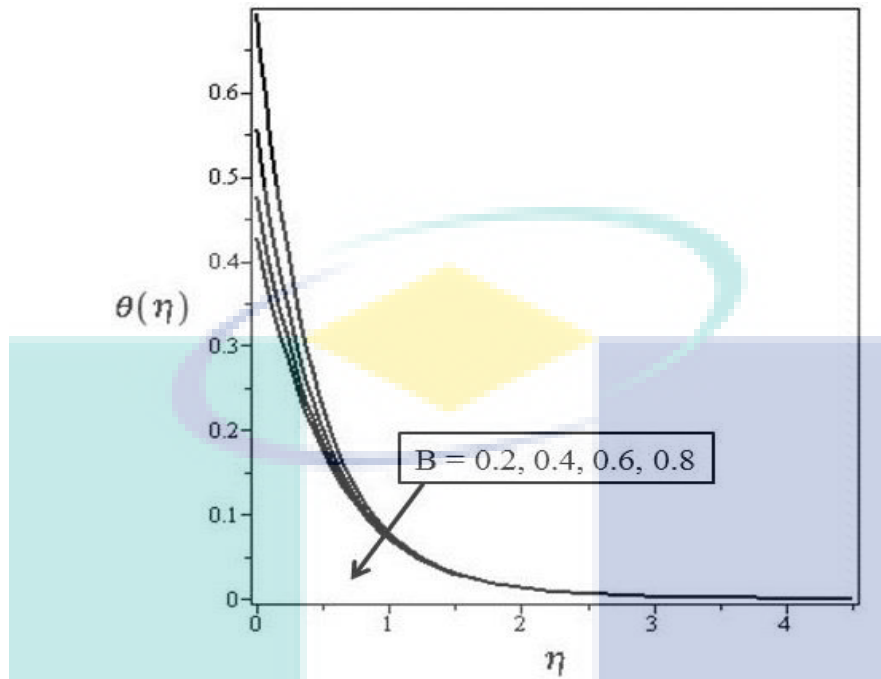
Figure 4.5 Temperature profile for various values of thermal slip parameter B, when $\lambda = 0.5,\ \delta = 0.5,\ Nc = 2.5,\ Nbt = 2,\ Le = 10,\ Sc = 5$ and $\Pr = 7$.
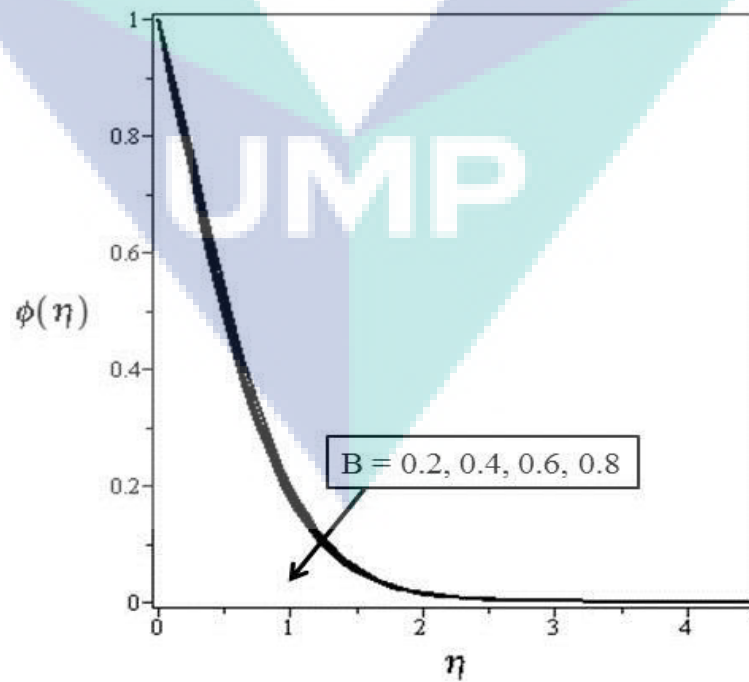
Figure 4.6 Concentration profile for various values of thermal slip parameter B, when $\lambda = 0.5,\ \delta = 0.5,\ Nc = 2.5,\ Nbt = 2,\ Le = 10,\ Sc = 5$ and $\text{Pr} = 7$.
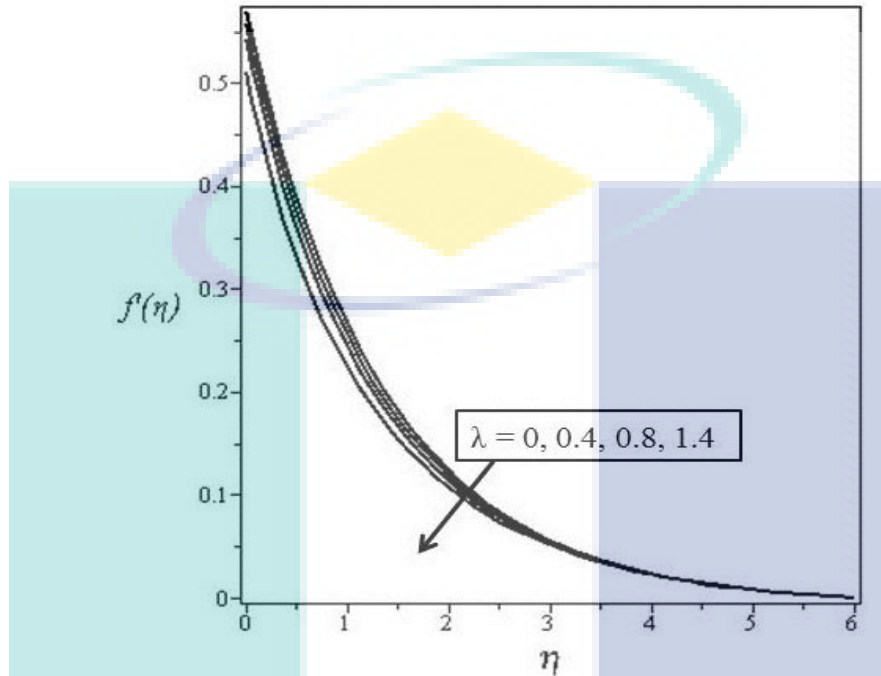
Figure 4.7 Velocity profile for various values of Williamson parameter λ, when $B = 0.5,\ \delta = 0.5,\ Nc = 2.5,\ Nbt = 2,\ Le = 10,\ Sc = 5$ and $\text{Pr} = 7$.
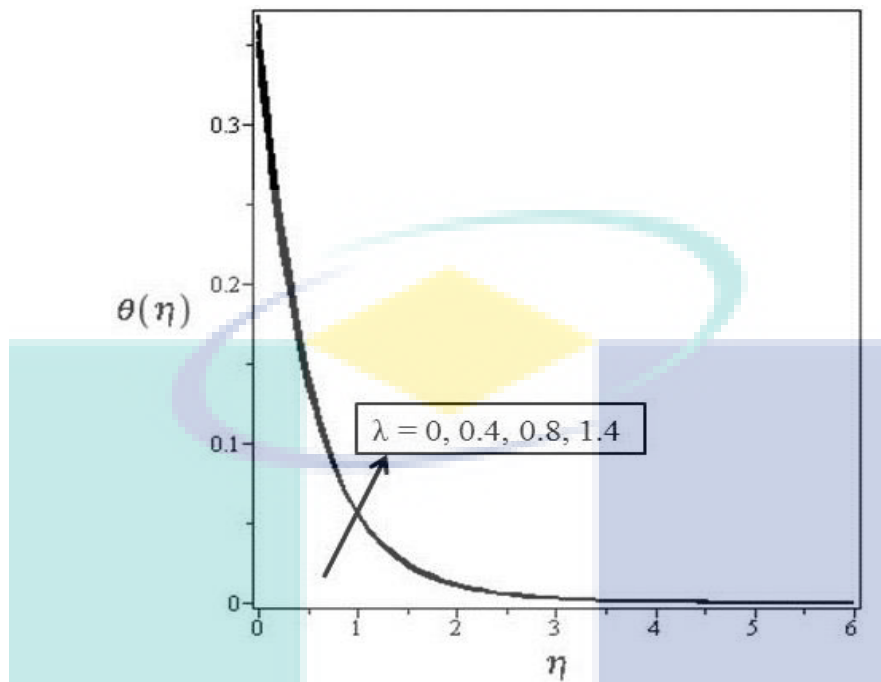
Figure 4.8 Temperature profile for various values of Williamson parameter λ, when $B = 0.5$, $\delta = 0.5$, $Nc = 2.5$, $Nbt = 2$, $Le = 10$, $Sc = 5$ and $\Pr = 7$.
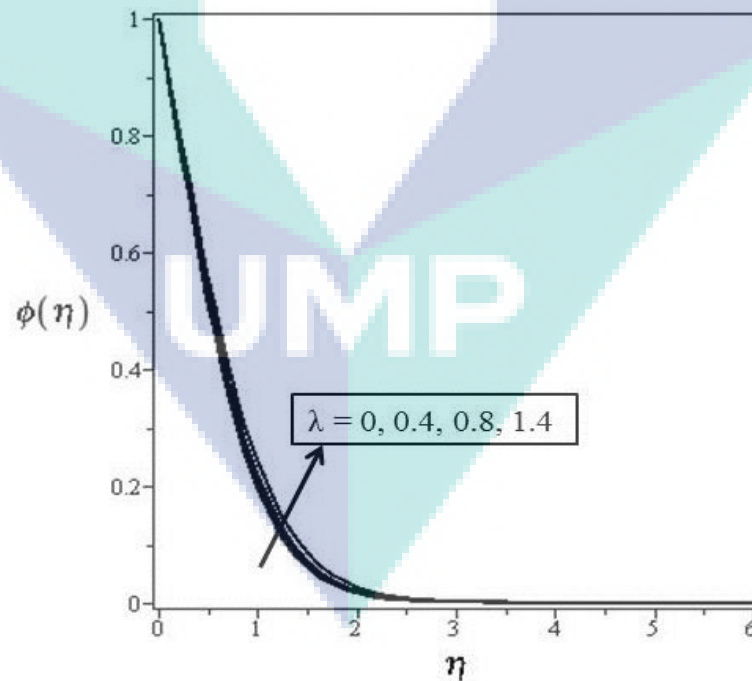
Figure 4.9 Concentration profile for various values of Williamson parameter λ, when $B = 0.5$, $\delta = 0.5$, $Nc = 2.5$, $Nbt = 2$, $Le = 10$, $Sc = 5$ and $\Pr = 7$.
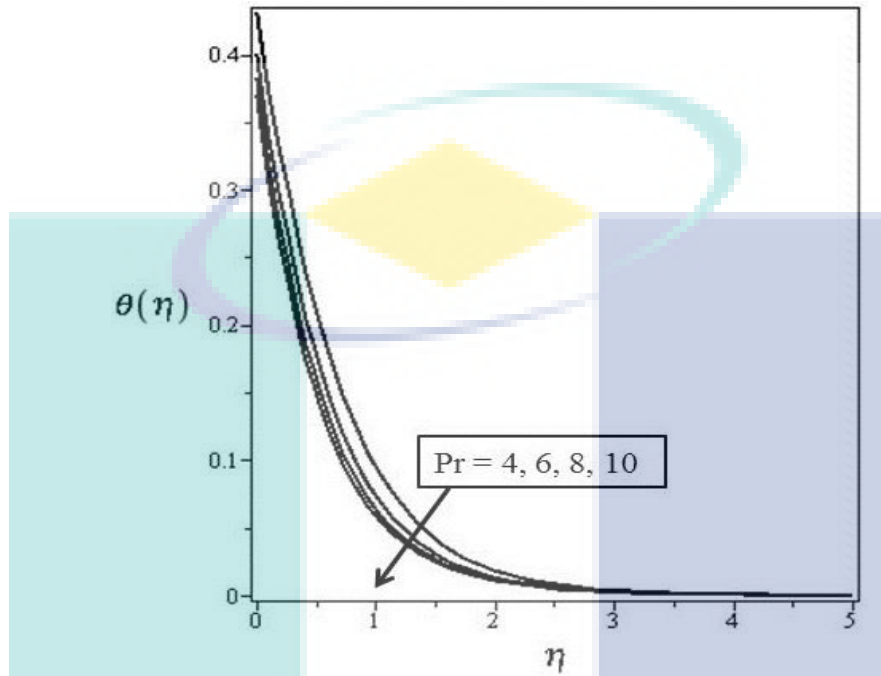
Figure 4.10 Temperature profile for various values of Prandlt number Pr, when $\lambda = 0.5$, $B = 0.5$, $\delta = 0.5$, $Nc = 2.5$, $Nbt = 2$, $Le = 10$ and $Sc = 5$.
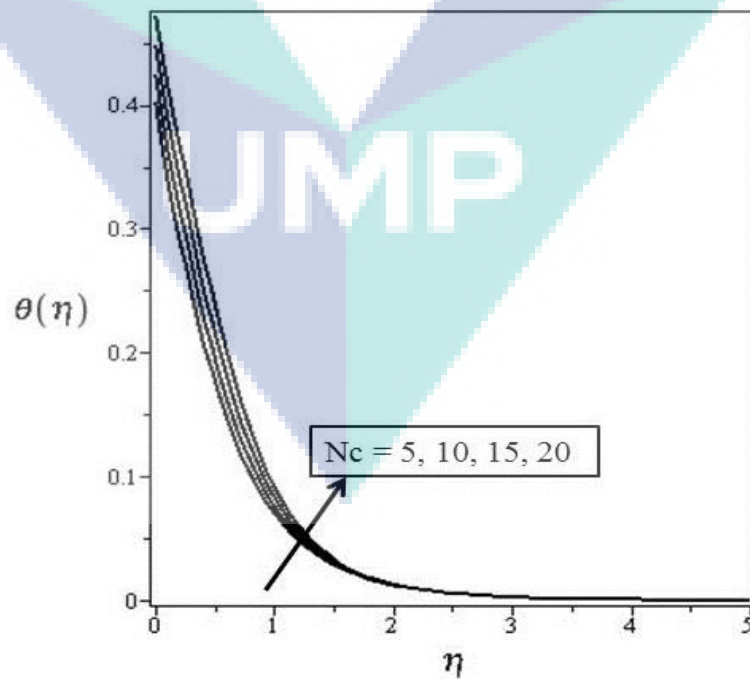
Figure 4.11 Temperature profile for various values of heat capacities ratio parameter Nc, when $\lambda = 0.5$, $B = 0.5$, $\delta = 0.5$, $Nbt = 2$, $Le = 10$, $Sc = 5$ and $\Pr = 7$.
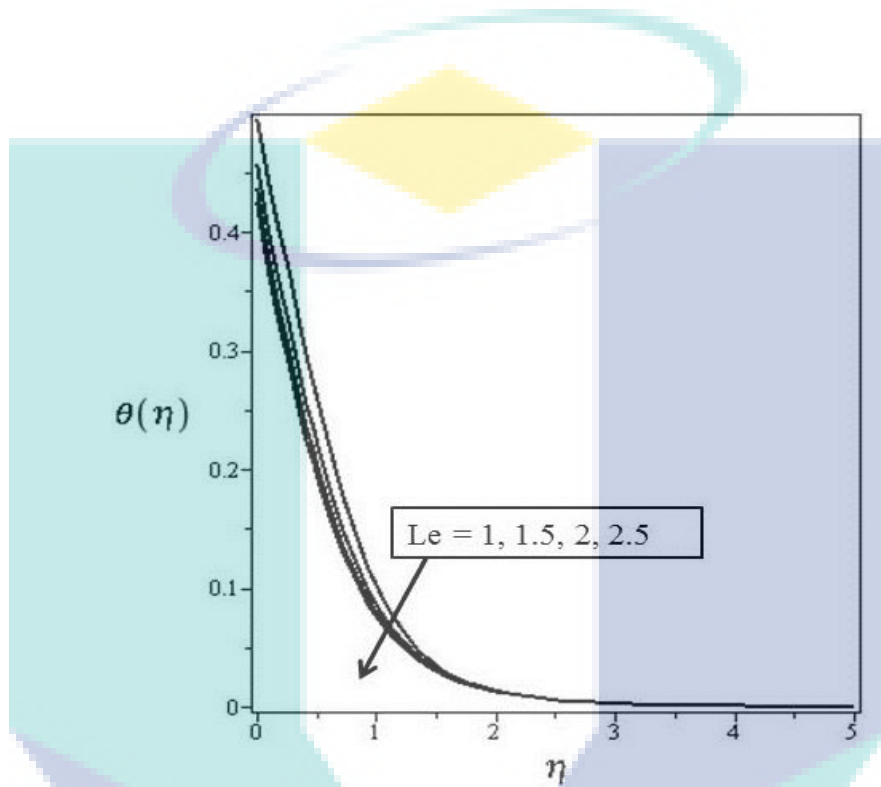
Figure 4.12 Temperature profile for various values of Lewis number Le, when $\lambda = 0.5$, $B = 0.5$, $\delta = 0.5$, $Nc = 2.5$, $Nbt = 2$, $Sc = 5$ and $\Pr = 7$.
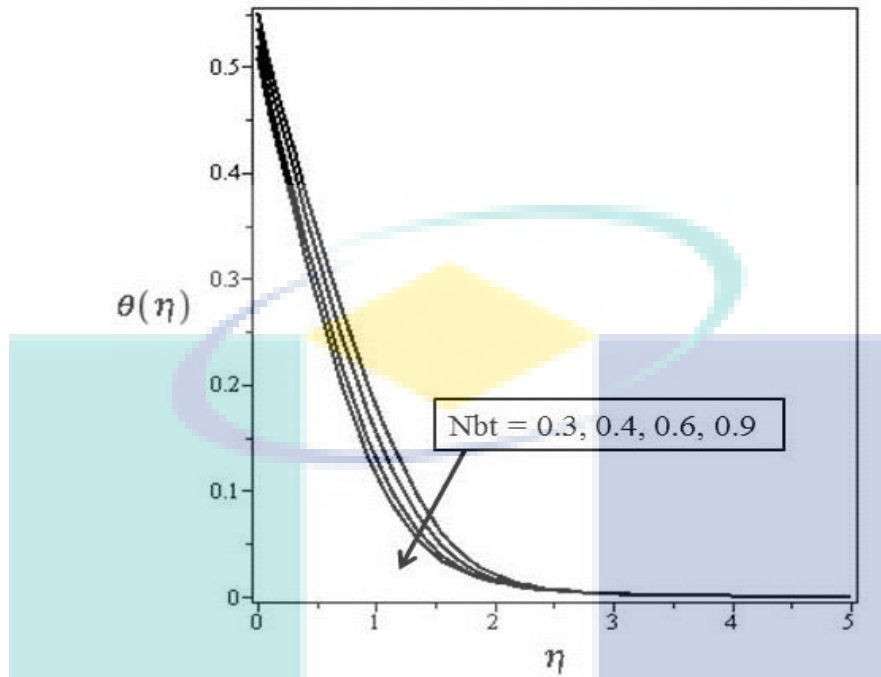
Figure 4.13 Temperature profile for various values of diffusivity ratio *Nbt*, when $\lambda = 0.5$, $B = 0.5$, $\delta = 0.5$, $Nc = 2.5$, Le=10, $Sc = 5$ and Pr $= 7$.
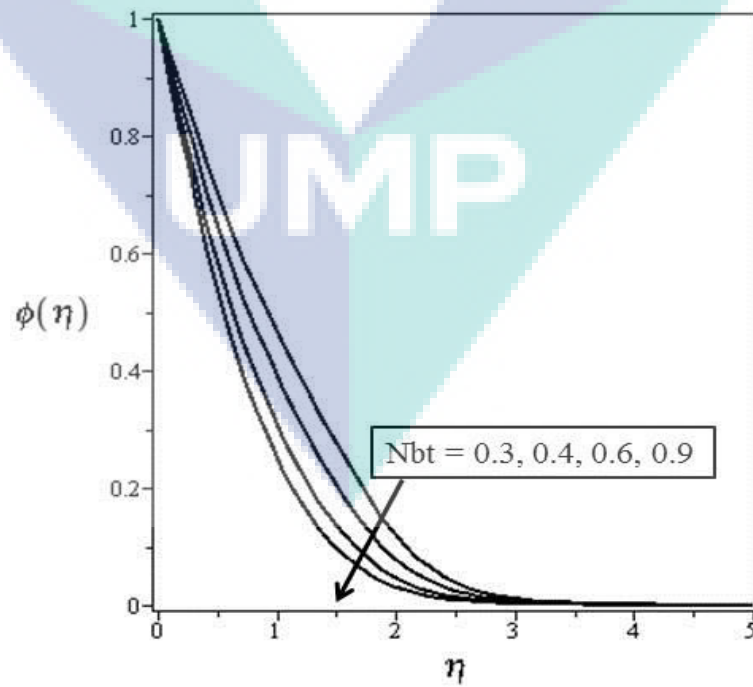
Figure 4.14 Concentration profile for various values of diffusivity ratio *Nbt*, when $\lambda = 0.5$, $B = 0.5$, $\delta = 0.5$, $Nc = 2.5$, $Le = 10$, $Sc = 5$ and $Pr = 7$.
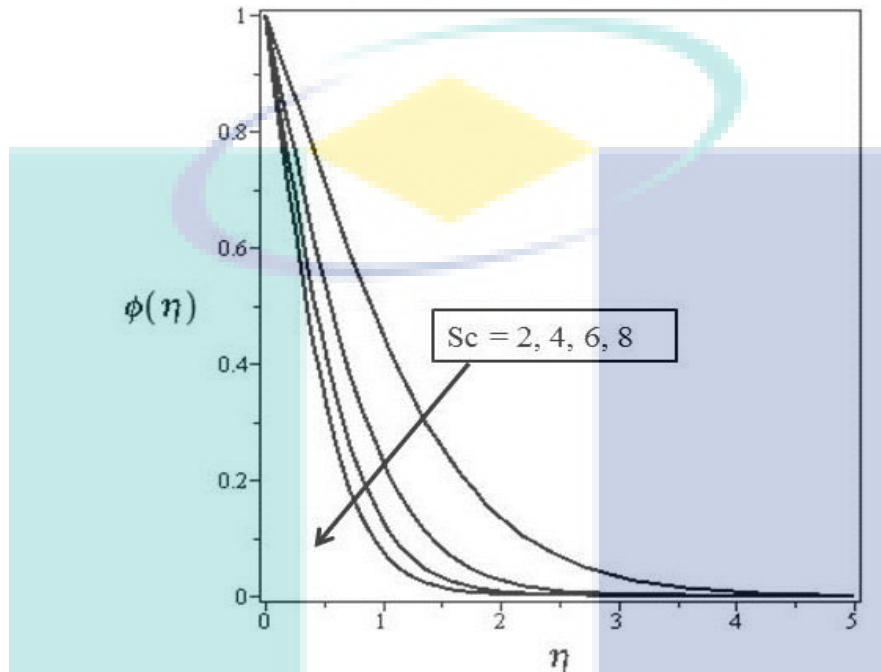
Figure 4.15 Temperature profile for various values of Schmidt number *Sc*, when $\lambda = 0.5$, $B = 0.5$, $\delta = 0.5$, $Nc = 2.5$, $Nbt = 2$, $Le = 10$ and $Pr = 7$.
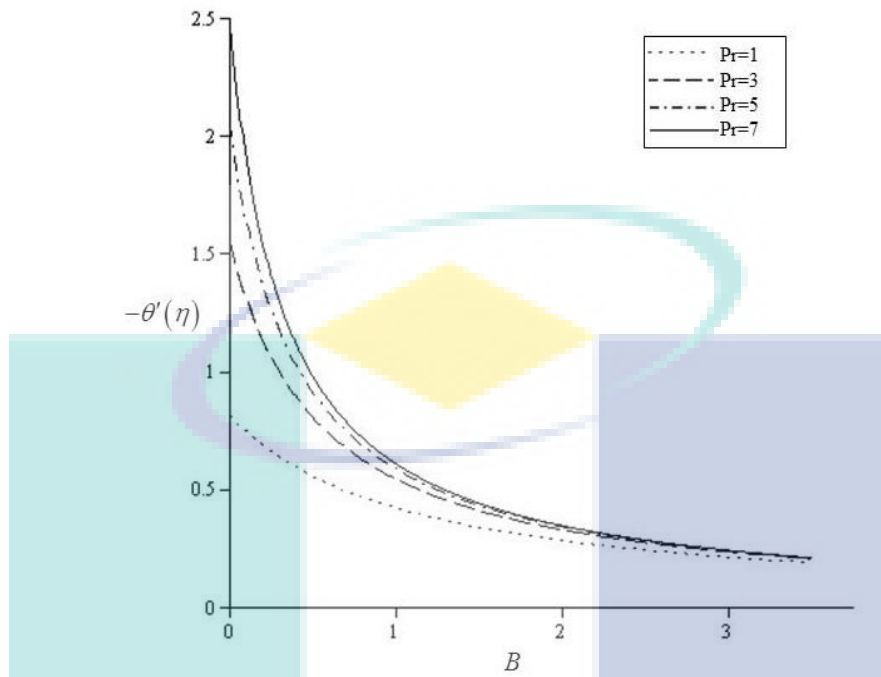
Figure 4.16 The effect of B and Pr on temperature gradient.
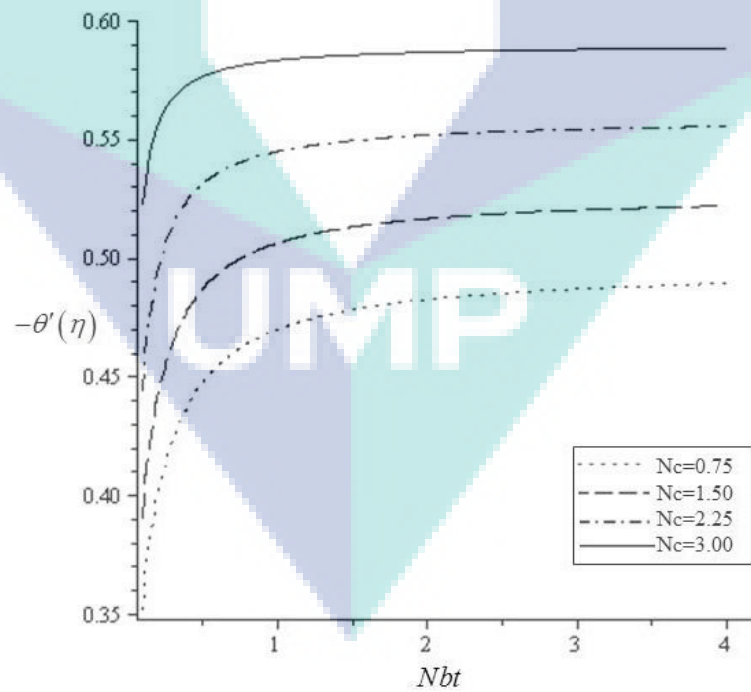
Figure 4.17 The effect of Nbt and Nc on temperature gradient.
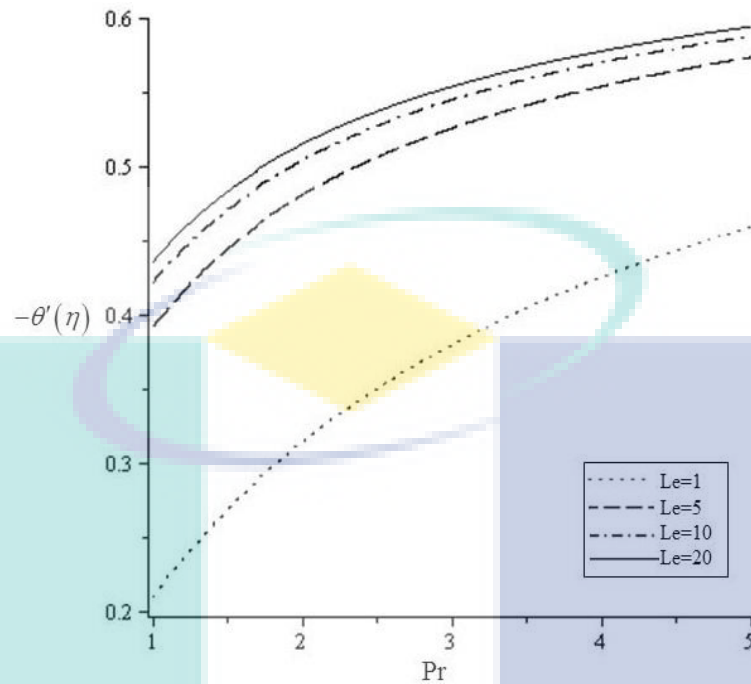
Figure 4.18 The effect of *Le* and Pr on temperature gradient.

4.4 Conclusion

The problem of slip conditions on flow and heat transfer analysis of Williamson nanofluid past over a stretching sheet were studied and analysed numerically. The important findings are summarized as below:

- Williamson nanofluid had lower skin friction coefficient when the non-Newtonian Williamson parameter increased.
- An increase in the velocity slip parameter would lead to an increase in the heat transfer rate.
- An increase in the thermal slip parameter wouldcause a drop in the temperature gradient.
- The higher the non-Newtonian Williamson parameter, the greater the thickness of boundary layer would be.

Table 4.2 The computation results for local skin friction coefficient, local Nusselt number and local Sherwood number respectively.

δ	B	λ	Pr	Nt	Nb	Le	Sc	$f''(0)$	$-\theta'(0)$	$-\phi'(0)$
0.25	1	0.5	7	2.5	2	10	5	-0.824627	0.560312	1.214397
0.75								-0.521313	0.634114	0.995300
1.25								-0.391317	0.653846	0.879335
1.75								-0.316124	0.659675	0.801841
0.5	0.2	0.5	7	2.5	2	10	5		1.531496	0.731268
	0.4								1.111056	0.890411
	0.6								0.871426	0.981179
	0.8								0.716725	1.039801
1	1	0	5	2.5	2	10	5	-0.430631	0.653863	0.952791
		0.4						-0.442676	0.648285	0.935371
		0.8						-0.457476	0.641978	0.914200
		1.4						-0.489301	0.631466	0.869951
0.5	1	0.5	4	2.5	2	10	5		0.593771	
			6						0.632611	
			8						0.656798	
			10						0.673705	
0.5	1	0.5	7	5	2	10	5		0.634617	
				10					0.611296	
				15					0.587304	
				20					0.563051	
0.5	1	0.5	7	2.5	0.3	10	5		0.479166	0.251699
					0.4				0.494843	0.446998
					0.6				0.512197	0.658669
					0.9				0.524636	0.811730
0.5	1	0.5	7	2.5	2	1	5		0.538971	
						1.5			0.579227	
						2			0.599359	
						2.5			0.611296	
0.5	1	0.5	7	2.5	2	10	2			0.409463
							4			0.780050
							6			1.062968
							8			1.299821

CHAPTER 5

**MHD FLOW AND HEAT TRANSFER ANALYSIS OF WILLIAMSON
NANOFLUID WITH THERMAL RADIATION EFFECT OVER A
STRETCHING SHEET**

5.1   Introduction

In this chapter, the results of investigation into the medium in pseudoplastics
materials flow using Williamson fluid as the chosen model proposed by Williamson
(1929), are presented. Tiwari and Das (2007) have suggested the nanofluid model
because nanofluids have great potential in the advancement of thermal conductivity.
Motivated by these studies, Williamson nanofluid was employed to study the present
problem with thermal radiation effect on MHD flow and heat transfer analysis over a
plate sheet. Studies on convective flow in porous medium with the influence of
magnetic field have attracted the interests of many researchers. In this regard, thermal
radiation and magnetic field, can be improved to produce great performance in
engineering and industrial activities such as biological fluid flow, cancer treatment,
chemical and agricultural engineering.

Numerical solutions for the present problem were carried out using the Shooting
method. As described in the previous chapter, the current study was divided into two
parts, namely, CWT and NH. The resulting local Nusselt number for viscous fluid was
then compared to the findings by other researchers such as Nadeem and Hussain (2014),
Goyal and Bhargava (2014) and Prasannakumara et al. (2016). As explained in the
preceding chapter, all the equations (momentum, energy and concentration) were first
transformed from PDE to ODE, subject to boundary conditions, respectively. The new
results were obtained for velocity, temperature and concentration profiles, as well as the
skin friction coefficient, local Nusselt number and local Sherwood number. Graphs for
the various embedded parameters were plotted and discussed in terms of velocity,

temperature and concentration profiles as well as gradient wall temperature and skin friction coefficient.

5.2   Mathematical Formulation

Assuming that a two-dimensional steady flow of an incompressible Williamson nanofluid flow over a stretching surface and the flow region would be defined as $y > 0$, and the plate was stretched along the x-axis with the velocity $U_w = ax$, where b was a positive constant. The two-dimensional boundary layer equations governing the flow would be given as

$$u\frac{\partial u}{\partial x} + v\frac{\partial u}{\partial y} = v\frac{\partial^2 u}{\partial y^2} + \sqrt{2}\,v\Gamma\frac{\partial u}{\partial y}\frac{\partial^2 u}{\partial y^2} - \frac{\sigma B_0^{\,2}u}{\rho}, \qquad 5.1$$

$$u\frac{\partial T}{\partial x} + v\frac{\partial T}{\partial y} = \alpha\frac{\partial^2 T}{\partial y^2} + \frac{\rho_p C_p}{\rho C}\left[D_B\frac{\partial C}{\partial y}\frac{\partial T}{\partial y} + \frac{D_T}{T_\infty}\left(\frac{\partial T}{\partial y}\right)^2\right] - \frac{\partial q_r}{\partial y}, \qquad 5.2$$

$$u\frac{\partial C}{\partial x} + v\frac{\partial C}{\partial y} = D_B\frac{\partial^2 C}{\partial y^2} + \frac{D_T}{T_\infty}\frac{\partial^2 T}{\partial y^2}. \qquad 2.4$$

subjected to boundary conditions (2.5) in Section 2.2. In order to solve equations (5.1), (5.2) and (2.4), we define stream function as equation (2.6) and similarity transformation in an equation (2.7). By applying equation (2.7) into equation (5.1), (5.2) and (2.4), the following equation have obtained

$$f'''(\eta) + \lambda f''(\eta) f'''(\eta) + f(\eta) f''(\eta) - f'^2(\eta) - Mf'(\eta) = 0 \qquad 5.3$$

$$\left(1 + \frac{4}{3}R\right)\theta''(\eta) + \Pr f(\eta)\theta'(\eta) + \frac{Nc}{Le}\phi'(\eta)\theta'(\eta) + \frac{Nc}{Le.Nbt}\theta'^2(\eta) = 0 \qquad 5.4$$

$$\phi''(\eta) + Scf(\eta)\phi'(\eta) + \frac{1}{Nbt}\theta''(\eta) = 0 \qquad 5.5$$

where $\lambda = \sqrt{\dfrac{2b^3}{v}}\Gamma x,\ M = \dfrac{\sigma B_o^2}{\rho b},\ R = \dfrac{4\sigma^* T_\infty^3}{k^*\alpha},\ \Pr = \dfrac{v}{\alpha},\ Nc = \dfrac{\rho_p C_p}{\rho C}(C_W - C_\infty),$

$$Le = \frac{\alpha}{D_B}, \ Sc = \frac{v}{D_B}, \ Nbt = \frac{T_\infty D_B \left(C_W - C_\infty\right)}{D_T \left(T_W - T_\infty\right)}.$$ The f, θ and ϕ would be functions of η

and prime would denote derivatives with respect to η and $R = \dfrac{4\sigma^* T_\infty^3}{kk^*}$. We used the

boundary conditions (2.42) as stated in Section 2.2. The physical quantities of interest

are skin friction coefficient C_f local Nusselt number Nu and local Sherwood number

Sh would be defined as:

$$C_f = \frac{\tau_w}{\rho U_W^2}, \ \mathrm{Nu} = -\frac{xq_w}{T_W - T_\infty} \frac{\partial T}{\partial y}_{y=0} \ \text{and} \ Sh = -\frac{x}{C_w - C_\infty} \frac{\partial C}{\partial y}, \qquad 4.13$$

where the shear stress $\tau_w = \mu\left[\dfrac{\partial u}{\partial y} + \dfrac{\Gamma}{\sqrt{2}}\left(\dfrac{\partial u}{\partial y}\right)^2\right]$. Using the non-dimensional variables, the

following was obtained:

$$C_f\sqrt{\mathrm{Re}} = f''(0) + \frac{\lambda}{2} f''^2(0), \ \frac{\mathrm{Nu}}{\sqrt{\mathrm{Re}}} = -\theta'(0) \ \text{and} \ \frac{Sh}{\sqrt{\mathrm{Re}}} = -\phi'(0). \qquad 4.14$$

where $\mathrm{Re} = \dfrac{a}{v}x^2$ would be the local Reynold's number. The detailed explanation for

mathematical formulation in this chapter is shown in Appendix C of this thesis.

5.2.1 Results and Discussion for Constant Wall Temperature (CWT)

The calculated boundary values should be similar to the real boundary values,
hence, the values should be as close to the boundary values as would be appropriate to
consider. In this study, there was no consideration of variation in temperature, velocity
and concentration where large infinity condition was adopted but a finite value for η.
The value at $\eta_{\max} = 8$, was chosen, which would be sufficient to achieve asymptotic
boundary conditions for all parameter values considered. Table 5.1 shows the
comparison of values of $-\theta'(0)$ with previous results by using different methods. From
our numerical solutions, it can be concluded that this method worked efficiently and the
results presented here are accurate.

Table 5.1 Comparison of results for viscous case $-\theta'(0)$ when $\lambda = \infty, Le=Nbt = 1,$ $Pr = R = M = Nc = 0.$

Pr	Nadeem and Hussain (2014) by HAM method	Goyal and Bhargava (2014) by FEM method	Prasannakumara et al. (2016) by RKF45	Present study by Shooting method
0.20	0.169	0.1691	0.1702	0.1698
0.70	0.454	0.4539	0.4544	0.4539
2.00	0.911	0.9113	0.9113	0.9113
7.00	-	1.8954	1.8954	1.8954
20.00	-	3.3539	3.3539	3.3539

This section includes the graphical results for temperature $\theta(\eta)$, velocity $f'(\eta)$ and concentration $\phi(\eta)$ fields for different parameters involved such as Williamson parameter λ, magnetic parameter M, radiation parameter R, Prandtl number Pr, heat capacities ratio parameter Nc, diffusivity ratio parameter Nbt and Schmidt number Sc.

Figures 5.1, 5.2 and 5.3 show magnetic parameter M effects on the velocity $f'(\eta)$, temperature $\theta(\eta)$ and concentration $\phi(\eta)$ fields, respectively. It was found that velocity $f'(\eta)$ field would decrease when the magnetic parameter M increased. The reason is that an increase in magnetic parameter M would mean an increase in the Lorentz force opposing the fluid motion. Meanwhile, Figures 5.2 and 5.3 show that an increase in the magnetic parameter M would lead to an increase in temperature $\theta(\eta)$ and concentration $\phi(\eta)$ fields. Further, this enhancement would be very significant near the sheet, however this effect is almost negligible farther away from the sheet.

Figure 5.4 reveals the temperature profile effect of radiation parameter. Based on the graph, the result shows that as R increased, the temperature profile would also increase. The observation shows that temperature would increase when R increased because the larger the value of radiation parameter, the more heat to fluid would be provided to the fluid, causing an enhancement in the temperature as well as the

thickness of thermal boundary layer. The variation of temperature profile of Prandtl number is shown in Figure 5.5. An increase in the Pr would cause the temperature distribution to decrease. Prandtl number corresponding to the weaker thermal diffusivity as a result of the fluids having weaker thermal diffusivity, had lower temperature. This is the reason for Prandtl number depicting a decrement in the temperature profile. Figure 5.6 illustrates the heat capacities ratio parameter of temperature profiles. Increasing the value of Nc would cause the temperature distribution to increase. This is because $Nc = 0$ would correspond to the Williamson fluid in the absence of nanoparticles. Thus, the heat transfer rate of Williamson nanofluid would increase as nanofluid heat capacity Nc increased.

Figures 5.7 and 5.8 show the temperature and concentration profiles of diffusivity ratio parameter, respectively. It was observed that by increasing the value of Nbt, the temperature and concentration profiles would decrease. Normally, Lewis number would rely upon Brownian diffusion coefficient and the larger values of Lewis number would tend to reduce the Brownian diffusion coefficient, depicting a weaker nanoparticle temperature profile as shown in Figure 5.9. Meanwhile Figure 5.10 illustrates the effect of Schmidt parameter on the concentration profiles. Based on the graph, the result shows that an increase in the value of Sc would cause the concentration profile to decrease. Figures 5.11, 5.12 and 5.13 were plotted to explain the effect of Williamson parameter and Magnetic parameter on skin friction coefficient, temperature gradient and concentration gradient, respectively. The results show that the skin friction coefficient, local Nusselt number and Sherwood number would decrease when the value of λ and M decreased. Thus, the heat transfer rate at the surface would also decreases because it was represented by a local Nusselt number.

Figures 5.14 and 5.15 show the effects of Prandtl number and radiation parameter on the temperature gradient. Based on Figure 5.14, the smaller values of Pr (0.72 & 1) and R were considered. With increasing Pr value, the value of temperature gradient would also increase. However, the heat transfer rate would decrease as the value of radiation parameter was increased. Figure 5.16 reveals the effect of λ and R on temperature gradient. The higher the λ and R, the lower the rate of heat transfer and resulting in the thinning of the boundary layer thickness would be. The influence of

heat capacities ratio parameter and thermophoretic diffusivity parameter on local Nusselt number is illustrated in Figure 5.17. It can be seen that the dimensionless temperature would decrease as the value of Nc increased. However, raising the value of Nbt would decrease the heat transfer rate of the temperature gradient. Figure 5.18 shows the effect of Lewis number and Prandtl number on temperature gradient. The heat transfer rate and wall temperature would increase in accordance with the increase in the value of both parameters. This is because when the Le increased, the thermal diffusivity would also increase which in turn would enhance the heat transfer rate, leading to an increase in the temperature gradient.
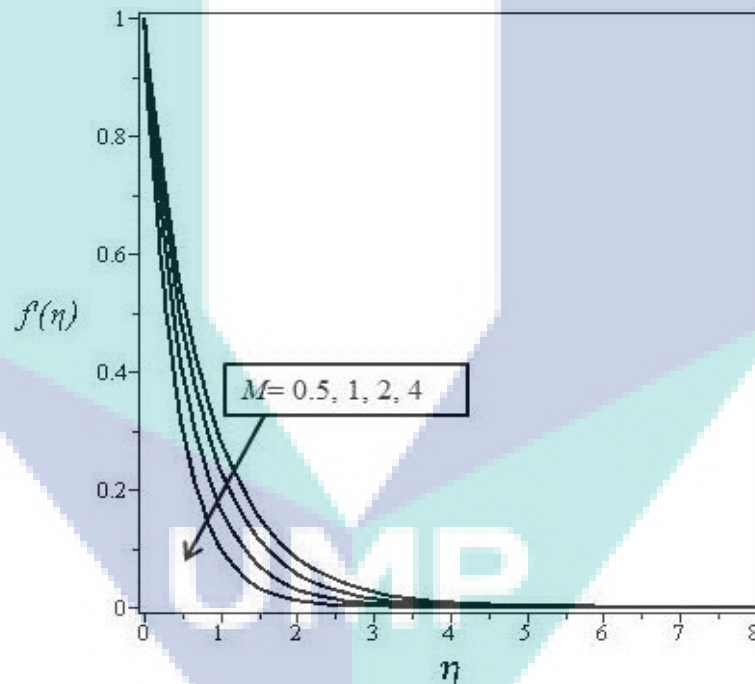
Figure 5.1 Velocity profile for various values of magnetic parameter M, when $\lambda = 0.1$, $Le = 5$, $R=0.3$, $Nc = 0.5$, $Nbt = 1$, $Sc = 2.5$ and $\Pr = 2$.
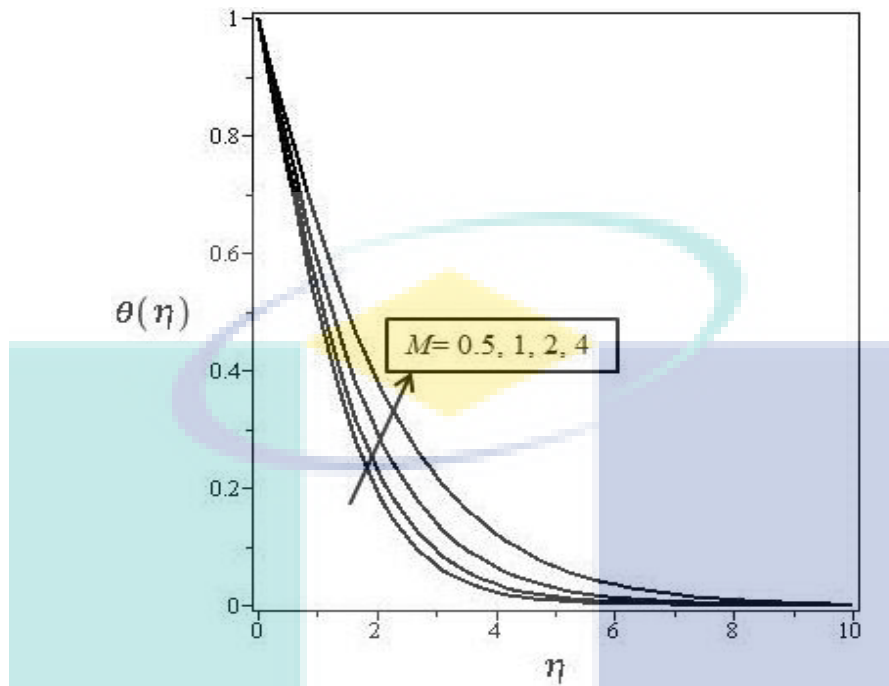
Figure 5.2 Temperature profile for various values of magnetic parameter M, when $\lambda = 0.1$, $R = 0.3$, $Le = 5$, $Nc = 0.5$, $Nbt = 1$, $Sc = 2.5$ and $\Pr = 2$.
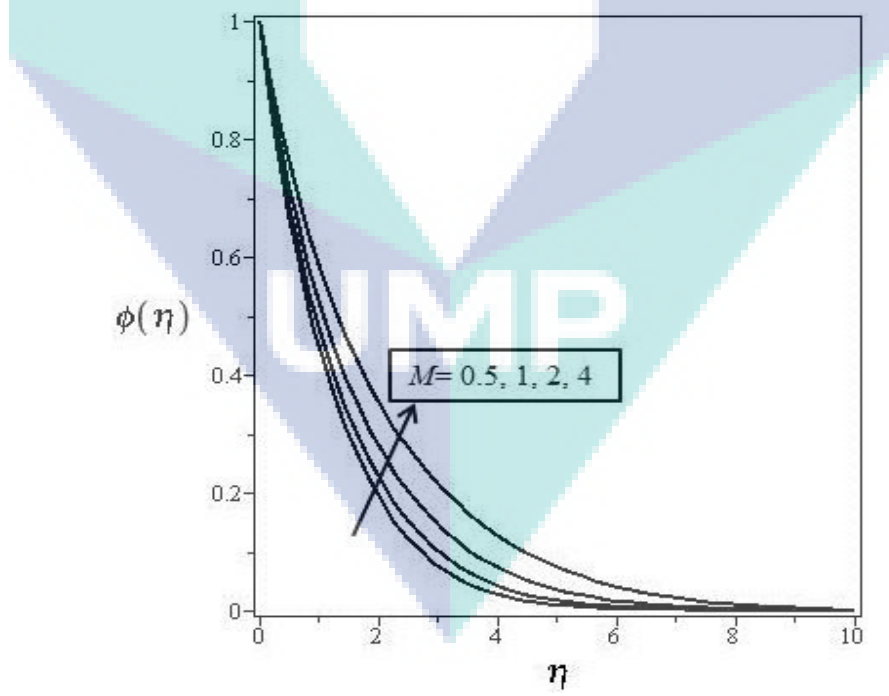
Figure 5.3 Concentration profile for various values of magnetic parameter M, when $\lambda = 0.1$, $R = 0.3$, $Le = 5$, $Nc = 0.5$, $Nbt = 1$, $Sc = 2.5$ and $\Pr = 2$.
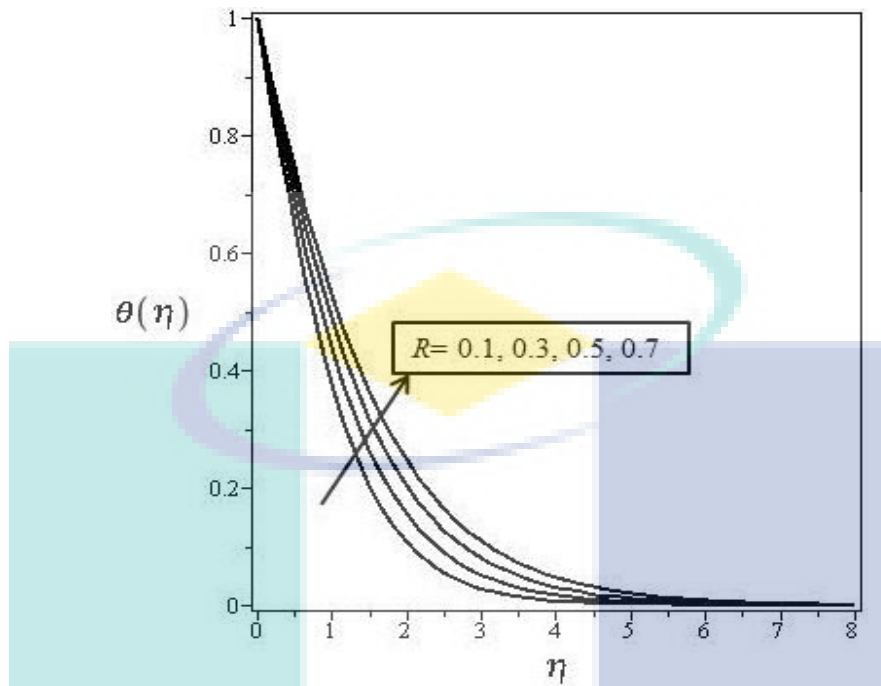
Figure 5.4 Temperature profile for various values of radiation parameter R, when $\lambda = 0.1$, $M = 0.5$, $Le = 5$, $Nc = 0.5$, $Nbt = 1$, $Sc = 2.5$ and $Pr = 2$.
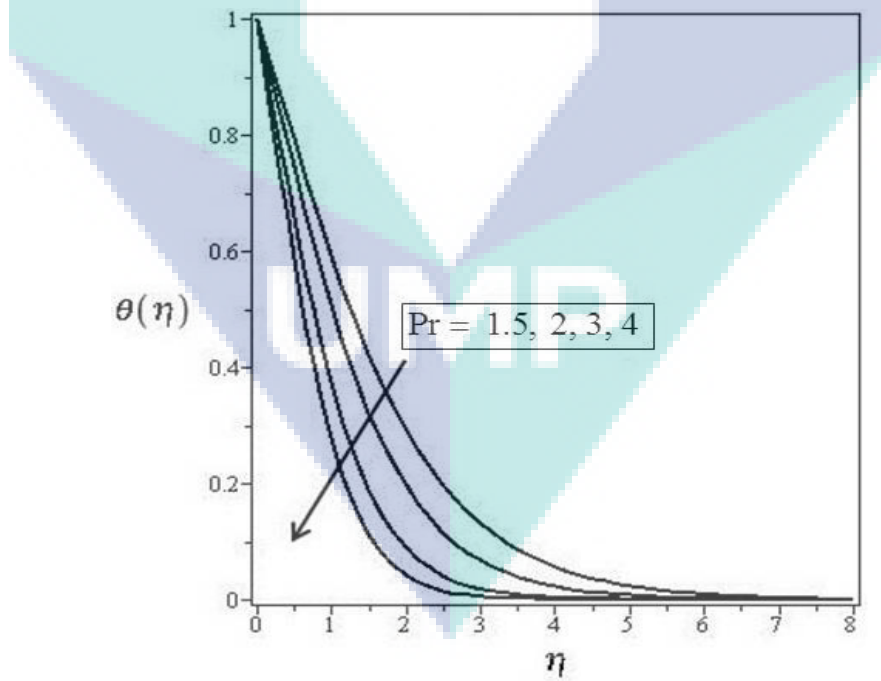
Figure 5.5 Temperature profile for various values of Prandtl parameter Pr, when $\lambda = 0.1$, $M = 0.5$, $R = 0.3$, $Le = 5$, $Nc = 0.5$, $Nbt = 1$ and $Sc = 2.5$.
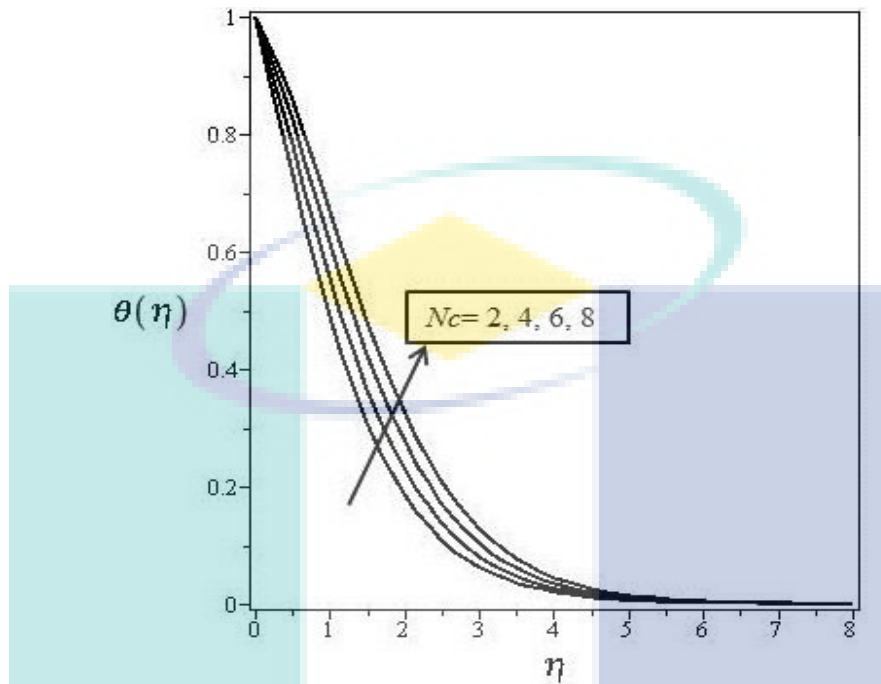
Figure 5.6 Temperature profile for various values of heat capacities ratio parameter Nc, when $\lambda = 0.1$, $M = 0.5$, $R = 0.3$, $Le = 5$, $Nbt = 1$, $Sc = 2.5$ and $Pr = 2$.
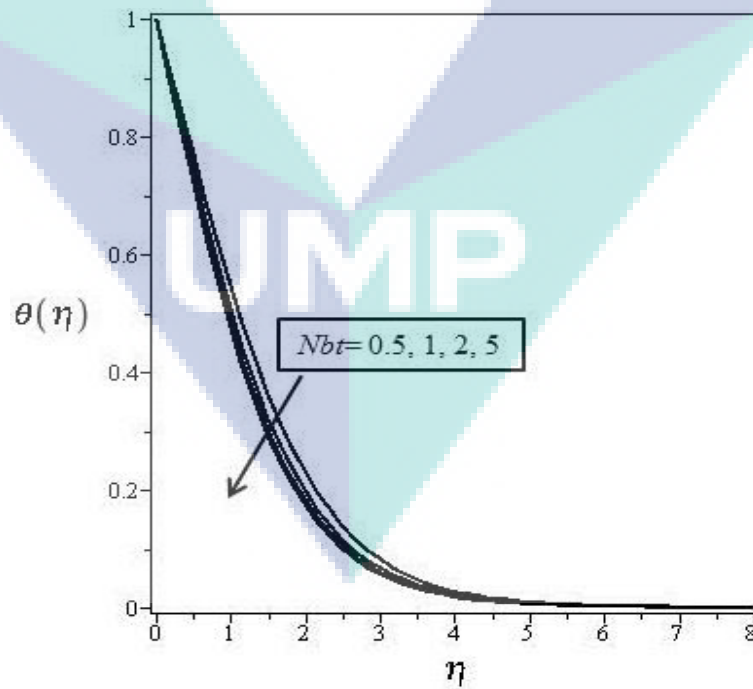
Figure 5.7 Temperature profile for various values of diffusivity ratio parameter Nbt, when $\lambda = 0.1$, $M = 0.5$, $R = 0.3$, $Le = 5$, $Nc = 0.5$, $Sc = 2.5$ and $Pr = 2$.
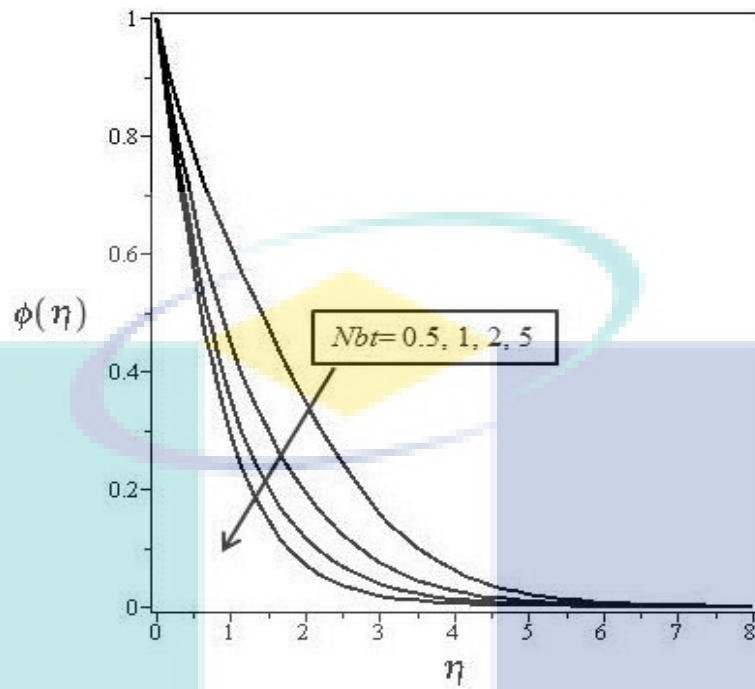
Figure 5.8 Concentration profile for various values of diffusivity ratio parameter Nbt, when $\lambda = 0.1$, $M = 0.5$, $R = 0.3$, $Le = 5$, $Nc = 0.5$, $Sc = 2.5$ and $\Pr = 2$.
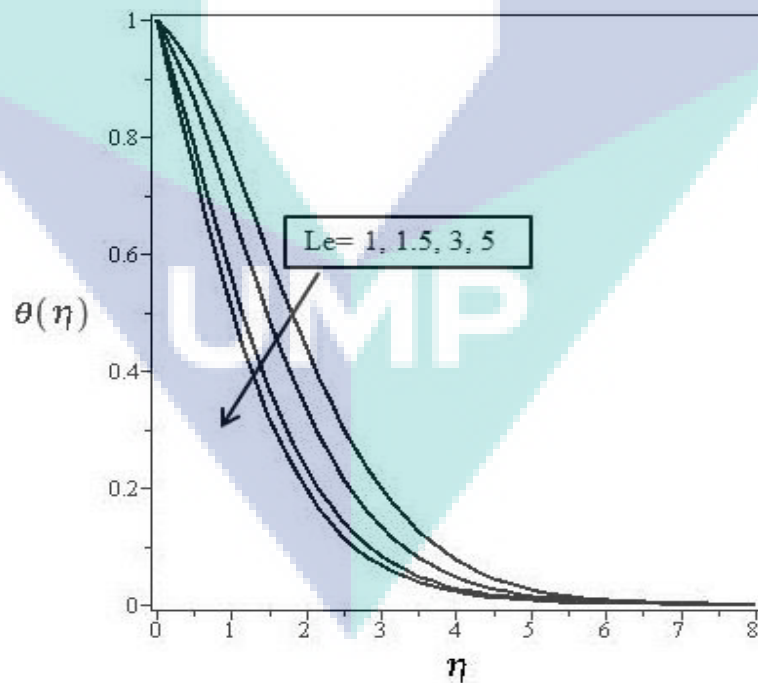
Figure 5.9 Temperature profile for various values of Lewis parameter Le, when $\lambda = 0.1$, $M = 0.5$, $Le = 5$, $Nc = 0.5$, $Nbt = 1$, $Sc = 2.5$ and $\Pr = 2$.
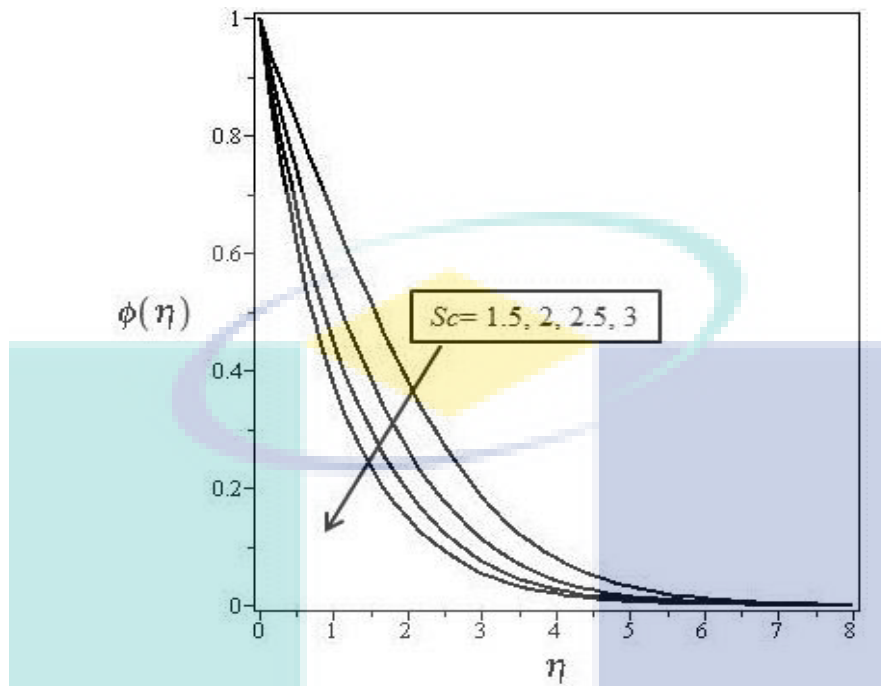
Figure 5.10 Concentration profile for various values of Schmidt parameter Sc, when $\lambda = 0.1$, $M = 0.5$, $R = 0.3$, $Le = 5$, $Nc = 0.5$, $Nbt = 1$ and $\text{Pr} = 2$.
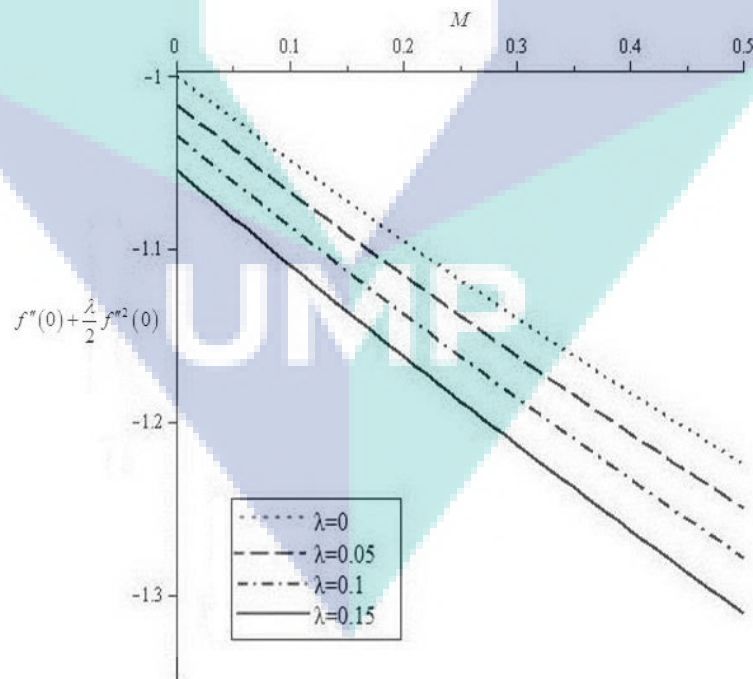
Figure 5.11 The effect of λ and M on skin friction coefficient.
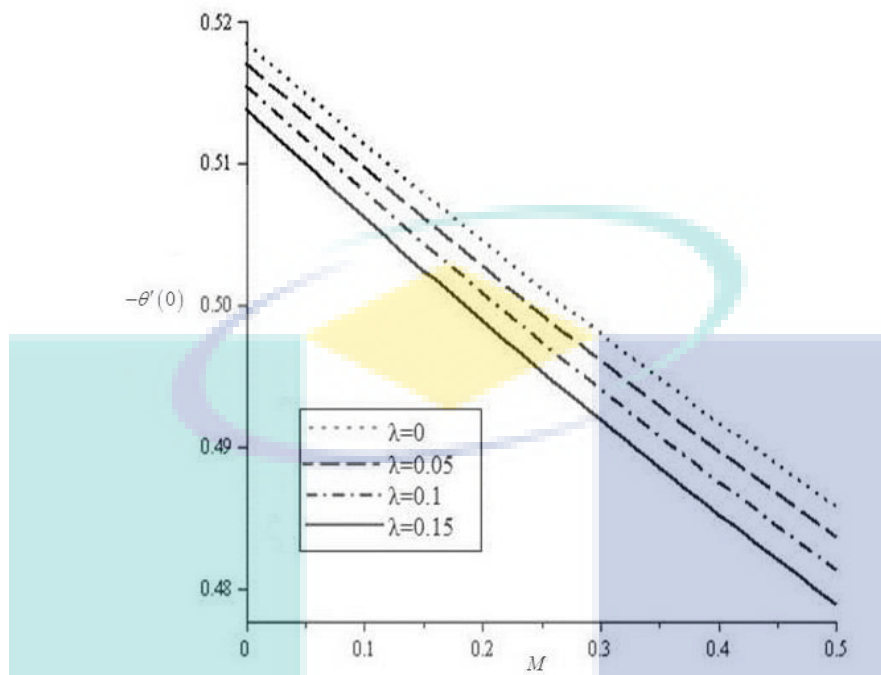
Figure 5.12 The effect of λ and M on temperature gradient.
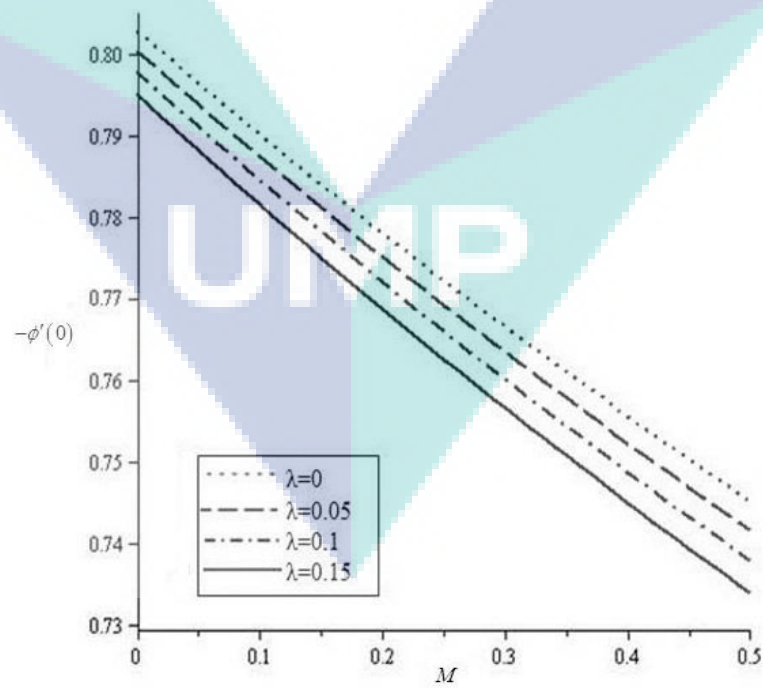
Figure 5.13 The effect of λ and M on concentration gradient.
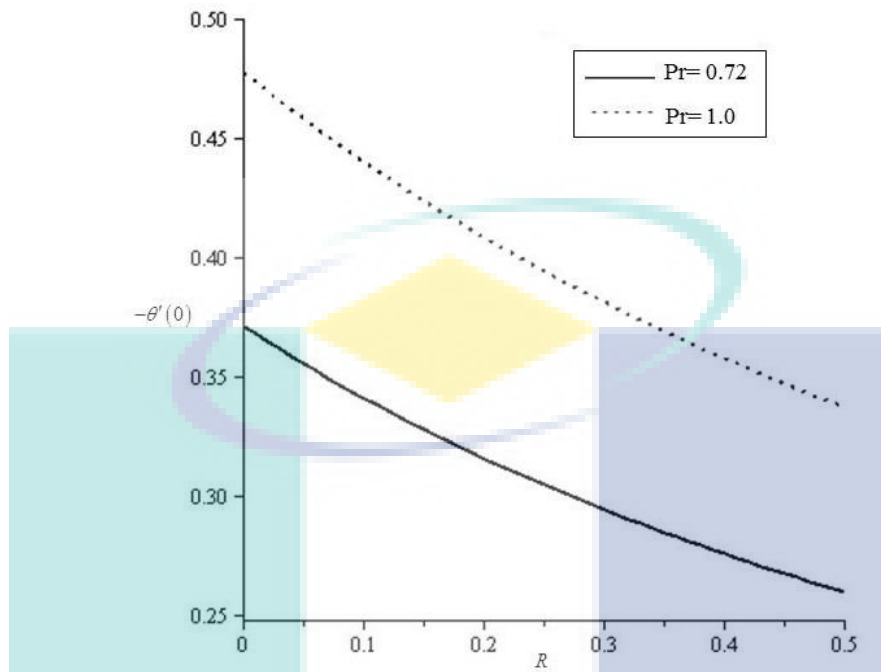
Figure 5.14 The effect of Pr and R on temperature gradient.
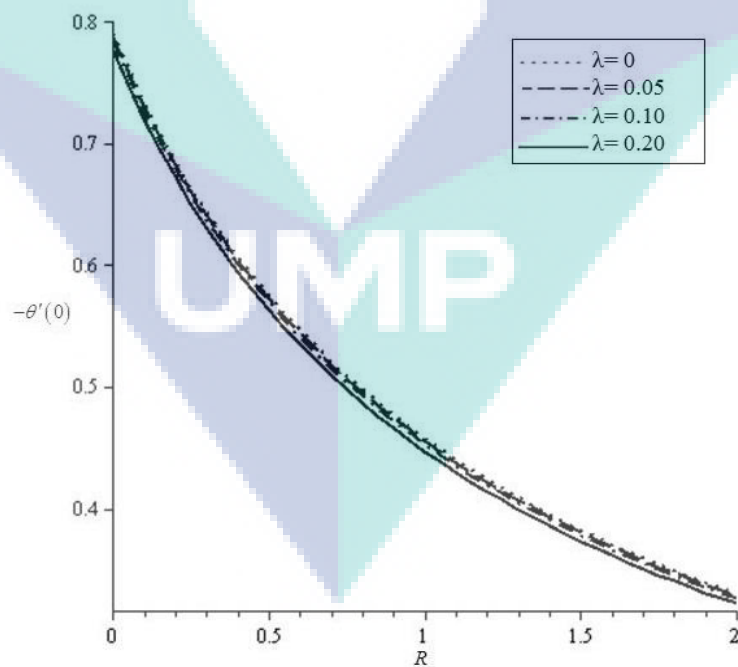
Figure 5.15 The effect of λ and R on temperature gradient.
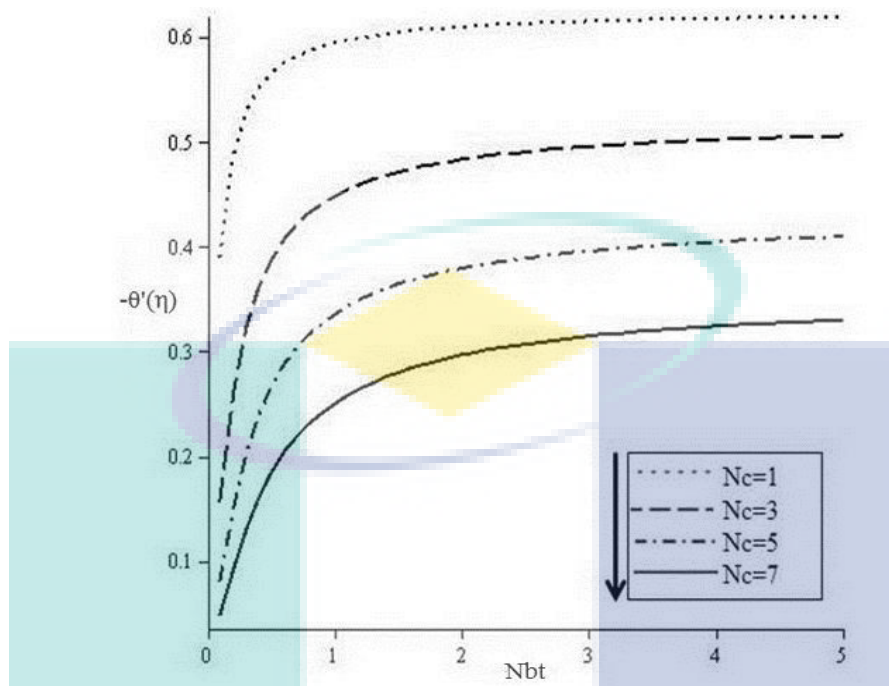
Figure 5.16 The effect of Nc and Nbt on temperature gradient.
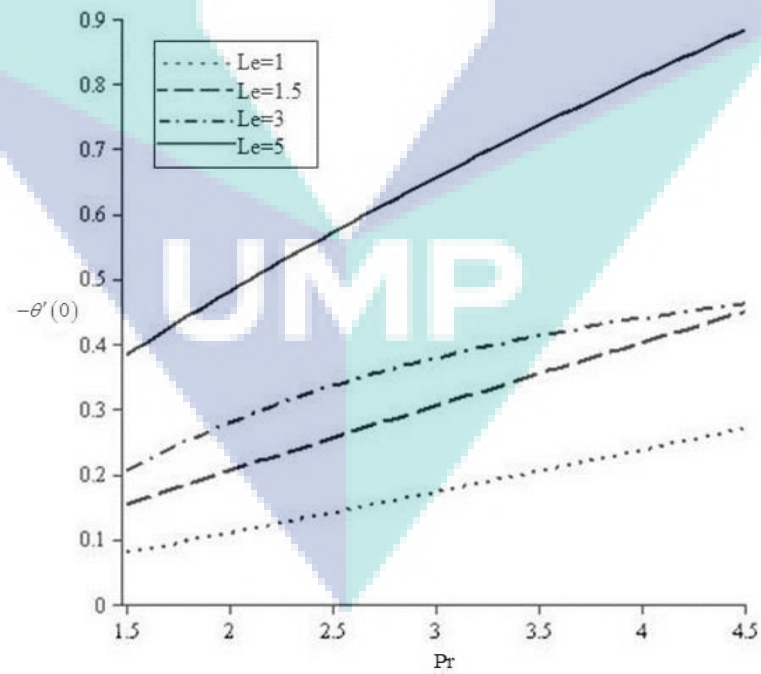
Figure 5.17 The effect of Le and $\Pr$ on temperature gradient.

Table 5.2 The computation results with all the parameters for local skin friction coefficient, local Nusselt number and local Sherwood number respectively.

λ	M	R	Nbt	Nc	Sc	Le	Pr	$f''(0)+\frac{\lambda}{2}f''^2(0)$	$-\theta'(0)$	$-\phi'(0)$
0	0.5	0.3	1	0.5	2.5	5	2	-1.224744	0.262878	0.861499
0.05								-1.250243	0.261291	0.858227
0.1								-1.278723	0.259629	0.854739
0.15								-1.310949	0.257879	0.850998
0.1	0.5	0.3	1	0.5	2.5	5	2	-1.278725	0.481279	0.737944
	1							-1.488267	0.453568	0.690693
	2							-1.847920	0.410392	0.619924
	4							-2.441922	0.352091	0.530775
0.1	0.5	0.1	1	0.5	2.5	5	2		0.727322	
		0.3							0.637636	
		0.5							0.569746	
		0.7							0.516376	
0.1	0.5	0.3	0.5	0.5	2.5	5	2		0.426029	0.562733
			1						0.481279	0.737944
			2						0.512394	0.852278
			5						0.532288	0.931103
0.1	0.5	0.3	1	2	2.5	5	2		0.516700	0.711117
				4					0.388042	0.806982
				6					0.289930	0.876478
				8					0.215816	0.925940
0.1	0.5	0.3	1	0.5	1.5	5	2		0.508351	0.387010
					2				0.492442	0.575847
					2.5				0.481279	0.737944
					3				0.472987	0.881338
0.1	0.5	0.3	1	0.5	2.5	1	2		0.110079	
						1.5			0.205395	
						3			0.378796	
						5			0.481279	

5.2.2 Summary

The thermal radiation effect on MHD flow and heat transfer analysis of Williamson nanofluids were studied numerically with CWT. The governing non-linear equations were solved by using the Shooting method. Numerical outcome for velocity profiles, surface heat transfer rate and nanoparticle volume fraction were obtained with various range of boundary conditions and different acceptable values of pertinent flow parameters. The important findings in this research are summarized as follows:

- Boundary layer thickness would increase for temperature and concentration profiles and velocity distribution would decrease with an increase in magnetic parameter.
- Temperature profile would increase with the increasing values of radiation parameter but the rate of heat transfer would decrease.
- Temperature profile would decrease as Prandtl number increased.
- An increase in heat capacities ratio parameter would also cause an increase in temperature profile.
- An increase in diffusivity ratio parameter would lead to a decrease in concentration and temperature profiles.
- Temperature profile would decrease with the increasing value of Lewis number.
- Concentration profile would decrease with the increasing value of Schmidt number.
- Skin friction coefficient as well as local Nusselt and Sherwood number would decrease at all times as λ and M increased in the fluid.
- The value of temperature gradient would decrease at all times as $\Pr$ and R increased.
- The value of temperature gradient would decrease at all times as λ and R increased.
- The temperature gradient would increase as value of Nbt increased. However, the higher the value of Nc, the lower the value of temperature gradient would be.

5.2.3 Results and Discussion of Newtonian Heating (NH)

The nonlinear ordinary differential equations were derived manually together with the boundary conditions. Then, these equations were solved by using the Shooting method. The nonlinear ordinary differential equations were of third order in f, second order in θ and ϕ, and were then reduced into simultaneous ordinary equations. With the initial conditions of $\eta \to \infty$, the following values could be obtained: $f'(\eta)$, $\theta(\eta)$ and $\phi(\eta)$. Thus, unknown initial conditions $\eta = 0$ were obtained by using the Shooting method and the initial values for boundary value problem were assumed. The calculated boundary values should be similar to the real boundary values; hence, the value should be as close to the boundary values would be as appropriate to consider. In this study, there were no considerations of variation in temperature, velocity and concentration where large infinity condition was adopted but finite value for η. The value at $\eta_{max} = 8$, which would be sufficient to achieve asymptotic boundary conditions for all parameter values considered, was chosen. Table 4.3 shows the comparison of values of $-\theta'(0)$ with previous results. It can be concluded that this method worked efficiently and the results presented here are accurate.

Table 5.3 Comparison of results for viscous case $-\theta'(0)$ when $\lambda = \infty$, $Le=Nbt = 1$, $\mathrm{Pr} = R = M = Nc = 0$.

Pr	Nadeem and Hussain (2014) by HAM method	Goyal and Bhargava (2014) by FEM method	Prasannakumara et al. (2016) by RKF45	Present study by Shooting method
0.20	0.169	0.1691	0.1702	0.1698
0.70	0.454	0.4539	0.4544	0.4539
2.00	0.911	0.9113	0.9113	0.9113
7.00	-	1.8954	1.8954	1.8954
20.00	-	3.3539	3.3539	3.3539

This section includes the graphical results for temperature $\theta(\eta)$, velocity $f'(\eta)$ and concentration $\phi(\eta)$ fields for different parameters involved such as Williamson

parameter λ, magnetic parameter M, radiation parameter R, Prandtl number Pr, heat capacities ratio parameter Nc, diffusivity ratio parameter Nbt and Schmidt number Sc. Figure 5.18 shows the Williamson parameter λ effects on velocity $f'(\eta)$. It was found that velocity $f'(\eta)$ field decrease with increase in the Williamson parameter λ. Figures 5.19 shows magnetic parameter M effects on velocity $f'(\eta)$. It is found that velocity $f'(\eta)$ field decreases with increases in the magnetic parameter M. The reason is that an increase in magnetic parameter M would mean increase in the Lorentz force opposing the fluid motion.

Figure 5.20 reveals the temperature profile with the effect of radiation parameter. Based on the graph, the result shows that increasing the value of R would cause an increase in temperature profile. The observation showed that temperature would increase with an increase in R because increasing the value of radiation parameter would provide more heat to the fluid, causing enhancement in the temperature and the thickness of thermal boundary layer. The variation of temperature profile by Prandtl number is shown in Figure 5.21. Increasing the value of Pr would cause a decrease in temperature distribution. Prandtl number is whose corresponding to the weaker thermal diffusivity as a result of those fluids having weaker thermal diffusivity and, contained lower temperature. This is the reason for Prandtl number depicting a decrement in the temperature profile. Figure 5.22 illustrates the heat capacities ratio parameter of temperature profiles. An increase in Nc would cause temperature profile to increase. This is because $Nc = 0$ would correspond to that of the Williamson fluid in the absence of nanoparticles. Thus, the heat transfer rate of the Williamson nanofluid would increase as the nanofluid heat capacity Nc increased.

Normally, Lewis number would rely upon Brownian diffusion coefficient and the larger value of Lewis number would tend to reduce the Brownian diffusion coefficient, depicting a weaker nanoparticle temperature profile, as shown in Figure 5.23. Figures 5.24 and 5.25 show the temperature and concentration profiles of diffusivity ratio parameter, respectively. It was observed that increasing the value of Nbt would decrease the temperature and concentration profiles. Figures 5.26 and 5.27 illustrate the temperature and concentration profiles of conjugate parameter γ, respectively. The wall temperature and concentration profiles would increase as the

112

value of γ increased. Figure 5.28 depicts the effect of Schmidt parameter to the concentration profile. Based on the graph, the result shows that increasing the value of Sc then decrease the concentration profile.

In the case of Newtonian heating (NH), Figure 5.29 illustrates the variation of wall temperature $\theta(0)$ with Prandlt number when $\gamma = 0.1$. To obtain a physically appropriate solution, $\Pr$ must be greater than the critical values $\Pr_c$ (critical value of $\Pr$), which would be dependent on γ. Based on the below diagram, it was found that the $\theta(0)$ would become large as $\Pr$ approached the critical value $\Pr_c = 0.276755$ when $\gamma = 0.1$. Figure 5.30 has shown the variation of the wall temperature $\theta(0)$ for various values of γ when $\Pr = 1$ and 7. Also, in order to obtain the appropriate solution, γ must be less than a certain value called γ_c, critical value of conjugate parameter, which would be dependent on $\Pr$. The surface temperature would become unbounded when $\gamma = \gamma_c$ was found in our numerical solution and the value of wall temperature $\theta(0)$ would become larger as γ approached the critical values, $\gamma_c = 0.221538$ and 0.934912 when $\Pr = 1$ and 7, respectively.
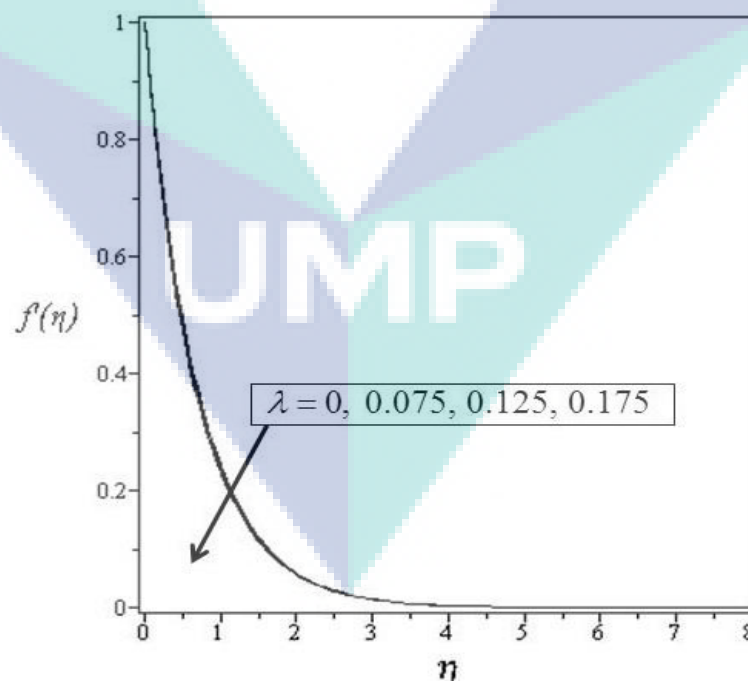
Figure 5.18 Velocity profile for various values of Williamson parameter λ, when $M = 1,\ Le = 5,\ R = 0.5,\ Nc = 1,\ Nbt = 2,\ Sc = 2.5,\ \Pr = 1$ and $\gamma = 0.1$.
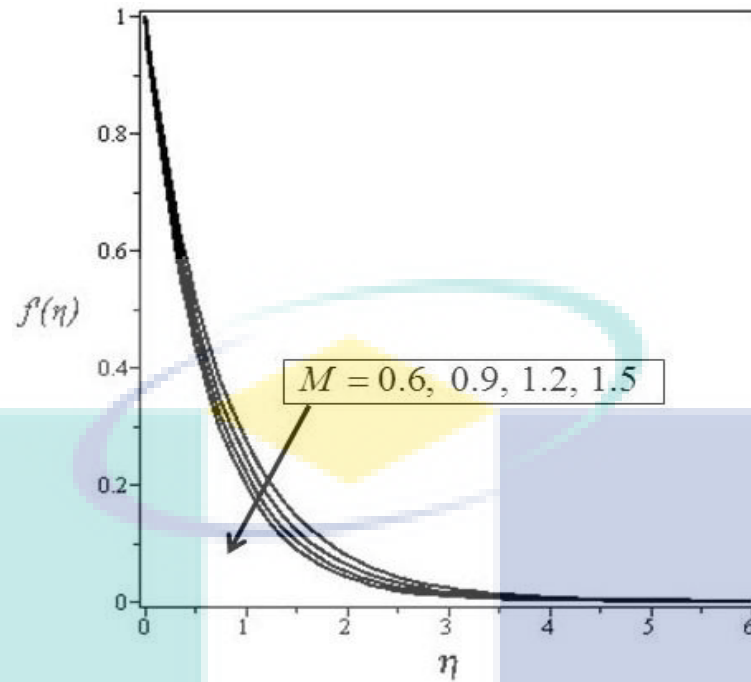
Figure 5.19 Velocity profile for various values of magnetic parameter M, when $\lambda = 0.1,\ Le = 5,\ R = 0.5,\ Nc = 1,\ Nbt = 2,\ Sc = 2.5,\ \mathrm{Pr} = 1$ and $\gamma = 0.1$.
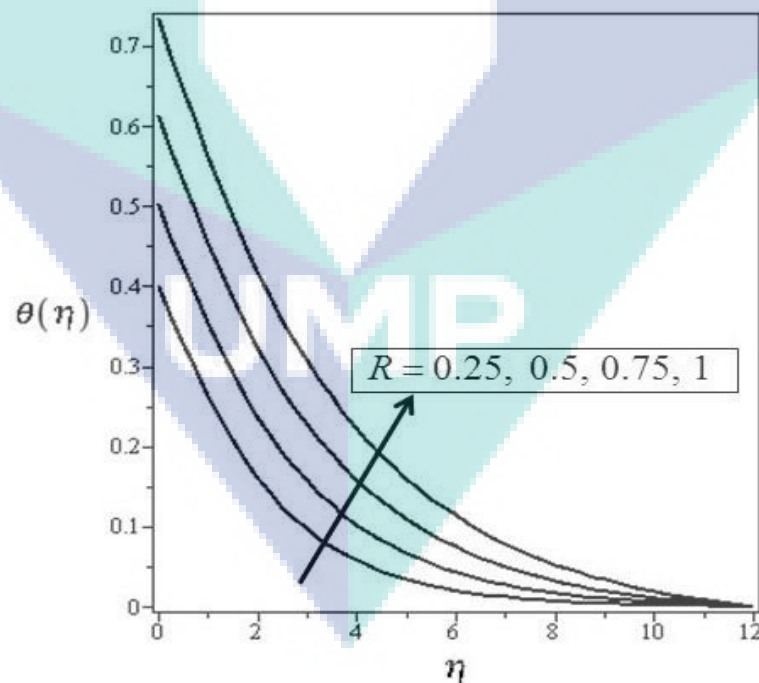
Figure 5.20 Temperature profile for various values of radiation parameter R, when $M = 1,\ \lambda = 0.1,\ Le = 5,\ Nc = 1,\ Nbt = 2,\ Sc = 2.5,\ \mathrm{Pr} = 1$ and $\gamma = 0.1$.
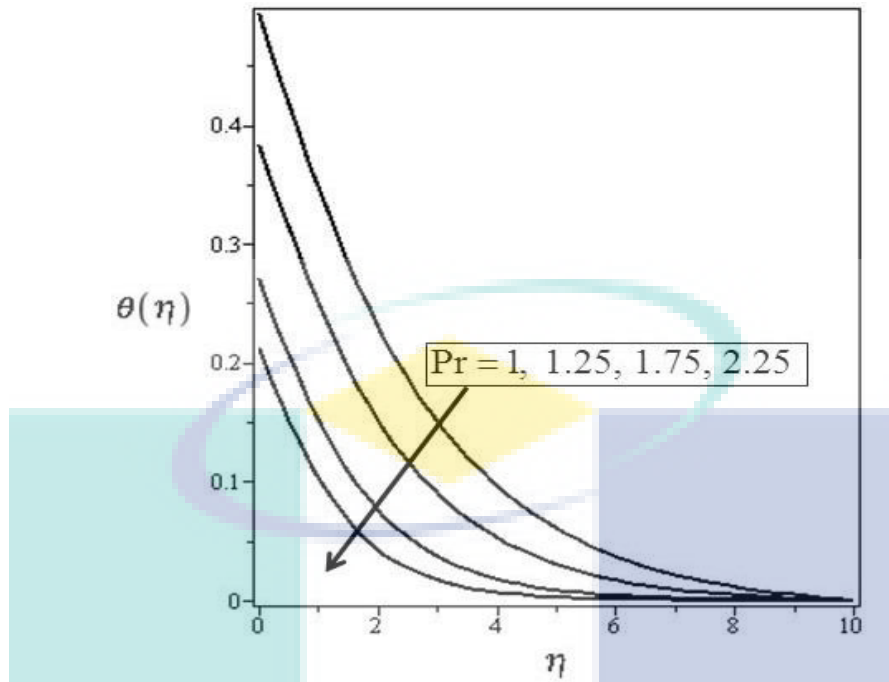
Figure 5.21 Temperature profile for various values of Prandlt number parameter Pr, when $M = 1,\ \lambda = 0.1,\ Le = 5,\ R = 0.5,\ Nc = 1,\ Nbt = 2,\ Sc = 2.5$ and $\gamma = 0.1$.
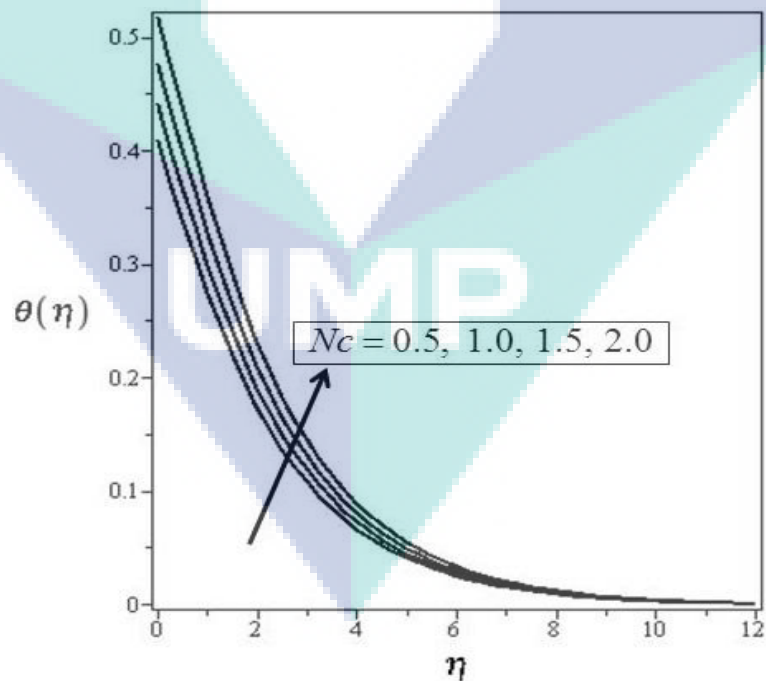
Figure 5.22 Temperature profile for various values of heat capacities ratio parameter $Nc,$ when $M = 1,\ \lambda = 0.1,\ Le = 5,\ R = 0.5,\ Nbt = 2,\ Sc = 2.5,\ \mathrm{Pr} = 1$ and $\gamma = 0.1$.
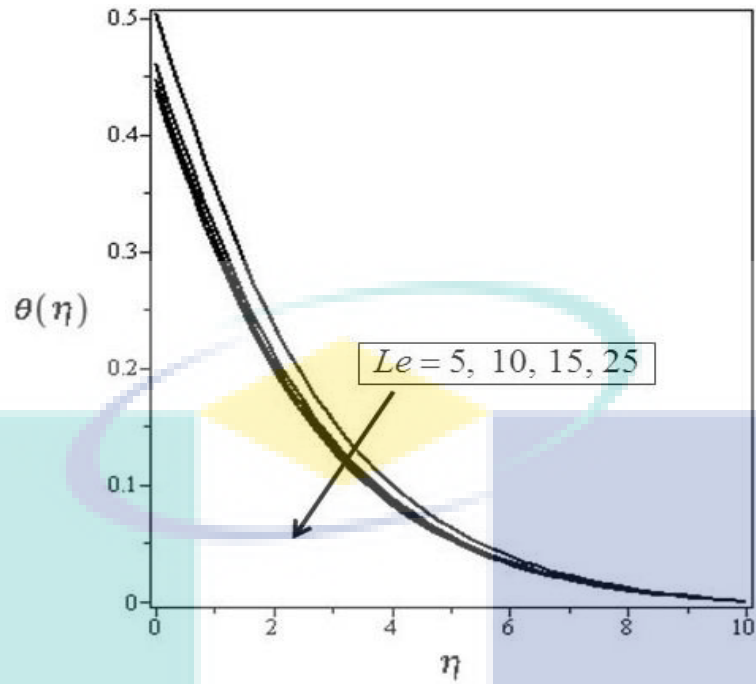
Figure 5.23 Temperature profile for various values of Lewis number *Le*, when $M = 1$, $\lambda = 0.1$, $R = 0.5$, $Nc = 1$, $Nbt = 2$, $Sc = 2.5$, $\Pr = 1$ and $\gamma = 0.1$.
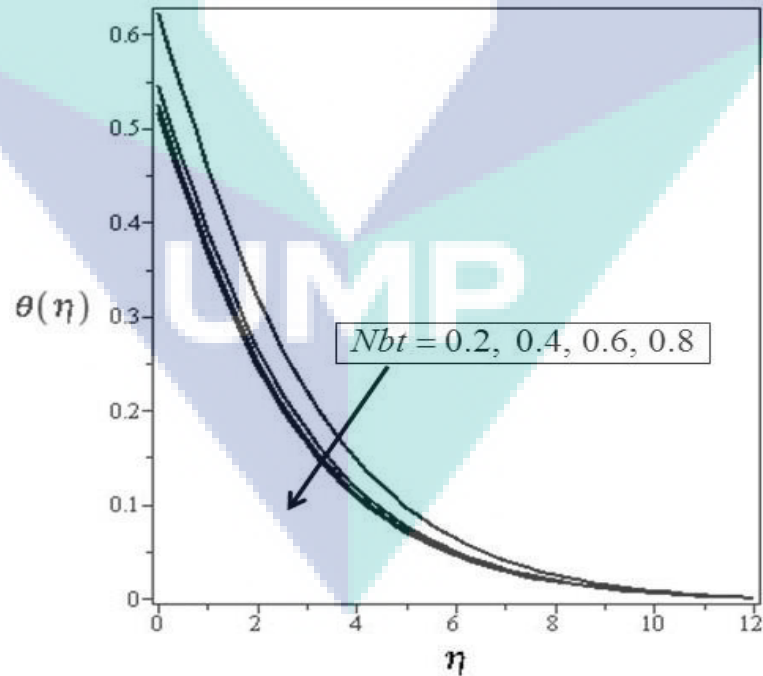
Figure 5.24 Temperature profile for various values of diffusivity ratio parameter *Nbt*, when $M = 1$, $\lambda = 0.1$, $Le = 5$, $R = 0.5$, $Nc = 1$, $Sc = 2.5$, $\Pr = 1$ and $\gamma = 0.1$.
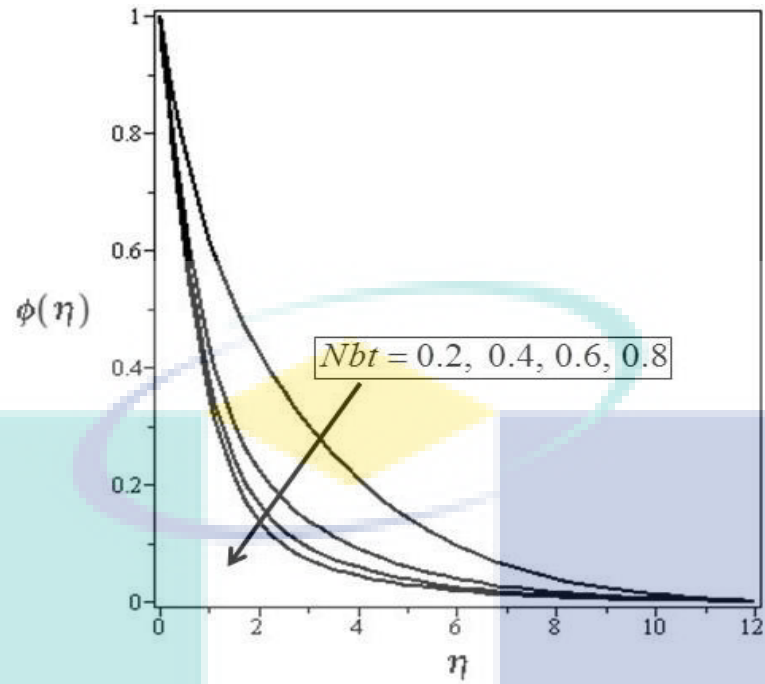
Figure 5.25 Concentration profile for various values of diffusivity ratio parameter *Nbt*, when $M = 1$, $Le = 5$, $R = 0.5$, $Nc = 1$, $Nbt = 2$, $Sc = 2.5$, $\Pr = 1$ and $\gamma = 0.1$.
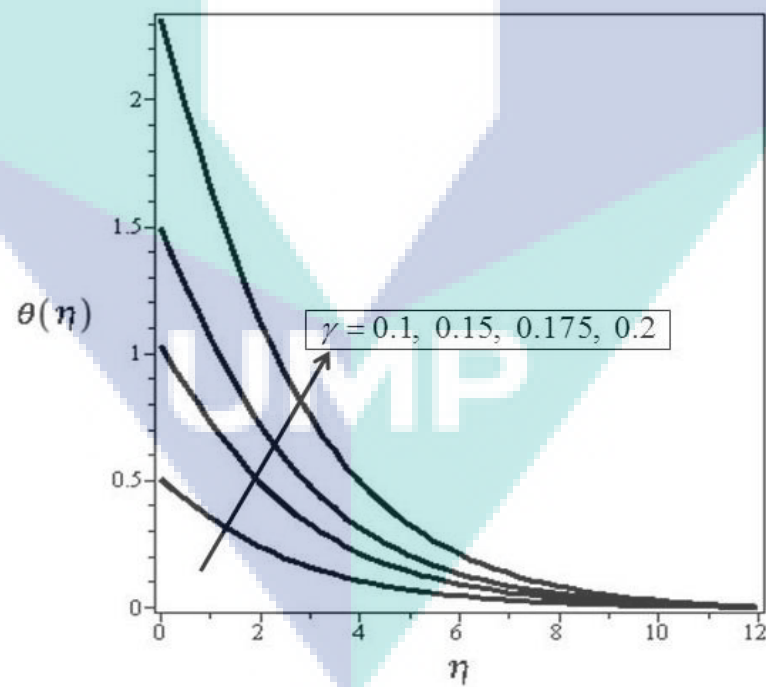
Figure 5.26 Temperature profile for various values of Newtonian heating parameter γ, when $M = 1$, $\lambda = 0.1$, $Le = 5$, $R = 0.5$, $Nc = 1$, $Nbt = 2$, $Sc = 2.5$ and $\Pr = 1$.
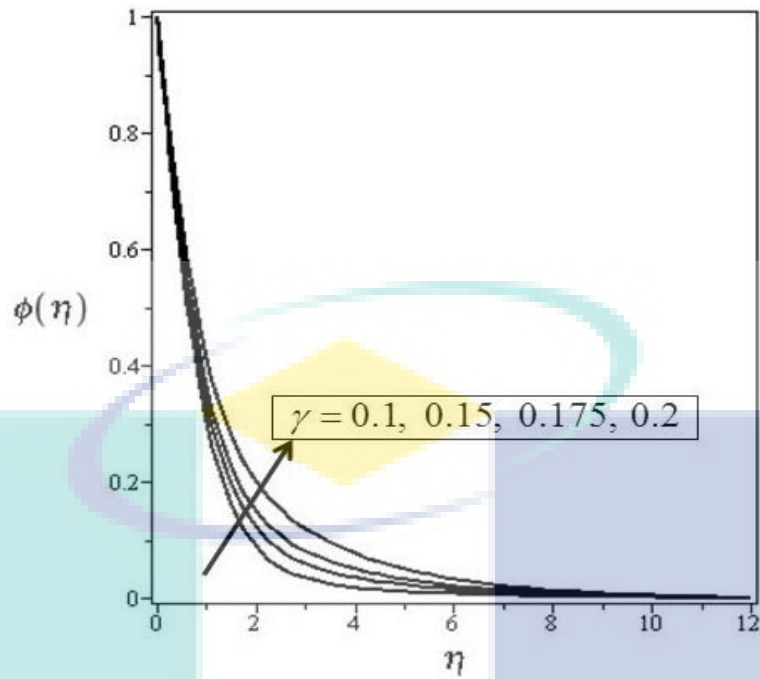
Figure 5.27 Concentration profile for various values of Newtonian heating parameter γ, when $M = 1$, $\lambda = 0.1$, $Le = 5$, $R = 0.5$, $Nc = 1$, $Nbt = 2$, $Sc = 2.5$ and $\Pr = 1$.
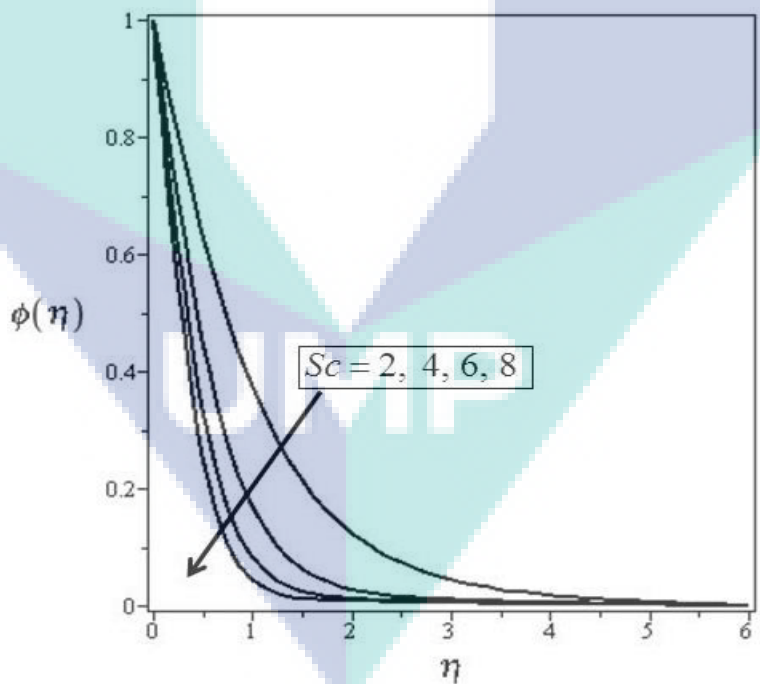
Figure 5.28 Concentration profile for various values of Schmidt number Sc, when $M = 1$, $\lambda = 0.1$, $Le = 5$, $R = 0.5$, $Nc = 1$, $Nbt = 2$, $\Pr = 1$ and $\gamma = 0.1$.
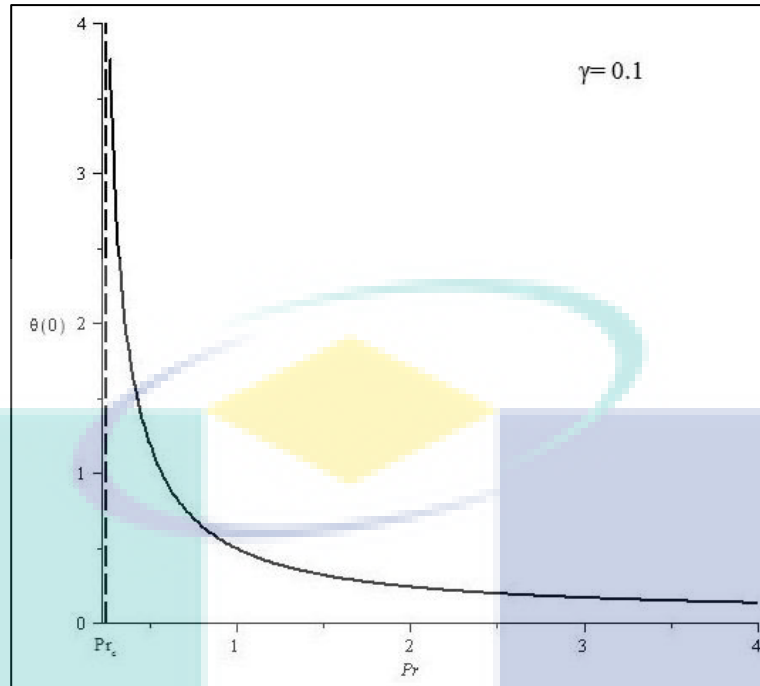
Figure 5.29 Variation of the wall temperature $\theta(0)$ with Prandlt number Pr when Newtonian heating parameter $\gamma = 0.1$.
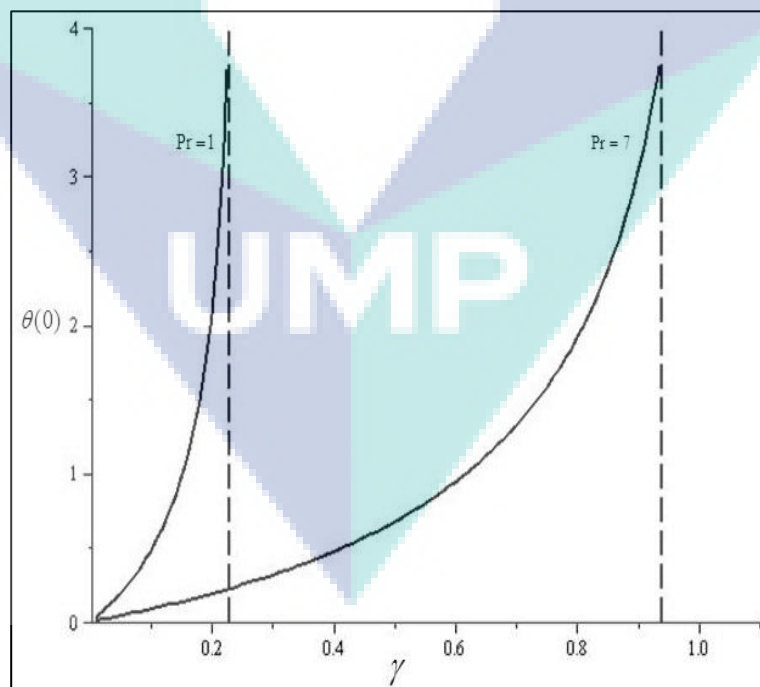
Figure 5.30 Variation of the wall temperature $\theta(0)$ with Newtonian heating parameter γ when Pr $= 1$ and 7.

5.2.4   Summary

The effect of thermal radiation on MHD boundary layer flow and heat transfer of Williamson nanofluid over a stretching sheet with Newtonian heating were studied numerically using the Shooting method. It was shown how each parameter affected the velocity, temperature and concentration profiles. It can therefore be concluded that:

- The velocity profile would decreases as the Williamson parameter and magnetic parameter increased simultaneously.

- The wall temperature would increase as the heat capacities ratio parameter increased. However, the temperature profile would decrease as Lewis number and diffusivity ratio parameter increased.

- The concentration profile would drop as the Schmidt number increased.

- The thickness of boundary layer would increase as the radiation parameter increased. Furthermore, an increase in Prandtl number result in a decrease the temperature profile.

- The Newtonian heating parameter would cause the temperature profile to increase significantly. To obtain a physically appropriate solution, the value of Pr must be greater than Pr_c and dependent on γ at all times. Also, the value of γ must be less than γ_c which would be dependent on Pr.

Table 5.4 The computation results with all the parameters for gradient temperature and concentration respectively.

λ	M	γ	R	Nbt	Nc	Sc	Le	Pr	$-\theta'(0)$	$-\phi'(0)$
0	1	0.1	0.5	2	1	2.5	5	7		
0.075										
0.125										
0.175										
0.1	0.6	0.1	0.5	2	1	2.5	5	7		
	0.9									
	1.2									
	1.5									
0.1	1	0.1	0.5	2	1	2.5	5	7	0.150153	0.903453
		0.15							0.304649	0.860298
		0.175							0.436449	0.823653
		0.2							0.663559	0.76089
0.1	1	0.1	0.25	2	1	2.5	5	7	0.13996	
			0.5						0.150153	
			0.75						0.161316	
			1						0.173432	
0.1	1	0.1	0.5	0.2	1	2.5	5	7	0.162293	0.501725
				0.4					0.15451	0.730947
				0.6					0.152551	0.803686
				0.8					0.151653	0.839569
0.1	1	0.1	0.5	2	0.5	2.5	5	7	0.140908	
					1				0.144079	
					1.5				0.147665	
					2				0.151761	
0.1	1	0.1	0.5	2	1	2	5	7		0.778071
						4				1.248462
						6				1.610977
						8				1.916295
0.1	1	0.1	0.5	2	1	2.5	5		0.15036	
							10		0.146055	
							15		0.144764	
							25		0.143777	
0.1	1	0.1	0.5	2	1	2.5	5	1	0.149409	
								1.25	0.138362	
								1.75	0.127014	
								2.25	0.121279	

CHAPTER 6

CONCLUSION

6.1   Summary of Research

The purpose of this study was to examine the numerical solutions for the problem of Casson and Williamson nanofluids with other variables such as thermal radiation, magnetic field, porous medium as well as heat transfer which has been explained in six chapters of this thesis. Three problems have been examined.

Chapter 1 was an introductory topic which included the research background, the problem statement, the research objective and scope, the methodology, significance of this study, literature review and thesis outline.

Chapter 2 presented the details of mathematical formulation work related to the thesis study problems. All of the problems were modelled in terms of partial differential equations with initial and boundary conditions. Appropriate non-dimensional variables were then introduced to transform the governing equations into the dimensionless forms. Numerical solutions for each problem were carried out by using the Shooting method.

In Chapter 3, the effect of thermal radiation on MHD flow of Casson nanofluid over a stretching sheet was examined. Two types of boundary conditions in this topic, namely, constant wall temperature and Newtonian heating, were considered. The results showed that velocity profiles decreased significantly while the wall temperature and concentration profile increased when the Casson parameter increased, under the two different cases of boundary conditions. Also, Casson nanofluid had greater fluid velocity than Newtonian fluids. The increment of Prandtl number caused the wall temperature of nanofluids to drop. The magnetic effect had caused retardation in velocity profiles in the presence of porous medium due to the effect of Lorentz force.

The thermal radiation parameter had led to an increase in the wall temperature since the higher the radiation, the greater the radiate, especially in high temperature. For the case of Newtonian heating, the temperature and concentration profiles increased when the Newtonian heating parameter was increased. However, in order to obtain an appropriate value for Newtonian heating parameter, it must not exceed its critical value and must depend on the Prandtl number.

Chapter 4 discussed the slip conditions on flow and heat transfer analysis of Williamson nanofluid over a stretching sheet. The velocity and thermal slip parameters were also introduced. After computing the mathematical formulation, it was found that Williamson nanofluid had lower skin friction coefficient when the non-Newtonian Williamson parameter increased. The thickness of thermal boundary layer increased as Williamson parameter increased. In addition, the rise of the velocity slip parameter led to an increase in the heat transfer rate. At the same time, an increase in thermal slip parameter caused the temperature wall as well as the temperature gradient to drop. The numerical solutions obtained in the present study would be significant because they would serve as the accuracy standards for approximate methods, especially asymptotic.

In Chapter 5, Williamson nanofluid as the medium with the effects of thermal radiation and MHD flow over a stretching sheet was discussed. The two types of boundary conditions as in previous chapter was considered. For the case of constant wall temperature, the results showed that the skin friction coefficient, temperature gradient and concentration decreased when the value of non-Newtonian Williamson parameter increased. Besides that, the temperature gradient was reduced as the radiation parameter and Prandtl number increased. The temperature gradient increased as Lewis number and heat capacities ratio parameter increased. For the case of Newtonian heating, the temperature profile increased when the Newtonian heating parameter and radiation parameter increased. In order to obtain the physically appropriate solutions for this study, the Prandtl number must be greater than its critical value, known as Pr_c; and must depend on the value of γ. Also, the value of Newtonian heating parameter must be less than the critical point γ_c and dependent on the value of Pr.

Overall, the consideration of boundary conditions by constant wall temperature and Newtonian heating of heat transfer flow of Casson and Williamson nanofluid due to

over the stretching plate with various effects have been investigated. Based on the finding results, it is noticed that Casson parameter and Williamson parameter with a similarities which if increase in these two parameters, the yield stress will be reduced and behave like Newtonian fluid. Besides, the finding results of present study revealed that the solutions are noticed to exist when the Newtonian parameter must less than the critical values then only flow like normal. Meanwhile, there is no solution if the Newtonian heating exceeds the limits. Based on these problems, the values of wall temperature of nanofluid is larger than compared to the viscous fluid. This explains why the Newtonian fluids always have greater thermal conductivity and effective during the heat rate transfer. Other than that, increase the velocity field lead to an increase in the magnitude of skin frictions coefficient by considering the absolute value for stretching surface. The absolute value has been taken due to these quantities give the negative values. Nevertheless, the Nusselt number and Sherwood number increases at most of the time.

In addition, the results were compared with studies published in journals to validate the efficiency of the method used. It should be noted that the problems discussed in this thesis are new and all the graphical results have been well illustrated in the form of tables and figures. Furthermore, these results could be used as the source of reference and comparison in future studies.

6.2   Contribution of Study

The main contribution of this study is the investigation and examination conducted on Casson and Williamson nanofluids in mathematical formulation such as momentum, energy and concentration. Furthermore, there were several parameters considered in the profiles like magnetic field, radiation parameter, porosity parameter, Newtonian heating parameter, Brownian parameter, Lewis number, Schmidt number and Prandtl number. The wall temperature, skin friction, Nusselt number and Sherwood number were also been studied and the findings were presented in graphical form. The solutions obtained and the explanantions could be used for validation purposes in the future.

6.3   Future Study

Even though the problem of nanofluids has received favourable attention in this century, the numerical solutions for non-Newtonian fluids with Newtonian heating conditions are not widely discussed in the literature. This is because such problem is relatively difficult and complicated compared to other boundary conditions. Besides, the method used for numerical solutions is easier compared to the method of exact solutions. Although exact solutions serve as accuracy for approximate methods, whether for numerical, asymptotic or experimental, these solutions are complicated and seldom used to solve the problem. In this thesis, only two nanofluids with convective boundary conditions were considered. Thus, there is much are still to be investigated in other aspects of the area to be undertaken in future studies. It is recommended that future research should consider the following:

- Other types of model fluids for internal flow like Jeffrey fluid and Maxwell fluid could be examined.
- Other geometries such as elliptic circular cylinder and solid sphere.
- Other effects such as chemical reaction, revised model rotating flow, etc should be studied.

REFERENCES

Abolbashari, M.H., Freidoonimehr, N., Nazari, F. and Rashidi, M.M. (2015). Analytical modeling of entropy generation for Casson nano-fluid flow induced by a stretching surface. *Advanced Powder Technology*, 26(2), 542-552.

Acheson, D.J. (1990). Elementary fluid dynamics. Oxford University Press.

Ahmad, S.B. (2009). Convection boundary layer flows over needles and cylinders in viscous fluids. Ph.D Thesis, Universiti Putra Malaysia, Malaysia.

Ahmad, S. and Pop. I. (2010). Mixed convection boundary layer flow from a vertical flat plate embedded in a porous medium filled with nanofluids. *International Communications in Heat and Mass Transfer*, 37, 987-991.

Ahmed, N. and Dutta, M. (2013). Transient mass transfer flow past an impulsively started infinite vertical plate with ramped plate velocity and ramped temperature. *International Journal of Physical Sciences*, 8(7), 254-263.

Akbar, N.S. and Khan, Z.H. (2015). Metachronal beating of cilia under the influence of Casson fluid and magnetic field. *Journal of Magnetism and Magnetic Materials*, 378, 320-326.

Akbar, N.S., Nadeem, S. and Ali, M. (2011). Jeffrey fluid model for blood flow through a tapered artery with a stenosis. *Journal of Mechanics in Medicine and Biology*, 11(03), 529-545.

Akbar, N.S., Nadeem, S., Lee, C., Khan, Z.H. and Haq, R.U. (2013). Numerical study of Williamson nano fluid flow in an asymmetric channel. *Results in Physics*, 3, 161-166.

Aly, E.H. (2015). Effect of the velocity slip boundary condition on the flow and heat transfer of nanofluids over a stretching sheet. *Journal of Computational and Theoretical Nanoscience*, 12(9), 2428-2436.

Amanulla, C.H., Nagendra, N., and Reddy, M. (2017). Numerical Study of Thermal and Momentum Slip Effects on MHD Williamson *Nanofluid from an Isothermal Sphere. Journal of Nanofluids, 6*(6), 1111-1126.

Anwar, M.I., Khan, I., Shafie, S. and Salleh, M.Z. (2012). Conjugate effects of heat and mass transfer of nanofluids over a nonlinear stretching sheet. *International Journal of Physical Sciences*, 7, 4081-4092.

Anwar, I., Kasim, A.R.M., Ismail, Z., Salleh, M.Z. and Shafie, S. (2013). Chemical reaction and uniform heat generation or absorption effects on MHD stagnation-

point flow of a nanofluid over a porous sheet. *World Applied Sciences Journal*, 24(10), 1390-1398.

Azizian, R., Doroodchi, E., McKrell, T., Buongiorno, J., Hu, L.W. and Moghtaderi B. (2014). Effect of magnetic field on laminar convective heat transfer of magnetite nanofluids. *International Journal of Heat and Mass Transfer*, 68, 94-109.

Bachok, B., Ishak. A. and Pop. I. (2010). Boundary layer flow of nanofluids over a moving surface in a flowing fluid. *International Journal of Thermal Sciences*, 49, 1663-1668.

Bataller, R.C. (2008). Radiation effects for the Blasius and Sakiadis flows with a convective surface boundary condition. *Applied Mathematics and Computation*, *206*(2), 832-840.

Bejan, A. (2013). Convection heat transfer. John Wiley & Sons.

Bhatti, M.M. and Rashidi, M.M. (2016). Effects of thermo-diffusion and thermal radiation on Williamson nanofluid over a porous shrinking/stretching sheet. *Journal of Molecular Liquids*, 221, 567-573.

Blasius, H. (1950). The boundary layers in fluids with little friction.

Brinkman, H.C. (1952). The viscosity of concentrated suspensions and solutions. The Journal of Chemical Physics, 20, 571-581.

Buongiorno, J. (2006). Convective transport in nanofluids. *ASME Journal of Heat Transfer*, 128, 240-250.

Burmeister, L.C. (1993). Convective heat transfer. New York: John Wiley and Sons Inc.

Casson, N. (1959). A flow equation for pigment-oil suspensions of the printing ink type. *Pergamon Press*.

Cebeci, T. and Bradshaw, P. (2012). Physical and computational aspects of convective heat transfer. *Springer Science & Business Media*.

Chamkha, A.J. and Aly, A.M. (2011). MHD Free Convection Flow of a Nanofluid past a Vertical Plate in the Presence of Heat Generation or Absorption Effects. *Chemical Engineering Communication*, 198, 425–441.

Choi, S. (1995). Enhancing thermal conductivity of fluids with nanoparticles in developments and applications of non-Newtonian flows. In: D.A. Siginer, H.P. Wang, editors, *ASME*, 66, 99-105.

Chol, S.U.S. (1995). Enhancing thermal conductivity of fluids with nanoparticles. *ASME-Publications-Fed*, 231, 99-106.

Cross, M.M. (1965). Rheology of non-Newtonian fluids: a new flow equation for pseudoplastic systems. *Journal of Colloid Science*, 20(5), 417-437.

Das, S.K., Choi, S.U. and Patel, H.E. (2006). Heat transfer in nanofluids—a review. *Heat transfer engineering*, 27(10), 3-19.

Dash, R.K., Jayaraman, G. and Mehta, K.N. (2000). Shear augmented dispersion of a solute in a Casson fluid flowing in a conduit. *Annals of Biomedical Engineering*, 28(4), 373-385.

Eastman, J.A., Choi, U.S., Li, S., Thompson, L.J. and Lee, S. (1996). Enhanced thermal conductivity through the development of nanofluids. In MRS proceedings (Vol. 457, p. 3). *Cambridge University Press*.

Ellahi, R. (2013). The effects of MHD and temperature dependent viscosity on the flow of non-Newtonian nanofluid in a pipe: Analytical solutions. *Applied Mathematical Modeling*, 37, 1451-1467.

Ellahi, R., Riaz, A. and Nadeem, S. (2013). Three dimensional peristaltic flow of Williamson fluid in a rectangular duct. *Indian Journal of Physics*, 87(12), 1275-1281.

Gad-el-Hak, M. (1999). The fluid mechanics of microdevices-the Freeman scholar lecture. *Transactions-American Society of Mechanical Engineers Journal of FLUIDS Engineering*, 121, 5-33.

Ganga, B., Ansari, S.M.Y., Ganesh, N.V. and Hakeem A.K.A. (2016). Hydromagnetic flow and radiative heat transfer of nanofluid past a vertical plate. *Journal of Taibah University for Science*, 268, 1-14.

Gireesha, B. J, Gorla, R.S.R. and Mahanthesh, B. (2015). Effect of suspended nanoparticles on three-dimensional MHD flow, heat and mass transfer of radiating Eyring-Powell fluid over a stretching sheet. *Journal of Nanofluids*, 4(4), 474-484.

Gorla, R.S.R., & Gireesha, B.J. (2016). Dual solutions for stagnation-point flow and convective heat transfer of a Williamson nanofluid past a stretching/shrinking sheet. *Heat and Mass Transfer*, 52(6), 1153-1162.

Gorla, R.S.R. and Sidawi, I. (1994). Free convection on a vertical stretching surface with suction and blowing. *Applied Scientific Research*, 52(3), 247-257.

Goyal, M., and Bhargava, R. (2014). Boundary layer flow and heat transfer of viscoelastic nanofluids past a stretching sheet with partial slip conditions. *Applied Nanoscience*, 4(6), 761-767.

Gupta, H. K., Agrawal, G. D. and Mathur, J. (2012). An overview of Nanofluids: A new media towards green environment. *International Journal of environmental sciences*, 3(1), 433-440.

Ha, S.N. (2001). A nonlinear shooting method for two-point boundary value problems. *Computers & Mathematics with Applications*, 42(10), 1411-1420.

Hadjiconstantinou, N.G. and Simek, O. (2002). Constant-wall-temperature Nusselt number in micro and nano-channels. *Journal of Heat Transfer*, 124(2), 356-64.

Hamad, M.A.A., Pop, I. and Ismail, A.I.M. (2011). Magnetic field effects on free convection flow of a nanofluid past vertical semi-infinite flat plate. *Nonlinear Analysis: Real World Applications*, 12, 1338-1346.

Haq, R., Nadeem, S., Khan, Z. and Okedayo, T. (2014). Convective heat transfer and MHD effects on Casson nanofluid flow over a shrinking sheet. *Open Physics*, 12(12), 862-871.

Haq, R.U., Khan, Z.H. and Khan, W.A. (2014). Thermophysical effects of carbon nanotubes on MHD flow over a stretching surface. *Physics. E*, 63, 215-222.

Haq, R.U., Nadeem, S., Khan, Z.H. and Akbar, N.S. (2015) Thermal radiation and slip effects on MHD stagnation point flow of nanofluid over a stretching sheet. *Physica E: Low-dimensional Systems and Nanostructures*, 65, 17-23.

Haq, R.U., Nadeem, S., Khan, Z.H. and Noor, N.F.M. (2015). Convective heat transfer in MHD slip flow over a stretching surface in the presence of carbon nanotubes. *Physica B: Condensed Matter*, 457, 40-47.

Hayat, T., Abbas, Z. and Javed, T. (2008). Mixed convection flow of a micropolar fluid over a non-linearly stretching sheet. *Physics Letters A*, 372(5), 637-647.

Hayat, T. and Ali, N. (2008). Peristaltic motion of a Jeffrey fluid under the effect of a magnetic field in a tube. *Communications in Nonlinear Science and Numerical Simulation*, 13(7), 1343-1352.

Hayat, T., Asad. S. and Alsaedi. A. (2015). Analysis for flow of Jeffrey fluid with nanoparticles. *Chin.Phys.B*, 24(4), 044702.

Hayat, T., Ashraf, M. B., Shehzad, S. A. and Alsaedi, A. (2015). Mixed convection flow of Casson nanofluid over a stretching sheet with convectively heated chemical reaction and heat source/sink. *Journal of Applied Fluid Mechanics*, 8(4), 803-813.

Hayat, T., Khan, M.I., Waqas, M., Yasmeen, T. and Alsaedi, A. (2016). Viscous dissipation effect in flow of magnetonanofluid with variable properties. *Journal of Molecular Liquids*, 222, 47-54.

Hayat, T., Rashid, M., Imtiaz, M., and Alsaedi, A. (2015). Magnetohydrodynamic (MHD) flow of Cu-water nanofluid due to a rotating disk with partial slip. *AIP Advances*, 5(6), 067169.

Hayat, T., Shehzad, S.A., and Alsaedi, A. (2012). Soret and Dufour effects on magnetohydrodynamic (MHD) flow of Casson fluid. *Applied mathematics and Mechanics*, 33(10), 1301-1312.

Herbert, O.J. and Prandtl, L. (2004). *Prandtl's Essentials of Fluid Mechanics*. Germany: Springer Verlag.

Heris, S.Z., Etemad, S.G. and Esfahany, M.N. (2006). Experimental investigation of oxide nanofluids laminar flow convective heat transfer. *International Communications in Heat and Mass Transfer*, 33(4), 529-535.

Hossain, M.A. and Pop, I. (1996). Magnetohydrodynamic boundary layer flow and heat transfer on a continuous moving wavy surface. *Archives of Mechanics*, 48(5), 813-823.

Hussain, T., Shehzad, S. A., Alsaedi, A., Hayat, T. and Ramzan, M. (2015). Flow of Casson nanofluid with viscous dissipation and convective conditions: a mathematical model. *Journal of Central South University*, 22(3), 1132-1140.

Hussanan, A., Khan, I., Hashim, H., Anuar, M. K.A, Ishak, N., Sarif, N. M. and Salleh, M.Z. (2016). Unsteady MHD flow of some nanofluids past an accelerated vertical plate embedded in a porous medium. *Journal of Teknologi*, 78(2), 5-10.

Hussanan. A., Khan.I. and Shafie.S. (2013). An exact analysis of heat and mass transfer past a vertical plate with Newtonian heating, *Journal of Applied Mathematics*, 1-9.

Hussanan. A, Salleh. M.Z., Khan I., Tahar. R.M. and Ismail. Z. (2015). Soret effects on unsteady magnetohydrodynamic mixed-convection heat-and-mass-transfer flow in a porous medium with Newtonian heating. *Maejo International Journal of Science and Technology*, 9(2), 224-245.

Ibrahim, W. and Makinde, O.D. (2015). Magnetohydrodynamic stagnation point flow and heat transfer of casson nanofluid past a stretching sheet with slip and convective boundary condition. *Journal of Aerospace Engineering*, 11, 040150371.

Ibrahim, W. and Shankar, B. (2013). MHD boundary layer flow and heat transfer of a nanofluid past a permeable stretching sheet with velocity, thermal and solutal slip boundary conditions. *Computers & Fluids*, 75, 1-10.

Incropera, F.P., DeWitt, D.P., Berqman, T.L. and Lavine, A.S. 2006. *Fundamentals of Heat and Mass Transfer 6th ed.* New York: John Wiley and Sons.

Ishak, A., Nazar, R., and Pop, I. (2009). Heat transfer over an unsteady stretching permeable surface with prescribed wall temperature. *Nonlinear Analysis: Real World Applications*, 10(5), 2909-2913.

Jang, S.P. and Choi, S.U.S (2004). Role of Brownian motion in the enhanced thermal conductivity of nanofluids. *Applied Physics Letters*, 84(21), 4316-4318.

Jang, S.P. and Choi, S.U.S. (2007). Effects of various parameters on nanofluid thermal conductivity. Journal of Heat Transfer, 129, 617-623.

Kakac, S. and Pramuanjaroenkij, A. (2009). Review of convective heat transfer enhancement with nanofluids. *International Journal of Heat and Mass Transfer*, 52(13), 3187-3196.

Khalid, A., Khan, I., Khan, A. and Shafie, S. (2015). Unsteady MHD free convection flow of Casson fluid past over an oscillating vertical plate embedded in a porous medium. *Engineering Science and Technology, an International Journal*, 18(3), 309-317.

Khan, M.S., Karim, I., Ali, L.E. and Islam, A. (2012) Unsteady MHD free convection boundary-layer flow of a nanofluid along a stretching sheet with thermal radiation and viscous dissipation effects. *International Nano Letters*, 2(1), 1-9.

Khan, N.A. and Khan, H. (2014). A Boundary layer flows of non-Newtonian Williamson fluid. *Nonlinear Engineering Nonlinear Engineering*, 3(2), 107-115.

Khan, W.A. and Pop, I. (2010). Boundary-layer flow of a nanofluid past a stretching sheet. *International Journal of Heat and Mass Transfer*, 53(11), 2477-2483.

Kothandapani, M. and Prakash, J. (2015). Effects of thermal radiation parameter and magnetic field on the peristaltic motion of Williamson nanofluids in a tapered asymmetric channel. *International Journal of Heat and Mass Transfer*, 81, 234-245.

Kreith, F., Manglik, R.M. and Bohn, M.S. 2010. *Principles of Heat Transfer*. Stamford USA: Cengage Learning.

Krishna, P.M., Sugunamma, V. and Sandeep, N. (2014). Radiation and magnetic field effects on unsteady natural convection flow of a nanofluid past an infinite vertical plate with heat source. *Chemical and Process Engineering Research*, 25, 39-52.

Krishnamurthy, M.R., Gireesha, B.J., Prasannakumara, B.C. and Gorla, R.S.R. (2016). Thermal radiation and chemical reaction effects on boundary layer slip flow and melting heat transfer of nanofluid induced by a nonlinear stretching sheet. *Nonlinear Engineering*, 5(3), 147-159.

Krishnamurthy, M.R., Prasannakumara, B.C., Gireesha, B.J. and Gorla, R.S.R. (2016). Effect of chemical reaction on MHD boundary layer flow and melting heat transfer of Williamson nanofluid in porous medium. *Engineering Science and Technology, an International Journal*, 19(1), 53-61.

Kumaran, G., and Sandeep, N. (2017). Thermophoresis and Brownian moment effects on parabolic flow of MHD Casson and Williamson fluids with cross diffusion. *Journal of Molecular Liquids*, *233*, 262-269.

Kumari, B.A., Prasad, K.R. and Kavitha, K. (2012). Fully developed free convective flow of a Williamson fluid in a vertical channel under the effect of a magnetic field. *Advanced Application Sciences Research*, 3, 2492-2499.

Kurtcebe, C. and Erim, M.Z. (2002). Heat Transfer of non-Newtonian Viscoinelastic Fluid in an Axisymmetric Channel with a Porous Wall for Turbine Cooling Application. *International Communications in Heat and Mass Transfer*, 29(7), 971-982.

Lapwood, E.R. (1948, October). Convection of a fluid in a porous medium. *In Mathematical Proceedings of the Cambridge Philosophical Society, Cambridge University Press*, 44(4), 508-521.

Lebon, G. and Jou, D. (2008). *Understanding Non-equilibrium Thermodynamics*. Springer-Verlag Berlin Heidelberg.

Lesnic, D., Ingham, D.B. and Pop, I. (1999). Free convection boundary-layer flow along a vertical surface in a porous medium with Newtonian heating. *International Journal of Heat and Mass Transfer*, 42(14), 2621-2627.

Loganathan, P. and Vimala, C. (2014). Unsteady flow of nanofluids past a vertical flat plate with leading edge accretion or ablation. *Indian Journal Physics*, 88(8), 855–859.

Magyari, E. and Keller, B. (1999). Heat and mass transfer in the boundary layers on an exponentially stretching continuous surface. *Journal of Physics D: Applied Physics*, 32(5), 577-581.

Mahanta, G. and Shaw, S. (2015). 3D Casson fluid flow past a porous linearly stretching sheet with convective boundary condition. *Alexandria Engineering Journal*, 54(3), 653-659.

Mahapatra, T.R., and Gupta, A.S. (2002). Heat transfer in stagnation-point flow towards a stretching sheet. *Heat and Mass Transfer*, 38(6), 517-521.

Mahdy, A. (2012). Unsteady mixed convection boundary layer flow and heat transfer of nanofluids due to stretching sheet. *Nuclear Engineering and Design*, 249, 248-255.

Majumder, M., Chopra, N., Andrews, R. and Hinds, B.J. (2005). Nanoscale hydrodynamics: enhanced flow in carbon nanotubes. *Nature*, 438(7064), 44-48.

Malik, M.Y., Khan, M., Salahuddin, T. and Khan, I. (2016). Variable viscosity and MHD flow in Casson fluid with Cattaneo–Christov heat flux model: Using Keller box method. *Engineering Science and Technology, an International Journal*, 19(4), 1985-1992.

Malik, M.Y., Naseer, M., Nadeem, S. and Rehman, A. (2014). The boundary layer flow of Casson nanofluid over a vertical exponentially stretching cylinder. *Applied Nanoscience*, 4(7), 869-873.

Malvandi, A., Hedayati, F. and Ganji, D.D. (2014). Slip effects on unsteady stagnation point flow of a nanofluid over a stretching sheet. *Powder Technology*, 253, 377-384.

Matin, M.H., and Pop, I. (2013). Forced convection heat and mass transfer flow of a nanofluid through a porous channel with a first order chemical reaction on the wall. *International Communication in Heat and Mass Transfer*, 46, 134–141.

Merkin, J.H. (1994). Natural-convection boundary-layer flow on a vertical surface with Newtonian heating. *International Journal of Heat and Fluid Flow*, 15(5), 392-398.

Metzner, A.B. (1965). Heat transfer in non-Newtonian fluids. *Advances in Heat Transfer*, 2, 357-397.

Mohamad, A.A. (2003). Heat transfer enhancements in heat exchangers fitted with porous media Part I: constant wall temperature. *International Journal of Thermal Sciences*, 42(4), 385-95.

Morrison, D.D, Riley, J.D. and Zancanaro, J.F. (1962). Multiple shooting method for two-point boundary value problems. *Communications of the ACM*, 5(12), 613-614.

Mustafa, M. and Khan, J.A. (2015). Model for flow of Casson nanofluid past a non-linearly stretching sheet considering magnetic field effects. *AIP Advances*, 5(7), 077148.

Nadeem, S. and Akram, S. (2010). Peristaltic flow of a Williamson fluid in an asymmetric channel. *Communications in Nonlinear Science and Numerical Simulation*, 15(7), 1705-1716.

Nadeem, S., Haq, R.U. and Akbar, N.S. (2014). MHD three-dimensional boundary layer flow of Casson nanofluid past a linearly stretching sheet with convective boundary condition. *IEE E Transactions on Nanotechnology*, 13(1), 109-115.

Nadeem, S., Haq, R.U., Akbar, N.S. and Khan, Z.H. (2013). MHD three-dimensional Casson fluid flow past a porous linearly stretching sheet. *Alexandria Engineering Journal*, 52(4), 577-582.

Nadeem, S. and Hussain, S. T. (2014). Flow and heat transfer analysis of Williamson nanofluid. *Applied Nanoscience*, 4(8), 1005-1012.

Nadeem. S. and Hussain. S.T. (2014). Heat transfer analysis of Williamson fluid over exponentially stretching surface. *Applied Mathematics Mechanical English Edition*, 35(4), 489–502.

Nadeem, S., Hussain, S.T. and Lee, C. (2013). Flow of a Williamson fluid over a stretching sheet. *Brazilian Journal of Chemical Engineering*, 30(3), 619-625.

Nadeem, S. and Hussain, S.T. (2016). Analysis of MHD Williamson Nano Fluid Flow over a Heated Surface. *Journal of Applied Fluid Mechanics*, 9(2), 729-739.

Nadeem, S., Mehmood, R. and Akbar, N.S. (2015). Combined effects of magnetic field and partial slip on obliquely striking rheological fluid over a stretching surface. *Journal of Magnetism and Magnetic Materials*, 378, 457-462.

Narahari, M. and Ishak, A. (2011). Radiation effects on free convection flow near a moving vertical plate with Newtonian heating. *Journal of Applied Sciences*, 11(7), 1096-1104.

Narayana, K.L., Gangadhar, K. and Subhakar, M.J. (2015). Effect of Viscous dissipation on Heat Transfer of Magneto-Williamson Nanofluid. *IOSR Journal of Mathematics*,11(4), 25-37.

Noghrehabadi, A., Pourrajab, R. and Ghalambaz, M. (2012). Effect of partial slip boundary condition on the flow and heat transfer of nanofluids past stretching sheet prescribed constant wall temperature. *International Journal of Thermal Sciences*, 54, 253-261.

Özışık, M.N. (1985). Heat transfer: a basic approach (Vol. 1). McGraw-Hill College.

Prasannakumara, B.C., Gireesha, B.J., Gorla, R.S. and Krishnamurthy, M.R. (2016). Effects of chemical reaction and nonlinear thermal radiation on Williamson nanofluid slip flow over a stretching sheet embedded in a porous medium. *Journal of Aerospace Engineering*, 29(5), 04016019.

Qasim, M., Khan. I. and Shafie, S. (2013). Heat and mass diffusion in nanofluids over a moving permeable convective surface. *Mathematical Problems in Engineering*, Vol.2013, 1-7.

Qasim, M., Khan, Z.H., Khan, W.A. and Shah, I.A. (2014). MHD boundary layer slip flow and heat transfer of ferrofluid along a stretching cylinder with prescribed heat flux. *Plos One*, 9, e83930.

Qasim, M. and Noreen, S. (2014). Heat transfer in the boundary layer flow of a Casson fluid over a permeable shrinking sheet with viscous dissipation. *The European Physical Journal Plus*, 129(1), 7.

Qing, J., Bhatti, M.M., Abbas, M.A., Rashidi, M.M. and Ali, M.E.S. (2016). Entropy generation on MHD Casson nanofluid flow over a porous stretching/shrinking surface. *Entropy*, 18(4), e18040123.

Raisi, A., Ghasemi, B. and Aminossadati, S.M. (2011). A numerical study on the forced convection of laminar nanofluid in a microchannel with both slip and no-slip conditions. *Numerical Heat Transfer, Part A: Applications*, 59(2), 114-129.

Raju, C.S.K. and Sandeep, N. (2017). Unsteady Casson nanofluid flow over a rotating cone in a rotating frame filled with ferrous nanoparticles: A numerical study. *Journal of Magnetism and Magnetic Materials*, 421, 216-224.

Raju, C.S.K., Sandeep, N. and Saleem, S. (2016). Effects of induced magnetic field and homogeneous–heterogeneous reactions on stagnation flow of a Casson fluid. *Engineering Science and Technology, an International Journal*, 19(2), 875-887.

Raju, C.S.K., Sandeep, N., Sugunamma, V., Babu, M.J. and Reddy, J.R. (2016). Heat and mass transfer in magnetohydrodynamic Casson fluid over an exponentially permeable stretching surface. *Engineering Science and Technology, an International Journal*, 19(1), 45-52.

Ramesh, G.K., Gireesha, B.J. and Gorla, R.S.R. (2015). Study on Sakiadis and Blasius flows of Williamson fluid with convective boundary condition. *Nonlinear Engineering*, 4(4), 215-221.

Ramzan, M. (2015). Influence of Newtonian heating on three dimensional MHD flow of couple stress nanofluid with viscous dissipation and joule heating. *PloS One*, 10(4), e0124699.

Rana, P. and Bhargava, R. (2012). Flow and heat transfer of a nanofluid over a nonlinearly stretching sheet. *A numerical study, Communication in Nonlinear Science and Numerical Simulation*, 17, 212-226.

Rashidi, M.M., Ganesh, N.V., Hakeem, A.A. and Ganga, B. (2014). Buoyancy effect on MHD flow of nanofluid over a stretching sheet in the presence of thermal radiation. *Journal of Molecular Liquids*, 198, 234-238.

Reddy, M.G. (2014). Influence of magnetohydrodynamic and thermal radiation boundary layer flow of a nanofluid past a stretching sheet. *Journal of Scientific Research*, 6(2), 257-272.

Reddy, S., Naikoti, K., and Rashidi, M.M. (2017). MHD flow and heat transfer characteristics of Williamson nanofluid over a stretching sheet with variable

thickness and variable thermal conductivity. *Transactions of A. Razmadze Mathematical Institute*, *171*(2), 195-211.

Renksizbulut, M., Niazmand, H. and Tercan, G. (2006). Slip-flow and heat transfer in rectangular microchannels with constant wall temperature. *International Journal of Thermal Sciences*, 45(9), 870-881.

Riehl, R.R. and dos Santos, N. (2012). Water-copper nanofluid application in an open loop pulsating heat pipe. *Applied Thermal Engineering*, 42, 6-10.

Roy, G., Nguyen, C.T. and Lajoie, P.R. (2004). Numerical investigation of laminar flow and heat transfer in a radial flow cooling system with the use of nanofluids. *Superlattices and Microstructures*, 35(3), 497-511.

Saffman, P.G. and Taylor, G. (1958). The penetration of a fluid into a porous medium or Hele-Shaw cell containing a more viscous liquid. *In Proceedings of the Royal Society of London A: Mathematical, Physical and Engineering Sciences*, 245(1242), 312-329.

Sakiadis, B.C. (1961). Boundary layer behavior on continuous solid surfaces: I. Boundary‐layer equations for two‐dimensional and axisymmetric flow. *AIChE Journal*, 7(1), 26-28.

Salahuddin, T., Malik, M.Y., Hussain, A., Bilal, S. and Awais, M. (2016). MHD flow of Cattanneo–Christov heat flux model for Williamson fluid over a stretching sheet with variable thickness: Using numerical approach. *Journal of Magnetism and Magnetic Materials*, 401, 991-997.

Salleh, M.Z., Nazar, R. and Pop, I. (2010). Boundary layer flow and heat transfer over a stretching sheet with Newtonian heating. *Journal of the Taiwan Institute of Chemical Engineers*, 41(6), 651-655.

Sarojamma, G. and Vendabai, K. (2015). Boundary layer flow of a Casson nanofluid past a vertical exponentially stretching cylinder in the presence of a transverse magnetic field with internal heat generation/absorption. *International Journal of Mechanical Aerospace Industrial Mechatronik Engineering,* 9(1).

Schlichting, H. (1979). Boundary-layer theory (Vol. 7). New York: McGraw-hill.

Seigel, R. and Howell, J.R. (2002). *Thermal Radiation Heat Transfer.* 4th ed. England: Taylor and Francis.

Sharma, A. K., Tiwari, A. K. and Dixit, A. R. (2015). Progress of nanofluid application in machining: a review. *Materials and Manufacturing Processes*, 30(7), 813-828.

Sheikholeslami, M., Bandpy, M.G. and Ganji, D.D. (2014). MHD free convection in an eccentric semi-annulus filled with nanofluid. *Journal of the Taiwan Institute of Chemical Engineers*, 45, 1204-1216.

Sheikholeslami, M., Ganji, D.D., Javed, M.Y. and Ellahi, R. (2015). Effect of thermal radiation on magnetohydrodynamics nanofluid flow and heat transfer by means of two phase model. *Journal of Magnetism and Magnetic Materials*, 374, 36-43.

Sheikholeslami, M., Ganji, D.D. and Rashidi, M.M. (2015). Ferrofluid flow and heat transfer in a semi annulus enclosure in the presence of magnetic source considering thermal radiation. *Journal of the Taiwan Institute of Chemical Engineers*, 47, 6-17.

Sheikholeslami, M., Vajravelu, K. and Rashidi, M.M. (2016). Forced convection heat transfer in a semi annulus under the influence of a variable magnetic field. *International Journal of Heat and Mass Transfer*, 92, 339-348.

Shima, P.D., Philip, J. and Raj, B. (2009). Magnetically controllable nanofluid with tunable thermal conductivity and viscosity. *Applied physics letters*, 95(13), 133112.

Sivaiah, M., Nagarajan, A.S. and Reddy, P.S. (2010). Radiation effects on MHD free convection flow over a vertical plate with heat and mass flux. *Emirates Journal for Engineering Research*, 15(1), 35-40.

Sivashanmugam, P. (2012). Application of nanofluids in heat transfer. *INTECH Open Access Publisher*.

Sparrow, E.M. and Cess, R.D. (1961). The effect of a magnetic field on free convection heat transfer. *International Journal of Heat and Mass Transfer*, 3(4), 267-74.

Sreenivasulu, P., Poornima, T. and Reddy, N.B. (2015). Influence of magnetic field and viscous dissipation on nanofluids past a nonlinear stretching sheet with radiation and uniform heat source. *International Conference on Frontiers in Mathematics*, 147-153.

Srivastava, V. P. and Saxena, M. (1994). Two-layered model of Casson fluid flow through stenotic blood vessels: applications to the cardiovascular system. *Journal of Biomechanics*, 27(7), 921-928.

Taylor, R., Coulombe, S., Otanicar, T., Phelan, P., Gunawan, A., Lv, W., Rosengarten, G., Prasher, R. and Tyagi, H. (2013). Small particles, big impacts: a review of the diverse applications of nanofluids. *Journal of Applied Physics*, 113(1), 1.

Tiwari, R.K., and Das, M.K. (2007). Heat transfer augmentation in a two-sided lid-driven differentially heated square cavity utilizing nanofluids. *International Journal of Heat and Mass Transfer*, *50*(9), 2002-2018.

Trisaksri, V. and Wongwises, S. (2007) Critical review of heat transfer characteristics of nanofluids. *Renewable and Sustainable Energy Reviews*, 11(3), 512-23.

Turkyilmazoglu, M. (2012). Exact analytical solutions for heat and mass transfer of MHD slip flow in nanofluids. *Chemical Engineering Science*, 84, 182-187.

Vafai, K. (1984). Convective flow and heat transfer in variable-porosity media. *Journal of Fluid Mechanics*, 147, 233-259.

Venkateswarlu, B. and Narayana, P.S. (2015). Chemical reaction and radiation absorption effects on the flow and heat transfer of a nanofluid in a rotating system. *Applied Nanoscience*, 5(3), 351-360.

Verma, S. K., and Tiwari, A. K. (2015). Progress of nanofluid application in solar collectors: a review. *Energy Conversion and Management*, 100, 324-346.

Wang, C.Y. (1989). Free convection on a vertical stretching surface. *ZAMM Journal of Applied Mathematics and Mechanics/Zeitschrift für Angewandte Mathematik und Mechanik*, 69(11), 418-420.

Wen, D., Lin, G., Vafaei, S. and Zhang, K. (2009) Review of nanofluids for heat transfer applications. *Particuology*, 7(2), 141-50.

Williamson, R.V. (1929). The flow of pseudoplastic materials. *Industrial & Engineering Chemistry*, 21(11), 1108-1111.

Wong, K.V. and De Leon, O. (2010). Applications of nanofluids: current and future. *Advances in Mechanical Engineering*.

Wu, J. M. and Zhao, J. (2013). A review of nanofluid heat transfer and critical heat flux enhancement—research gap to engineering application. *Progress in Nuclear Energy*, 66, 13-24.

Xuan, Y. and Li, Q. (2000). Heat transfer enhancement of nanofluids. *International Journal of Heat and Fluid Flow*, 21(1), 58-64.

Xuan, Y. and Li, Q. (2003). Investigation on convective heat transfer and flow features of nanofluids. *Journal of Heat Transfer*, 125(1), 151-155.

Xuan, Y. and Roetzel, W. (2000). Conceptions for heat transfer correlation of nanofluids. *International Journal of Heat and Mass Transfer*, 43(19), 3701-3707.

Yacob, N.A., Ishak, A., Pop. I. and Vajravelu. K. (2011). Boundary layer flow past a stretching/shrinking surface beneath an external uniform shear flow with a convective surface boundary condition in a nanofluid. *Nanoscale Research Letters*, 6, 1-7.

Yang, F. (2009). Slip boundary condition for viscous flow over solid surfaces. *Chemical Engineering Communications*, 197(4), 544-550.

Yang, Y., Zhang, Z.G., Grulke, E.A., Anderson, W.B. and Wu, G. (2005). Heat transfer properties of nanoparticle-in-fluid dispersions (nanofluids) in laminar flow. *International Journal of Heat and Mass Transfer*, 48(6), 1107-16.

Yasin, M.H, Ishak, A. and Pop, I. (2016) MHD heat and mass transfer flow over a permeable stretching/shrinking sheet with radiation effect. *Journal of Magnetism and Magnetic Material*,. 407, 235-40.

Yoshimura, A. and Prud'homme, R.K. (1988). Wall slip corrections for Couette and parallel disk viscometers. *Journal of Rheology*, 32(1), 53-67.
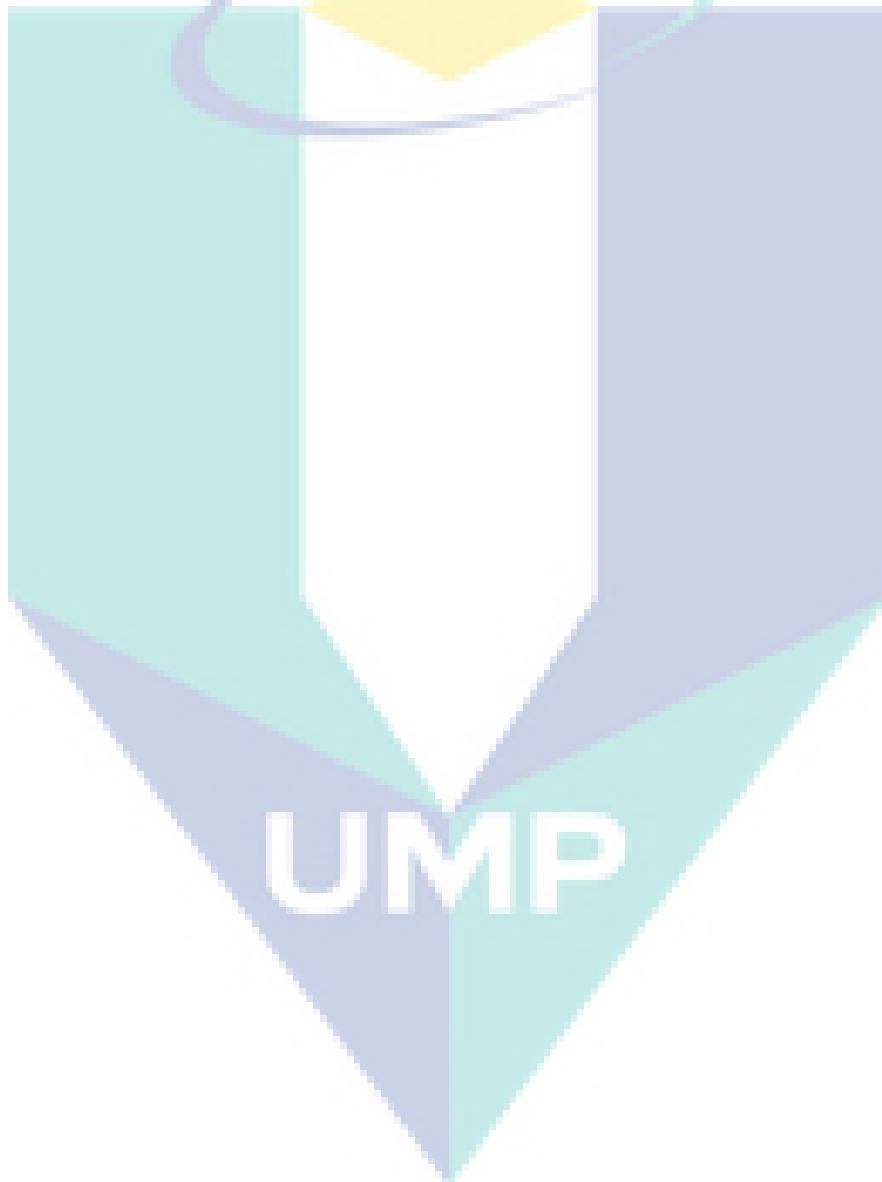
APPENDIX A

Maple (Shoot) Program .

```
> restart;
> Shootlib := "C:\\Program Files (x86)/Maple 13/Shoot9/";
```
$$Shootlib := \text{"C:\\Program Files (x86)/Maple 13/Shoot9/"} \tag{1}$$

```
> libname := Shootlib, libname;
```
$$libname := \text{"C:\Program Files (x86)/Maple 13/Shoot9/", "C:\Program Files (x86)\Maple 13/lib"} \tag{2}$$

```
> with (Shoot);
```
$$with \ Shoot \tag{3}$$

```
> with (plots);
```
$$with \ plots \tag{4}$$

```
> blt := 8; Pr := 1; Nc := 2; Le := 10; Nbt := 5; d := 5; Sc := 2; k := 2; λ := 0.5;
```
$$blt := 8$$
$$Pr := 1$$
$$Nc := 2$$
$$Le := 10$$
$$Nbt := 5$$
$$d := 5$$
$$Sc := 2$$
$$k := 2$$
$$\lambda := 0.5 \tag{5}$$

```
> FNS := {F(Z), Fp(Z), Fpp(Z), T(Z), Tp(Z), H(Z), Hp(Z)} :
> ODE := {diff(F(Z), Z) = Fp(Z), diff(Fp(Z), Z) = Fpp(Z), diff(Fpp(Z), Z) − Fp(Z)² + F(Z)·Fpp(Z) + λ·Fpp(Z)·diff(Fpp(Z), Z) + k·Fp(Z) = 0, diff(T(Z), Z)
```
$$= Tp(Z), diff(Tp(Z), Z) + Pr \cdot F(Z) \cdot Tp(Z) + \left(\frac{Nc}{Le \cdot Nbt} \right) \cdot Tp(Z)^2 + d \cdot T(Z) = 0, diff(H(Z), Z) = Hp(Z), diff(Hp(Z), Z) + Sc \cdot F(Z) \cdot Hp(Z) + \left(\frac{1}{Nbt} \right) \cdot diff(Tp(Z),$$
$$Z) = 0\};$$

$$ODE := \left\{ \frac{d}{dZ} Hp(Z) + 2 F(Z) Hp(Z) + \frac{1}{5} \frac{d}{dZ} Tp(Z) = 0, \frac{d}{dZ} Tp(Z) + F(Z) Tp(Z) + \frac{1}{25} Tp(Z)^2 + 5 T(Z) = 0, \frac{d}{dZ} Fpp(Z) − Fp(Z)^2 + F(Z) Fpp(Z) \right. \tag{6}$$
$$\left. + 0.5 Fpp(Z) \left(\frac{d}{dZ} Fpp(Z) \right) + 2 Fp(Z) = 0, \frac{d}{dZ} F(Z) = Fp(Z), \frac{d}{dZ} Fp(Z) = Fpp(Z), \frac{d}{dZ} H(Z) = Hp(Z), \frac{d}{dZ} T(Z) = Tp(Z) \right\}$$

```
> IC := {F(0) = s, Fp(0) = −1, H(0) = 0, T(0) = 1, Fpp(0) = α, Hp(0) = β, Tp(0) = −δ};
>
>
> BC := {Fp(L) = 0, H(L) = 0, T(L) = 0} :
> infolevel[shoot] := 1 :
> S := shoot( ODE, IC, BC, FNS, [α = 2.90, β = 0.01, δ = 0]);
shoot: Step #  1
shoot: Parameter values :  alpha = 2.90 beta = 0.1e-1 delta = 0
shoot: Step #  2
shoot: Parameter values :  alpha = HFloat(2.9633704507721084) beta = HFloat(-3.1365036772782256e-4) delta = HFloat
(11.010517362372283)
shoot: Step #  3
shoot: Parameter values :  alpha = HFloat(2.9556737159922366) beta = HFloat(9.883658291798664e-4) delta = HFloat
(11.012299389644127)
shoot: Step #  4
shoot: Parameter values :  alpha = HFloat(2.9555412362663622) beta = HFloat(0.0010116616237919492) delta = HFloat
(11.012295073515109)
```
$$S := \mathbf{proc}(x\_rkf45) \ \dots \ \mathbf{end \ proc} \tag{7}$$

```
> p := odeplot( S, [η, Fp(η)], 0 ..20, color = red, linestyle = solid, numpoints = 2000 )
> q := odeplot( S, [η, H(η)], 0 ..20, color = red, linestyle = solid, numpoints = 2000 )
> r := odeplot( S, [η, T(η)], 0 ..5, color = red, linestyle = solid, numpoints = 2000 ) :
```

> display(q);
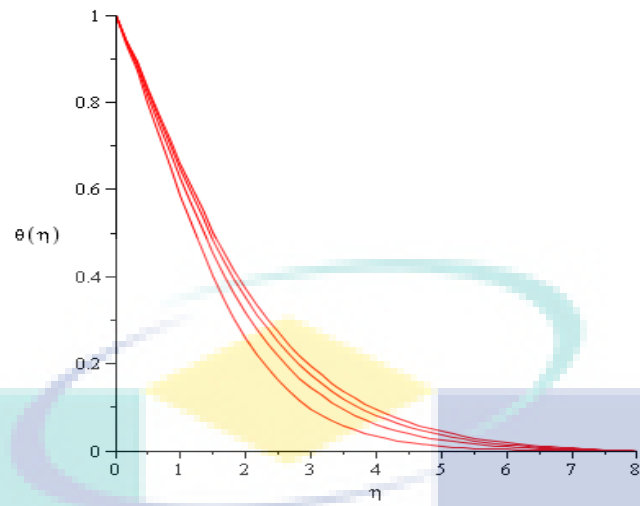
> display(p);

> display(r);

141
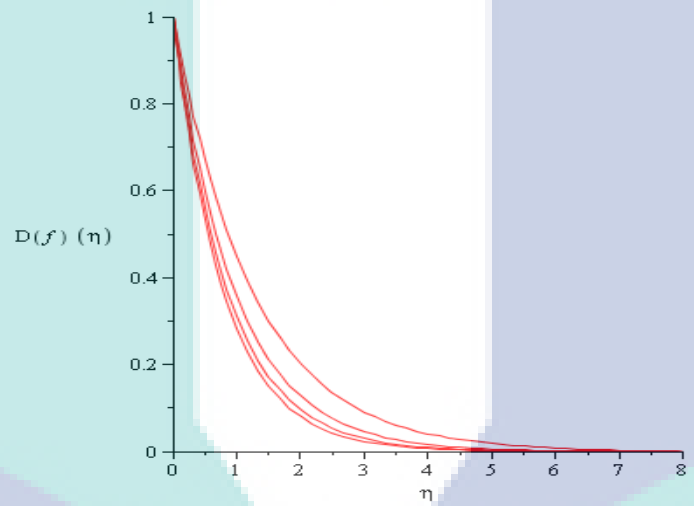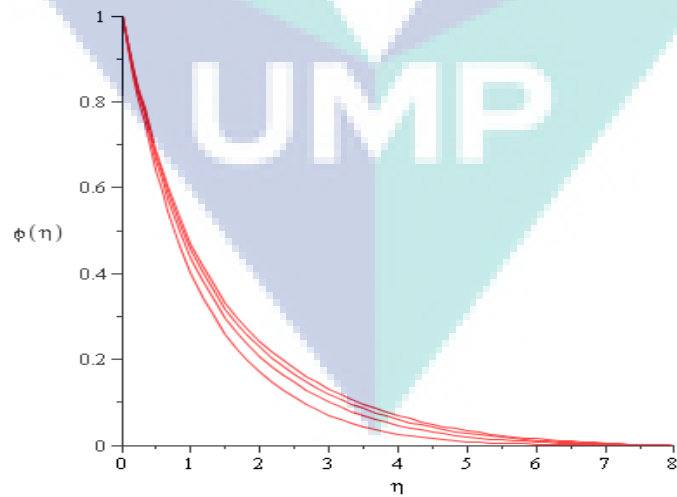
APPENDIX B

In this appendix, the transformation of PDEs to ODEs in Chapter 4 will be discussed in detail by using a similarity transformation in exponential form. The governing equations are shown as below:

Continuity equation:

$$\frac{\partial u}{\partial x} + \frac{\partial v}{\partial y} = 0 \qquad\qquad\text{B.1}$$

Momentum equation:

$$u\frac{\partial u}{\partial x} + v\frac{\partial u}{\partial y} = \nu\frac{\partial^2 u}{\partial y^2} + \sqrt{2}\,\nu\Gamma\frac{\partial u}{\partial y}\frac{\partial^2 u}{\partial y^2} - \frac{\sigma B_0^{\,2} u}{\rho} \qquad\qquad\text{B.2}$$

Energy equation:

$$u\frac{\partial T}{\partial x} + v\frac{\partial T}{\partial y} = \alpha\frac{\partial^2 T}{\partial y^2} + \frac{\rho_p C_p}{\rho C}\left[D_B\frac{\partial C}{\partial y}\frac{\partial T}{\partial y} + \frac{D_T}{T_\infty}\left(\frac{\partial T}{\partial y}\right)^2 \right] - \frac{\partial q_r}{\partial y} \qquad\qquad\text{B.3}$$

Concentration equation:

$$u\frac{\partial C}{\partial x} + v\frac{\partial C}{\partial y} = D_B\frac{\partial^2 C}{\partial y^2} + \frac{D_T}{T_\infty}\frac{\partial^2 T}{\partial y^2} \qquad\qquad\text{B.4}$$

The following equations (B.1), (B.2), (B.3) and (B.4) are transformed to ODEs by using the similarity transformations in exponential form below

$$u = bxf'(\eta) \qquad\qquad\text{B.5}$$

$$v = -\sqrt{b\nu}\,f(\eta) \qquad\qquad\text{B.6}$$

$$\eta = \sqrt{\frac{b}{\nu}}\,y \qquad\qquad\text{B.7}$$

$$\theta(\eta) = \frac{T - T_\infty}{T_W - T_\infty} \qquad\qquad\text{B.8}$$

$$T = \theta(\eta)(T_w - T_\infty) + T_\infty \qquad \text{B.9}$$

$$\phi(\eta) = \frac{C - C_\infty}{C_W - C_\infty} \qquad \text{B.10}$$

$$C = \phi(\eta)(C_W - C_\infty) + C_\infty \qquad \text{B.11}$$

To solve the problem of continuity equation (B.1), find the first derivatives for $\dfrac{\partial u}{\partial x}$ and $\dfrac{\partial v}{\partial y}$ by using equations (B.5), (B.6) and (B.7), respectively

$$\begin{aligned}
\frac{\partial u}{\partial x} &= \frac{\partial}{\partial x}\left(bxf'(\eta)\right) \\
&= bf'(\eta)
\end{aligned} \qquad \text{B.12}$$

$$\begin{aligned}
\frac{\partial v}{\partial y} &= \frac{\partial v}{\partial \eta}\cdot\frac{\partial \eta}{\partial y} \\
&= \frac{\partial}{\partial \eta}\left(-\sqrt{bv}\,f(\eta)\right)\cdot\frac{\partial}{\partial y}\left(\sqrt{\frac{b}{v}}\,y\right) \\
&= \left(-\sqrt{bv}\,f'(\eta)\right)\left(\sqrt{\frac{b}{v}}\right) \\
&= -bf'(\eta)
\end{aligned} \qquad \text{B.13}$$

After that, substitute equations (B.12) and (B.13) into the continuity equations (B.1) to obtain

$$\begin{aligned}
\frac{\partial u}{\partial x} + \frac{\partial v}{\partial y} &= bf'(\eta) + \left(-bf'(\eta)\right) \\
&= 0
\end{aligned} \qquad \text{B.14}$$

It is proved that the continuity equation is satisfied by looking at the above equation.

Furthermore, to reduce the momentum equation to a dimensionless form, the following terms of $u\dfrac{\partial u}{\partial x}$, $v\dfrac{\partial u}{\partial y}$, $v\dfrac{\partial^2 u}{\partial y^2}$, $\dfrac{\partial u}{\partial y}\dfrac{\partial^2 u}{\partial y^2}$, $u\dfrac{\partial T}{\partial x}$, $v\dfrac{\partial T}{\partial y}$, $\alpha\dfrac{\partial^2 T}{\partial y^2}$ and $\left(\dfrac{\partial T}{\partial y}\right)^2$ as shown below

$$u \frac{\partial u}{\partial x} = bxf'(\eta).bf'(\eta)$$
$$= b^2 x f'^2(\eta)$$

<div align="right">B.15</div>

$$v \frac{\partial u}{\partial y} = v \frac{\partial u}{\partial \eta} \cdot \frac{\partial \eta}{\partial y} = -\sqrt{bv} f(\eta) \frac{\partial}{\partial \eta} (bxf'(\eta)) \cdot \frac{\partial}{\partial y} \left(\sqrt{\frac{b}{v}} y \right)$$
$$= -\sqrt{bv} f(\eta).bxf''(\eta).\sqrt{\frac{b}{v}}$$
$$= -b^2 x f(\eta) f''(\eta)$$

<div align="right">B.16</div>

$$v \frac{\partial^2 u}{\partial y^2} = v \frac{\partial}{\partial y} \left(\frac{\partial u}{\partial y} \right)$$
$$= v \frac{\partial}{\partial \eta} \left(\frac{\partial u}{\partial \eta} \frac{\partial \eta}{\partial y} \right) \cdot \frac{\partial \eta}{\partial y}$$
$$= v \frac{\partial}{\partial \eta} \left(\frac{\partial}{\partial \eta} (bxf'(\eta)) \cdot \frac{\partial}{\partial y} \left(\sqrt{\frac{b}{v}} y \right) \right) \cdot \frac{\partial}{\partial y} \left(\sqrt{\frac{b}{v}} y \right)$$
$$= v \frac{\partial}{\partial \eta} \left(b \sqrt{\frac{b}{v}} x f''(\eta) \right) \cdot \left(\sqrt{\frac{b}{v}} \right)$$
$$= v \left(b \sqrt{\frac{b}{v}} x f'''(\eta) \right) \cdot \left(\sqrt{\frac{b}{v}} \right)$$
$$= b^2 x f'''(\eta)$$

<div align="right">B.17</div>

$$\frac{\partial u}{\partial y} \frac{\partial^2 u}{\partial y^2} = \left(b \sqrt{\frac{b}{v}} x f''(\eta) \right) \left(b^2 x f'''(\eta) \right)$$
$$= \left(b^2 x \right) \left(b \sqrt{\frac{b}{v}} x \right) f''(\eta) f'''(\eta)$$

<div align="right">B.18</div>

$$v \frac{\partial T}{\partial y} = v \frac{\partial T}{\partial \eta} \frac{\partial \eta}{\partial y}$$
$$= -\sqrt{bv} f(\eta) \cdot \frac{\partial}{\partial n} (\theta(\eta)(T_w - T_\infty) + T_\infty) \frac{\partial}{\partial y} \left(\sqrt{\frac{b}{v}} y \right)$$
$$= -\sqrt{bv} f(\eta) \cdot (\theta'(\eta)(T_w - T_\infty)) \left(\sqrt{\frac{b}{v}} \right)$$
$$= -b(T_w - T_\infty) f(\eta) \theta'(\eta)$$

<div align="right">B.19</div>

$$\alpha \frac{\partial^2 T}{\partial y^2} = \alpha \frac{\partial}{\partial \eta} \left(\frac{\partial T}{\partial \eta} \frac{\partial \eta}{\partial y} \right) \cdot \frac{\partial \eta}{\partial y}$$

$$= \alpha \frac{\partial}{\partial \eta} \left(\frac{\partial}{\partial \eta} \left(\theta(\eta)(T_w - T_\infty) + T_\infty \right) \frac{\partial}{\partial y} \left(\sqrt{\frac{b}{\nu}} y \right) \right) \cdot \frac{\partial}{\partial y} \left(\sqrt{\frac{b}{\nu}} y \right) \qquad \text{B.20}$$

$$= \alpha \frac{\partial}{\partial \eta} \left(\theta'(\eta)(T_w - T_\infty) \left(\sqrt{\frac{b}{\nu}} \right) \right) \cdot \left(\sqrt{\frac{b}{\nu}} \right)$$

$$= \alpha \frac{b}{\nu} (T_w - T_\infty) \theta''(\eta)$$

$$\left(\frac{\partial T}{\partial y} \right)^2 = \left(\theta'(\eta)(T_w - T_\infty) \left(\sqrt{\frac{b}{\nu}} \right) \right)^2 \qquad \text{B.21}$$

$$= \frac{b}{\nu} (T_w - T_\infty)^2 \theta'^2(\eta)$$

Then, substitute the following terms (B.15) (B.16) (B.17) (B.18) (B.19) (B.20) and (B.21) into equation of momentum (B.2) transform

$$b^2 x f'^2(\eta) + \left(-b^2 x f(\eta) f''(\eta) \right) = b^2 x f'''(\eta) + \sqrt{2} \nu \Gamma \left(b^2 x \right) \left(b \sqrt{\frac{b}{\nu}} x \right) f''(\eta) f'''(\eta)$$

$$- \frac{\sigma B_0^2}{\rho} b x f'(\eta)$$

by dividing with $b^2 x$, then the equation become

$$f'^2(\eta) - f(\eta) f''(\eta) = f'''(\eta) + \sqrt{2} \nu \Gamma \left(b \sqrt{\frac{b}{\nu}} x \right) f''(\eta) f'''(\eta) - \frac{\sigma B_0^2}{\rho b} f'(\eta)$$

By rearrange the position and substitute $\lambda = \sqrt{2} \nu \Gamma \left(b \sqrt{\frac{b}{\nu}} x \right)$ and $M = \frac{\sigma B_0^2}{\rho b}$

$$f'''(\eta) + \sqrt{2} \nu \Gamma \left(b \sqrt{\frac{b}{\nu}} x \right) f''(\eta) f'''(\eta) + f(\eta) f''(\eta) - f'^2(\eta) - \frac{\sigma B_0^2}{\rho b} f'(\eta) = 0$$

$$f'''(\eta) + \lambda f''(\eta) f'''(\eta) + f(\eta) f''(\eta) - f'^2(\eta) - M f'(\eta) = 0 \qquad \text{B.23}$$

Next, to reduce the energy equation to a dimensionless form, the following terms of $u\dfrac{\partial T}{\partial x}$ and $\dfrac{\partial C}{\partial y}$ as shown below

$$u\frac{\partial T}{\partial x} = u\frac{\partial T}{\partial n}\frac{\partial n}{\partial x}$$

$$= bxf'(\eta)\cdot\frac{\partial}{\partial n}\big(\theta(\eta)(T_w - T_\infty) + T_\infty\big)\frac{\partial}{\partial x}\left(\sqrt{\frac{b}{v}}\,y\right) \qquad \text{B.24}$$

$$= bxf'(\eta)\cdot\big(\theta'(\eta)(T_w - T_\infty)\big)(0)$$

$$= 0$$

$$\frac{\partial C}{\partial y} = \frac{\partial C}{\partial \eta}\frac{\partial \eta}{\partial y}$$

$$= \frac{\partial}{\partial \eta}\big(\phi(\eta)(C_w - C_\infty) + C_\infty\big)\frac{\partial}{\partial y}\left(\sqrt{\frac{b}{v}}\,y\right) \qquad \text{B.25}$$

$$= \sqrt{\frac{b}{v}}\,(C_w - C_\infty)\phi'(\eta)$$

After that, substitute the following terms (B.19), (B.24) and (B.25) into energy equation (B.3) to obtain

$$0 - b(T_w - T_\infty)f(\eta)\theta'(\eta) = \alpha\frac{b}{v}(T_w - T_\infty)\theta''(\eta) - \left[-\frac{16\sigma^* T_\infty^3}{3k^*}\frac{b}{v}(T_w - T_\infty)\theta''(\eta)\right]$$

$$+ \frac{\rho_p C_p}{\rho C}\left[D_B\sqrt{\frac{b}{v}}(C_w - C_\infty)\phi'(\eta)\theta'(\eta)(T_w - T_\infty)\left(\sqrt{\frac{b}{v}}\right) + \frac{D_T}{T_\infty}\left(\theta'(\eta)(T_w - T_\infty)\left(\sqrt{\frac{b}{v}}\right)\right)^2\right]$$

Reposition the above equation

$$\alpha\frac{b}{v}(T_w - T_\infty)\theta''(\eta) + b(T_w - T_\infty)f(\eta)\theta'(\eta) + \frac{16\sigma^* T_\infty^3}{3k^*}\frac{b}{v}(T_w - T_\infty)\theta''(\eta)$$

$$+ \frac{\rho_p C_p}{\rho C}\left[D_B\frac{b}{v}(C_w - C_\infty)\phi'(\eta)\theta'(\eta)(T_w - T_\infty) + \frac{D_T}{T_\infty}\left(\frac{b}{v}\theta'^2(\eta)(T_w - T_\infty)^2\right)\right] = 0$$

By dividing $b(T_w - T_\infty)$ and multiply $\dfrac{v}{\alpha}$

$$\theta''(\eta) + \frac{v}{\alpha} f(\eta) \theta'(\eta) + \frac{\rho_p C_p}{\rho C} \frac{D_B}{\alpha} (C_W - C_\infty) \phi'(\eta) \theta'(\eta) + \frac{\rho_p C_p}{\rho C} \frac{D_T}{\alpha T_\infty} (T_W - T_\infty) \theta'^2(\eta)$$

$$+ \frac{4}{3} \left(\frac{4\sigma^* T_\infty^3}{k^*} \frac{1}{\alpha} \right) \theta''(\eta) = 0$$

$$\theta''(\eta) + \frac{v}{\alpha} f(\eta) \theta'(\eta) + \frac{\rho_p C_p}{\rho C} \frac{D_B}{\alpha} (C_W - C_\infty) \phi'(\eta) \theta'(\eta) + \frac{4}{3} \left(\frac{4\sigma^* T_\infty^3}{k^*} \frac{1}{\alpha} \right) \theta''(\eta)$$

$$+ \frac{D_B(C_W - C_\infty)}{D_B(C_W - C_\infty)} \left[\frac{\rho_p C_p}{\rho C} \frac{D_T}{\alpha T_\infty} (T_W - T_\infty) \theta'^2(\eta) \right] = 0$$

$$\theta''(\eta) + \frac{v}{\alpha} f(\eta) \theta'(\eta) + \frac{\rho_p C_p}{\rho C} \frac{D_B}{\alpha} (C_W - C_\infty) \phi'(\eta) \theta'(\eta) + \frac{4}{3} \left(\frac{4\sigma^* T_\infty^3}{k^*} \frac{1}{\alpha} \right) \theta''(\eta)$$

$$+ \frac{D_B}{\alpha} \cdot \frac{\rho_p C_p}{\rho C} (C_W - C_\infty) \cdot \frac{D_T}{D_B T_\infty} \frac{(T_W - T_\infty)}{(C_W - C_\infty)} \theta'^2(\eta) = 0$$

Substitute that $R = \left(\frac{4\sigma^* T_\infty^3}{k^*} \frac{1}{\alpha} \right)$, $Nc = \frac{\rho_p C_p}{\rho C} (C_W - C_\infty)$, $Nbt = \frac{D_B T_\infty}{D_T} \frac{(C_W - C_\infty)}{(T_W - T_\infty)}$

and $Le = \frac{\alpha}{D_B}$

$$\theta''(\eta) + \Pr f(\eta) \theta'(\eta) + \frac{Nc}{Le} \phi'(\eta) \theta'(\eta) + \frac{4}{3} R \theta''(\eta) + \frac{Nc}{Le.Nbt} \theta'^2(\eta) = 0$$

$$\left(1 + \frac{4}{3} R \right) \theta''(\eta) + \Pr f(\eta) \theta'(\eta) + \frac{Nc}{Le} \phi'(\eta) \theta'(\eta) + \frac{Nc}{Le.Nbt} \theta'^2(\eta) = 0 \qquad \text{B.26}$$

Also, to reduce the concentration equation to a dimensionless form, the following terms

of $u \frac{\partial C}{\partial x}$, $v \frac{\partial C}{\partial y}$ and $\frac{\partial^2 C}{\partial y^2}$ have been carried.

$$u \frac{\partial C}{\partial x} = u \frac{\partial C}{\partial \eta} \frac{\partial \eta}{\partial x}$$

$$= bx f'(\eta) \cdot \frac{\partial}{\partial \eta} (\phi(\eta)(C_W - C_\infty) + C_\infty) \frac{\partial}{\partial x} \left(\sqrt{\frac{b}{v}} y \right) \qquad \text{B.27}$$

$$= bx f'(\eta) \phi'(\eta)(C_W - C_\infty)(0)$$

$$= 0$$

$$v\frac{\partial C}{\partial y} = v\frac{\partial C}{\partial \eta}\frac{\partial \eta}{\partial y}$$

$$= -\sqrt{bv}f(\eta).\frac{\partial}{\partial \eta}\left(\phi(\eta)(C_W - C_\infty) + C_\infty\right)\frac{\partial}{\partial y}\left(\sqrt{\frac{b}{v}}y\right) \qquad \text{B.28}$$

$$= -\sqrt{bv}f(\eta).\sqrt{\frac{b}{v}}(C_W - C_\infty)\phi'(\eta)$$

$$= -b(C_W - C_\infty)f(\eta)\phi'(\eta)$$

$$\frac{\partial^2 C}{\partial y^2} = \frac{\partial}{\partial \eta}\left(\frac{\partial C}{\partial \eta}\frac{\partial \eta}{\partial y}\right).\frac{\partial \eta}{\partial y}$$

$$= \frac{\partial}{\partial \eta}\left(\sqrt{\frac{b}{v}}(C_W - C_\infty)\phi'(\eta)\right).\frac{\partial}{\partial y}\left(\sqrt{\frac{b}{v}}y\right) \qquad \text{B.29}$$

$$= \sqrt{\frac{b}{v}}(C_W - C_\infty)\phi''(\eta).\sqrt{\frac{b}{v}}$$

$$= \frac{b}{v}(C_W - C_\infty)\phi''(\eta)$$

Then, substitute the equations of (B.27), (B.28) and (B.29) into the dimensionless of concentration equation (B.4)

$$0 + \left(-b(C_W - C_\infty)f(\eta)\phi'(\eta)\right) = D_B\frac{b}{v}(C_W - C_\infty)\phi''(\eta) + \frac{D_T}{T_\infty}\frac{b}{v}(T_W - T_\infty)\theta''(\eta)$$

By dividing $b(C_W - C_\infty)$ and multiply $\dfrac{v}{D_B}$ then we obtain that

$$\phi''(\eta) + \frac{v}{D_B}f(\eta)\phi'(\eta) + \frac{D_T}{D_B T_\infty}\frac{(T_W - T_\infty)}{(C_W - C_\infty)}\theta''(\eta) = 0$$

And substitute that $Sc = \dfrac{v}{D_B}$

$$\phi''(\eta) + Scf(\eta)\phi'(\eta) + \frac{1}{Nbt}\theta''(\eta) = 0 \qquad \text{B.30}$$

The boundary conditions for the variables are carried out as follows when $y = 0$,

$$u = bx$$

$$bxf'(0) = bx$$

$$f'(0) = \frac{bx}{bx}$$

$$= 1$$

$$v = 0$$

$$-\sqrt{bv}\, f(0) = 0$$

$$f(0) = \frac{0}{-\sqrt{bv}}$$

$$= 0$$

$$T = T_w \ \text{(Constant Wall Temperature)}$$

$$\theta(0) = \frac{T - T_\infty}{T_w - T_\infty}$$

$$= \frac{T_w - T_\infty}{T_w - T_\infty}$$

$$= 1$$

$$\frac{\partial T}{\partial y} = -h_s T \ \text{(Newtonian Heating)}$$

$$\sqrt{\frac{a}{v}}\, T_\infty \theta'(0) = -h_s T_\infty \left(\theta(0) + 1\right)$$

$$\theta'(0) = -h_s \sqrt{\frac{v}{a}} \left(\theta(0) + 1\right)$$

$$\theta'(0) = -\gamma \left(\theta(0) + 1\right)$$

$$C = C_w$$

$$\phi(0) = \frac{C - C_\infty}{C_w - C_\infty}$$

$$= \frac{C - C_\infty}{C_w - C_\infty}$$

$$= 1$$

Boundary conditions when $y \rightarrow \infty$,

$$u \rightarrow \infty$$
$$bxf'(\infty) = 0$$
$$f'(\infty) = \frac{0}{bx}$$
$$= 0$$

$$T \rightarrow T_\infty$$
$$\theta(\infty) = \frac{T - T_\infty}{T_W - T_\infty}$$
$$= \frac{T_\infty - T_\infty}{T_W - T_\infty}$$
$$= 0$$

$$C \rightarrow C_\infty$$
$$\phi(\infty) = \frac{C - C_\infty}{C_W - C_\infty}$$
$$= \frac{C_\infty - C_\infty}{C_W - C_\infty}$$
$$= 0$$

The Reynold number

$$\mathrm{Re}_x = \frac{xU_w(x)}{v}$$
$$= \frac{x(bx)}{v}$$
$$= \frac{x^2 b}{v}$$

Thus, the boundary conditions are obtained after the similirarity transformations as shown below:

$$f'(0) = 1, \, f(0) = 0, \, \theta(0) = 1 \, (\mathrm{CWT}), \, \theta'(0) = -\gamma(\theta(0) + 1) \, (\mathrm{NH}), \, \phi(0) = 1,$$
$$f'(\infty) \rightarrow 0, \, f(\infty) \rightarrow 0, \, \theta(\infty) \rightarrow 0, \, \phi(\infty) \rightarrow 0$$

(B.31)

The physical quantities for skin friction coeffiecient, local Nusselt number and local Sherwood number have been obtained respectively.

150

Local skin friction coefficient C_f and shear stress $\tau_w = \mu\left[\dfrac{\partial u}{\partial y} + \dfrac{\Gamma}{\sqrt{2}}\left(\dfrac{\partial u}{\partial y}\right)^2\right]$

$$C_f = \frac{\tau_w}{\rho\left(U_w\right)^2}_{y=0}$$

$$= \frac{\mu\left[\dfrac{\partial u}{\partial y} + \dfrac{\Gamma}{\sqrt{2}}\left(\dfrac{\partial u}{\partial y}\right)^2\right]}{\rho\left(U_w\right)^2}$$

$$= \frac{\mu\left[\sqrt{\dfrac{b^3}{\nu}}xf''(\eta) + \dfrac{\Gamma}{\sqrt{2}}\left(\sqrt{\dfrac{b^3}{\nu}}xf''(0).\sqrt{\dfrac{b^3}{\nu}}xf''(0)\right)\right]}{\rho\left(bx\right)^2}$$

$$= \frac{\mu\left[\sqrt{\dfrac{b^3}{\nu}}xf''(0) + \dfrac{\sqrt{2}\Gamma}{2}\sqrt{\dfrac{b^3}{\nu}}x\left(\sqrt{\dfrac{b^3}{\nu}}xf''^2(0)\right)\right]}{\rho\left(bx\right)^2}$$

$$= \frac{\mu}{\rho}\frac{\left[\sqrt{\dfrac{b^3}{\nu}}xf''(0) + \dfrac{\lambda}{2}\left(\sqrt{\dfrac{b^3}{\nu}}xf''^2(0)\right)\right]}{\left(bx\right)^2}$$

$$= \nu\frac{\sqrt{\dfrac{b^3}{\nu}}x\left[f''(0) + \dfrac{\lambda}{2}f''^2(0)\right]}{\left(bx\right)^2}$$

$$= \frac{\sqrt{\dfrac{\nu}{b}}\left[f''(0) + \dfrac{\lambda}{2}f''^2(0)\right]}{x}$$

$$\left(\mathrm{Re}_x\right)^{\frac{1}{2}}C_f = \left(x\sqrt{\dfrac{b}{\nu}}\right)\frac{\sqrt{\dfrac{\nu}{b}}\left[f''(0) + \dfrac{\lambda}{2}\left(f''^2(0)\right)\right]}{x} \qquad\text{B.32}$$

$$= f''(0) + \frac{\lambda}{2}f''^2(0)$$

Local Nusselt number Nu,

$$Nu = \frac{-x}{T_W - T_\infty} \frac{\partial T}{\partial y}\bigg|_{y=0}$$

$$= \frac{-x}{T_W - T_\infty} \left(\theta'(0)(T_W - T_\infty)\right)\left(\sqrt{\frac{b}{\nu}}\right)$$

$$= -x\sqrt{\frac{b}{\nu}}\theta'(0)$$

$$\frac{Nu}{\left(\text{Re}_x\right)^{\frac{1}{2}}} = \frac{-x\sqrt{\frac{b}{\nu}}\theta'(0)}{x\sqrt{\frac{b}{\nu}}} \qquad\qquad \text{B.32}$$

$$= -\theta'(0)$$

Sherwood number Sh,

$$Sh = \frac{-x}{C_W - C_\infty} \frac{\partial C}{\partial y}\bigg|_{y=0}$$

$$= \frac{-x}{C_W - C_\infty} \left(\phi'(0)(C_W - C_\infty)\right)\left(\sqrt{\frac{b}{\nu}}\right)$$

$$= -x\sqrt{\frac{b}{\nu}}\phi'(0)$$

$$\frac{Sh}{\left(\text{Re}_x\right)^{\frac{1}{2}}} = \frac{-x\sqrt{\frac{b}{\nu}}\phi'(0)}{x\sqrt{\frac{b}{\nu}}} \qquad\qquad \text{B.33}$$

$$= -\phi'(0)$$

APPENDIX C

In this appendix, the transformation of PDEs to ODEs in Chapter 5 will be discussed in detail by using a similarity transformation in exponential form. The governing equations are shown as below:

Continuity equation:

$$\frac{\partial u}{\partial x} + \frac{\partial v}{\partial y} = 0,$$

C.1

Momentum equation:

$$u\frac{\partial u}{\partial x} + v\frac{\partial u}{\partial y} = \nu\frac{\partial^2 u}{\partial y^2} + \sqrt{2}\,\nu\Gamma\frac{\partial u}{\partial y}\frac{\partial^2 u}{\partial y^2},$$

C.2

Energy equation:

$$u\frac{\partial T}{\partial x} + v\frac{\partial T}{\partial y} = \alpha\frac{\partial^2 T}{\partial y^2} + \frac{\rho_p C_p}{\rho C}\left[D_B\frac{\partial C}{\partial y}\frac{\partial T}{\partial y} + \frac{D_T}{T_\infty}\left(\frac{\partial T}{\partial y}\right)^2\right],$$

C.3

Concentration equation:

$$u\frac{\partial C}{\partial x} + v\frac{\partial C}{\partial y} = D_B\frac{\partial^2 C}{\partial y^2} + \frac{D_T}{T_\infty}\frac{\partial^2 T}{\partial y^2}.$$

C.4

The following equations (C.1), (C.2), (C.3) and (C.4) are transformed to ODEs by using the similarity transformations in exponential form below

$$u = bxf'(\eta)$$

C.5

$$v = -\sqrt{b\nu}\,f(\eta)$$

C.6

$$\eta = \sqrt{\frac{b}{\nu}}\,y$$

C.7

$$\theta(\eta) = \frac{T - T_\infty}{T_W - T_\infty}$$

C.8

$$\phi(\eta) = \frac{C - C_\infty}{C_w - C_\infty} \tag{C.9}$$

To solve the problem of continuity equation (C.1), find the first derivatives for $\dfrac{\partial u}{\partial x}$ and $\dfrac{\partial v}{\partial y}$ by using equations (C.5), (C.6) and (C.7), respectively

$$\begin{aligned}\frac{\partial u}{\partial x} &= \frac{\partial}{\partial x}\big(bxf'(\eta)\big) \\ &= bf'(\eta)\end{aligned} \tag{C.10}$$

$$\begin{aligned}\frac{\partial v}{\partial y} &= \frac{\partial v}{\partial \eta} \cdot \frac{\partial \eta}{\partial y} \\ &= \frac{\partial}{\partial \eta}\big(-\sqrt{bv}\, f(\eta)\big) \cdot \frac{\partial}{\partial y}\left(\sqrt{\frac{b}{v}}\, y\right) \\ &= \big(-\sqrt{bv}\, f'(\eta)\big)\left(\sqrt{\frac{b}{v}}\right) \\ &= -bf'(\eta)\end{aligned} \tag{C.11}$$

After that, substitute equations (C.10) and (C.11) into the continuity equations (C.1) to obtain

$$\begin{aligned}\frac{\partial u}{\partial x} + \frac{\partial v}{\partial y} &= bf'(\eta) + \big(-bf'(\eta)\big) \\ &= 0\end{aligned} \tag{C.12}$$

It is proved that the continuity equation is satisfied by looking at the equation (C.12)

Furthermore, to reduce the momentum equation to a dimensionless form, the following terms of $u\dfrac{\partial u}{\partial x}$, $v\dfrac{\partial u}{\partial y}$, $v\dfrac{\partial^2 u}{\partial y^2}$ and $\dfrac{\partial u}{\partial y}\dfrac{\partial^2 u}{\partial y^2}$ as shown below

$$\begin{aligned}u\frac{\partial u}{\partial x} &= bxf'(\eta) \cdot bf'(\eta) \\ &= b^2 x f'^2(\eta)\end{aligned} \tag{C.13}$$

154

$$v \frac{\partial u}{\partial y} = v \frac{\partial u}{\partial \eta} \cdot \frac{\partial \eta}{\partial y}$$

$$= -\sqrt{bv} f(\eta) \frac{\partial}{\partial \eta} (bxf'(\eta)) \cdot \frac{\partial}{\partial y} \left(\sqrt{\frac{b}{v}} y \right) \qquad \text{C.14}$$

$$= -\sqrt{bv} f(\eta).bxf''(\eta). \sqrt{\frac{b}{v}}$$

$$= -b^2 xf(\eta) f''(\eta)$$

$$v \frac{\partial^2 u}{\partial y^2} = v \frac{\partial}{\partial y} \left(\frac{\partial u}{\partial y} \right)$$

$$= v \frac{\partial}{\partial \eta} \left(\frac{\partial u}{\partial \eta} \frac{\partial \eta}{\partial y} \right) \cdot \frac{\partial \eta}{\partial y}$$

$$= v \frac{\partial}{\partial \eta} \left(\frac{\partial}{\partial \eta} (bxf'(\eta)) \cdot \frac{\partial}{\partial y} \left(\sqrt{\frac{b}{v}} y \right) \right) \cdot \frac{\partial}{\partial y} \left(\sqrt{\frac{b}{v}} y \right) \qquad \text{C.15}$$

$$= v \frac{\partial}{\partial \eta} \left(b \sqrt{\frac{b}{v}} xf''(\eta) \right) \cdot \left(\sqrt{\frac{b}{v}} \right)$$

$$= v \left(b \sqrt{\frac{b}{v}} xf'''(\eta) \right) \cdot \left(\sqrt{\frac{b}{v}} \right)$$

$$= b^2 xf'''(\eta)$$

$$\frac{\partial u}{\partial y} \frac{\partial^2 u}{\partial y^2} = \left(b \sqrt{\frac{b}{v}} xf''(\eta) \right) (b^2 xf'''(\eta))$$

$$\qquad \text{C.16}$$

$$= (b^2 x) \left(b \sqrt{\frac{b}{v}} x \right) f''(\eta) f'''(\eta)$$

Then, substitute the following terms (C.13) (C.14) (C.15) and (C.16) into equation of momentum (C.2) transform

$$b^2 xf'^2(\eta) + \left(-b^2 xf(\eta) f''(\eta) \right) = b^2 xf'''(\eta) + \sqrt{2} v \Gamma (b^2 x) \left(b \sqrt{\frac{b}{v}} x \right) f''(\eta) f'''(\eta),$$

by dividing with $b^2 x$, then the equation become

$$f'^2(\eta) - f(\eta) f''(\eta) = f'''(\eta) + \sqrt{2} v \Gamma \left(b \sqrt{\frac{b}{v}} x \right) f''(\eta) f'''(\eta),$$

By rearrange the position and substitute $\lambda = \sqrt{2}\nu\Gamma\left(b\sqrt{\dfrac{b}{\nu}}x\right)$

$$f'''(\eta)+\sqrt{2}\nu\Gamma\left(b\sqrt{\dfrac{b}{\nu}}x\right)f''(\eta)f'''(\eta)+f(\eta)f''(\eta)-f'^2(\eta)=0$$

Then, we will obtain the final equation as below

$$f'''(\eta)+\lambda f''(\eta)f'''(\eta)+f(\eta)f''(\eta)-f'^2(\eta)=0 \quad \text{(C.17)}$$

Next, to reduce the energy equation to a dimensionless form, the following terms of

$\dfrac{\partial C}{\partial y}$, $v\dfrac{\partial T}{\partial y}$, $\alpha\dfrac{\partial^2 T}{\partial y^2}$ and $\left(\dfrac{\partial T}{\partial y}\right)^2$ as shown below

$$\frac{\partial C}{\partial y}=\frac{\partial C}{\partial \eta}\frac{\partial \eta}{\partial y}$$

$$=\frac{\partial}{\partial \eta}\big(\phi(\eta)(C_w-C_\infty)+C_\infty\big)\frac{\partial}{\partial y}\left(\sqrt{\frac{b}{\nu}}y\right) \qquad \text{C.18}$$

$$=\sqrt{\frac{b}{\nu}}(C_w-C_\infty)\phi'(\eta)$$

$$v\frac{\partial T}{\partial y}=v\frac{\partial T}{\partial \eta}\frac{\partial \eta}{\partial y}$$

$$=-\sqrt{b\nu}\,f(\eta).\frac{\partial}{\partial n}\big(\theta(\eta)(T_w-T_\infty)+T_\infty\big)\frac{\partial}{\partial y}\left(\sqrt{\frac{b}{\nu}}y\right) \qquad \text{C.19}$$

$$=-\sqrt{b\nu}\,f(\eta).\big(\theta'(\eta)(T_w-T_\infty)\big)\left(\sqrt{\frac{b}{\nu}}\right)$$

$$=-b(T_w-T_\infty)f(\eta)\theta'(\eta)$$

$$\alpha\frac{\partial^2 T}{\partial y^2}=\alpha\frac{\partial}{\partial \eta}\left(\frac{\partial T}{\partial \eta}\frac{\partial \eta}{\partial y}\right).\frac{\partial \eta}{\partial y}$$

$$=\alpha\frac{\partial}{\partial \eta}\left(\frac{\partial}{\partial \eta}\big(\theta(\eta)(T_w-T_\infty)+T_\infty\big)\frac{\partial}{\partial y}\left(\sqrt{\frac{b}{\nu}}y\right)\right).\frac{\partial}{\partial y}\left(\sqrt{\frac{b}{\nu}}y\right) \qquad \text{C.20}$$

$$=\alpha\frac{\partial}{\partial \eta}\left(\theta'(\eta)(T_w-T_\infty)\left(\sqrt{\frac{b}{\nu}}\right)\right).\left(\sqrt{\frac{b}{\nu}}\right)$$

$$=\alpha\frac{b}{\nu}(T_w-T_\infty)\theta''(\eta)$$

156

$$\left(\frac{\partial T}{\partial y}\right)^2 = \left(\theta'(\eta)(T_W - T_\infty)\left(\sqrt{\frac{b}{v}}\right)\right)^2$$

$$= \frac{b}{v}(T_W - T_\infty)^2 \theta'^2(\eta)$$

<div style="text-align:right">C.21</div>

Then, substitute the following terms (C.18) (C.19) (C.20) and (C.21) into **equation of momentum (C.3) transform**

$$0 - b(T_W - T_\infty)f(\eta)\theta'(\eta) = \alpha\frac{b}{v}(T_W - T_\infty)\theta''(\eta) -$$

$$+\frac{\rho_p C_p}{\rho C}\left[D_B\sqrt{\frac{b}{v}}(C_W - C_\infty)\phi'(\eta)\theta'(\eta)(T_W - T_\infty)\left(\sqrt{\frac{b}{v}}\right) + \frac{D_T}{T_\infty}\left(\theta'(\eta)(T_W - T_\infty)\left(\sqrt{\frac{b}{v}}\right)\right)^2\right]$$

Reposition the equation

$$\alpha\frac{b}{v}(T_W - T_\infty)\theta''(\eta) + b(T_W - T_\infty)f(\eta)\theta'(\eta) +$$

$$\frac{\rho_p C_p}{\rho C}\left[D_B\frac{b}{v}(C_W - C_\infty)\phi'(\eta)\theta'(\eta)(T_W - T_\infty) + \frac{D_T}{T_\infty}\left(\frac{b}{v}\theta'^2(\eta)(T_W - T_\infty)^2\right)\right] = 0$$

By dividing $b(T_W - T_\infty)$, we will obtain the equation as follows

$$\frac{\alpha}{v}\theta''(\eta) + \frac{v}{\alpha}f(\eta)\theta'(\eta) + \frac{\rho_p C_p}{\rho C}\frac{D_B}{\alpha}(C_W - C_\infty)\phi'(\eta)\theta'(\eta) + \frac{\rho_p C_p}{\rho C}\frac{D_T}{\alpha T_\infty}(T_W - T_\infty)\theta'^2(\eta)$$

$$= 0$$

and multiply $\frac{v}{\alpha}$, we will get the equation as follows

$$\theta''(\eta) + \frac{v}{\alpha}f(\eta)\theta'(\eta) + \frac{\rho_p C_p}{\rho C}\frac{D_B}{\alpha}(C_W - C_\infty)\phi'(\eta)\theta'(\eta)$$

$$+ \frac{D_B(C_W - C_\infty)}{D_B(C_W - C_\infty)}\left[\frac{\rho_p C_p}{\rho C}\frac{D_T}{\alpha T_\infty}(T_W - T_\infty)\theta'^2(\eta)\right] = 0$$

Then, rearrage the position of the variables

$$\frac{\rho_p C_p}{\rho C}\frac{D_B}{\alpha}(C_W - C_\infty)\phi'(\eta)\theta'(\eta) + \frac{D_B}{\alpha}.\frac{\rho_p C_p}{\rho C}(C_W - C_\infty).\frac{D_T}{D_B T_\infty}\frac{(T_W - T_\infty)}{(C_W - C_\infty)}\theta'^2(\eta)$$

$$+\theta''(\eta) + \frac{\nu}{\alpha}f(\eta)\theta'(\eta) = 0$$

Substitute that $Nc = \frac{\rho_p C_p}{\rho C}(C_W - C_\infty)$, $Nbt = \frac{D_B T_\infty}{D_T}\frac{(C_W - C_\infty)}{(T_W - T_\infty)}$ and $Le = \frac{\alpha}{D_B}$

$$\theta''(\eta) + \Pr f(\eta)\theta'(\eta) + \frac{Nc}{Le}\phi'(\eta)\theta'(\eta) + \frac{Nc}{Le.Nbt}\theta'^2(\eta) = 0$$

Hence, the final term of energy equation is shown below

$$\theta''(\eta) + \Pr f(\eta)\theta'(\eta) + \frac{Nc}{Le}\phi'(\eta)\theta'(\eta) + \frac{Nc}{Le.Nbt}\theta'^2(\eta) = 0 \qquad \text{C.22}$$

Also, to reduce the concentration equation to a dimensionless form, the following terms of $u\frac{\partial C}{\partial x}$, $v\frac{\partial C}{\partial y}$ and $\frac{\partial^2 C}{\partial y^2}$ have been worked out.

$$u\frac{\partial C}{\partial x} = u\frac{\partial C}{\partial \eta}\frac{\partial \eta}{\partial x}$$

$$= bxf'(\eta).\frac{\partial}{\partial \eta}(\phi(\eta)(C_W - C_\infty) + C_\infty)\frac{\partial}{\partial x}\left(\sqrt{\frac{b}{\nu}}y\right) \qquad \text{C.23}$$

$$= bxf'(\eta)\phi'(\eta)(C_W - C_\infty)(0)$$

$$= 0$$

$$v\frac{\partial C}{\partial y} = v\frac{\partial C}{\partial \eta}\frac{\partial \eta}{\partial y}$$

$$= -\sqrt{b\nu}f(\eta).\frac{\partial}{\partial \eta}(\phi(\eta)(C_W - C_\infty) + C_\infty)\frac{\partial}{\partial y}\left(\sqrt{\frac{b}{\nu}}y\right) \qquad \text{C.24}$$

$$= -\sqrt{b\nu}f(\eta).\sqrt{\frac{b}{\nu}}(C_W - C_\infty)\phi'(\eta)$$

$$= -b(C_W - C_\infty)f(\eta)\phi'(\eta)$$

$$\frac{\partial^2 C}{\partial y^2} = \frac{\partial}{\partial \eta}\left(\frac{\partial C}{\partial \eta}\frac{\partial \eta}{\partial y}\right)\cdot\frac{\partial \eta}{\partial y}$$

$$= \frac{\partial}{\partial \eta}\left(\sqrt{\frac{b}{v}}(C_W - C_\infty)\phi'(\eta)\right)\cdot\frac{\partial}{\partial y}\left(\sqrt{\frac{b}{v}}y\right)$$

$$= \sqrt{\frac{b}{v}}(C_W - C_\infty)\phi''(\eta)\cdot\sqrt{\frac{b}{v}}$$

$$= \frac{b}{v}(C_W - C_\infty)\phi''(\eta)$$

C.25

Then, substitute the equations of (B.23), (B.24) and (B.25) into the dimensionless of concentration equation (B.4)

$$0 + \left(-b(C_W - C_\infty)f(\eta)\phi'(\eta)\right) = D_B\frac{b}{v}(C_W - C_\infty)\phi''(\eta) + \frac{D_T}{T_\infty}\frac{b}{v}(T_W - T_\infty)\theta''(\eta)$$

By dividing $b(C_W - C_\infty)$ and multiply $\dfrac{v}{D_B}$ then we obtain that

$$\phi''(\eta) + \frac{v}{D_B}f(\eta)\phi'(\eta) + \frac{D_T}{D_B T_\infty}\frac{(T_W - T_\infty)}{(C_W - C_\infty)}\theta''(\eta) = 0$$

And substitute that $Sc = \dfrac{v}{D_B}$, the final concentration equation as shown below

$$\phi''(\eta) + Scf(\eta)\phi'(\eta) + \frac{1}{Nbt}\theta''(\eta) = 0$$

C.26

The boundary conditions for the variables are carried out as follows when $y = 0$,

$$v = 0$$
$$-\sqrt{bv}f(0) = 0$$
$$f(0) = \frac{0}{-\sqrt{bv}}$$
$$= 0$$

$$u = u_w + \delta^* \mu \left(\frac{\partial u}{\partial y} \right)$$

$$bxf'(0) = bx + \delta^* (\rho v) \left(b\sqrt{\frac{b}{v}} xf''(\eta) \right)$$

$$bxf'(0) = bx \left(1 + \delta^* (\rho v) \left(\sqrt{\frac{b}{v}} f''(\eta) \right) \right)$$

$$= \frac{bx}{bx} \left(1 + \delta^* (\rho v) \left(\sqrt{\frac{b}{v}} f''(\eta) \right) \right)$$

$$= 1 + \delta^* (\rho v) \sqrt{\frac{b}{v}} f''(\eta)$$

$$= 1 + \delta f''(\eta)$$

$$T = T_w + B^* \frac{\partial T}{\partial y}$$

$$\theta(0) = \frac{T - T_\infty}{T_W - T_\infty}$$

$$T = \theta(0)(T_W - T_\infty) + T_\infty$$

$$T_w + B^* \frac{\partial T}{\partial y} = \theta(0)(T_W - T_\infty) + T_\infty$$

$$T_w + B^* \left(\theta'(0)(T_W - T_\infty) \right) \left(\sqrt{\frac{b}{v}} \right) = \theta(0)(T_W - T_\infty) + T_\infty$$

$$\theta(0)(T_W - T_\infty) = T_w - T_\infty + B^* (T_W - T_\infty) \left(\sqrt{\frac{b}{v}} \right) \theta'(0)$$

$$(T_W - T_\infty) \theta(0) = (T_W - T_\infty) \left[1 + B^* \left(\sqrt{\frac{b}{v}} \right) \theta'(0) \right]$$

$$\theta(0) = \frac{(T_W - T_\infty)}{(T_W - T_\infty)} \left[1 + B^* \left(\sqrt{\frac{b}{v}} \right) \theta'(0) \right]$$

$$\theta(0) = 1 + B^* \left(\sqrt{\frac{b}{v}} \right) \theta'(0)$$

$$\theta(0) = 1 + B\theta'(0)$$

$$C = C_w$$

$$\phi(0) = \frac{C - C_\infty}{C_W - C_\infty}$$

$$= \frac{C - C_\infty}{C_W - C_\infty}$$

$$= 1$$

Boundary conditions when $y \rightarrow \infty$,

$$u \rightarrow \infty$$

$$bxf'(\infty) = 0$$

$$f'(\infty) = \frac{0}{bx}$$

$$= 0$$

$$T \rightarrow T_\infty$$

$$\theta(\infty) = \frac{T - T_\infty}{T_W - T_\infty}$$

$$= \frac{T_\infty - T_\infty}{T_W - T_\infty}$$

$$= 0$$

$$C \rightarrow C_\infty$$

$$\phi(\infty) = \frac{C - C_\infty}{C_W - C_\infty}$$

$$= \frac{C_\infty - C_\infty}{C_W - C_\infty}$$

$$= 0$$

The Reynold number

$$\mathrm{Re}_x = \frac{xU_w(x)}{v}$$

$$= \frac{x(bx)}{v}$$

$$= \frac{x^2 b}{v}$$

161

Thus, the boundary conditions obtained after the similirarity transformations are as follows:

$$f(0) = 0, \ f'(0) = 1 + \delta f''(0), \ \theta(0) = 1 + B\theta'(0), \ \phi(0) = 1 \quad \text{as } y = 0.$$
$$f'(\infty) = 0, \ \theta(\infty) = 0, \ \phi(\infty) = 0 \quad \text{as } y \to 0.$$

The physical quantities for skin friction coeffiecient, local Nusselt number and local Sherwood number have been obtained respectively.

Local skin friction coefficient C_f and shear stress $\tau_w = \mu\left[\dfrac{\partial u}{\partial y} + \dfrac{\Gamma}{\sqrt{2}}\left(\dfrac{\partial u}{\partial y}\right)^2\right]$

$$C_f = \frac{\tau_w}{\rho(U_w)^2}\Bigg|_{y=0}$$

$$= \frac{\mu\left[\dfrac{\partial u}{\partial y} + \dfrac{\Gamma}{\sqrt{2}}\left(\dfrac{\partial u}{\partial y}\right)^2\right]}{\rho(U_w)^2}$$

$$= \frac{\mu\left[\sqrt{\dfrac{b^3}{v}}xf''(\eta) + \dfrac{\Gamma}{\sqrt{2}}\left(\sqrt{\dfrac{b^3}{v}}xf''(0).\sqrt{\dfrac{b^3}{v}}xf''(0)\right)\right]}{\rho(bx)^2}$$

$$= \frac{\mu\left[\sqrt{\dfrac{b^3}{v}}xf''(0) + \dfrac{\sqrt{2}\Gamma}{2}\sqrt{\dfrac{b^3}{v}}x\left(\sqrt{\dfrac{b^3}{v}}xf''^2(0)\right)\right]}{\rho(bx)^2}$$

$$= \frac{\mu}{\rho}\frac{\left[\sqrt{\dfrac{b^3}{v}}xf''(0) + \dfrac{\lambda}{2}\left(\sqrt{\dfrac{b^3}{v}}xf''^2(0)\right)\right]}{(bx)^2}$$

$$= v\frac{\sqrt{\dfrac{b^3}{v}}x\left[f''(0) + \dfrac{\lambda}{2}f''^2(0)\right]}{(bx)^2}$$

$$= \frac{\sqrt{\dfrac{v}{b}}\left[f''(0) + \dfrac{\lambda}{2}f''^2(0)\right]}{x}$$

$$\left(\mathrm{Re}_x\right)^{\frac{1}{2}} C_f = \left(x\sqrt{\frac{b}{v}}\right) \frac{\sqrt{\frac{v}{b}}\left[f''(0)+\frac{\lambda}{2}\left(f''^2(0)\right)\right]}{x} \qquad \text{C.28}$$

$$= f''(0)+\frac{\lambda}{2}f''^2(0)$$

Local Nusselt number Nu,

$$Nu = \frac{-x}{T_W - T_\infty}\frac{\partial T}{\partial y}\bigg|_{y=0}$$

$$= \frac{-x}{T_W - T_\infty}\left(\theta'(0)(T_W - T_\infty)\right)\left(\sqrt{\frac{b}{v}}\right)$$

$$= -x\sqrt{\frac{b}{v}}\theta'(0)$$

$$\frac{Nu}{\left(\mathrm{Re}_x\right)^{\frac{1}{2}}} = \frac{-x\sqrt{\frac{b}{v}}\theta'(0)}{x\sqrt{\frac{b}{v}}} \qquad \text{C.29}$$

$$= -\theta'(0)$$

Sherwood number Sh,

$$Sh = \frac{-x}{C_W - C_\infty}\frac{\partial C}{\partial y}\bigg|_{y=0}$$

$$= \frac{-x}{C_W - C_\infty}\left(\phi'(0)(C_W - C_\infty)\right)\left(\sqrt{\frac{b}{v}}\right)$$

$$= -x\sqrt{\frac{b}{v}}\phi'(0)$$

$$\frac{Sh}{\left(\mathrm{Re}_x\right)^{\frac{1}{2}}} = \frac{-x\sqrt{\frac{b}{v}}\phi'(0)}{x\sqrt{\frac{b}{v}}} \qquad \text{C.30}$$

$$= -\phi'(0)$$